Ensemble weather forecast using a stochastic weather generator and analogs of the atmospheric circulation

Meriem Krouma

université PARIS-SACLAY

Ensemble weather forecast using a stochastic weather generator and analogs of the atmospheric circulation

Prévision météorologique d'ensemble avec un générateur de temps stochastique basé sur des analogues de circulation

Thèse de doctorat de l'université Paris-Saclay

École doctorale n° 129 : sciences de l'environnement d'Île-de-France (SEIF)
Spécialité de doctorat : Géosciences
Graduate School : Géosciences, climat, environnement et planètes,

Référent : Université de Versailles-Saint-Quentin-en-Yvelines

Thèse préparée dans l'unité de recherche LSCE (Université Paris-Saclay, CNRS, CEA, UVSQ), sous la direction de Pascal Yiou, directeur de recherche et le Co-encadrement de Céline Déandreis, Ingénieure de recherche.

Thèse soutenue à Paris-Saclay, 5 Juin 2023 , par

Meriem Krouma

Composition du jury
Membres du jury avec voix délibérative

Sylvie Joussaume Directrice de recherche CNRS, LSCE-IPSL, Gif-sur-Yvette	Présidente
Juliette Blanchet Chargée de recherche CNRS, IGE, Grenoble	Rapporteur et Examinateur
Grégoire Mariéthoz Professeur à l'Université de Lausanne, Suisse	Rapporteur et Examinateur
Lauriane Batté Direction de la Climatologie et des Services Climatiques, Météo France	Examinatrice
Frédéric Vitart Principal Investigator, ECMWF, Reading, UK	Examinateur

THESE DE DOCTORAT
NNT : 2023UPASJ010

université PARIS-SACLAY

ÉCOLE DOCTORALE
Sciences de l'Environnement d'Île-de-France (SEIF)

Titre : Prévision météorologique d'ensemble avec un générateur de temps stochastique basé sur les analogues de circulation

Mots clés : SWG, analogues, statistiques, prévision, intra-saisonnier, précipitation, Oscillation de Madden et Julian, Prédictabilité.

Résumé: Les prévisions météorologiques d'ensemble peuvent aider à anticiper les risques d'événements météorologiques extrêmes. Cependant, le comportement chaotique de l'atmosphère représente une source majeure d'incertitudes pour les prévisions météorologiques, en particulier pour des échéances sous-saisonnières (de quelques jours à un mois). Un grand nombre de simulations numériques peut permettre de résoudre ce problème d'incertitude et de déterminer la distribution statistique des variables climatiques. Dans cette thèse, nous avons développé un outil de prévision d'ensemble basé sur des méthodes statistiques et probabilistes pour générer des prévisions météorologiques d'ensemble.

Nous utilisons un générateur de temps stochastique conçu pour imiter le comportement des variables climatiques en se basant sur des analogues de circulation atmosphérique. Nous avons testé cet outil pour prévoir différentes variables climatiques telles que les précipitations en Europe et l'oscillation de Madden et Julian. Nous avons évalué la performance de nos prévisions par rapport à des prévisions des centres météorologiques.

Dans un premier temps, nous avons testé le générateur stochastique de temps pour simuler des moyennes précipitations en Europe à l'échelle locale (au niveau des villes) pour des périodes de 3 à 30 jours. Nous avons obtenu de bonnes performances dans différentes régions d'Europe pour 10 jours. Ces performances sont basées sur l'importance de la circulation atmosphérique dans la prévision des paramètres météorologiques tels que les précipitations. Nous avons également identifié l'influence des types de circulation atmosphérique sur les bonnes et mauvaises prévisions.

Dans un deuxième temps, nous avons combiné le générateur stochastique de temps avec des sorties de modèles numériques pour obtenir de grands ensembles de prévisions de précipitations en Europe. Nous avons vérifié que les scores de prévision sont intéressants pour des moyennes jusqu'à 35 jours à l'avance, à une échelle très locale. Cela a conduit à une amélioration significative par rapport aux prévisions du centre européen ECMWF et de Météo-France.

Dans un troisième temps, nous avons configuré notre modèle stochastique pour prévoir l'oscillation Madden Julian (MJO). La MJO est responsable de fortes précipitations dans des régions très peuplées comme l'Inde. Nous avons cherché à prévoir la moyenne d'indices de l'activité MJO sur des périodes allant de 3 jours à 60 jours. Notre modèle fournit une prévision de ces indices dont les scores probabilistes sont satisfaisant jusqu'à 40 jours à l'avance et donne des résultats compétitifs par rapport aux prévisions météorologiques numériques.

Les travaux présentés dans ce manuscrit ont fait l'objet de plusieurs articles scientifiques. Des travaux complémentaires concernant la prévisibilité des variables météorologiques ont aussi été réalisés.

université PARIS-SACLAY

ÉCOLE DOCTORALE
Sciences de l'Environnement d'Île-de-France (SEIF)

Title: Ensemble weather forecast using a stochastic weather generator and analogs of the atmospheric circulation

Keywords: SWG, analogs, statistics, forecast, sub-seasonal, precipitation, Madden Julian Oscillation, Predictability

Abstract: Ensemble weather forecasts can help to better manage and anticipate the risks of extreme weather events. Nevertheless, weather forecasting is a complex task due to the chaotic behaviour of the atmosphere, which is a major source of uncertainties for sub-seasonal time scale (days to a month). To overcome these uncertainties, a large number of numerical simulations are required. It allows to determine the statistical distribution of the climate variables. In this thesis, we have developed a weather ensemble forecasting tool based on statistical and probabilistic methods to generate weather ensemble forecasts. We used a stochastic weather generator designed to mimic the behaviour of climate variables, based on atmospheric circulation analogs. We have tested this tool to forecast different climate variables such as European precipitation and the Madden-Julian oscillation. We have evaluated the performance of our forecasts using several forecast verification methods. In addition, we compared the performance of our forecast to other forecasts from international weather centers.

We start by assessing the capacity of the stochastic weather generator to simulate precipitation in Europe at the local scale (city level). We evaluated the ensemble forecasts of averages over 3 to 60 days ahead. We found good performances in different regions of Europe for up to 10 days. We assessed the role of atmospheric circulation patterns on the forecast scores of meteorological parameters. We also identified the influence of weather regimes on forecast performances. Then, we combined the stochastic weather generator with dynamical model outputs to obtain large ensembles of European precipitation forecasts. We obtain interesting forecast scores for averages up to 35 days ahead at a very local scale. This led to a significant improvement over the forecasts of the European Centre for Medium-Range Weather Forecasts and Météo-France.

Finally, we adjusted our model to forecast the Madden Julian Oscillation (MJO). The MJO is responsible for heavy precipitation in densely populated regions such as India. Our model provides a forecast of averages of MJO indices up to 40 days in advance and is competitive with numerical weather predictions. The results of this thesis have been the subject of published scientific papers. Some other work on the predictability of meteorological variables has also been developed.

"La nature produit des horloges qui ne sont pas périodiques."

Ilya Prigogine & Isabelle Stengers. Entre le temps et l'éternité, 2009. [1]

[1] "Nature produces clocks that are not periodic."

Remerciements

Ce fut une merveilleuse aventure scientifique! La thèse m'a permis d'approfondir mes connaissances scientifiques, de découvrir le monde, de me redécouvrir aussi, d'apprendre des grandes leçons et de rencontrer de belles âmes qui ont illuminé d'une manière ou d'une autre ce long chemin, et que je tiens ainsi à les remercier.

Tout d'abord je tiens à exprimer mes sincères remerciements ainsi que ma grande reconnaissance à Pascal Yiou, mon directeur de thèse. Son savoir, sa perspicacité, son calme et surtout sa modestie m'ont beaucoup appris et inspirée. Je le remercie pour ses conseils et aussi ses critiques judicieux, son soutien aussi scientifique que moral, ses petites attentions, et sa grande humanité, qui m'ont permis d'aller jusqu'au bout. Je le remercie de m'avoir soutenue dans les différentes épreuves que j'ai passées durant ces trois ans. C'est un grand plaisir pour moi de travailler avec lui.

J'ai eu le plaisir d'avoir dans mon jury de thèse Sylvie Joussaume, Juliette Blanchet, Grégoire Mariéthoz, Lauriane Batté, Frédéric Vitard et Alvaro Corral, qui m'ont fait l'honneur de juger mes travaux écrits ainsi que ma présentation orale de soutenance de thèse. Je les remercie pour les remarques, les questions, les critiques et les compliments qu'ils m'ont fait. Je les remercie aussi pour leur temps et leur soutien durant les derniers mois de mon doctorat. Aussi je tiens à remercier Pierre Tandéo, Julien Cattiaux et Jérôme Servonnat, les membres de mon comité de thèse durant ces trois ans, pour leur temps et toutes les discussions que nous avons eues.

J'ai eu la chance de pouvoir passer les trois ans de ma thèse dans le laboratoire des sciences du climat et de l'environnement, que je considère comme ma première maison et au sein de l'équipe ESTIMR qui est pour moi ma deuxième famille. Je remercie toutes les personnes qui m'ont aidée, encouragée, avec qui j'ai partagé un repas, un café, une réflexion, un sourire. Je remercie tous les membres de l'équipe ESTIMR, surtout Davide Faranda pour sa gentillesse, son soutien moral et sa bonne humeur. Soulivanh Theo pour sa gentillesse infinie, son écoute, ses conseils et surtout pour ses réponses à toutes mes questions sur R au début de ma thèse. Je remercie également Florence Gerry de m'avoir aidée dans les démarches administratives et répondu à toutes mes questions. Aussi je remercie mes collègues Robin, Camille, Mireia et Flavio pour leur amitié et leur support, aussi Burak, George, Pradeebane, Bastien et Florentin pour toutes les discussions que nous avons eues sur l'histoire, la politique et la science!

Ma thèse a été conduite en collaboration avec ARIA Technologies, ce qui m'a permis de découvrir le monde de l'entreprise et de faire des nouvelles rencontres. Mes remerciements s'adressent tout d'abord à ma co-encadrante Céline Déandreis pour ses conseils et pour les discussions que nous avons eues. Je la remercie aussi de m'avoir accueillie à Toulouse. Je remercie ainsi de ARIA Technologies, Armand Albergel et Fanny Velay, le directeur de SUEZ Adrien De Soria, et mes collègues Alex, Assia et Ines. Je remercie particulièrement Ingrid Jooris,

qui était pour moi une amie, une collègue et une chère sœur durant ces années. Elle m'a toujours guidée dans toutes les démarches, elle m'a toujours aidée, écoutée et a répondu à toutes mes questions. Elle m'a toujours remonté le moral. Je la remercie sincèrement et du fond du cœur pour son amitié, son grand cœur, pour tous les sourires et les discussions partagées dans son bureau à Boulogne ou par téléphone!

Ma thèse a été réalisée dans le cadre du projet Européen ITN CAFE. Au cours de ce projet, j'ai rencontré des personnes super agréables qui m'ont aidée et encouragée, des personnes qui ont vraiment cru en moi. Je tiens à remercier tous les ESRs : Noémie, Nikos, Pedro, Niclas, Emmanuel, Amal, Iago, Monica, Riccardo, Xinjia et Shraddha. J'ai un souvenir avec chacun d'entre eux. On a pu sûrement partager un café, un bubble tea, des churros, des cookies, des vacances, un zoom, un appel téléphonique et aussi un papier scientifique. Je tiens à remercier aussi tous les encadrants du projet pour leurs temps, leurs conseils et leurs critiques à chaque réunions du projet qui m'ont beaucoup aidé ! En particulier, je tiens à remercier Alvaro Corral pour sa gentillesse et son écoute, Linus Magnusson pour ses explications et ses réponses à mes questions, Hervé Douville pour son chaleureux accueil à Météo France, aussi de m'avoir toujours incluse dans les discussions et de m'avoir consacré de son temps et son expérience à plusieurs reprises, et Jörg Matschullat pour son support moral tout au long de ce parcours.

Au cours de ma thèse et grâce au projet ITN CAFE, j'ai eu la chance de visiter plusieurs instituts scientifiques en Europe et à chaque visite, j'ai eu l'occasion de rencontrer ou de partager mon temps avec des personnes superbes et agréables. Je remercie toutes les personnes du PIK qui m'ont accueilli en particulier Abhirup Banerjee pour son aide et Norbert Marwan pour le livre qui m'offert et pour le temps qui m'accordé pour m'expliquer les recurrences plots. Je remercie toutes les personnes du CRM, Pau, Vanessa, Jordi, Aranxta, Alvaro pour leur chaleureux accueil sous les positive vibes de Barcelone. Je remercie Lauriane Batté, Damien Specq et Constantin Ardilouze de m'avoir acceptée pour une visite scientifique au CNRM à Toulouse qui n'était pas programmée au début de ma thèse; c'était un plaisir de travailler avec eux. Je les remercie de m'avoir accueillie aussi chaleureusement, d'avoir pris le temps de m'expliquer les choses et pour leurs sourires et leur soutien durant les dernière mois de ma thèse.

Au cours de mes années d'étude, j'ai eu la chance de rencontrer des chercheurs qui m'ont beaucoup inspirée et aidée. Je tiens à remercier Redouane Lguensat pour son amitié et ses conseils durant ces années, Jacopo Riboldi pour ses réponses à mes questions sur le climat et la météo. Je remercie aussi Prof. Ramzi Touchan pour ces conseils et ses encouragements malgré la distance et de m'avoir rendu visite à Paris depuis les USA. Aussi je remercie mes prof Madame Layla Ben Ayed, Monsieur Issam Nouiri et Madame Jamila Tarhouni de m'avoir encouragé pour entamer ce parcours.

Les amis pour moi sont le plus beau cadeau de la vie, et j'ai eu la chance d'en avoir quelques perles que je remercie ici: ma chère tayti, ma jiji Lamorosa, Sa7bi Camillia, la douce Emna merci d'être restées toujours à mes côtés malgré la distance, à chaque fois que je vous appelle ou que je rentre même sans prévenir vous laisser tout tomber pour partager avec moi une journée ou quelques petites minutes ! J'ai eu le privilège d'en connaitre davantage ici, je commence par Eya qui m'a accompagnée depuis mon premier jour à l'aéroport jusqu'à ma soutenance de thèse, je la remcercie pour tout et d'avoir été une chère sœurette! Je remercie aussi Noémie pour son soutien continu et pour son amitié, de m'avoir invité chez elle à Strasbourg et me faire découvrir l'Alsace aussi pour tous les moments qu'on a partagé ensemble malgré le covid et toutes les discussions qu'on a eues à Potsdam. Nikos mon cher ami grec avec qui je peux

sentir les Mediterranean vibes je le remercie d'avoir été toujours à mes côtés et à chaque fois que j'en ai eu besoin. Mon cher Pedro que je remercie pour toutes les belles choses qu'on a pu partager, les voyages, les discussions, les moments de joie et de faiblesse, de m'avoir appris plein des belles choses, de m'avoir donné de son temps et de m'avoir offrir cette belle et très précieuse amitié. Je remercie Amal pour ses encouragements et nos discussions sur la justice et le monde parfait, Niclas pour sa grande humanité et son énergie positive, Emmanuel pour ses conseils et son aide. Je remercie Maureen pour notre belle amitié et tous les beaux moments qu'on a partagé ensemble, Le Cyrilou pour ses encouragements et les repas libanais qu'il m'a fait découvrir, Alice pour son amitié et tous les repas italiens qu'on a partagés, aussi Jaime, et Mikel et beaucoup bien d'autres, que je tiens à les remercier pour tous les moments qu'on a passés et qu'on continue à partager ensemble !

Tout ce que j'ai toujours voulu de cette vie est de rendre mes parents fiers de moi afin que je puisse leur rendre un peu de ce qu'ils ont fait pour moi! et c'est ainsi que je les remercie pour leur confiance, pour leur amour inconditionnel, pour tous les sacrifices. Hayouta et Kamoula je vous aime énormément! Je suis extrêmement reconnaissante à ma chère sœur ou ma deuxième petite maman Malek qui m'a toujours encouragée, de m'avoir accompagnée virtuellement dans tous mes voyages, de m'avoir toujours écoutée, et d'avoir fait partie de sa vie malgré la distance. Mes deux frères Adel et Aziz, Adoula pour son support et son amour et Azouz pour les sourires et les bêtises. Je remercie aussi ma nièce Minyar et mes neuves Loulou, Hamidou, Kamoula et Salmlam qui m'ont rendu la vie aussi joyeuse grâce à leur amour infini. Je remercie ma chère famille d'avoir toujours été à mes côtés malgré la distance et le covid, de m'avoir toujours incluse dans toutes les occasions familiales, et de ne jamais me laisser seule! Durant ces années, j'ai reçu beaucoup d'encouragements de ma grand-mère, ma grande famille, mes voisins, les amis de la famille que je tiens à remercie pour leur amour.

Finalement et grâce à cette opportunité, j'ai pu réaliser un rêve d'une petite fille, qui a toujours rêver de partir faire des études à l'étranger et de visiter Paris, la ville de la lumière et d'amour, et c'était un petit peu la raison qui m'a toujours poussé à tenir le coup, à garder le sourire et à savourer chaque instant. A toutes les personnes qui m'ont toujours posé la question voilà la réponse :

Well, maybe it started that way. As a dream,
but doesn't everything?
Those buildings. These lights. This whole city.
Somebody had to dream about it first.
And maybe that is what I did.
I dreamed about coming here,
but then I did it.
And as someone said
those who don't believe in magic,
will never find it!
And I do believe in it!
Roald Dahl - James and the Giant Peach

Summary

Ensemble weather forecasts can help to better manage and anticipate the risks of extreme weather events. Nevertheless, weather forecasting is a complex task due to the chaotic behaviour of the atmosphere, which is a major source of uncertainties for sub-seasonal time scale (days to a month). To overcome these uncertainties, a large number of numerical simulations are required. It allows to determine the statistical distribution of the climate variables. In this thesis, we have developed a weather ensemble forecasting tool based on statistical and probabilistic methods to generate weather ensemble forecasts. We used a stochastic weather generator designed to mimic the behaviour of climate variables, based on atmospheric circulation analogs. We have tested this tool to forecast different climate variables such as European precipitation and the Madden-Julian oscillation. We have evaluated the performance of our forecasts using several forecast verification methods. In addition, we compared the performance of our forecast to other forecasts from international weather centers.

We start by assessing the capacity of the stochastic weather generator to simulate precipitation in Europe at the local scale (city level). We evaluated the ensemble forecasts of averages over 3 to 60 days ahead. We found good performances in different regions of Europe for up to 10 days. We assessed the role of atmospheric circulation patterns on the forecast scores of meteorological parameters. We also identified the influence of weather regimes on forecast performances. Then, we combined the stochastic weather generator with dynamical model outputs to obtain large ensembles of European precipitation forecasts. We obtain interesting forecast scores for averages up to 35 days ahead at a very local scale. This led to a significant improvement over the forecasts of the European Centre for Medium-Range Weather Forecasts and Météo-France.

Finally, we adjusted our model to forecast the Madden Julian Oscillation (MJO). The MJO is responsible for heavy precipitation in densely populated regions such as India. Our model provides a forecast of averages of MJO indices up to 40 days in advance and is competitive with numerical weather predictions. The results of this thesis have been the subject of published scientific papers. Some other work on the predictability of meteorological variables has also been developed.

Résumé

Les prévisions météorologiques d'ensemble peuvent aider à anticiper les risques d'événements météorologiques extrêmes. Cependant, le comportement chaotique de l'atmosphère représente une source majeure d'incertitudes pour les prévisions météorologiques, en particulier pour des échéances sous-saisonnières (de quelques jours à un mois). Un grand nombre de simulations numériques peut permettre de résoudre ce problème d'incertitude et de déterminer la distribution statistique des variables climatiques. Dans cette thèse, nous avons développé un outil de prévision d'ensemble basé sur des méthodes statistiques et probabilistes pour générer des prévisions météorologiques d'ensemble.

Nous utilisons un générateur de temps stochastique conçu pour imiter le comportement des variables climatiques en se basant sur des analogues de circulation atmosphérique. Nous avons testé cet outil pour prévoir différentes variables climatiques telles que les précipitations en Europe et l'oscillation de Madden et Julian. Nous avons évalué la performance de nos prévisions par rapport à des prévisions des centres météorologiques.

Dans un premier temps, nous avons testé le générateur stochastique de temps pour simuler des moyennes précipitations en Europe à l'échelle locale (au niveau des villes) pour des périodes de 3 à 30 jours. Nous avons obtenu de bonnes performances dans différentes régions d'Europe pour 10 jours. Ces performances sont basées sur l'importance de la circulation atmosphérique dans la prévision des paramètres météorologiques tels que les précipitations. Nous avons également identifié l'influence des types de circulation atmosphérique sur les bonnes et mauvaises prévisions.

Dans un deuxième temps, nous avons combiné le générateur stochastique de temps avec des sorties de modèles numériques pour obtenir de grands ensembles de prévisions de précipitations en Europe. Nous avons vérifié que les scores de prévision sont intéressants pour des moyennes jusqu'à 35 jours à l'avance, à une échelle très locale. Cela a conduit à une amélioration significative par rapport aux prévisions du centre européen ECMWF et de Météo-France.

Dans un troisième temps, nous avons configuré notre modèle stochastique pour prévoir l'oscillation Madden Julian (MJO). La MJO est responsable de fortes précipitations dans des régions très peuplées comme l'Inde. Nous avons cherché à prévoir la moyenne d'indices de l'activité MJO sur des périodes allant de 3 jours à 60 jours. Notre modèle fournit une prévision de ces indices dont les scores probabilistes sont satisfaisant jusqu'à 40 jours à l'avance et donne des résultats compétitifs par rapport aux prévisions météorologiques numériques.

Les travaux présentés dans ce manuscrit ont fait l'objet de plusieurs articles scientifiques. Des travaux complémentaires concernant la prévisibilité des variables météorologiques ont aussi été réalisés.

Contents

Chapter 1

Introduction, context and objectives

1.1 General context

In January 2021, cyclone Filomena affected Spain inducing strong winds and heavy rain in the Canary Islands and southern Andalusia as well as extreme snowfall in large areas of the Iberian Peninsula. Madrid saw snow accumulations up to 50 cm in 30 hours, which was the most intense snowstorm since 1971. The snow episode forced Madrid-Barajas Airport to close and led to the cancellation of the entire rail service in the region. Schools were also closed for several days. The European Centre for Medium-Range Weather Forecasts (ECMWF) predicted snowfall three days in advance as well as large amounts of precipitation in southeast Spain (Gascón et al., 2021). The forecasts included uncertainties associated with the exact location of the polar and subtropical air mass convergence, the total amount and extension of the most affected areas, but they contained enough information to issue the corresponding weather warnings in advance (Gascón et al., 2021). The July 2021 floods in Germany, Belgium, and other neighbouring countries caused 200 deaths and catastrophic flooding in small and medium-sized rivers. The magnitude of rainfall in the worst-affected region broke the record in the ERA-5 reanalysis by a large margin. ECMWF forecasts predicted an extreme event with high confidence 3 days before the start of the 2-day event, but with large uncertainties about the absolute magnitude and the runoff over rivers (Magnusson et al., 2021).

During the summer of 2022, Europe experienced several heatwaves and drier conditions than normal, particularly in western Europe. For example, on July 19, the UK reached temperatures above 40 °C for the first time since the beginning of the 20th century. This summer also saw extreme weather in the northern hemisphere, with severe flooding in Pakistan and severe droughts in parts of China (Magnusson et al., 2022). The skill of forecasts for European heatwaves in the summer of 2022 on different timescales showed a signal for a warmer-than-normal summer in the 6-week forecasts from the extended-range system. However, the forecasts failed to capture the magnitude of the record-breaking day in the UK (Magnusson et al., 2022). The same findings were found for the heatwaves of 2015, 2018, and 2019.

The extreme weather events I have been citing above and many others are, of course, not new. Indeed, high-impact weather events have always occurred because they are an expression of climate variability. But, despite the dramatic consequences for both human societies and ecosystems, the examples of the extreme weather events that occurred all over the world during the development of this thesis were well forecasted in advance. However, the information was

not enough to implement additional measures. For instance, having the forecast of those events a few weeks in advance would help to better manage their dramatic consequences. This is why improving the understanding and prediction of these phenomena at different time scales has been and will always be crucial for societies.

The goal of this thesis is to assess the ability of statistical approaches to improve forecasts of climate variables and how they can contribute to improve the quality and timescales of the forecast. The work presented in this thesis was carried out in this context by evaluating and designing a new forecasting tool that takes into account the dependence between large and local climate variables. First, I was interested in applying and evaluating the forecasting tool and verifying whether it could simulate precipitation over Europe from large-scale information at different locations and time scales. Then, a new methodology based on combining the output of dynamical models with our stochastic forecasting tool has been developed in order to improve the forecasting skill to the sub-seasonal time scale. And finally, the forecasting tool was adapted to forecast one of the sources of predictability on the sub-seasonal time scale, the Madden-Julian oscillation (Kim et al., 2018).

This first chapter will introduce the main concepts of sub-seasonal forecasting used in my thesis. It will also provide a context for the work done in this manuscript. This chapter gives a few reasons about the importance of the sub-seasonal forecast, how it has been improved, the role of the ensemble forecast, and its utility for society as well as its interest to the scientific community. The goal of this chapter is not to be exhaustive, as several books that give a broader overview of sub-seasonal forecasting, ensemble forecast, as well as forecast verification methods, already exist (e.g. Robertson and Vitart, 2019; Wilks, 2011; Jolliffe and Stephenson, 2011).

1.2 Sub-seasonal timescale

The sub-seasonal to seasonal (S2S) prediction covers the gap between medium-range weather forecasting and seasonal forecasting (Robertson and Vitart, 2019). Different approximate ranges have been considered to define the S2S time scale. The World Meteorological Organization (WMO) defines the S2S scale as the scale associated with extended-range weather forecasting (from 10 to 30 days), and the first part of long-range forecasting (30 days up to 2 years) (WMO, 2012). Another definition formed by the National Academy of Sciences in the United States defines the S2S range as the time scale between 2 weeks and 12 months (Board et al., 2016). The sub-seasonal scale in many studies has been considered as the time scale between 2 weeks and a season ahead (Rashid et al., 2011; Kim et al., 2014).

The sub-seasonal forecast tends to be qualified as a "difficult" scale. The main reason behind this qualification is that the sub-seasonal time scale is considered too long for the atmospheric initial conditions memory and, at the same time, too short for the ocean conditions memory (Robertson and Vitart, 2019). Indeed, longer-term climate forecasting requires knowledge about components of the Earth's natural system such as sea-surface temperature, El Niño-Southern Oscillation, and snow cover, which are conditions that evolve more slowly. In contrast, predicting day-to-day weather requires an understanding of rapidly changing conditions like temperature, pressure, and so on, within the atmosphere. However, the key to accurate sub-seasonal forecasting is knowing which processes are responsible for predicting weather changes on this timescale. Sub-seasonal predictability is linked to both real-time initial conditions and atmospheric processes, including soil moisture (Koster et al., 2010), snow cover (Lin and Wu, 2011),

stratospheric-tropospheric interactions, ocean-atmosphere interactions, and natural oscillations such as the Madden Julian Oscillations (Lau and Waliser, 2011) and Monsoon Intraseasonal Oscillations. Significant effort was expended to understand these various processes to improve forecasting, initialization, and ensemble forecast generation at the sub-seasonal scale (Vitart, 2014; Rashid et al., 2011; Newman et al., 2003).

The first sub-seasonal forecast was made by Miyakoda et al. (1983) to predict, 10 days in advance, a blocking event that induced exceptional snow over Florida in 1977. The success of forecasts beyond the tenth day generated a great deal of interest at that time, and many operational forecast centers around the world began testing long-range forecasts for 10 to 30 days in advance (Tracton et al., 1989; Molteni et al., 1986; Déqué and Royer, 1992). Consequently, several attempts by different meteorological centers have been tested. For example, ECMWF produced a pair of 31-day forecasts from two consecutive days for each month from April 1985 to January 1989 (Palmer et al., 1990). These forecasts were found to be averaged after 10 days with respect to climatology and poor with respect to long-term persistence (Déqué and Royer, 1992; Miyakoda et al., 1986). ECMWF extended range experiments failed to produce significantly better 10-day forecasts than operational medium-range persistence forecasts (Molteni et al., 1986). Other forecast trials demonstrated that the high-quality long-range forecasts that generated the initial interest in monthly forecasts may have been the result of chance (Anderson and van den Dool, 1994). The same findings were obtained by the National Centers for Environmental Prediction (NCEP) model (Tracton et al., 1989). Indeed, they found that after 12 days, their model did not produce better predictions than an uncontrolled forecast. These poor results supported for many years the idea that the sub-seasonal to seasonal time scale was an "unpredictable" scale (Robertson and Vitart, 2019). The S2S time scale gained more interest later by (i) discovering the atmospheric, oceanic and land processes associated with the predictability of S2S (Koster et al., 2010; Lin and Wu, 2011; Lau and Waliser, 2011), (ii) the significant improvement in numerical weather prediction (NWP) that was mainly related to the improvement of the models and better available data (Hendon et al., 1999). Another factor that played a crucial role in the S2S forecast is the application of dynamical systems theory to S2S timescales. Indeed, understanding and adjusting the theoretical limits of Lorenz to longer time scales helped with the use of predictable phenomena specific to this time scale. And finally, the societal (WMO, 2012) need for such kind of forecast pushed further the enhancement of S2S forecasts.

In recent decades, a lot of progress has been made in the S2S forecast (Vitart, 2017b; Vitart and Robertson, 2018; Kim et al., 2018). For instance, due to the improvement of the forecast skill of the Madden Julian oscillation (Kim et al., 2018; Vitart and Molteni, 2010) and understanding its influence on the extra-tropics (Cassou, 2008), Vitart (2014) showed a significant improvement in 2-m temperature weekly mean prediction in the extra-tropics within the 3^{rd} and 4^{th} weeks. Similar results were found by Newman et al. (2003) where strong predictability of week 2 and week 3 averages was proved for some regions of the Northern Hemisphere.

Through this thesis manuscript, I will expand more about the sub-seasonal lead time in each chapter and give more details about other aspects that helped to improve the understanding of the sub-seasonal time scale, such as the use of dynamical models in Chapter 4 and the Madden Julian oscillation in Chapter 5.

Why is the sub-seasonal forecast important?

The improvement and understanding of the S2S time scale can satisfy the scientific community's questions and society's needs. The S2S prediction represents a great opportunity to help decision-makers through skilful forecasts of extreme weather risk. As explained before, weather and climate span a continuum of time scales, and forecast information with different lead times is relevant to different sorts of decisions and early warnings.

For instance, a seasonal forecast might inform a crop-planting choice, while sub-seasonal forecasts could help irrigation scheduling and pesticide or fertilizer application by making the cropping calendar as a function of the S2S forecast and thus dynamic in time. In situations where seasonal forecasts are already in use, sub-seasonal ones could be used as updates, as in estimating end-of-season crop yields. Sub-seasonal forecasts may play an especially important role where initial conditions and intra-seasonal oscillation yield strong sub-seasonal predictability, while seasonal predictability is weak, such as in the case of the Indian summer monsoon.

The potential benefits of S2S applications in developing nations are very diverse, especially in Africa, where at least 30 climate-sensitive diseases pose a major threat to the lives and livelihoods of millions of people. More than 500 million Africans live in regions where malaria is endemic, which is highly correlated with the seasonal climate (Brunet et al., 2010). Malaria forecasting on seasonal timescales has been well documented (Rogers et al., 2010; Jones and Morse, 2012). Morse et al. (2005) showed skilful 1-month lead seasonal predictions using a malaria transmission model driven with output from seasonal predictions. MacLeod et al. (2015) demonstrated skilful malaria epidemic forecasts in Africa 2 months before the start of the season.

In the context of humanitarian aid and disaster preparedness, the Red Cross Climate Centre and the International Research Institute for Climate and Society (IRI) have proposed a 'Ready-Set-Go' concept (Bazo et al., 2019) for making use of forecasts, from weather to seasonal. The concept consists on establishing different actions related to each forecast. The 'Ready-Set-Go' concept is defined as follows (Bazo et al., 2019):

- **Ready** is when seasonal forecasts are used to begin monitoring sub-seasonal and short-range forecasts, update contingency plans, train volunteers, and enable early warning systems.
- **Set** is when sub-seasonal predictions are used to alert volunteers and warn communities,
- Then **Go**, where weather forecasts are used to activate volunteers, distribute instructions to communities, and activate evacuation protocols if needed.

Aside from its benefits in the agriculture sector and humanitarian activities, rigorous S2S forecasts provide greater confidence in various other sectors, such as:

(i) The water management sector, where most international operational forecast centers provide flood forecasting and warning services based on short-range rainfall forecasts. However, with the use of advanced NWP applications, there is a potential opportunity to extend flood forecasting with rainfall-runoff hydraulic models to longer time frames. In addition, the amount of water allocated based on seasonal forecasts issued at the beginning of the season requires revision using updated sub-seasonal forecasts throughout the season (Sankarasubramanian et al., 2009).

(ii) The energy sector, where weather-related risk is a primary driver of energy pricing, production, and usage. For instance, it is routine practice for the wind energy sector to use short-range weather forecasts (Foley et al., 2012) and, to a lesser degree, seasonal outlooks. Roulston et al. (2003) showed that energy demand scenarios based on ensemble predictions are more accurate than those produced using traditional weather forecasts up to 10 days in advance. Therefore, S2S forecasts could be used to support these activities by hedging for anticipated energy peaks and other weather-related energy trading opportunities and risks.

1.3 Ensemble forecast

The sub-seasonal forecasts have been more accurate with the improvement of numerical weather prediction (NWP) models (Robertson and Vitart, 2019). NWP forecasting has improved over the past decades due to model improvements and the availability of better data and forecast initialization. NWP models have shifted in the past decades from a deterministic approach to the probabilistic one. Ensemble (probabilistic) forecasts help to catch atmospheric chaos by producing a set of probabilities for the predicted variable (Palmer, 2000). Today, ensemble forecasts are used on short- and medium-range forecasts, monthly and seasonal forecasts, and even decadal forecasts and climate projections. Indeed, ensemble forecasts provide both the most likely scenario and the uncertainty associated with it. The ensemble forecasts give the forecaster a much better idea of what weather events may occur at a particular time. By comparing these different forecasts the forecaster can decide how likely a particular weather event will be. If the forecast varies a lot then the forecaster knows that there is a lot of uncertainty about the weather behaviour, but if the forecast converges towards a similar behaviour, that will give more confidence in predicting a particular event.

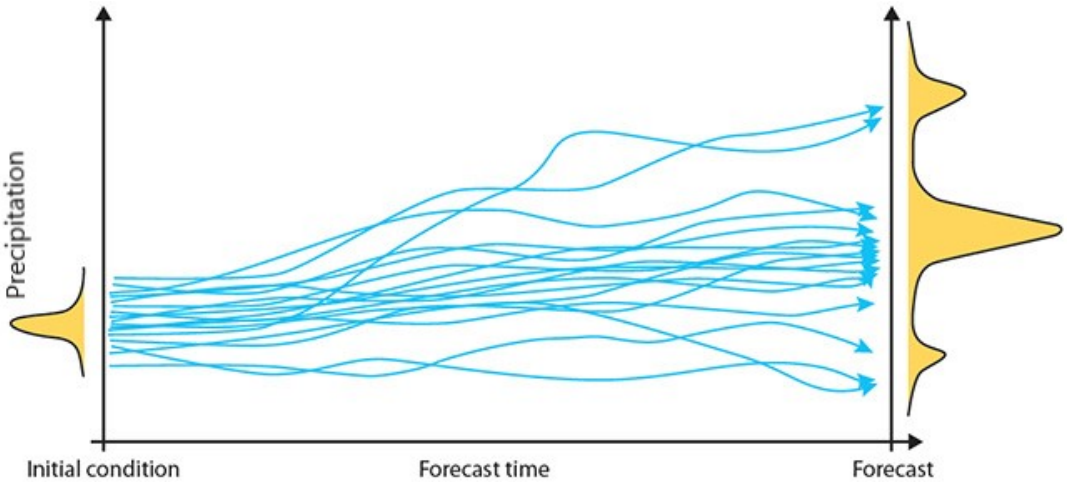

Figure 1.1: Illustration of the ensemble forecast concept. The starting point consists of initial conditions that already comprise a multitude of possible states. The initial conditions are used to estimate the associated probability distribution functions (PDF) at a selected forecast lead time. Figure modified, initially taken from Robertson and Vitart (2019).

The main concept behind the ensemble approach is to generate a set of S perturbed forecasts (Wilks, 2011), as illustrated in Figure 1.1. Each member of the ensemble S is designed in order to

simulate the effect of possible uncertainties associated with the unperturbed (or control) forecast. Moreover, the S perturbed forecasts are used to estimate the range of possible outcomes, the most probable set of values, and/or the probability that a future parameter, for example, the amount of precipitation in a particular place, will be higher or lower than a certain value. There are different methods to determine uncertainties in a forecast. The first method involves computing uncertainties around the predicted parameters, as shown in Figure 1.1. This method of ensemble forecasting is the most popular and is mostly used as it predicts the likelihood that a predicted event will occur. Another method consists of computing uncertainties from the starting point (uncertainties of atmospheric variables at the time of the analysis). This method considers ensembles of short-range forecasts or data assimilation.

Probabilistic forecast models use the same set of parameter values and initial conditions as the NWP models, although the output from the two models is different. However, the performance of the ensemble (probabilistic) forecast is usually expected to be similar to NWP models. For the S2S lead time, the use of probabilistic forecasts with the increase of model resolution and physical parameterizations as well as understanding the sources of predictability helped to improve the forecast skill of many meteorological variables as for example, for the ECMWF model, as shown in Figure 1.2. This illustrates that a portion of large-scale and low-frequency variability can be successfully predicted with NWP systems at a seasonal lead time. The forecast skill of the ECMWF ensemble forecast at a medium-range scale has greatly improved in recent years. However, it is still much less than 10 days for very detailed forecasts such as the forecast of precipitation and extreme Figure 1.2.

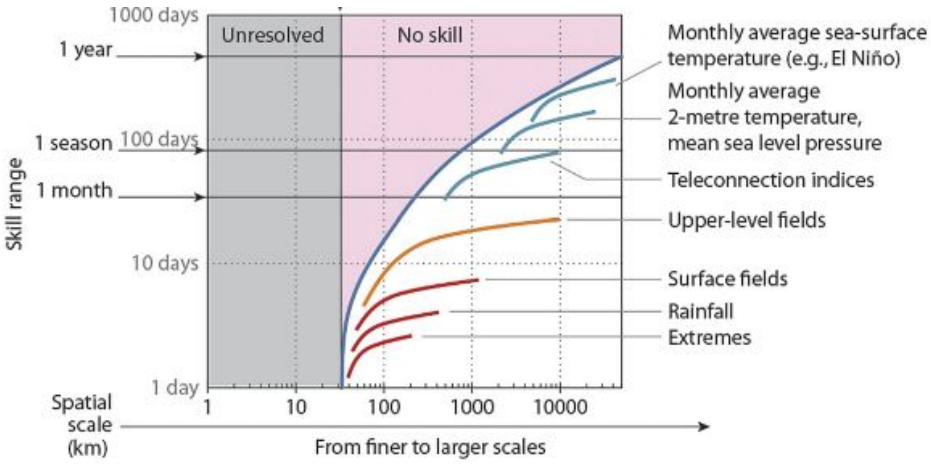

Figure 1.2: The Forecast Skill Diagram of the ECMWF for 2014. The figure shows the time and spatial scales up to which the ensemble forecasts are skilful. The x-axis represents the spatial scale. The y-axis (logarithmic scale) shows the time scale. Figure taken from Robertson and Vitart (2019).

1.4 Forecast Verification

The philosophy behind using forecast verification methods is to give meaning to the forecast. A weather forecast, or any other range of forecast, is made to predict in advance an event or quantity of a variable. Therefore, it is always important to verify a posteriori the "truth" behind the predicted values (Jolliffe and Stephenson, 2012).

Forecast verification methods differ depending on the type of data, the forecast lead time, and the predictand-predictor relationship. Forecast verification measurements are usually adjusted to the type of the forecasted event. For instance, the verification of extreme events forecast, such as tornadoes, may be extremely difficult to do in a comprehensive way as the forecast includes predictions of several different weather variables at different time scales, spatial locations, and vertical levels of the atmosphere. However, all forecast verification methods have one common purpose, which is to be "informative" (Casati et al., 2008). Forecast verification tends to be informative as it gives an idea about the quality of the forecast to the scientific community, which helps to understand and improve the forecast tool. Forecast verification is also informative to the entire society, as it provides concrete information about the forecast that allows better preparation to weather extreme event risks. For example, consider a daily forecast of temperatures in winter. The actual temperature is relevant to an electricity company as demand for electricity varies with temperature in a relatively smooth manner. In contrast, a local road authority is concerned with the value of the temperature relative to some threshold below which it should treat the roads to prevent ice formation. Forecast verification in both examples can help better manage risks and optimize economic decisions and daily operations.

A range of verification methods exist. I will list some of them below, as a range of books (Jolliffe and Stephenson, 2012; Wilks, 2011) and papers are available and they are well-suited to discuss and explain each metric. Some exploratory methods can be used to examine forecasted and observed data graphically using boxplots or histograms, which can provide a good and simple visualization of the forecast and observation distributions. Nevertheless, it is also helpful to use descriptive numerical measures using correlation or percentiles. Meteorological phenomena can be considered simple binary events, such as rain, floods, and tornadoes, known as unconditional events that will or will not occur. Their forecasts are referred to as yes-or-no forecasts and represent the simplest type of forecasting and decision-making situation. For these events, metrics of hits, false alarms, misses and correct rejections can be suitable.

		Occurred events	
forecasted events		yes	no
	yes	hit	false alarm
	no	miss	correct rejection

Figure 1.3: Forecast verification for binary events.

The verification can be extended to forecast problems in more than two categories, for example, forecasts of low, normal, or high precipitation where the categories are defined by some threshold. The continuous rank probability score skill (CRPSS) (Zamo and Naveau, 2018; Hersbach, 2000) could be well adapted to assess the forecast skill of this kind of forecast. In my thesis work, I will be using different forecast verification methods that I will explain and define in the next chapters, mainly on the papers.

Forecast verification measurements should be specific and adapted to users. This concept

is known as "user-oriented" verification. Indeed, users have different interests. For instance, a seasonal forecast of summer rainfall may be of interest to both a farmer and an insurance company. However, different aspects of the forecast are relevant to each. The farmer will be interested in total rainfall and its distribution across the season, whereas the insurance company's interest is mainly in the risk of event cancellations due to wet weather during the weekends. Hence, communicating the verification metrics should consider the needs of a particular user and provided in various ways going from simple and less informative to more informative way.

1.5 Objectives of the Thesis

The first objective of the thesis is to explore the prediction skills of the stochastic weather generator. This will be done through a proof-of-concept study that will aim to:

- Forecast European precipitation with analogs of circulation and stochastic weather generator,
- Evaluate the performance of the stochastic weather generator with forecast verification metrics,
- Compare the predictive skill of the stochastic weather generator to forecast precipitation with precipitation forecasts from other meteorological centers.

The second objective of the thesis is to improve the stochastic weather generator forecast of precipitation in order to reach the sub-seasonal lead time. The questions underlying this objective that will be addressed are mainly related to the technique that I will be applying/associating to the stochastic weather generator in order to improve ensemble forecast of European precipitation.

The third objective is to apply the stochastic weather generator to forecast other meteorological variables. This will be done by applying our forecast technique, composed of analogs of the atmospheric circulation and the stochastic weather generator, to forecast the Madden Julian oscillation.

1.6 Outline of the manuscript

The rest of the manuscript is organized as follows: Chapter 2 introduces the forecasting tool composed of analogs and the stochastic weather generator giving an overview of each approach and its applications in this thesis. It specifies as well some definitions. Chapters 3 and 4 cover the subject of the forecast of European precipitation. Chapter 3 examines the capacity of the stochastic weather generator and analogs of the atmospheric circulation to forecast precipitation over different European areas. Chapter 4 explores the potential techniques applied to improve the European precipitation forecast with the stochastic weather generator. Chapters 3 and 4 contain respectively published and to-be-submitted articles and additional perspectives. Then, Chapter 5 focuses on the forecast of the Madden Julian oscillation. It contains a published paper. Chapter 6 is dedicated to present two theoretical studies related to the predictability of precipitation that I performed. Finally, Chapter 7 will summarize the work carried out and the results obtained. It will also specify some perspectives for future research.

Chapter 2

Methodological framework

This chapter is a specific introduction to the forecasting tools used in this thesis. The chapter aims to provide a reminder of some key notions to facilitate the understanding of the global methodologies applied in the rest of the thesis manuscript. The chapter is composed of three sections concerning the analogs of atmospheric circulation, the stochastic weather generator approach and the forecast time range definition. In each section, I give an overview of the used approach and briefly introduce how it has been applied in this thesis work, as the specific methodological details are also explained in each of the following chapters and papers.

2.1 Analogs of atmospheric circulation

2.1.1 Definition

An analog circulation of a reference (atmospheric) pattern is an atmospheric circulation pattern **similar** to that reference state (Platzer, 2020). Atmospheric circulation analogs were introduced by Lorenz (1969) to study atmospheric predictability by considering a current state of the atmosphere and its best analogs. As analogs are searched in the past, which is considered to be known, this offers an opportunity to predict a future state from known states. In his study, Lorenz (1969) uses the difference between future states and known successors of the analogs (in the past) of the current state to assess its predictability.

Several measures, mainly mathematical distances, can be used to quantify the similarity of atmospheric circulation (e.g. Toth, 1991). One of the most commonly used distances to define analogs is the Euclidean distance. Many reasons can justify this choice. The mathematical properties of the Euclidean distance make it a suitable tool as they are well known and widely used in the search for nearest neighbours. The Euclidean distance can also be adapted to search for analogs. For instance, Yiou et al. (2013) used the Euclidean distance to find analogs from atmospheric fields and added other statistical quantities such as the correlation to select best analogs. Fraedrich and Rückert (1998) adjusted the Euclidean distance using weights to optimize the analog forecasting task. A similar procedure was used by Wetterhall et al. (2005) to select the best analogs of the sea level pressure fields projected into their first principal components. Alternatively, Blanchet et al. (2018) use the Teweles-Wobus score to measure similarity in the shape instead of the actual value of geopotential height fields. Other distances, such as the Wasserstein and Mahalanobis distances, can be used in finding analogs (Platzer, 2020).

The Wasserstein distance finds the smallest path from one distribution to another and can thus identify patterns that are similar to a translation. This distance can be useful for some specific physical features. It was used by Robin et al. (2017) to detect changes in the attractor structure of dynamical systems. However, this distance is computationally expensive and is originally designed to measure changes of probability distributions, which can complicate its use for real-valued vector fields (Thorpe et al., 2017; Platzer, 2020). The Mahalanobis distance can be a good candidate to search for analogs. It normalizes the data by their spatial covariance structure, which might be interesting for atmospheric sciences, because SLP variance increases with latitude. But this involves products of large matrices which also slows down the computation. Finally, the distance choice can be defined depending on the aim of the study and the used variables.

Distance choice is important to define analogs. Nevertheless, additional conditions may be imposed for a state to be considered an analog of a given target state. For instance, Yiou and Déandréis (2019) selected analogs with a probability proportional to the calendar distance to the target state to ensure an averaged seasonal cycle in the simulated time series. Similar conditions may be imposed for the analogs to respect the seasonality or the life cycle of the target state, as it is shown in Chapters 2 and 4 to compute analogs for respectively European precipitation and the Madden-Julian Oscillation (Krouma et al., 2022, 2023).

2.1.2 Applications of analogs in climate sciences

The analogs have found many applications in climate studies. For instance, they can be useful for **downscaling** by estimating the possible states at a meteorological station given large-scale information. Wetterhall et al. (2005) produce statistics of precipitation at stations in Sweden from analogs of large-scale sea-level pressure fields and associated local precipitation values. Vaittinada Ayar et al. (2016) demonstrated that analog methods are very competitive for downscaling precipitation in Europe. Other examples of a similar procedure are given in the next chapters 3,4 and 5. Analogs also allow **upscaling** by estimating from local information the probability of large-scale patterns. This helps to reconstruct high-resolution fields at dates for which only local observations are available (Yiou et al., 2013).

Analogs have been used to evaluate the role of atmospheric circulation in **the occurrence of extreme events**, such as cold winters (Cattiaux et al., 2010) and heatwaves (Jézéquel et al., 2018b) and other studies of **attibution of extreme events to climate change** (Stott et al., 2016; Faranda et al., 2022). Using analogs in those studies helped to estimate the probability of observing extreme events assuming similar circulation patterns as done in a recent study by (Faranda et al., 2022) that I co-authored, to study the occurrence of some extreme events in 2021.

Analog forecasting was also combined with **data assimilation** (Lguensat et al., 2017). This approach was developed for data assimilation when models are not available. A direct application of analog forecasting with data assimilation is to fill gaps in observation maps as in Zhen et al. (2020).

In addition, analogs were combined with statistical techniques to **generate ensemble weather forecast**. Yiou (2014) used analogs with a stochastic weather generator to assess the probability of observing a given atmospheric state. Alexander et al. (2017) combined analogs with Gaussian kernels to perform forecasts of tropical intraseasonal oscillations. Delle Monache

et al. (2019); Atencia and Zawadzki (2014) have compared ensemble forecasts generated from analogs to other ensemble generating techniques. Hamill and Whitaker (2006) used analog ensemble reforecasts to estimate rainfall cumulative probability distributions. Arroyo and Maté (2009) produced histogram forecasts of monthly precipitation at stations in China, using analogs of histograms based on the Wasserstein and Mallows distances to measure similarity.

2.1.3 Advantages and caveats

The analog approach has many advantages. One of the advantages of using analogs is that it is a non-parametric method. It needs a few settings (mainly related to the number of used analogs, the choice of the distance...) to be performed. This simple principle behind analogs makes them easy to implement and interpret compared to other black-boxes methods that are hard to understand. Analog methods are also computationally cheap compared to the high computational cost of physical models, particularly for ensemble forecast tasks. In many ways, analogs are prototypes of machine learning approaches. They allow to easily perform ensemble forecasts, especially with developing techniques that can faster search for analogs. Generating large ensemble forecasts can be useful to evaluate uncertainties.

The analog methods showed the capacity to preserve features of the analysed systems. Atencia and Zawadzki (2017) noted that contrarily to other initial condition perturbation methods, analog ensemble forecasts are consistent with the system's fractal dimension. Zhen et al. (2020) note that the analog data assimilation technique allows to build reconstructed sea-surface height maps with a temporal spectra that is more consistent with the true spectra than optimal interpolation.

The analog approach lost its appeal for forecast applications, particularly with the development of numerical weather models, as they are based on physical models and vast amounts of observed data. However, analogs can still be used for other applications such as downscaling, upscaling, event attribution, interpolation, or ensemble forecasts.

The main criticism attributed to the analog approach since Lorenz's work is mainly related to the relative small size of a learning period (i.e. the number of data that is necessary to obtain good efficiency). This number should be an exponentially growing function of the dimension of the observables. This problem represents a generic concern for data-based methods. Many studies like the one from Van den Dool (1994); Nicolis and Daems (1998); Platzer et al. (2021a) helped to understand this issue. Indeed, Van den Dool (1994) explained that considering analogs of circulation for the whole North Hemisphere can not help to find "good analogs". This issue can be solved nowadays with the existence of big datasets of climate projections and reanalyses. For example, ERA5 reanalyses start (at the moment of writing this manuscript) to be available from 1940 [1], which is much longer than the data available to Lorenz in 1969. In addition, many studies (e.g. Yiou, 2014; Blanchet et al., 2018), where the analog methods have been applied to specific domains, showed the relevant value of the analog approach. The reason for those successful results is that analogs are not searched over the whole sphere, but on a rather limited subdomain, with few spatial degrees of freedom, so that the search for "good" analogs is promising. In this thesis, I also consider small domains to define analogs and large datasets as shown in Figure 2.1 and explained in the following chapters.

A possible (mathematical) drawback for the interpretation of analog methods is that they

[1] ERA5 new database 2023.

are based on the hypothesis of ergodicity, which may apply an inability to generalize out of the previously observed states of the system (Platzer, 2020). Analog forecasts are likely to be biased, in the case where the dynamics of the system change (e.g., due to global warming, change in land use...). However, this drawback is turned into a feature as explained earlier, with studies that aim to attribute a given event to climate change.

2.1.4 How analogs are used in this thesis

In this thesis, analogs circulation are defined using the Euclidean distance over two different "small" domains as indicated in figure 2.1. Analog are computed over Europe considering the blue dashed rectangle in Figure 2.1 to generate an ensemble forecast of European precipitation as shown in (Krouma et al., 2022). Analogs were also computed over the tropics, mainly over the red rectangle as illustrated in Figure 2.1, to forecast the Madden-Julian oscillation (Krouma et al., 2023).

For verification purposes and the context of each study, analog has been computed from different data sources: reanalyses from the National Centers for Environmental Prediction (NCEP, (Kistler et al., 2001)), reanalyses from the ECMWF (ERA5, (Hersbach et al., 2020)) and reforecasts from S2S models of the centre national de la recherche météorologique (CNRM) of Météo France (Ardilouze et al., 2021) and ECMWF(Vitart et al., 2017), and over different period lengths. Some tuning related to the adjustment of the domain of computation of analogs, the chosen atmospheric fields, and the use of statistical approaches such as empirical orthogonal function have been applied with respect to the studied variables. More details about the analogs approach can be found in Chapters 2, 3 and 4 and the following papers.

2.2 Stochastic weather generator

Stochastic weather generators (SWGs) are statistical models that aim to provide realistic simulations of random sequences of atmospheric variables such as temperature, precipitation and wind (Wilks and Wilby, 1999; Richardson, 1981; Horton, 2019). SWGs tend to reproduce accurately the spatio-temporal dynamics of the variables of interest, as well as weather persistence and natural variability (Ailliot et al., 2015).

SWGs focus on small spatial scales with a faster computationally, which can provide numerous random simulations that have the same distributional properties as observed time series, mainly at the daily or sub-daily scales. SWGs are computationally inexpensive tools as they can provide large ensembles in a short time compared to numerical models, which reproduce the behaviour of the whole atmosphere and its interactions with other Earth system components at the global scale and for a long time period. The two reasons explained earlier make SWGs widely useful for impact studies. By generating daily time series of atmospheric variables at local sites, SWG can be used as inputs into impact models such as the ones for electricity demand or crop growth (Ailliot et al., 2015). Like any approach, SWGs have disadvantages. One of the principal disadvantages of the SWGs is that they assume a priori physical relations between the climate variables, so they remain always dependent on available training datasets. Consequently, an SWG that is tuned to present climate variability might not be necessarily relevant for the future because the relationship between large scale predictors and local variables could be altered. In section 3.3 of Chapter 3, I propose some assumptions that can be used to adapt SWGs to a changing climate.

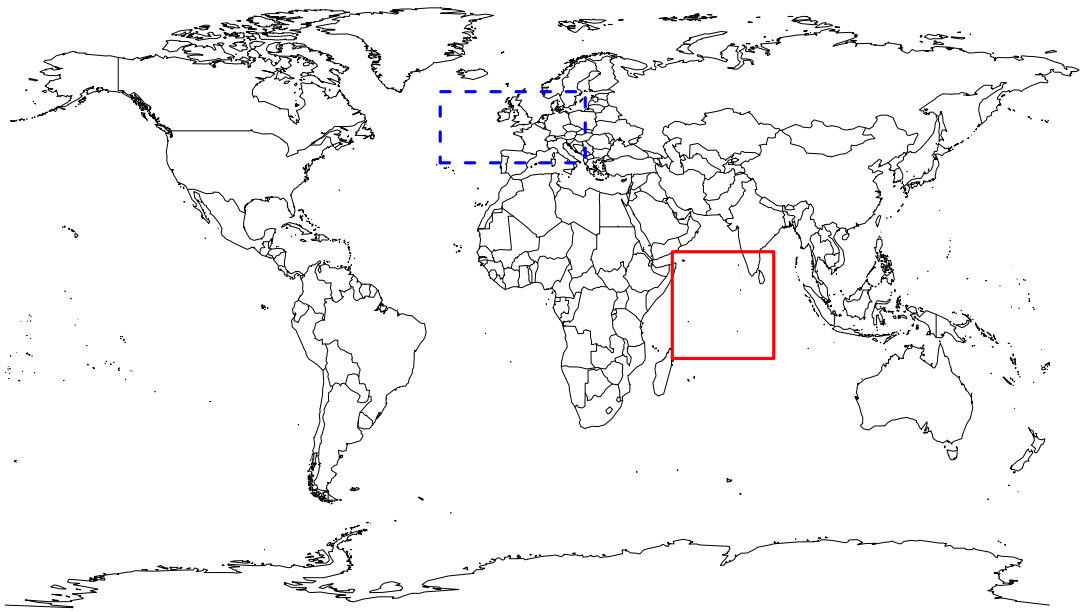

Figure 2.1: Domains of computation of analogs. We computed analogs over different domains. The first domain with coordinates [30°W – 20°E; 40° – 60°N] represented by dash blue rectangle is used to compute analogs to forecast European precipitation (Krouma et al., 2022). The second domain (red rectangle) over the tropics with coordinates [50°E – 85°E; 15°S – 15°N] is used to forecast the Madden-Julian oscillation (Krouma et al., 2023).

SWGs can be divided into four groups as follow: resampling methods as in Yiou (2014); Rajagopalan and Lall (1999), Box-Jenkins methodology (Nihan and Holmesland, 1980), point process models and hierarchical models. The SWGs types depend on the used statistical method. More details about those different groups of SWGs and many others can be found in Maraun and Widmann (2018, chap.13).

2.2.1 SWG procedure

In this thesis, SWG developed by Yiou (2014) has been adapted and adjusted to generate ensembles forecast of precipitation and Madden-Julian oscillation. The SWG has been tested to forecast temperature and North Atlantic oscillation (Yiou and Déandréis, 2019). The SWG consists of generating $S = 100$ members for a given day t_0 based on analogs of the atmospheric circulation. As illustrated in Figure 2.2, for a day t_0, the SWG selects randomly an analog from the K best analogs of $t_0 + 1$. This operation is repeated S time until $t_0 + T$. In this thesis, the random selection of the analog of t_0 is proportional to weights defined in the methodological sections in Krouma et al. (2022, 2023).

2.3 Forecast time range

In my thesis, I provide studies concerning the ensemble forecast of European precipitation and the Madden-Julian oscillation for the sub-seasonal time range. The provided forecast is an averaged-time forecast at a time range T as illustrated in Figure 2.2. During the development

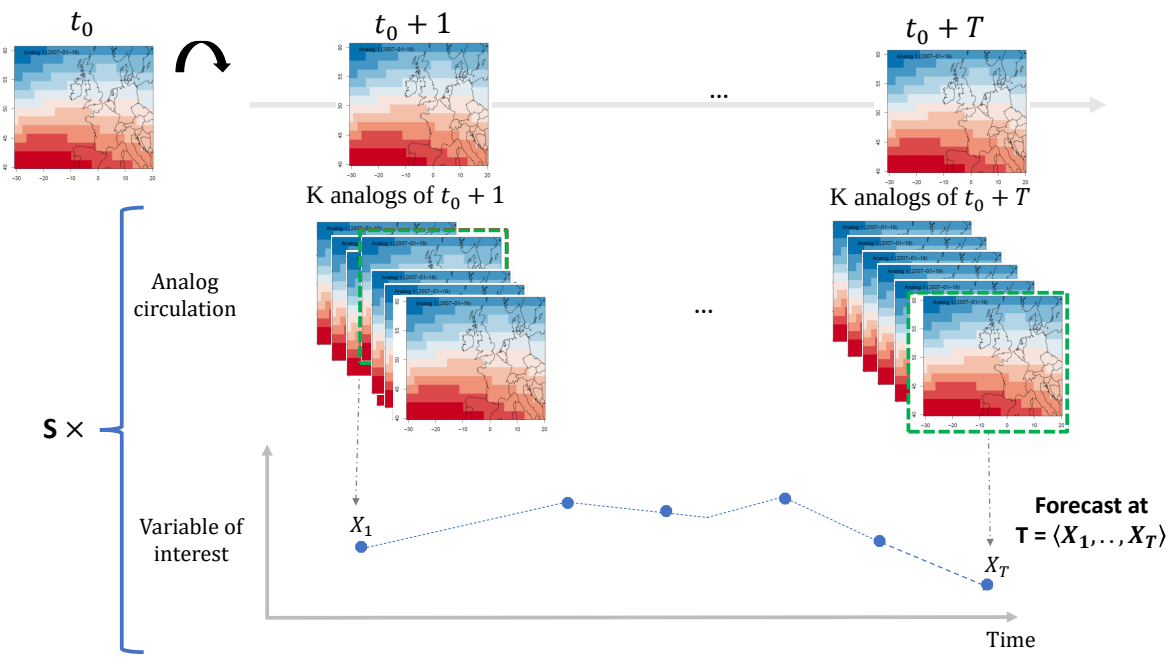

Figure 2.2: Illustration of the SWG process. The input of the SWG is analogs circulation. For one given day t_0, the SWG turns the information gained from the pre-defined K analogs circulation to the associated variable of interest X.

of this thesis, the term "lead time" has been used to design the time range T of the forecast.

Therefore, I would like to outline the definition of "lead time" used in this thesis. In this work, we do an averaging forecast of a meteorological variable X, at a time t_0, between a time $t_0 + \tau$ and $t_0 + \tau + T$. This is explained earlier in the section 2.2.1 and mentioned in (Yiou and Déandréis, 2019; Krouma et al., 2023, 2022). Then we associate the forecast with a range time $T > 0$ that can vary from 1 to 40 days. Therefore, the lead time forecast (or forecast range time) is defined with a fixed τ equal to 0 for an T-averaged-time forecast of X defined as follows:

$$\langle X \rangle_\tau^T = \frac{1}{T} \sum_{t=\tau}^{t=\tau+T} X_t. \tag{2.1}$$

In some textbooks (Vannitsem et al., 2018; van den Dool, 2007), $\tau > 0$ is called the lead time as it refers to a forecast of $\langle X \rangle^T$ for time τ ahead. In my work, τ is fixed to a small value (0 or 5 days), and the averaging time is varied from $T = 5$ to $T = 40$ days, which corresponds to T days ahead of the last day. In this thesis, I will hence investigate the statistical properties of the ensemble forecast of an average of X over T days in advance. This justifies the use of "lead time" for T, which should not be confused with τ.

Chapter 3

Prediction skill of SWG for precipitation in Europe

The core of this chapter is an article published in the journal *Geoscientific Model Development*. The article is preceded by a preamble giving some methodological information on the work carried out. It is then completed by a discussion recalling the main conclusions and highlighting some perspectives.

3.1 Preamble and a methodology summary

In this chapter, we aim to provide an ensemble forecast of precipitation in Europe using statistical and probabilistic approaches. We aim to give a common approach to forecast European precipitation. We assess the skill of a stochastic weather generator (SWG) to forecast precipitation in several cities in western Europe. The SWG was developed by Yiou (2014). It is based on a random sampling of circulation analogs. The SWG can be configured to simulate large ensembles forecasts of climate variables related to the atmospheric circulation (Yiou and Déandréis, 2019). The analogs are computed from the geopotential height at 500 hPa (Z500). The choice of such input was made in order to evaluate the impact of large-scale circulation on local weather variables (Jézéquel et al., 2018b; Xoplaki et al., 2000; Türkes et al., 2002). As a first step, we built a data-set of analogs of circulation. We define an analog as a day with a similar atmospheric circulation configuration as a target day (Krouma et al., 2022). We used the Euclidean distance as a criterion for the selection of analogs. We apply some rules to select an analog: (i) the analogs must be in a different year than the target day and (ii) the calendar distance between the target day and its analogs should be of 30 days. Then, we simulate ensemble forecasts with 100 members on a daily time increment. We optimized the parameters of the SWG in order to get better forecast skill. I give below a summary of the main adjustments:

- We adapted **the geographical area to compute analogs**. We computed sample trajectories of the SWG from different domains in order to find an optimal region that allows verifying the relationship between precipitation and Z500. Each domain includes a part of the Atlantic and a part of western Europe (Jézéquel et al., 2018a). We chose a widest domain with the coordinates 80°W – 20°E and 30°– 70°N in order to catch the variability in the whole Euro-Atlantic region. However, this large domain gave the poorest skill

scores for precipitation forecasting for the studied areas. Then we focused on two smaller domains: one centred over northern Europe and the other centred over southern Europe. We found better forecast skills for specific locations. The same level of performance was found for the domain with coordinates 30°W – 20°E and 40° – 60°N. Therefore, we kept this domain for the subsequent analyses, because it helps to optimize at the same time the correlations between Z500 and precipitation for the four studied areas and the time of computation of analogs.

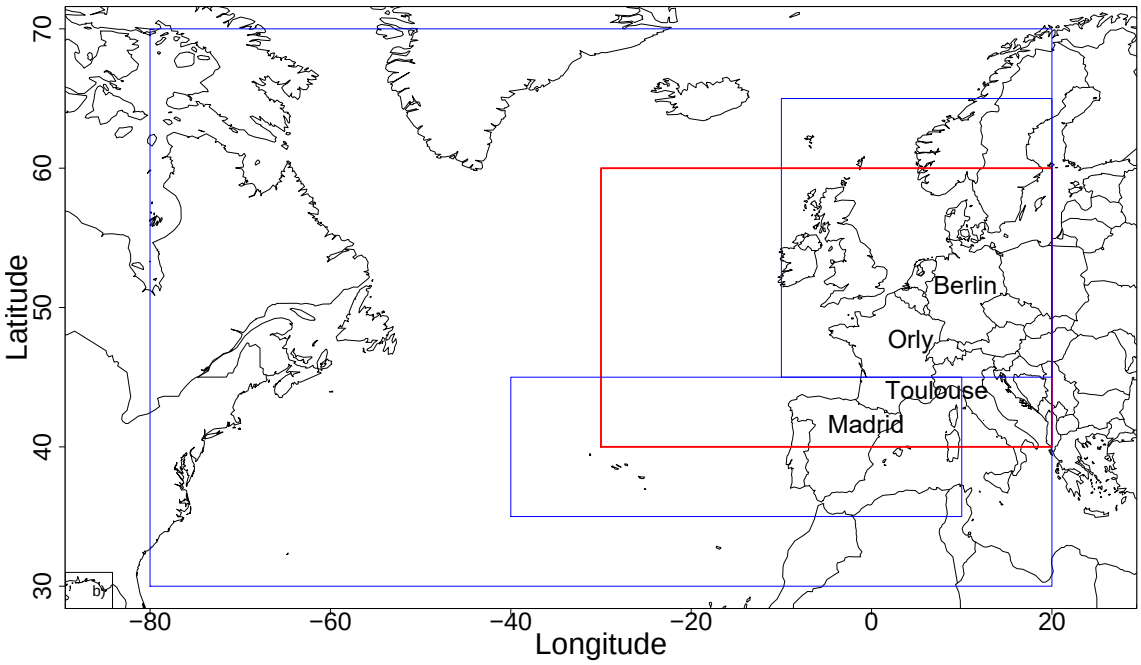

Figure 3.1: Domains of computation of analogs. We computed analogs over different domains, each one including a part of the Atlantic and focusing on a part of Western Europe, in order to test the sensitivity of our model to different geographic areas. The optimizing area was [30°W-20°E; 40°-60°N], indicated by the red rectangle.

- **The number of best analogs** that we use to simulate the precipitation. Our choice was based on numerical experiments and previous works. We performed different SWG simulations where we varied the number of best analogs from 5 to 20. We notice an improvement in the skill scores by increasing the number of analogs. Therefore, we considered 20 best analogs to ensure that we have enough analog dates for the simulations. It appears that the Euclidean distance of analogs grows rather slowly after a certain threshold. Our choice was also comforted by a theoretical study by Platzer et al. (2021b) who showed that, for complex systems, the use of a large number of analogs ($K > 30$ analogs) does not change the prediction properties (More details are available on Table 2 in Krouma et al. (2022)).
- We quantify the dependence of the forecast on **large analog** [1]. We define "large analog" as an analog computed taking into consideration the Z500 patterns during days from 1 to 4 days. We find that a large analog of 4 days helped to better catch the persistence

[1]We referred to "large analog" as analogs computed with an embedding of x consecutive days in (Krouma et al., 2022). The nomination has been modified after a discussion with some colleagues from Météo France

and improve the skill scores for the forecast compared to 1 day (see Table 3 in Krouma et al. (2022)). Therefore we kept the forecast based on a 4-day analog. This choice was based on the numerical experiments performed for the studied locations. Our choice is also supported by the study of Yiou et al. (2013), where large analog computation with time embedding was argued to improve the temporal smoothness of simulations.

- We explored the sensitivity of our approach to different **reanalyses and observations sources**. We computed analogs from reanalyses of NCEP (Kistler et al., 2001) and ERA5 (Hersbach et al., 2020). By comparing their skill scores, we found that SWG simulations based on NCEP and ERA5 have the same skill score values. The computations were made using observations of precipitation from the ECAD (Klein Tank et al., 2002) and E-Obs (Haylock et al., 2008) databases. We found the same results because the ECAD and E-Obs are highly correlated (by the construction of E-Obs).

We evaluate the performance of SWG by comparing it to the persistence and climatological forecasts (Jolliffe and Stephenson, 2011). To measure the forecast skill of the SWG we used skill scores such as the continuous ranked probability scores (CRPS) and its normalization the CRPSS (Zamo and Naveau, 2018; Hersbach, 2000). Finally, we compare the SWG forecast to ECMWF precipitation forecasts (Vitart, 2017a) to evaluate the performance of the SWG forecast to other forecasts. We compared the cumulative distribution function of the two forecasts as well as the properties of each forecast.

This forecast of European precipitation with the SWG based on analogs of Z500 is a proof of concept for a stochastic regional ensemble precipitation forecast.

3.2 Article published in *Geoscientific Model Development*: Assessment of stochastic weather forecast of precipitation near European cities, based on analogs of circulation

This paper is included in the Appendix A (Krouma et al., 2022).

3.3 Conclusions and perspectives

We explored the performance of the stochastic weather generator to simulate precipitation averages over different locations in western Europe at a local scale and for lead times of 5 to 20 days. In this work, we confirmed the importance of atmospheric circulation to forecast precipitation averages as explained in previous work (Xoplaki et al., 2000; Molteni et al., 2015; Jézéquel et al., 2018b). The forecast skill of the SWG was confirmed by positive CRPSS with a respect to climatology and persistence at the four studied areas. However, the SWG forecast tends to be sensitive to seasons. High values of CRPSS with a respect to climatology and persistence were mostly associated with winter for lead times of 5 and 10 days. The rank correlation between observations of precipitation and the SWG simulations is high for a lead time of 5 and 10 days. However, the CRPSS does not show any improvement in summer at a lead time of 20 days as in the case of Orly (Paris) forecast. The SWG showed a capacity to forecast precipitation better than climatology for small lead times (5 days). The SWG forecast

showed a sensitivity to the geographical regions. Indeed, the skill scores are higher for southern Europe, e.g. for Madrid.

We also investigated the role of North Atlantic weather patterns on the forecast quality. We evaluated the relationship between the forecast skill of the SWG forecast (using the CRPS) and the European weather regimes. Due to the seasonality of the large-scale atmospheric circulation, the weather regimes vary with seasons (Yiou et al., 2008). Hence, we evaluated the dependence of the forecast skill to weather regimes for winter and summer. We found that low predictability (defined when the values of CRPS are below the 75th quantile) and high predictability (values of CRPS that exceed the 25th quantile) were related to specific weather regimes. This is in agreement with other studies (Faranda et al., 2017b). For instance, the high forecast skill is obtained with Blocking weather regime in both winter and summer for Orly. In general, the dependence on weather regimes is more significant in winter than in summer. We mainly found that good predictability of European precipitation is related to Blocking.

The comparison with the ECMWF forecast system over Western Europe confirmed quantitatively and qualitatively the forecast skill of the SWG. We evaluated the added value of the ECMWF forecast over the SWG forecast using the CRPSS. We found that the ECMWF forecast has no improvement over the SWG forecast for the different lead times. The improvement of the SWG is more important for a lead time of 20 days, particularly for Berlin. This confirms the relatively good skill of the SWG to forecast precipitation, compared to ECMWF. This could be explained by the difference in the average of the CRPS of the two forecasts (Krouma et al., 2022). Although, we notice that the ECMWF forecast yields good skill scores (CRPS equal to 0) for small values of precipitations.

This work shows promising forecast skills of the SWG for local precipitation from large-scale information. The performance of the SWG relies on the relation between precipitation and the synoptic atmospheric circulation, which is verified for western Europe. The work developed in this chapter leads to several perspectives. I will provide more details to some of them.

Adapting SWG parameters for other regions

In the paper (Krouma et al., 2022), we suggest to transpose the SWG forecast to other regions of the globe and for an operational use. This requires observations covering several decades. Numerical weather models obviously do not yield this constraint. The SWG forecast showed a capacity to forecast European precipitation (Krouma et al., 2022) and temperature (Yiou and Déandréis, 2019). However, the SWG model cannot replace a numerical weather prediction, as the SWG parameters (e.g. region of analogs) need to be tuned to local variables, and rely on the existence of a fairly large database to compute analogs.

In this work, we used the same domain of circulation analogs for stations from Madrid to Berlin. Obviously, this region should be optimized for each individual station. Therefore, the main utility of the SWG forecast system is to make local ensemble simulations, where its performances can challenge a numerical weather prediction if the parameters are well-tuned. To deal with this issue, other sources of predictability can be used to compute the analogs.

SWG and climate change

The SWG is based on atmospheric circulation. However, climate change effects on temperature and large-scale circulation have been identified and they are likely to intensify in the future (IPCC, 2021). Figure 3.2 shows the observed and projected upper air temperature and circulation changes (Arias et al., 2021). We can see the increase of the temperature at the different pressure levels either from the observations or the projections with a high model agreement at 250 hPa, particularly for the mid-latitude (Arias et al., 2021). Our SWG forecasting tool is based on Z500 which is affected by climate change for different scenarios as shown in Figure 3.2. The forecast of precipitation or temperature would be affected. In our case, we did not notice a clear change in the analogs distribution. It means that the computed analogs (dates) are uniformly distributed between past and future dates. However, possible measures can be taken to mitigate the impact of climate change on SWG weather forecast either considering the changes in Z500 or precipitation.

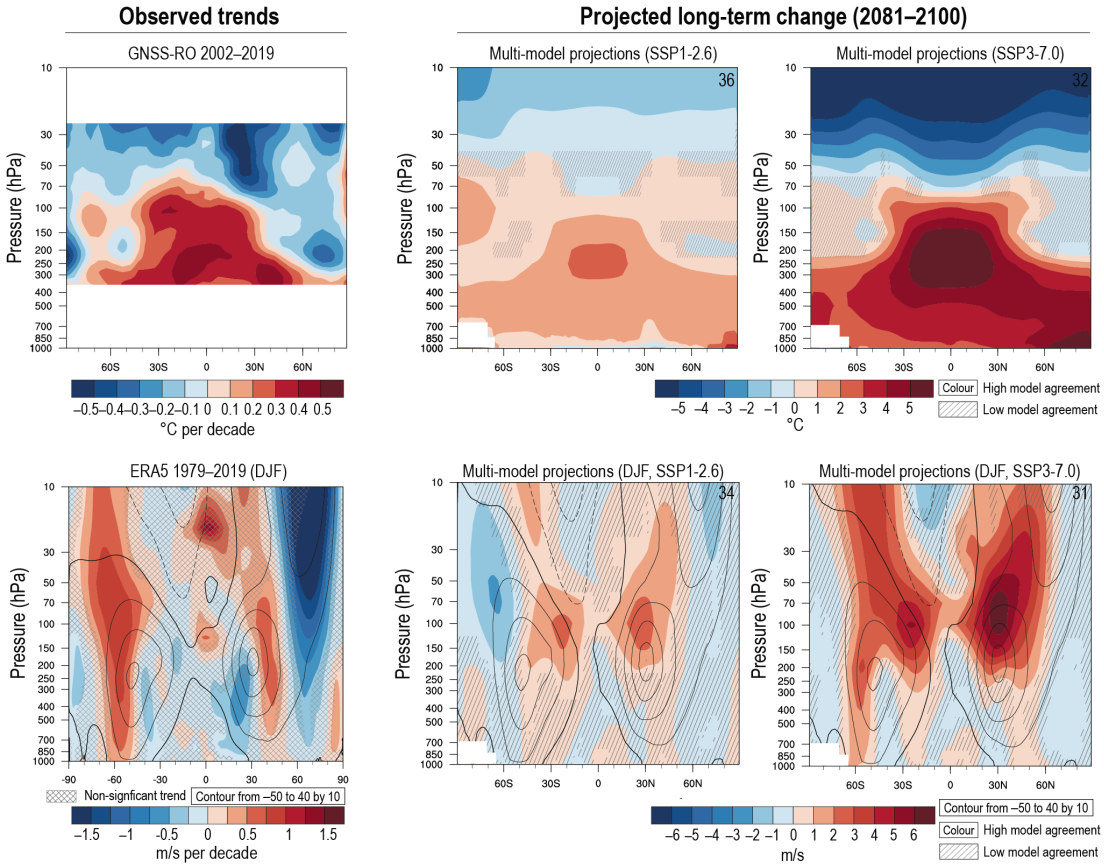

Figure 3.2: Observed and projected upper air temperature and circulation changes. The similarity between observed (2002 - 2019) and projected changes (2081 - 2100) on the upper air temperature and circulation changes. Figure from the IPCC Technical Summary (Arias et al., 2021)

Maraun and Widmann (2018) propose to use "Change-factor" weather generators. They suggest to induce a factor representing the changes in the atmospheric circulation. The approach, as explained by Bartholy et al. (1995), consists of calibrating the weather generator to climate model simulations of present and future climate in addition to calibrating it to observations. The "observed" weather generator parameters are then modified by the change in the simulated

parameters by an additive term. However, only simulated changes between present and future long-term climatological properties could be used to modify the weather generator parameters. The change-factor weather generators are unconditional weather generators that are not synchronised with a climate model. This would be a solution to adapt SWG and analogs, a "low-cost solution" for weather forecast (Ailliot et al., 2015), to climate change.

Résumé

Contexte et objectifs

La précipitation constitue une variable météorologique d'intêret. Elle joue un rôle crucial dans toutes les activités de vie. Elle constitue une composante fondamentale de cycle de l'eau. La prévision des précipitations est une étape essentielle pour appréhender l'état des réserves en eau et mieux les gérer. Dans ce chapitre, nous présentons une méthode statistique de prévision des précipitations. Notre objectif pricipal est d'évaluer la capacité d'une méthode statistique composée d'un générateur stochastique de temps et des analogues de la circulation atmospherique à prévoir la précipitation en Europe.

Méthodes

Nous avons évalué la compétence d'un générateur stochastique de temps (SWG) pour prévoir les précipitations dans plusieurs villes européennes. Le générateur stochastique de temps a été développé par Yiou (2014). Il est basé sur un échantillonnage aléatoire d'analogues de la circulation atmosphérique. Les analogues sont calculés à partir du géopotentiel à une hauteur de 500 hPa (Z500). Le choix du géopotentiel permet d'évaluer la relation entre la circulation à grande échelle et les variables météorologiques locales comme les précipitations et les températures (Lorenz, 1969). Dans un premier temps, nous avons constitué un ensemble de données d'analogues. Nous considérons un analogue pour un jour donné t, un jour avec une circulation atmosphérique similaire à t. Nous utilisons la distance euclidienne comme critère de sélection des analogues. Nous appliquons quelques règles pour sélectionner un analogue : (i) les analogues doivent appartenir à une année différente de celle du jour t et (ii) ayant une distance calendaire de 30 jours par rapport au jour t. Ensuite, nous générons des trajectoires aléatoires avec le générateur de temps. Un ensemble de 100 membres de prévisions des précipitations à differents pas de temps allant de 5 à 20 jours est créé. Dans cette étude, nous avons optimisé les paramètres du générateur stochastique de temps afin d'obtenir une meilleure qualité de prévision. Les évaluations de l'ensemble de prévision ont été faites par des scores probabilistes (CRPS, CRPSS, corrélation de rang), qui permettent d'évaluer notre prévision par rapport à d'autres prévisisons.

Résultats

Les valeurs positives de CRPSS qui ont été obtenues vis à vis de la climatologie et de la persistance démontrent la capacité du SWG a prédire les précipitations aux échelles de temps étudiées. Cependant, les prévisions du SWG ont tendance à être sensibles aux saisons. En effet, des CRPSS élevés vis-à-vis de la climatologie et de la persistance ont été constatés particulièrement en hiver pour des délais de 5 et 10 jours. La corrélation de rang entre les observations de précipitations et les simulations SWG est élevée pour un horizon de 5 à 10 jours.

Chapter 4

Improving the ensemble forecast of the European precipitation

The objective of this chapter is to propose a statistical approach to improve the European precipitation forecast for the sub-seasonal period (from 2 to 4 weeks). In this chapter, I describe two different methods that have been employed to enhance the ensemble weather forecast of European precipitation. The chapter is composed of two sections: the first one gives details on the combination of a stochastic weather generator (SWG) and dynamical models to enhance the skill forecast. This section is presented in the format of an article submitted to the *Quarterly Journal of the Royal Meteorological Society*. The second section contains another study where we combine analogs of several physical predictors. The two sections are followed by a discussion explaining the interest of each approach, the differences between them and the main conclusions and perspectives.

4.1 Combining a stochastic weather generator with dynamical models (paper submitted to *Quarterly Journal of the Royal Meteorological Society)*

4.1.1 Combining statistical and dynamical models

What is a dynamical model?

Numerical Weather Prediction (NWP) models have been developed to solve the complex set of the laws of physics and fluid mechanics of the atmosphere. NWP models solve equations of the evolution of the atmosphere such as the equation of motion, the equation of conservation of total mass, the equation of state of perfect gases and the equation of thermodynamics (Lynch, 2006). NWP models provide approximate solutions to the complex differential equations of the atmosphere.

NWP models describe the essential physical processes in the atmosphere, at the surface and in the soil. They also include the interaction between the different processes and their impact on the temporal evolution of variables such as pressure, temperature, or wind. The NWP models can be coupled with ocean processes (leading to so-called dynamical models). Atmosphere-Ocean

Coupled Models help to capture at the same time atmospheric initial conditions and changes in the ocean conditions, which both impact weather forecast depending on the time scale.

NWP are all based on the same physical laws. However, they differ in the concrete mathematical formulation and in the numerical solution procedures of the set of equations (Rodwell and Palmer, 2007). For instance, including some physical processes in the atmosphere or at the surface such as the formation of clouds or the interaction between solar radiation and cloud droplets that occur on very small spatial scales, cannot be resolved explicitly by the NWP models. The impact of these unresolved processes on the model variables can be included approximately via parameterisation schemes (Robertson and Vitart, 2019).

NWP calculate the evolution of a number of physical parameters within a portion of the atmosphere over successive time frames taking into account the state of the atmospheric fluid at each instant. Initial conditions are fundamental for NWP models as they represent the initial point from where a prediction scenario will emerge. Initial conditions should be carefully chosen. Because, otherwise, the whole prediction scenario will be illusory. To build a NWP model, two steps should be fulfilled that I will describe briefly. The first step, called data assimilation, consists of collecting all the observation data conform to calculation standards' center (Bauer et al., 2011). The second step consists on solving the equations based on the initial states defined before and modelling at successive times the parameters evolving in each portion of the atmosphere (Zhao et al., 2016). At the end of these two steps, a run is created. Since meteorological observations are continuous and constantly changing, it is necessary to run the NWP models several times a day in order to have scenarios that are as close as possible to reality.

NWP models help to predict weather behaviour from different time scales going from hours to days, weeks and seasons. They also provide prediction and trajectory of severe events, such as tropical cyclones, rainfall and flooding, ocean waves, storm surges and tsunamis.

Combining statistical and numerical approaches

Combining statistical and NWP models have been the subject of many studies (Specq and Batté, 2020b; Schepen et al., 2012; Dayon et al., 2015) and in different locations on the globe. The combination of dynamic and statistical modelling often improves forecast skills at relevant spatial scales. Schepen et al. (2012) claimed that merging statistical and dynamic forecasts maximises the spatial and temporal skill of the seasonal precipitation forecast in Australia. Indeed, despite the fact that NWP models reproduce most of the relevant atmospheric processes and include ocean information, which represents a main driver of the climate system (Shukla, 1998) and a main source of predictability for temperature and precipitation (Shukla et al., 2006; Goddard et al., 2001), the NWP forecast skill is still insufficient for some weather variables such as precipitation, particularly for sub-seasonal lead times. This is because the design of NWP models tends to homogenize and simplify surface conditions (Karl et al., 1990). Moreover, small-scale effects such as topography or orography are not well taken into consideration by NWP models and this is important for local weather (Wilks and Wilby, 1999).

There are different ways to achieve improvements using dynamical and statistical models combination, such as increasing the spatio-temporal resolution of forecasting systems, correcting/adjusting the systematic errors (or biases) of such a system through downscaling or building a statistical model linking a variable to predict and its predictors.

In this chapter, I will mostly use the last approach which consists in using a statistical model to link large-scale information to the meteorological variables (precipitation).

4.1.2 Summary of the paper

In this work, we explain how we improved the European precipitation forecast for sub-seasonal lead time at a local scale combining dynamical model forecasts and the SWG approach described in the previous chapter. In chapter 2, we explored the forecast skill of the SWG to forecast European precipitation. We showed that the SWG forecast skill of precipitation based on analogs of Z500 was satisfying within 10 days (Krouma et al., 2022). Therefore, we kept the Z500 as a predictor of European precipitation. Instead of using reanalysis as in (Krouma et al., 2022), in this work we aim to use the **reforecast** of Z500 from S2S models (Vitart et al., 2017). Dynamical models have good forecast skills for upper-level fields for up to 1 month (Robertson and Vitart, 2019). As shown in the figure 4.1 below, the skill score of Z500 from the ECMWF has been improving over the years and for different lead times. The improvement until a lead time of $T + 168$ h, has been related to the enhancement of the NWP models and the use of the ensemble forecast techniques as explained by Robertson and Vitart (2019, Chap2).

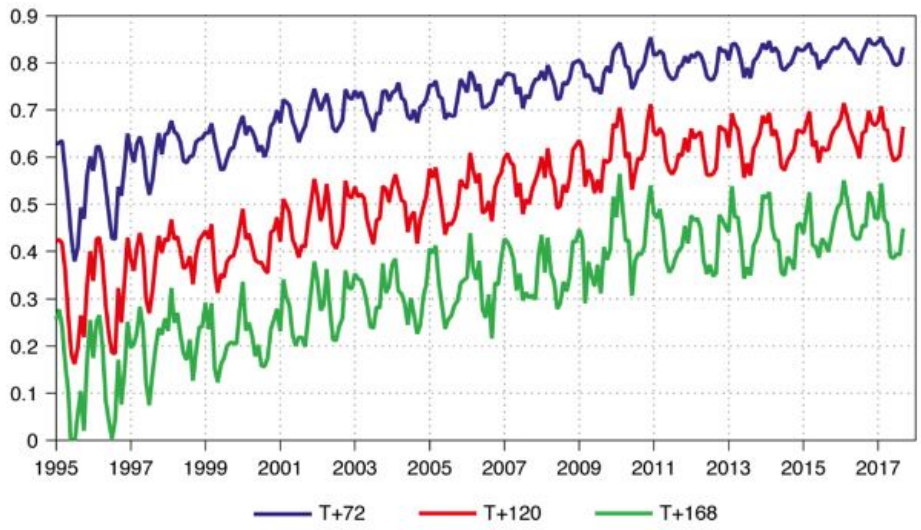

Figure 4.1: Improvement of the continuous rank probability skill score (CRPSS) of ECMWF probabilistic predictions of the 500 hPa geopotential height over the Northern Hemisphere. Each coloured line represents a lead time, blue for 3 days (72 h) lead time, red line for 5 days (120 h) and green line for 7 days (168 h). The CRPSS is obtained in comparison with climatologically based probabilistic information. Figure taken from Robertson and Vitart (2019).

In this study, we aim to take advantage of the high quality of the reforecast (or Hindcast (HC)) [1] of Z500 from S2S models to forecast European precipitation. We adapt the parameters of the SWG to optimize the simulation of European precipitation from ensembles dynamical reforecast of ECMWF and CNRM. The analogs of Z500 are computed from the ensemble member reforecast of ECMWF and CNRM. The ECMWF ensemble reforecast is composed of 11 members computed with the CY47R2 model with an horizontal resolution that varies from 15 to 31

[1] In this work, Hindcast and reforecast have the same definition.

km (Vitart, 2017a). The ECMWF reforecast is provided twice a week (Vitart, 2017a). The CNRM ensemble reforecast is composed of 10 members (Ardilouze et al., 2021). Data from the CNRM model is available on a weekly basis with an horizontal resolution of 50km (Ardilouze et al., 2021; Batté and Déqué, 2016) Both models are part of sub-seasonal to seasonal (S2S) project (Robertson and Vitart, 2019). They are coupled models and provide data with different initialization.

First, we assessed the quality of the reforecasts ensembles of ECMWF and CNRM for 5 days ahead. The aim is to verify the spread of the ensemble and to check whether we should use the whole ensemble to compute analogs. We computed the Euclidean distance between the members of each ensemble and we compared it to the average distance between analogs. We found that the distance between the members of the ensemble is smaller than the average distance between analogs. Hence, we computed analogs from the ensemble mean of the reforecast for either ECMWF and CNRM on the 5th day. We then generate an ensemble of 100 members for precipitation over Europe using the SWG. In this study, the new version of the SWG is called HC-SWG (HindCast SWG).

We evaluate the skill of the ensemble forecast using the CRPS (Hersbach, 2000; Ferro, 2007), the decomposition of the CRPS (Zamo and Naveau, 2018), the rank correlation and ROC curve (Fawcett, 2006). The fair CRPS was used to compare the forecast skill of the HC-SWG to ECMWF forecast of precipitation as the two ensemble forecasts have different sizes. The fair CRPS takes into consideration the differences in ensemble size between the forecasts and the reference forecasts via an unbiased estimator for the score that would be obtained as the ensemble size increases to infinity (Ferro, 2014). The decomposition of the CRPS was used to explain further the difference between the improvement of the HC-SWG in each studied area. The ROC curve helps to evaluate the discrimination skill of the HC-SWG. The discrimination skill defines the capacity of the model to distinguish between events and non-events (Krouma et al., 2023; Specq et al., 2022). Skill scores were performed for the whole Europe to evaluate the predictability of the HC-SWG.

Reasonable forecast skill scores (CRPSS $\in [0.4, 0.7]$ and AUC > 0.5) were obtained for lead times up to 35 days for different locations in Europe. This has been obtained with positive CRPSS with respect to climatology and persistence as well as a positive correlation between simulated and observed values of precipitation for the different lead times. We compared our HC-SWG forecast with other precipitation forecasts such as the forecast of ECMWF to further confirm the benefit of our method, and we compared the difference between the performance of the forecast using the two different reforecasts.

4.1.3 Article submitted to *Quarterly Journal of the Royal Meteorological Society*: Improving the ensemble forecast of precipitation in Europe by combining a stochastic weather generator with dynamical models

The manuscript of this paper is included in Appendix B.

4.1.4 Extra analyses

We did some extra analyses to improve the HC-SWG forecasts that are not shown in our paper. I will explain them in this part. We applied some other rules to define analogs based on previous conclusions (Krouma et al., 2022). In section 3.1, I explained the importance of using large analogs to compute analogs, which helps to increase the forecast skill. And in section 3.3, I explained the dependence of the forecast quality in European weather regimes. I assessed the added value of using a large analog as well as analogs from the same weather regime in the HC-SWG precipitation forecast.

We considered a large analogs searching for analogs of Z500 from reforecast of ECMWF and CNRM. We found that the HC-SWG forecast, using large analog, shows a positive CRPSS against the climatology and the persistence as illustrated in Figure 4.2. But the improvement is the same with or without using the large analog. Hence, in our case, the use of dynamical model can be enough in order to reduce computational costs.

In addition, we added another step to the HC-SWG that consists of selecting analogs that are in the same weather regime as the target day. The motivation behind using this step is to avoid climatology effect for long lead times. Therefore, the number of K best analogs varies from one day to another. However, as shown in figure 4.2, the HC-SWG forecast does not show any improvement against climatology or persistence over 10 days. That can be explained by the decrease in the number of analogs which plays a role in the forecast skill as shown in (Krouma et al., 2022). It can also be related to the fact that we have just four European weather regimes either in summer or winter, which does not take into consideration the transition from one regime to another.

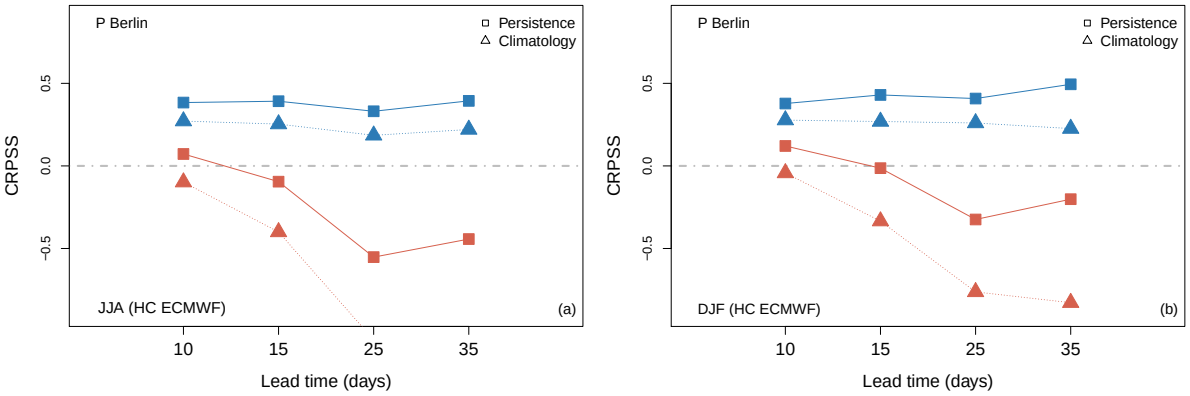

Figure 4.2: CRPSS of the HC-SWG forecast over the climatology and persistence forecasts of precipitation in Berlin for lead times $T \in [5, 10, 20, 30]$ days for JJA (a) and DJF (b) using Large analogs (blue) and analogs from the same weather regime (red). The grey dashed line indicates a $CRPSS = 0$, which means no improvement against climatology and persistence forecasts.

4.2 Improving the ensemble forecast of precipitation in Europe by multi-analog

4.2.1 Objective and Methodology

In this work, I propose another approach that I used to improve the forecast skill of the stochastic weather generator for the precipitation at sub-seasonal lead time. I aim to use multi-analogs of atmospheric circulation.

Forecasting European precipitation from analogs of Z500, although satisfactory, shows a weak forecast skill for lead times of 20 days (Krouma et al., 2022), as explained in Chapter 2. Hence, including other atmospheric predictors related to precipitation would help to exceed these limits. To apply this in our forecasting approach, we need to compute analogs from different predictors (atmospheric fields), containing additional information that can benefit precipitation forecast. However, computing analogs from several parameters can be challenging because (i) of the use of several atmospheric fields that are physically different and have different units. This applies that we need to be aware when weighting each predictor in order to properly include information from each field. (ii) We have to deal with big data, which could increase computational time and cost. In this section, I propose a method that takes into consideration those challenging points and helps to improve the European precipitation forecast at the sub-seasonal lead time.

Multi-analogs were defined as analogs computed from different atmospheric fields. To compute multi-analogs, I used Empirical Orthogonal Function (EOFs) from the reanalyses of the geopotential heights at 500 hPa (Z500) and at 1000 hPa (Z1000), as well as the relative humidity (HR). The choice of those different atmospheric fields is based on the interaction between large-scale parameters and local weather variables, in our case precipitation, as mentioned in other studies (Horton, 2019; Jézéquel et al., 2018b). For instance, in our previous work (Krouma et al., 2022), we found that the precipitation is predictable from the geopotential height at 500 hPa. Therefore, we start by defining analogs from EOFs of Z500.

I considered the daily average of Z500, Z1000 and HR from 1948 to 2020, over the geographic region with coordinates [30W – 20E; 40 – 60N]. The choice of the data length and geographical region is based on our previous work (Krouma et al., 2022). Z500, Z1000 and HR data have the same resolution 2.5×2.5. Daily data are available from NCEP (Kistler et al., 2001).

The three used atmospheric fields have different units (m for geopotential height and % for HR), before computing the EOFs, I normalised each field by dividing the anomalies with the standard deviation of the other field. The EOFs were calculated separately from the anomalies of each field using a spatial weight (this takes into consideration the variation in the latitude). We kept s principal components that contain 90% of the variance ($s = 6$ for Z1000 and Z500, and $s = 10$ for HR).

Therefore, we have a daily database from 1948 to 2020 composed of the s principal components EOFs of the selected variables. Analogs were computed from the constructed database using the Euclidean distance as expressed in the following equation 4.1, with a calendar window of 30 days between each day and its analogs.

$$D(t, t') = \left[|EOF(t) - EOF(t')|^2 \right]^{\frac{1}{2}} . \tag{4.1}$$

To compute analogs, I tested several combinations between the different atmospheric variables mentioned above. The two retained successful combinations are the multi-analogs of Z500 and Z1000 and the multi-analogs of Z500 and HR. These two combinations have been qualified as successful as the forecast skill was higher (more explanations in the results in section 4.2.2). This can be explained by the fact that using Z500 and Z1000 help to catch most of the atmospheric motions that occur between the upper and lower layers of the atmosphere. Combining Z500 and HR would help to improve the forecast of the precipitation, as from one side, increasing the HR raises the chances of having precipitation and on the other side Z500 brings information about the high and low pressures. The maximum distance found for analogs of Z500 is of 600 m and for the analogs of Z500 and Z1000 is around 1000 m.

Then, we generated members of precipitation using the SWG based on the analogs computed. The SWG proceeds following the same procedure described previously in Chapter 2 and in (Yiou and Déandréis, 2019; Krouma et al., 2022). Mainly, for each given day t_0 in year y_0, we generate a set of $N = 100$ simulations until a time $t_0 + T$, with T is the lead time going from 5 to 30 days.

We evaluated the SWG forecast using the CRPSS over the climatology and the persistence. The computations of the CRPS were made using observations of precipitation from ECA&D databases (Klein Tank et al., 2002). In addition, we compared the forecast skill of the SWG with the S2S ECMWF precipitation forecast using the CRPSS. For this, we considered the ECMWF precipitation forecast as a reference to the CRPSS.

4.2.2 Results of the simulations

We evaluate the SWG forecast of precipitation using multi-analogs. The assessment of the forecast skill of the SWG forecast was made in different areas in Western Europe (Orly, Berlin, Toulouse, Madrid). As a skill score, we used the CRPSS that was computed for winter (DJF) and summer (JJA). We consider these two seasons for verification purposes.

We found that the CRPSS shows a positive improvement until 30 days for the different studied locations for both seasons (winter and summer) from simulations of different multi-analogs. Figure 4.3 illustrates skill scores for Berlin. We found that the CRPSS against persistence is higher and stable in both seasons. The CRPSS against climatology shows a positive improvement with higher values in winter and for small lead times.

The use of analogs computed from EOFs of Z500 and from separate multi-analogs of (Z500, Z1000) and (Z500, HR) leads practically to the same skill scores with slightly higher CRPSS with respect to climatology and persistence for the different lead times $T = 5$ to 30 days using multi-analogs of Z500 and HR in summer as shown in figure 4.3 for Berlin. That can be explained by the fact that in summer different synoptic situations where the humidity and pressure can lead to precipitation. Depending on the locations, precipitation can be induced by (i) convection that could result from the enhancement in air humidity, (ii) advection, from the Mediterranean to southern Europe or from the Atlantic to the north/east coasts, that can cause instability or increase humidity, (iii) and cooler breeze near mountain regions All these situations could lead to precipitation.

In winter, we notice that the forecast with the multi-analogs of Z500 and Z1000 has positive improvement than climatology and persistence for lead times of 5 and 10 days. But after 20

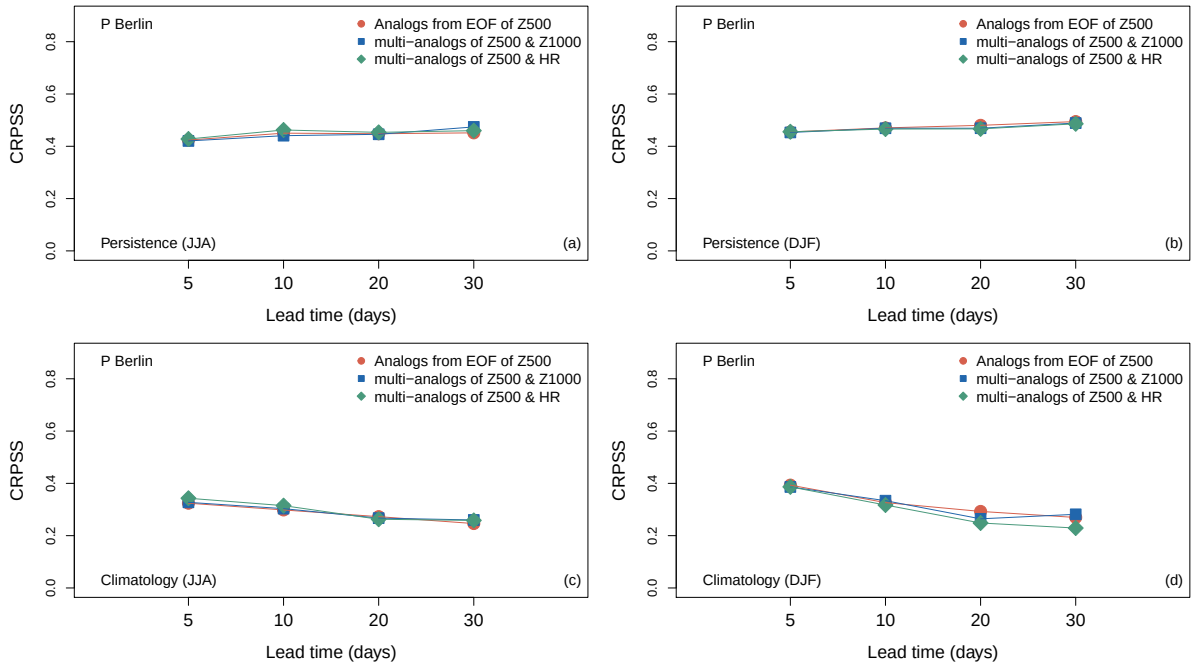

Figure 4.3: CRPSS of the SWG forecast over the climatology (c – d) and persistence (a – b) forecasts of precipitation in Berlin for lead times $T \in [5, 10, 20, 30]$ days for summer (JJA) a - c and winter (DJF) b - d using analogs from EOFs of Z500 (red cercle) and multi-analogs of Z500 and Z1000 (blue triangle) and Z500 and humidity relative (green diamond).

days, the forecast using analogs computed from the EOFs of Z500 has slightly higher CRPSS with respect to climatology. The same conclusion is observed for the other studied areas, where the combination of HR and Z500 seems to work better in summer and the use of multi-analogs of Z500 and Z1000 gives better skill for winter. Considering a thick layer of the atmosphere (from 1000 hPa to 500 hPa), particularly in the case of strong low pressure, would include additional information about the surface circulations (Jones et al., 2014; Fealy and Mills, 2018) that play an important role in synoptic weather and in driving precipitation in Europe. However, as the forecast skill of the multi-analogs shows similar improvements as the EOFs of Z500 and for computation efficiency, we can use only analogs from EOFs of Z500 for western Europe or depending on the areas of the study and the season we can choose the best combination to use.

We compared the SWG forecast using the multi-analogs approach to the ECMWF precipitation forecast. I present the results of this comparison for precipitation forecast in Berlin using the EOFs of Z500 just for simplification as the magnitude of the improvement using the two other multi-analogs led to similar results. The comparison with the ECMWF precipitation forecast showed a positive improvement of the SWG over the ECMWF as shown in table 4.1. We can notice that the improvement of the SWG is positive over the ECMWF forecast at the different lead times. The CRPSS is still showing improvement, despite the small CRPSS for Orly and the negative values for Toulouse at 30 days.

Comparing these forecasts with the SWG forecast in Krouma et al. (2022), we notice that the SWG (Krouma et al., 2022) shows higher score skills within 5 – 10 days (CRPSS $\in [0.6, 0.5]$ with respect to climatology or persistence), while the SWG based on multi-analogs shows significant improvement within a lead time of 20 – 30 days. Thus, the choice of SWG (Krouma et al., 2022)

or SWG based on multi-analogs forecasts would depend on the end-use goal.

Table 4.1: CRPSS of the SWG forecast of precipitation using multi-analogs of Z500 taking as a reference the ECMWF precipitation forecast.

Lead time	$T = 5$ **days**	$T = 10$ **days**	$T = 20$ **days**	$T = 30$ **days**
CRPSS Orly	0.17	0.1	0.1	0.1
CRPSS Toulouse	0.20	0.15	0.12	-0.1
CRPSS Madrid	0.22	0.15	0.13	0.15
CRPSS Berlin	0.15	0.12	0.12	0.2

4.3 Conclusions & perspectives

In this chapter, we applied two different approaches to improve the forecast skill of European precipitation within the sub-seasonal lead time. The first approach is based on the **HC-SWG** which is a benchmark of the SWG with analogs computed from the **Hindcast (HC)** [2] of S2S dynamical models. The second technique consists on the use of **Multi-Analogs**. The two approaches are technically different but they both contributed to provide a better forecast skill of precipitation over Europe within 30 days.

The use of the ensemble mean reforecasts of the geopotential at 500 hPa, 5 days ahead from ECMWF and CNRM models improved the forecast of European precipitation. The HC-SWG showed a capacity to forecast precipitation with a meaningful skill for up to 35 days in Europe and at the station level. The forecast skill varies from one region to another. It remains higher for the south for either summer or winter. This can be explained by the fact that precipitation is lower in the south than in the north, and in summer than in winter. This can be considered a drawback of our method. The HC-SWG kept its capacity to forecast the precipitation at a local scale (Krouma et al., 2022), with positive CRPSS over climatology and persistence for all the lead times (from 10 to 35 days) and in different regions despite the variety of local weather. The discrimination skill of the HC-SWG was also confirmed. The HC-SWG showed its capacity to distinguish between events and non-events of precipitation as well as extreme precipitation for a lead time of 10 days. In addition, the comparison with the ECMWF precipitation forecast supports the performance of the HC-SWG forecasts until 35 days. Combining dynamical models with the SWG allows an improvement of the forecast of precipitation at the sub-seasonal lead time. This work highlights the contribution of dynamical models and the importance of using a correct initialisation (Zuo et al., 2016) to get a skilful forecast.

The use of multi-analogs has improved precipitation forecasting over Europe. Forecast scores such as CRPSS show a positive improvement up to 30 days compared to climatology and persistence. The comparison with the ECMWF confirmed this skill. The use of multi-analogs helps to improve the forecast of European precipitation to the sub-seasonal time compared to the use of one atmospheric variable the Z500. However, the different atmospheric fields that we used and the different combinations between them to define multi-analogs led to the same skill scores. Hence, the EOFs of Z500 are sufficient to forecast European precipitation. The added value of the other combinations should be verified in other regions.

Moreover, in this study, we defined multi-analogs only from atmospheric circulation fields.

[2] In this work, Hindcast and reforecast have the same definition.

However, atmospheric processes can not be the only sources of predictability of the weather at different time scales. Adding ocean variables such as the sea surface temperature (SST) can contribute to improve the quality of precipitation forecasts as the ocean variables provide slow information about the evolution of the weather. To do so, some machine learning techniques can be used to optimize the choice of variables and their areas of influence in our target region. Therefore, more information can be included such as information about teleconnections between the tropics/subtropics as the influence of the Madden-Julian Oscillation (Cassou, 2008; Robertson and Vitart, 2019; Zhang, 2013). This could lead to a potential gain in forecast skill and not only over Europe.

As explained above, the use of either dynamical models or multi-analogs helped to improve the forecast skill of European precipitation within 30 days. The use of each method in future works or in operational forecasts mode may depend on the availability of the data either for S2S models or reanalyses and the quality of the data over the considered region.

Résumé

Contexte et objectifs

L'objectif de cette étude est d'améliorer les prévisions des précipitations en Europe pour atteindre l'échelle intrasaisonnière (de 2 à 4 semaines). Dans ce chapitre, on propose deux techniques pour améliorer les prévisions des précipitations en Europe avec le générateur stochastique de temps et les analogues de la circulation atmosphérique.

Méthodes

Dans un premier temps, nous présentons le "HC-SWG", qui est une nouvelle version du générateur de temps. Le HC-SWG consiste à utiliser les sorties des modèles numériques de prévision du temps pour définir les analogues. Nous utilisons les prévisions du centre Européen (ECMWF) et de Météo France (CNRM) du géopotentiel à 500 hPa pour calculer les analogues.
La deuxième méthode consiste en l'utilisation de "multi-analogues". Les multi-analogues sont des analogues calculés à partir de differentes variables atmosphériques. Pour les définir, nous avons utilisé les composantes principales du Z500, Z1000 et de l'humidité relative. Nous avons réalisé plusieurs combinaisons. Les deux méthodes de prévisions ont été évaluées par des scores de performance et comparées à la prévision de précipitation du centre Européen.

Résultats

Les deux méthodes d'amélioration des prévisions des précipitations ont contribué à fournir de meilleures prévisions jusqu'à 30 jours. Bien qu'elles soient différentes, les scores de performance des prévisions sont positifs. La comparaison avec les prévisions de précipitations d'ECMWF a permis de confirmer ce résultat.

Chapter 5

SWG ensemble forecast of the Madden Julian Oscillation

The Madden Julian Oscillation (MJO) is one of the sources of predictability for sub-seasonal time scales. It has a direct impact on weather in the tropics by organising convection and precipitation. Many studies have provided evidence that the variability of tropical convection associated with the MJO has a significant influence on extratropical weather and climate (Cassou, 2008). This global impact can provide an important signal for sub-seasonal climate prediction. Therefore, the forecast of the MJO is of considerable scientific interest. This chapter is dedicated to the forecast of the MJO with the Analog-SWG. The main focus of this chapter is a published article in *Earth System Dynamics*. This chapter starts with a brief summary explaining the importance of the MJO, its impacts and its prediction as well as a summary of the methodology. It will then be completed by a discussion pointing the main conclusions and highlighting some perspectives.

5.1 Overview about the Madden Julian Oscillation

The Madden-Julian Oscillation is a tropical convection pattern characterised by an eastward propagation on large areas of enhanced and suppressed tropical precipitation (Robertson and Vitart, 2019). It represents the dominant mode of sub-seasonal variability in the tropics (Vitart, 2017a). The MJO is mainly observed in the Indian Ocean and the Pacific Ocean. The MJO was first identified by Madden and Julian (1972) while studying tropical wind and pressure patterns. They noticed regular wind oscillations between Singapore and Canton Island in the west-central Pacific. The phenomena starts with an area of increased tropical precipitation that first appears over the western Indian Ocean and then extends eastward into the warm waters of the tropical Pacific. This tropical precipitation pattern tends to lose its intensity as it moves over the cooler waters of the eastern Pacific, before reappearing at some point over the Indian Ocean. A wet phase of increased convection is followed by a dry phase, where thunderstorm activity is suppressed (Madden and Julian, 1972).

The life cycle of the MJO is around 40 – 60 days (Kim et al., 2018). During the MJO cycle, there is a 'dipole' in rainfall anomalies (Zhang, 2013). For instance, while enhanced convection is over the western Pacific, convection is suppressed over the Indian Ocean.

Propagation of the MJO

The MJO exhibits two main modes of propagation based largely on the seasonal cycle as suggested by Madden and Julian (1972). In boreal winter, the MJO exhibits the strongest signals spatially and temporally (Lafleur et al., 2015; Hendon et al., 1999). A clear eastward propagation of convection and zonal wind anomalies are then observed at low latitudes (Hsu and Lee, 2005). By contrast, in boreal summer, a meridional migration of anomalous structures tends to become dominant (Cassou, 2008; Lawrence and Webster, 2002). The MJO is particularly pronounced over the Indian and western Pacific areas, where a secondary westward propagation tends to emerge in boreal autumn, starting from the Indo-Pacific Warm Pool [1] and heading towards the Philippines (Wu et al., 2006; Hsu and Weng, 2001). Many studies (Khalsa and Steiner, 1988; Goulet and Duvel, 2000) suggested that the MJO could present stationary characteristics at the regional level. Hsu and Lee (2005) showed that the eastward mean propagation of convection, which is widely described in the literature, tends to occur at the regional level. Zhang and Hendon (1997) consider this assumption of stationarity as a false impression given by the local amplification of convection within a continuous and very clearly dominant eastward propagation. Different theories derived from numerical modelling or in situ observation campaigns have emerged to explain the large-scale migrations of anomalous structures by the MJO (Zhang et al., 2020a). The MJO theories differ from each other in terms of the value of main parameters and constants used (More details can be found in Zhang et al. (2020b)). However, none of them is fully satisfactory and accomplishes realistic numerical simulations of the MJO due to the different assumed processes, approximations, parameterizations, and constants applied to the MJO theories. Further research is still in progress to determine processes and parameters sufficient for the MJO (Zhang, 2005; Lin et al., 2006; Zhang et al., 2020a). The nature of the phenomena explaining the propagation of the signal is still a matter of debate within the scientific community. Indeed, despite the advancement in the understanding of the MJO it is still a challenge to determine the fundamental mechanisms of the observed MJO.

Impacts of the MJO

There are many links between the MJO and synoptic weather. The MJO impacts the precipitation variability in the tropics in particular during the boreal winter (Zhang, 2013). The impacts of the MJO on precipitation are not limited to the tropics. For instance, anomalies in precipitation change signs between MJO phases in many parts of the world such as North American summertime and wintertime precipitation events (Whitaker and Weickmann, 2001), South American precipitation (Paegle et al., 2000). The MJO is also a source of the monsoon fluctuations (Zhang, 2013). It affects mainly the Asian summer monsoon and induces variations in the Australian monsoon (Hendon and Liebmann, 1990). The MJO creates favourable conditions for tropical cyclone activity (Zhang, 2013). Indeed, it has been shown that the number of tropical cyclones tends to increase by a factor of 2.6 on periods of negative convective anomalies of the MJO over the Indian ocean (Bessafi and Wheeler, 2006). This makes the MJO important to monitor during the Atlantic hurricane season. Many studies have identified connections between the MJO and extratropical climate modes. For instance, the MJO influences the El Niño Southern Oscillation (ENSO) cycle (Zhang, 2005) as well as the North Atlantic Oscillation (NAO) (Cassou, 2008). There is also evidence that the MJO can influence the onset of a Sudden

[1] Known also as Tropical Warm Pool, it is a mass of ocean water located in the western Pacific Ocean and eastern Indian Ocean which consistently exhibits the highest water temperatures over the largest expanse of the Earth's surface.

Stratospheric Warming (SSW) event (Baldwin et al., 2003; Tripathi et al., 2015).

Proxies of the MJO

The most common index used to define the MJO and also on prediction studies is the Real-time Multivariate MJO (RMM) index developed by Wheeler and Hendon (2004). RMM1 and RMM2 are the first and second principal components of the combined empirical orthogonal functions (EOFs) of outgoing longwave radiation (OLR), zonal wind at 200 and 850 hPa averaged between 15°N and 15°S (Rashid et al., 2011). They represent the observed MJO life cycle in eight different phases (phases 1–8) as shown in figure 5.1. MJO phases can be defined in terms of the timing and locations of its center of convection and associated wind fields (Robertson and Vitart, 2019).

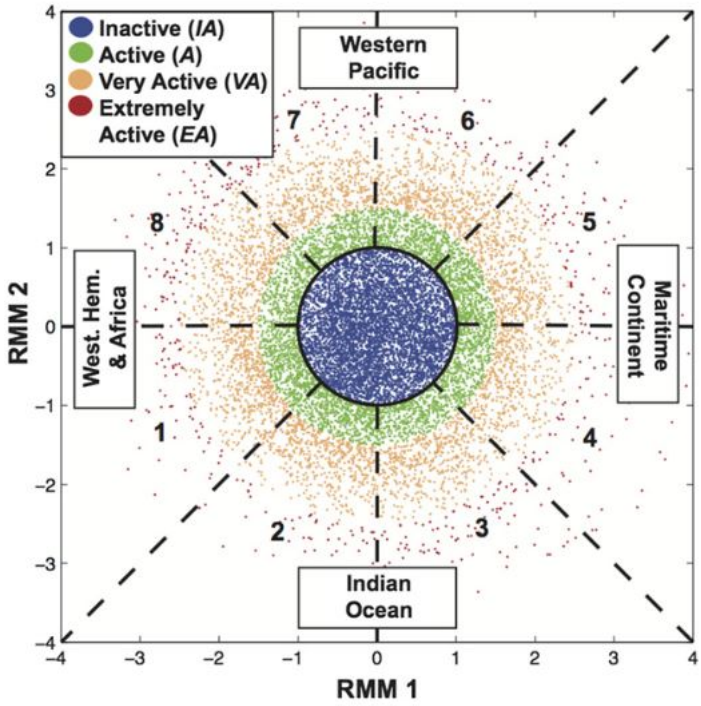

Figure 5.1: Phase-space diagram of the RMM index showing daily phase (quadrant) and magnitude (distance from center) of the MJO from 1 Jun 1974 through 31 Mar 2014. Colours indicate thresholds of activity (Lafleur et al., 2015).

RMM1 and RMM2 help both to locate the MJO and define the intensity of its convective activity. We are giving a summary of the main climatological aspect of the MJO from a study developed by Lafleur et al. (2015) based on RMMs. The MJO tends to be more active during December – March. The extreme amplitude of active MJO is sensitive and related to particular seasons. For instance, Lafleur et al. (2015) found that the frequency of extremely active MJO in March – May is of 8% of days while it is only 1% in June – August. In addition, MJO phases 1 and 2 occurred more often, and phase 8 occurred less often than the other phases throughout the year.

MJO prediction

The improvement of the forecast skill of the MJO has been the subject of several studies over time. Several numerical and probabilistic models have been used to forecast the MJO index (Kim et al., 2018). I will give a brief summary of the different efforts made to understand the MJO predictability. To start, the predictability of the MJO was shown to be possible up to 3 – 4 weeks using the upper filtered intraseasonal circulation field (Waliser et al., 2003; Liess et al., 2005). Such level of predictability of the MJO was obtained later by several numerical models (Reichler and Roads, 2005; Kim et al., 2008). Moreover, studies suggested that the predictability of the MJO can be extended to several days further when ocean-atmosphere coupled processes are involved (Pegion and Kirtman, 2008) However, (Kim et al., 2008) showed that the improvement was negligible above 3-4 weeks using the Sea surface temperature. Later, Kim et al. (2014) showed that with multi-model forecasting systems, the predictability of the MJO can reach up to 6 – 7 weeks using RMM indices.

Figure 5.2 shows the multimodel prediction skill from (Kim et al., 2018). The forecast skill of the MJO is usually measured with scalar metrics such as the bivariate correlation and the RMSE. Figure 5.2 shows the bivariate correlation over the period 1999 - 2010 for all seasons and for the winter from different S2S models. The predictability of the ensemble mean of RMM in most models is between 35 and 45 days. However, the highest predictability is obtained with the ECMWF and ABOM2 models of up to 45 days (Neena et al., 2014) and about 40 days for the Beijing climate center (BCC) (Wu et al., 2016).

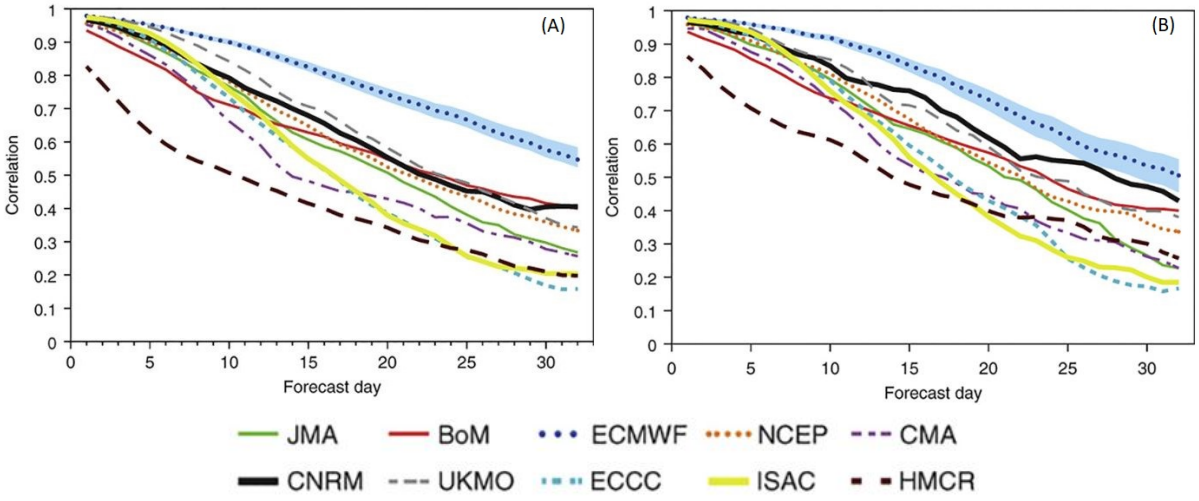

Figure 5.2: Evolution of the bivariate correlation between the model ensemble means and ERA-Interim as a function of lead time for 10 S2S models. The MJO bivariate correlation has been computed over the period 1999–2010 for (A) all seasons and (B) extended winters (December-March). The shaded area represents the 95% level of confidence computed from a 10,000 bootstrap resampling procedure (Robertson and Vitart, 2019)

The prediction skill using a probabilistic approach is still lower and less explored. This work is motivated by this gap. Marshall et al. (2016) proposed an ensemble predictions tool of the MJO for a real-time forecast that overcomes some of the difficulties compared with other tools. Forecast verification using probability-based skill scores (instead of scalar skill measures) is introduced to evaluate the model performance (Marshall et al., 2016). Probabilistic forecasts have been recently implemented for the real-time forecast of the MJO at the Bureau of Meteorology,

Australia (Marshall et al., 2016).

5.2 Methodology summary

In this study, we explored the skill of SWG to forecast the amplitude ($A(t)$) from the RMM indices of the MJO using analogs of atmospheric circulation. We forecasted the amplitude directly and by using the RMM1 and RMM2. Therefore, we generate separately an ensemble of 100 members of the amplitude $A(t)$ of the MJO and RMMs using the same approach. The goal is to have a probabilistic forecast of $A(t)$ for a sub-seasonal lead time (2 to 4 weeks). As input to the SWG, we are using analogs of the atmospheric circulations. We computed analogs separately from the geopotential heights at 300 and 500 hPa (Z300 and Z500), the OLR and the zonal wind at upper and lower levels. We choose to keep analogs from the geopotential height at 500 hPa (Z500) instead of the other fields. Three main reasons lead to this choice:

1. The composition of the RMMs index. Indeed, the OLR is used as a proxy for organized moist convection (Kim et al., 2018). However, the fractional contribution of the convection to the variance of RMMs is considerably lower than the fraction of the zonal wind fields (Kim et al., 2018; Straub, 2013).

2. The MJO predictability can be improved by including atmospheric and oceanic processes (Pegion and Kirtman, 2008). According to some theories that explain the MJO, the geopotential height and the moisture are considered as a driver of precipitation and convection (Zhang et al., 2020b). For instance, in the gravity-wave theory for MJO (Yang and Ingersoll, 2013), the convection and precipitation are triggered by a specific geopotential threshold.

3. Another reason is related to our forecast approach. The composites of OLR and wind speed highly depend on the phase of the MJO (Kim et al., 2018). As our analog approach is constrained by the choice of a geographical region, it misses the spatio-temporal variability of OLR and wind speed during the MJO. We computed analogs from other regions. However, we obtain better forecast scores by focusing on the "small" area shown in Krouma et al. (2023). This is explained by the higher quality of analogs. Indeed, choosing a "large" region to compute analogs yields rather large distances or low correlations for analogs. This implies that the analog SWG gets lower skill scores because the analogs are not very informative. The OLR or zonal wind speed analogs were computed on the optimal window obtained for Z500 or Z300 which is not appropriate for OLR or wind speed, as reflected by Kim et al. (2018). Therefore, we find lower COR and RMSE scores compared to the forecast using Z300 and Z500. This is a potential feature of analogs. The analog geometry needs to be imposed a priori in a rather simplistic way, which does not follow the spatio-temporal features of the MJO, which are known independently.

Then, we adjusted the geographical region and the temporal window search of analogs. Indeed, the SWG forecast skill of the MJO depends on the geographical region for analogs. We choose to compute the analogs over the Indian Ocean with coordinates (50°E – 85°E; 15°S –15°N). We argued our choice by the fact that (i) the Indian Ocean corresponds to the first phase of the MJO in the phase-space diagram, where the MJO starts. (ii) Different models found good results by initiating their forecast in this region (Kim et al., 2018). We search for analogs within

30 calendar days. This duration corresponds to the life cycle of the MJO. In addition, we adjust the SWG in order to select analogs from the same phase.

To evaluate the skill score of our forecasts, we used two approaches. We used probabilistic scores such as CRPS, rank correlation and ROC curve to evaluate the ensemble forecast of the amplitude. Then, we evaluate the ensembles mean of RMM1 and RMM2. We used scalar metrics such as the COR and the RMSE, as they are commonly used to evaluate MJO forecast (Rashid et al., 2011; Lim et al., 2018). Those scores are described in the article below (Rashid et al., 2011; Krouma et al., 2023).

5.3 Article published in *Earth System Dynamics*: Ensemble forecast of an index of the Madden Julian Oscillation using a stochastic weather generator based on circulation analogs

The manuscript of this paper is included in Appendix C (Krouma et al., 2023).

5.4 Conclusions and perspectives

We performed an ensemble forecast of the MJO amplitude using analogs of atmospheric circulation and a stochastic weather generator. We used the Z500 as a driver of the circulation over the Indian Ocean and we considered analogs from the same phase to do the forecast. We explored two ways to forecast the MJO, starting by forecasting directly the daily amplitude, then the daily MJO indices, RMM1 and RMM2, from 1979 to 2020. We assessed the forecast skill of the MJO forecast by evaluating the ensemble member and the mean of the ensemble member, using respectively probabilistic and scalar verification methods. This allowed us to evaluate the forecast and also to explore the difference between the two verification methods.

Using probabilistic skill scores (CRPSS and ROC), we found that the forecast is good within 40 days. With scalar scores (COR and RMSE) and the ensemble mean of the forecast of RMM1 and RMM2, we found that the SWG is able to forecast the MJO indices (RMM1 and RMM2) within 30 – 40 days. We noticed that the forecast is sensitive to seasons. The forecast has skill up to 30 days for the boreal winter (DJF and MAM), while it goes to 40 days for the boreal summer (JJA) and SON. This is consistent with previous studies (Silini et al., 2021; Rashid et al., 2011). We also notice that the forecast of the phase is better than of the amplitude. Finally, we showed that the SWG had improvement over the ECMWF and machine learning (Silini et al., 2021) forecasts, especially for long lead times. This work hence confirms the skill of the SWG to generate ensembles of MJO indices forecasts from analogs of circulation.

The work developed in this chapter leads to several perspectives. I will provide more details about some of them.

- In our study, we mentioned that the SWG forecast has skill using analogs computed at a "small" geographical area. Our method of calculating analogs shows limitations in computing analogs for a large geographical area. It can be interesting to find methods to search for analogs at large windows. This will help to verify the predictability of other

variables such as wind at different levels and OLR.

- Another important point concerns improving the MJO skill forecast over the Maritime Continent barrier (Wu and Hsu, 2009; Ahn et al., 2020; Kim et al., 2016) [2]. Indeed, improving the MJO forecast in this area may contribute to improve the ENSO forecast due to the influence of MJO on ENSO. In our study (Krouma et al., 2023), we found that the SWG forecasts of the MJO over the Maritime Continent are skilful until 30 days (using COR and RMSE). The same result was found by Silini et al. (2022) using an hybrid method that combines machine learning techniques and dynamical models. Hence, it could be interesting to combine dynamical models and SWG. This could improve the forecast of the MJO over this area as shown for precipitation in chapter 2.

- A final point, that is not directly related to the forecasting of the MJO but to the modelling of the MJO. Indeed, different theories have been developed to describe the MJO (Zhang et al., 2020a). Nevertheless, they do not help to improve the representation of the MJO in numerical models as there is still no consensual theory (Zhang et al., 2020a; Robertson and Vitart, 2019). Indeed, improving the understanding of the MJO processes will help to improve the predictions of MJO. Moreover, more studies are needed to link the forecast skill of the MJO to its capacity to forecast the weather and its impact. Few studies evaluate the forecasting models' skill to predict the impact of the MJO (Marshall et al., 2016; Specq and Batté, 2020a; Vitart, 2014; Cassou, 2008), despite the improvement in forecasting the MJO during recent years. Models need to be able to predict the influence of the MJO on meteorological variables of interest such as precipitation. This helps to maximise the potential of the MJO as a source of predictability on sub-seasonal timescales.

[2] is the name given by meteorologists and oceanographers to the region of Southeast Asia which comprises, amongst other countries, Indonesia, Philippines and Papua New Guinea. Located between the Indian and Pacific Oceans, it is situated within a warm ocean region known as the Tropical Warm Pool.

Résumé

Contexte et objectifs

L'oscillation de Madden-Julian (MJO) est le mode de variabilité dominant à l'échelle intrasaisonnière dans l'atmosphère tropicale. Elle a longtemps été considérée comme un phénomène interne aux bassins océaniques Indien et Pacifique, mais tend de plus en plus à être décrite comme un phénomène d'extension quasi-planétaire. La MJO est à l'origine de perturbations convectives de large échelle, dont la périodicité est comprise entre 30 et 60 jours, et qui présentent en moyenne une propagation vers l'est au cours du temps (en particulier, de l'océan Indien vers l'Indonésie, puis vers le Pacifique ouest). De nombreuses études se sont concentrées sur la prévision de la MJO car elle représente un phénomène majeur au vu de son importance à l'échelle sub-saisonnière et de ses impacts sur les variables météorologiques d'intérêt. Les modèles numériques ont montré des scores de prévision satisfaisants. Ce chapitre propose une méthode statistique de prévision de l'amplitude de la MJO basé sur les analogues de la circulation atmosphérique et le générateur stochastique de temps. Notre objectif est de prévoir l'amplitude de la MJO et les indices RMM1 et RMM2 de la MJO pour une échéance allant de 2 à 4 semaines.

Méthodes

La méthode de prévision consiste tout d'abord à définir les analogues de la circulation atmosphérique que nous utiliserons par la suite pour la prévision de la MJO. Dans cette étude, les analogues ont été calculés à partir de la hauteur du géopotentiel à 500 hPa. J'ai testé d'autres champs de circulation comme la vitesse du vent et le rayonnement ascendant de grande longueur d'onde (OLR) mais les scores de prévisions étaient plus faibles. Notre choix était conforté par plusieurs raisons, dont les théories de modélisation de la MJO. La deuxième étape consiste à générer des trajectoires avec le générateur de temps à partir des analogues préalablement sélectionnés. Finalement, des scores de prévision comme le CRPS ont été calculés afin d'évaluer la performance de notre méthode de prévision. Ils ont été comparés aux scores du modèle du centre Européen et d'un modèle de prévision basé sur l'intelligence artificielle.

Résultats

Notre modèle stochatique de prévision a permis de prévoir l'amplitude d'indices de la MJO (indices RMMs) pour des moyennes allant jusqu'à 40 jours à l'avance. Nous avons vérifié la performance de notre prévision par des scores probabilistes et des scores scalaires. Nous avons constaté que les prévisions sont sensibles aux saisons. Notre modèle de prévision est capable de prévoir la MJO jusqu'à 30 jours à l'avance pendant l'hiver boréal et jusqu'à 40 jours pendant l'été boréal. Cela est en accord avec des études précédentes (Silini et al., 2021; Rashid et al., 2011). Notre modèle de prévision montre des améliorations dans la prévision de la MJO par rapport aux prévisions du centre Européen et du modèle basé sur l'intelligence artificielle (Silini et al., 2021), en particulier pour de longs délais. Ce travail confirme la capacité du générateur stochastique de temps à générer des ensembles de prévisions d'indices de MJO à partir d'analogues de circulation.

Chapter 6

Recurrences and predictability

This chapter presents two theoretical studies that I performed during my thesis. Those studies are related to the use of non-linear approaches to investigate the predictability and the relationship between meteorological variables. I have focused mainly on precipitation. The chapter is composed of an introduction that gives an overview of dynamical and non-linear processes. Then, I present in each section one study by introducing the used technique and the relevant results. This will be completed by a general conclusion including a brief comparison between the two techniques.

6.1 Introduction

Most physical systems are described by ordinary or partial differential equations with a time dependence (e.g. the laws of geophysical fluid mechanics). Integrating those equations from all possible initial conditions defines a dynamical system. Dynamical system theory describes how the space of initial conditions evolves through time when the solutions of the dynamical equations are solved. Since the pioneering work of H. Poincaré, interesting notions that describe the behaviour of physical dynamical systems have emerged (Poincaré, 1900). The first one is the notion of **attractor** (or strange attractor) for dissipating systems. Many hydro-dynamical systems yield bounded trajectories, due to the dissipation of energy. It can be shown that those trajectories wind around a single subset of space, a so-called attractor (Weisstein, 2002). There are "trivial" attractors, such as fixed points or limit cycles. If the phase space had a fractal dimension then the attractor is called "strange" (Weisstein, 2003). The second crucial notion is **chaos**: the high sensitivity to initial conditions. Hence, trajectories from two arbitrarily close initial conditions diverge exponentially fast from each other (Lorenz, 1963). This makes all long-term prediction of the system very uncertain (Boeing, 2015). It has been shown that most dynamical systems from fluid dynamics are chaotic. E.N. Lorenz (re) introduced this notion in atmospheric sciences and illustrated it with the famous "butterfly effect" aphorism (Lorenz, 1962, 1963). A technical consequence of those notions (chaos and attractors) is **recurrence**. A theorem by H. Poincaré states that for any point in the surroundings of the attractor, one can find trajectories of the system in any arbitrary neighbourhood of that point (Poincaré, 1900). This is called a recurrence. This notion of recurrence may not be used directly from the observable of a physical system (an observable is a function of the variables of the system). For instance, meteorological variables in climate models cover the entire planet. However, one of the variables

may only have one measurement, say, one value once a day, which means that it is represented by a univariate quantity, whereas the whole system has an infinite number of variables.Ruelle and Takens (1971) showed that under generic assumptions, an embedding of the time variations of a univariate variable, with sufficiently large dimension, provides a good approximation of the underlying attractor. The methods I will describe and apply are hence based on analyses of observables of the climate system (precipitation), with the strong hypothesis that recurrences on embedded observables can be analysed.

6.2 Recurrence Plots of precipitation

To study recurrence states of the atmosphere, several approaches have been developed such as the analogs approach that I have been using during my thesis work. But not only, the analogs have been used in many other studies such as the work of Blanchet et al. (2018) and Yiou et al. (2013) where they are considering different ways to define analogs. However, the analogs are not the only metric to quantify recurrence, other techniques in statistical physics exist such as **recurrence plots** (RP) (Eckmann, 1987; Marwan et al., 2007).

Recurrence plots are based on recurrence theorem states. The recurrence theorem is based on the work of Poincaré on the three-body system (Poincaré, 1900) where he found that a conservative system recurs infinitely many times as close as one wishes to its initial state (Poincaré, 1900). This theoretical result can be observed in the real world, where recurrences occur across our daily activities as well as in different scientific disciplines (Marwan, 2008). The weather is a good example as it represents dynamics at different scales.

By definition, recurrence states are states in a (small) neighbourhood in phase space. For a given trajectory $\overrightarrow{x_i}$ ($i \in \{1, \ldots, N\}$) in a phase space ($\overrightarrow{x_i} \in \mathbb{R}^m$), the recurrence R around a given point is defined as:

$$R_{i,j} = \Theta(\epsilon - ||\overrightarrow{x_i} - \overrightarrow{x_j}||), \tag{6.1}$$

where

$$\Theta(x) = \begin{cases} 1 & \text{if } x \geq 0, \\ 0 & \text{if } x < 0. \end{cases}$$

N is the number of considered states $\overrightarrow{x_i}$ and ϵ is a threshold value (predefined) for the construction of a recurrence. There are several methods to choose ϵ (Eroglu et al., 2014). ϵ can be defined as the 10% of the mean or the maximum of phase space values of all distances, or a value that ensures a recurrence point density of 1% (Eroglu et al., 2014).

The spatial distance ($||.||$) between two states $\overrightarrow{x_i}$ and $\overrightarrow{x_j}$ is used as a recurrence criterion if it falls below a threshold ϵ. Then, $R_{i,j} = 1$ whenever states at times i and j are recurrent and $R_{i,j} = 0$ otherwise. Eckmann (1987) introduced RP to visualize when a state in the phase space nearly recurs. Every point of the phase space trajectory is tested in order to determine whether it is close to another point of the trajectory. The distance between these two points should be less than the specified threshold ϵ.

RP can be applied to different systems as illustrated in Figure 6.1. In this Figure, I show three examples of RPs which result from three different systems: a chaotic system (Lorenz system) shown in Figure 6.1 (A); a periodic system (sinus function) shown in Figure 6.1 (B);

and a stochastic system (red noise) shown in Figure 6.1 (C).

The Lorenz system is defined by a (non-linear) ordinary differential equation:

$$\begin{cases} \frac{dx}{dt} & = \sigma(y(t) - x(t)), \\ \frac{dy}{dt} & = x(t)(\rho - z(t)) - y(t), \\ \frac{dy}{dt} & = x(t)y(t) - \beta z(t). \end{cases} \tag{6.2}$$

where $\rho = 28$, $\sigma = 10$, $\beta = 8/3$. In the following, I considered $x_L(t) \equiv x(t)$ with time $t = 3000$ to obtain RP shown in Figure 6.1 (A).

The sinus function x_s was computed as follow for $t = 3000$:

$$x_s(t) = A \sin(\pi/180 \times t), \tag{6.3}$$

where A is the standard deviation of x_L. The RP obtained is represented in Figure 6.1 (B).

The red noise x_r was defined as follow:

$$x_r(t) = a \times x_r(t-1) + b(t), \tag{6.4}$$

where a is the memory with values $0 < a < 1$ and b is the white noise $(0, \sigma)$. a is defined as:

$$a = \frac{C_x(1)}{C_x(0)}, \tag{6.5}$$

where $C_x(1)$ is the covariance of $x_L(t)$ and $C_x(0)$ is the variance. And σ is defined as follows:

$$\sigma = \sqrt{\frac{C_x(1) - a^2}{a^2}}. \tag{6.6}$$

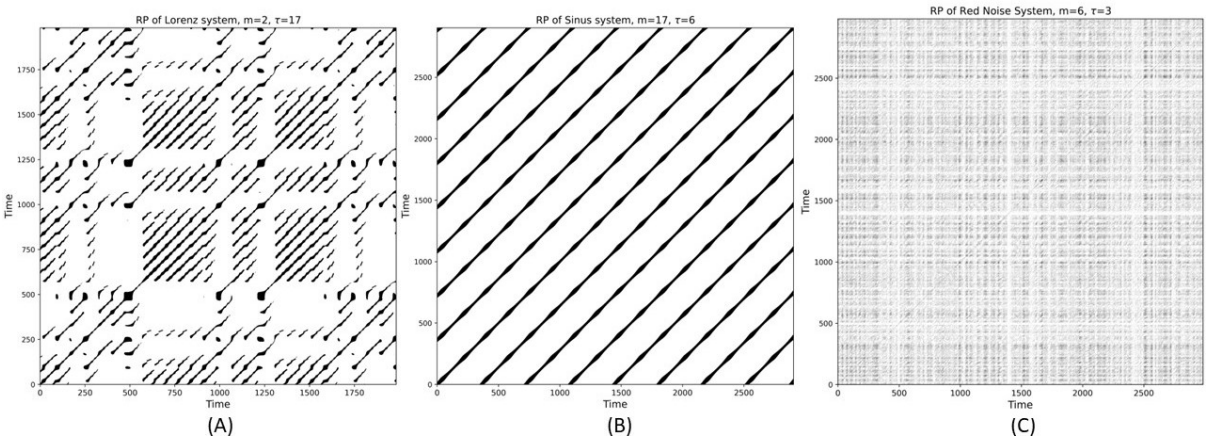

Figure 6.1: Comparison of the RPs of chaotic (Lorenz) dynamics, periodic (sinus) and stochastic (red noise). The x and y axes represent time. Figures made with data of the same length.

RPs have been applied to study external forcing (Goswami et al., 2013), landscape dynamics (Marwan et al., 2015) and changes in the paleoclimate variations (Rousseau et al., 2022; Goswami et al., 2018). RP analysis can be completed with recurrence quantification analysis (Webber Jr and Zbilut, 2005), which helps to determine predictability and other recurrence parameters (Marwan, 2008). I will give more details about that in the next sections 6.2.1 & 6.2.2.

6.2.1 Interpretation of Recurrence plots

A Recurrence plot (RP) is a tool to visualize the recurrence of a state of a dynamical system (Eckmann, 1987; Marwan, 2020) as illustrated in Figure 6.2. Recurrence states in RP are defined from equation (6.1) as follow:

$$R_{i,j} = \begin{cases} 1, & \text{if } ||x_i - x_j|| \leq \epsilon, \\ 0, & \text{if } ||x_i - x_j|| > \epsilon. \end{cases}$$

RP is a representation of a binary square matrix with black and white dots and two-time axes (Figure 6.2). Each black dot at the coordinates (i, j) represents a recurrence of the system state $\overrightarrow{x_i}$ at time j. However, white dot/space shows non-recurrence, as illustrated in Figure 6.2. The main diagonal of the RP, $R_{i,i} = 1$, represents the line of identity (LOI) (Figure 6.2). RP is a symmetric, binary matrix. The structures formed by line segments, which are parallel to the LOI in an RP, characterize typical dynamical indicators (Marwan, 2008). If the system is stochastic, homogeneously distributed recurrence points can be observed (Marwan, 2020). If the system is deterministic, diagonal line segments which are parallel to the LOI will dominate (Marwan, 2020). The dynamics are related to the length of the diagonal line segments: chaotic dynamics cause mainly short line segments, but contrary, regular (periodic) dynamics cause long line segments (Marwan, 2020), as illustrated respectively in Figure 6.1 (A) and (B).

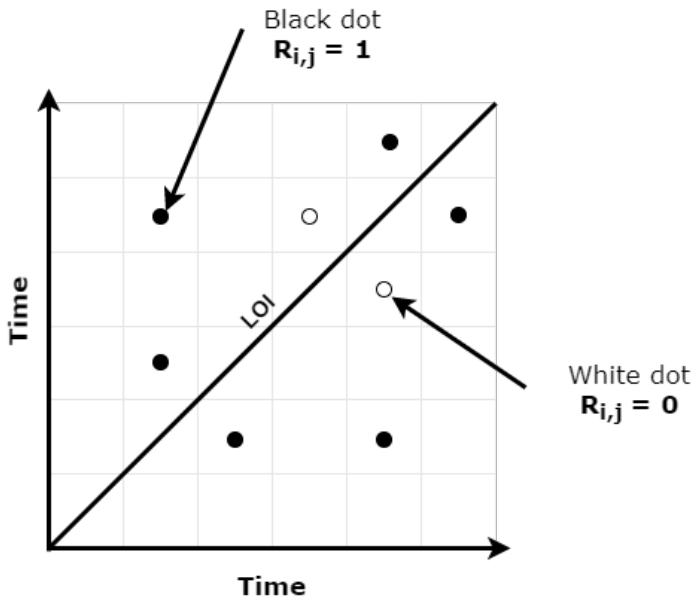

Figure 6.2: Illustration of a recurrence plot. Axes represent the time (daily, monthly, or yearly). Black dots indicate recurrence states. LOI is the line of identity or diagonal line.

Applying recurrence plot, or any other non-linear techniques, rely on reconstructing the phase space, thus determining the dimension m of the attractor. A big set of data is usually needed to reconstruct an attractor in order to keep it as close as possible to the state of the system as explained before in section 6.1. Hence, a trajectory in the phase space can be reconstructed using time delay τ and embedding m from a time series x_k defined (Kantz and Schreiber, 2004) as follows:

$$\overrightarrow{x}(t) = \overrightarrow{x_i} = (x_i, x_{i+\tau}, \ldots, x_{i+(m-1)\tau}), \tag{6.7}$$

with $t = i\Delta t$, $\overrightarrow{x}(t)$ is the vector of reconstructed states in the phase-space at the time t, and Δt is the time increment.

The delay embedding τ is a technique for constructing a set of likely state variables from an output (Semmlow, 2018). τ represents the time lags in each axis. The embedding dimension m is the dimension of the phase space (Cheng and Zhao, 2017). m can be found by false nearest neighbours and the τ by mutual information or autocorrelation (Goswami et al., 2013).

6.2.2 Recurrence Quantification analysis

The Recurrence Quantification analysis (RQA) represents several metrics established to provide a better understanding of RP (Marwan, 2008). As explained before, RP is just a visualization tool, the interpretation and analysis of all the structure and features of RP can be difficult and subjective (Webber Jr and Zbilut, 2005). To overcome this caveat, RQA measures were developed to quantify RP structures (Webber Jr and Zbilut, 2005). RQA uses small structures of the plot such as the diagonal and the vertical/horizontal lines to assess the complexity of the system (Schultz et al., 2015; Marwan et al., 2009). Several RQA measures have been developed. Each measure is dedicated to a specific aspect of the RP and has a defined interpretation (Marwan, 2020), which should be adapted to the physical meaning of the studied variable. In this study we mainly focus on two RQA measures:

- Determinism (DET) which is the fraction of recurrence points forming diagonal lines of at least length l in the RP as shown in Figure 6.3 (A). DET measures the likelihood that the dynamics of the system sustain to follow a dynamic that had already occurred at a previous time (Schultz et al., 2015). DET can also be defined as a measure of the likelihood of unstable limit cycles. Indeed, Lucarini and Gritsun (2020) explained that chaotic attractors are generically a superposition of unstable limit cycles. This implies that a deterministic chaotic system behaves locally (in time) like a periodic system, whose RP presents lines parallel to the bisector as illustrated in Figure 6.3 (A). DET can help to distinguish between stochastic and deterministic processes. For instance, RPs of stochastic processes reveal fewer diagonal lines compared to RPs of deterministic processes. DET can also be interpreted as the probability of the closeness between two segments of the phase space trajectory during the next time (Marwan, 2008). DET is a measurement of the predictability of the system, when DET is high (close to 1), the system is predictable (Marwan, 2020). Det is defined as:

$$DET = \frac{\sum_{l \geq l_{min}}^{N} l H_d(l)}{\sum_{l}^{N} l H_d(l)}, \tag{6.8}$$

  where H_d is the frequency distribution of the lengths l of the oblique lines, l_{min} is the necessary minimal length of the diagonal line, and in many studies, $l_{min} = 2$.

- Laminarity (LAM) measures vertical recurrence lines as explained in Figure 6.3 (B). LAM measures the probability that a state will not change for the next time step (Marwan, 2020). The Laminarity is related to the number of laminar phases in the system and its intermittency (Marwan et al., 2002). LAM is defined as follows:

$$LAM = \frac{\sum_{v \geq v_{min}}^{N} v H_l(v)}{\sum_{v}^{N} v H_l(v)}, \tag{6.9}$$

where H_l is the frequency distribution of the lengths v of the vertical lines, v_{min} is the length of the minimal vertical line.

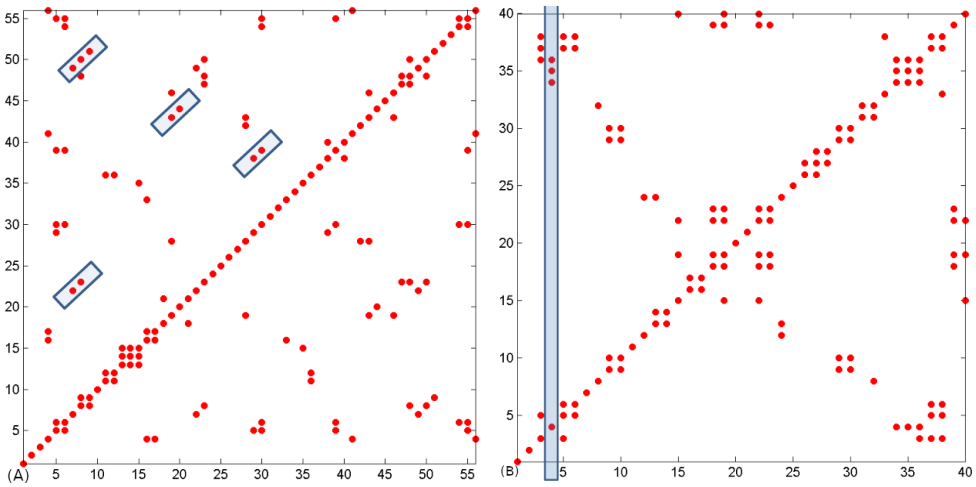

Figure 6.3: Schematic to explain the difference between Determinism (A) where diagonal lines are considered and Laminarity (B) where the vertical recurrence lines are considered. Inspired by a presentation of Nicola C Anderson where they studied the eye movement (Anderson et al., 2013).

The choice of the RQA depends on the nature of the studied phenomena. In this study, we choose DET and LAM as they are more adapted to our scientific question: the predictability of European precipitation.

6.2.3 Application to precipitation

I applied RP and RQA to precipitation at three different locations in western Europe (Berlin, Madrid and Orly). **The aim is to study the predictability of European precipitation**. For that, daily precipitation data were used. Precipitation data are obtained from the European Climate Assessment and Data (ECA&D) project (Klein Tank et al., 2002). Data are available from 1948 to 2023. I choose the period from 1948 to 2019.

Applying recurrence plot directly to precipitation can lead to false recurrence states due to the high frequency of zero in precipitation daily time series as shown in Figure 6.4 (a). To deal with this problem, the time series of the precipitation was normalised using the Standardized Precipitation Index (SPI) with a monthly time step (Figure 6.4 (b)). The SPI measures precipitation anomalies at a given location, based on a comparison of observed total precipitation amounts for an accumulation period of interest with the long-term historical rainfall record for that period (Wu et al., 2005; Livada and Assimakopoulos, 2007). SPI measures the monthly average of precipitation to which the Recurrence plot was applied.

As explained above, RP relies on finding the suitable embedding m, τ delay and recurrence threshold ϵ. Indeed, m and τ are important coordinates for phase space reconstruction. For a given time series, m and τ represent the m-dimensional delay space (Semmlow, 2018; Cheng and Zhao, 2017). Despite the large literature about those two parameters and the different techniques to compute them, the optimal choice of m and τ largely depends on the application (or studied variable/process) (Grassberger et al., 1991; Kantz and Schreiber, 2004).

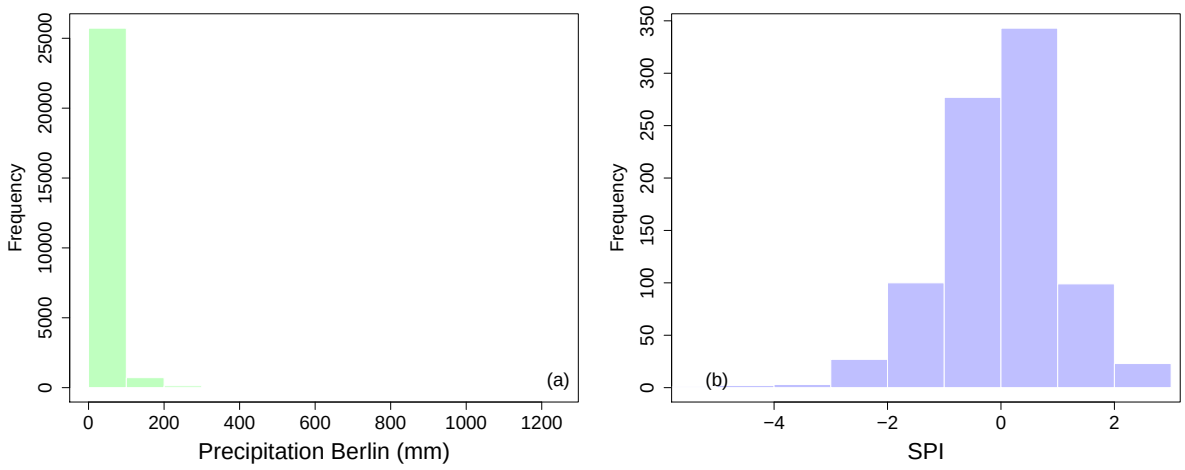

Figure 6.4: Histograms of precipitation of Berlin (a) and (b) the SPI of precipitation.

In this study, I determine the three RP parameters (m, τ and ϵ) as follows:

- m was determined using the *false nearest neighbours*. The false nearest neighbours technique consists in finding for a time series the nearest dimension for an m-dimensional space (Kennel et al., 1992). This guarantees that the reconstructed attractor is a one-to-one image of the attractor in the original phase space.
- τ was computed from the first local minimum of the mutual information. Mutual information is a quantity to measure the dependence between two random states. The mutual information determines a reasonable delay, unlike the autocorrelation function. Indeed, mutual information takes into account nonlinear correlations. It has no systematic dependence on the size of the time series (Fraser and Swinney, 1986).
- ϵ is defined as the 90 the quantile of x values.

I used scripts provided by Norbert Marwan at the PIK [1]. Indeed, this work has been done in the framework of a two-month secondment that I did in PIK - Potsdam within the CAFE project during the summer of 2020.

6.2.4 Significance tests for the RQA parameters

I was interested in verifying the sensitivity of the laminarity and determinism to the RP parameters (m, τ and ϵ). I verified whether DET and LAM are related to precipitation or to noise. For that, I applied a Monte Carlo simulation of Autoregressive model of order 1 (AR1) (Harrison, 2010). Monte Carlo analysis is a method that uses statistical sampling techniques to obtain a probabilistic approximation to the solution of a mathematical equation or model (Harrison, 2010). It is a method in which a large number of randomly generated sets of values are created. As a model, I choose an autoregressive model of order 1 (Eq. (6.10)).

$$x(t) = ax(t-1) + b(t) \tag{6.10}$$

[1] Recurrence Plots software http://www.recurrence-plot.tk/online/

$$\text{with } b \sim \mathcal{N}(0, \sigma),$$

where a and σ are the parameters of the model and $b(t)$ is a Gaussian white noise.

The Monte Carlo simulation follows a three-step process. In the first step, a and σ are determined from the variance and covariance of the time series of SPI by assuming that:

$$C_x(0) = C_{SPI}(0),$$
$$C_x(1) = C_{SPI}(1).$$

Once a and σ are determined using Eqs 6.5 and 6.6. The second step consists of selecting a random value from the time series of SPI as the initial x. Then, the generated time series from Eq. (6.10), is used to compute RP and the values of LAM and DET. The next step involves repeating step 2, 1000 times and storing the result of each calculation.

6.2.5 Results

I computed recurrence plot for precipitation in Berlin, Madrid and Orly. Figure 6.5 shows below a case study for Berlin. The computed values of m and τ are respectively equal to 5 and 3. I notice that by decreasing m to 3 the RP is no longer interpretable. Hence, I choose to keep an embedding $m = 5$ and a delay $\tau = 1$ as small delays lead to strongly correlated vectors in the new space. By analyzing the RP ($m = 5$, $\tau = 1$) of precipitation at Berlin from 1948 to 2019 (Figure 6.5), I found that the distribution is homogeneous. It indicates a stationary stochastic process. That means the process has a probability distribution that varies more or less constantly over a certain period of time. By looking at the RP (Figure 6.5), I notice that there are three different features related to each period from 1948 to 1969, 1970 to 1999, and 2000 to 2019. Therefore, I decided to split the RP into three different RPs keeping the same value of m and τ. The RP of the period from 1948 to 1969, shows mostly a periodicity in the monthly average of precipitation or the SPI. I notice an important sparse point that indicates a state that is not likely to happen often. For example, in 1954 I noticed a big sparse which corresponds to a high value of SPI (which indicates high precipitation) in July 1954. In the RP of 1970 to 1999, there are more strong colones which indicate more irregular states, and the RP of 2000 to 2019 shows more sparse.

As the visual interpretation of RPs is a bit difficult, RQA measures, mainly DET and LAM, were used to better understand the dynamic behaviour of precipitation and confirm our interpretation. The value of DET with $m = 5$ and $\tau = 1$ is high, mostly close to 1 as illustrated in table 6.1. This value of $DET = 0.85(\approx 1)$ indicates that the monthly average of precipitation (or SPI) is predictable. However, the LAM confirms that there has been a change in the state over time. Moreover, by modifying the values of m and τ the RQA parameters change in particular the values of DET as represented in Table 6.1. The same results were found for the Orly and Madrid SPIs.

Table 6.1: Laminarity (LAM) and determinism (DET) of SPI (normalized monthly precipitation) for Berlin. The RQA parameters are computed after modifying the delay τ and then m.

RQA	m=5 , $\tau = 1$	m=5 , $\tau = 2$	m=5 , $\tau = 3$	m=3 , $\tau = 1$	m=4 , $\tau = 1$
DET	**0.85**	0.14	0.20	0.68	**0.77**
LAM	**0.46**	0.29	0.33	0.38	**0.42**

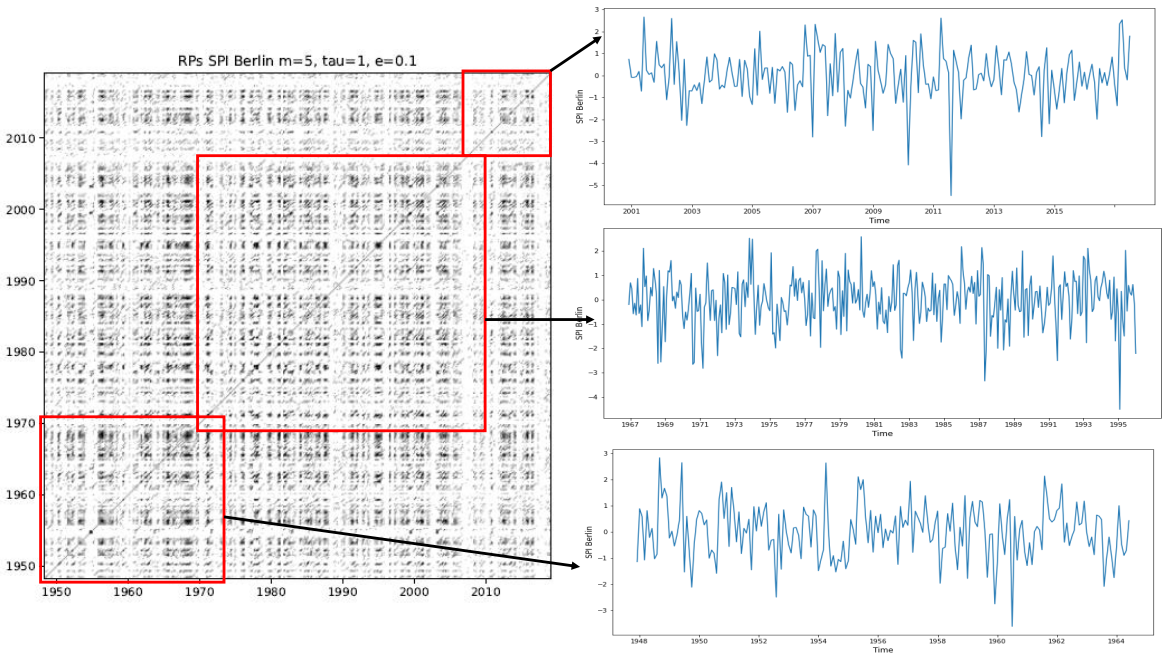

Figure 6.5: Recurrence plot of SPI of Berlin

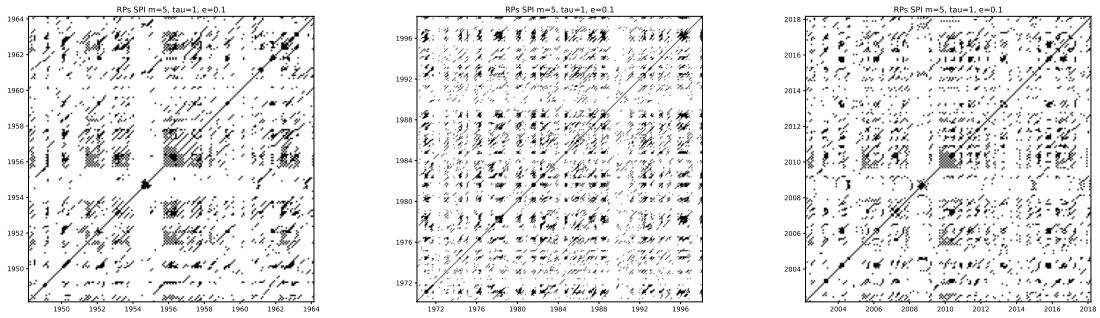

Figure 6.6: RPs of SPI of Berlin for the period (a) 1948 to 1969 ; (b) 1970 to 1999, (c) 2000 to 2019.

Therefore, I was interested in verifying whether the values of laminarity and determinism with an embedding $m = 5$ and a delay $\tau = 1$ are proper to precipitation or could be related to noise. For that, I used Monte Carlo simulations of Autoregressive model of order 1 (AR1). The verification with the Monte Carlo simulation will help to assess our choices for the delay and the embedding. As explained before, a reasonable choice of delay and embedding is important to deal with a finite amount of noise.

Results of Significance tests for the RQA parameters

I compute the distributions of DET and LAM with the Monte Carlo simulation, as represented respectively in Figures 6.7 and 6.8. The same DET value for $m = 5$ and a delay $\tau = 1$ previously obtained for SPI can be easily obtained from a noise. Indeed, the range values of DET for the SPI of Berlin, Madrid and Orly which are between $[0.85, 0.87]$ are included in the distribution of DET obtained from the 1000 simulations computed by AR1 as illustrated in Fig-

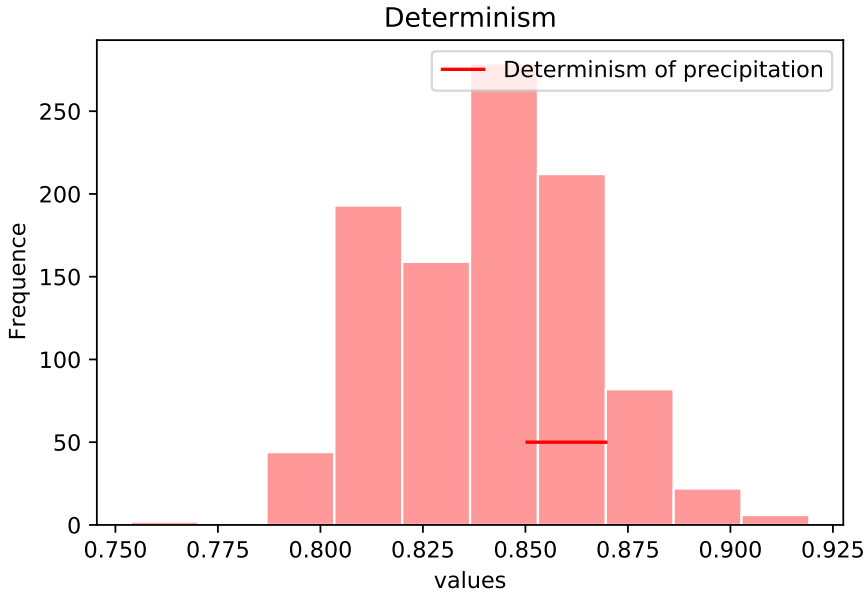

Figure 6.7: Determinism computed from AR1 using random values of a and σ.

ure 6.7. The LAM values in Figure 6.8 also represents a Gaussian distribution, and the values computed from SPI that are between $[0.46, 0.47]$, are approximately included in this distribution. Therefore, I can not reject the fact that the values found for DET with $m = 5$ and $\tau = 1$ are similar to those of a random series. Therefore, $m = 4$ and $\tau = 1$ are considered the best delay embedding values as they guarantee at the same time clear RP and RQA measures that are related to precipitation.

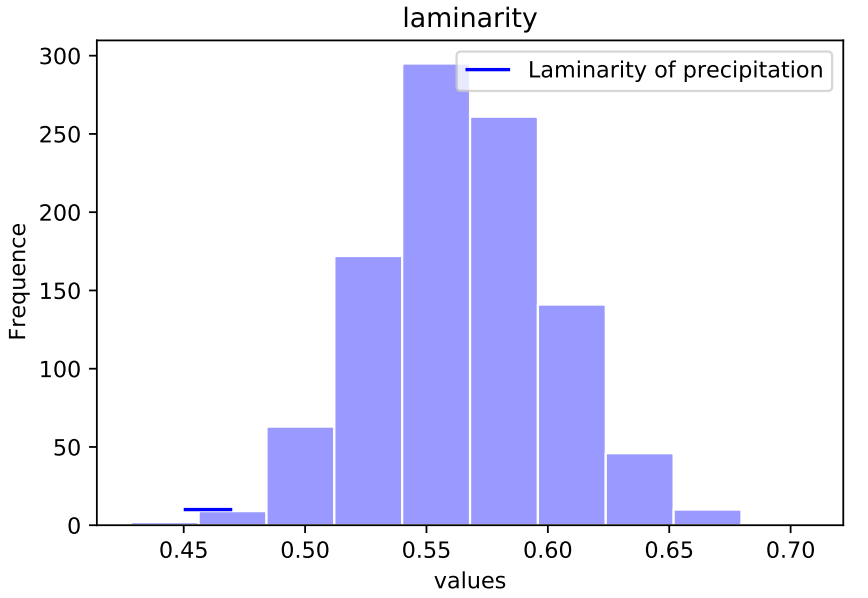

Figure 6.8: Laminarity computed from AR1 using random values of a and σ.

6.2.6 Conclusion

To sum up, applying the recurrence plot and recurrence quantification analysis to study the dynamics of precipitation helped to understand the behaviour of the precipitation system. RP showed that precipitation over Europe from 1948 to 2019 has a stationary stochastic behaviour. It showed that precipitation has three transition periods, as three different RPs configurations were found at different time periods. This indicates that European precipitation switched from periodic (1948 to 1969) to more stochastic behaviour with more frequent extremes in particular in the period from 2000 to 2019. Using the RQA, I found that the monthly average of precipitation (SPI) over Europe is predictable but shows non-stable states. In this study, I proposed a new approach to study precipitation dynamics. I emphasize the importance of choosing an "optimal" or "correct" delay and embedding the RP. I also proposed a method to better select those two parameters. However, very few studies have investigated precipitation with recurrence plots, therefore comparing parameters and results is rather difficult.

6.3 Predictability of precipitation using local indicators

Other techniques can be used to study the recurrence and predictability of meteorological variables known as **local indicators** (Caby et al., 2020; Faranda et al., 2017b). Local indicators are defined by two parameters which are the local dimension (d) and the inverse of persistence (θ) (Faranda et al., 2017b) of the attractor. Local indicators allow studying the evolution of the state of a system $x(t)$ approaching a point ζ of the attractor (Caby et al., 2020). More precisely, they give an idea about the trajectories of the dynamical system by measuring the density of neighbouring points and defining the persistence of the trajectories around a state ζ in the attractor at each instant t as illustrated in the following Figure 6.9.Local indicators have been successfully applied to describe the evolution of sea-level pressure (Faranda et al., 2017b) and geopotential height fields (Messori et al., 2017) over the North Atlantic, as well as to study the evolution of the sea-level pressure, temperature and precipitation fields at hemispheric scale (Faranda et al., 2017a) and the changes in the atmospheric circulation with CMIP5 models (Rodrigues et al., 2018).

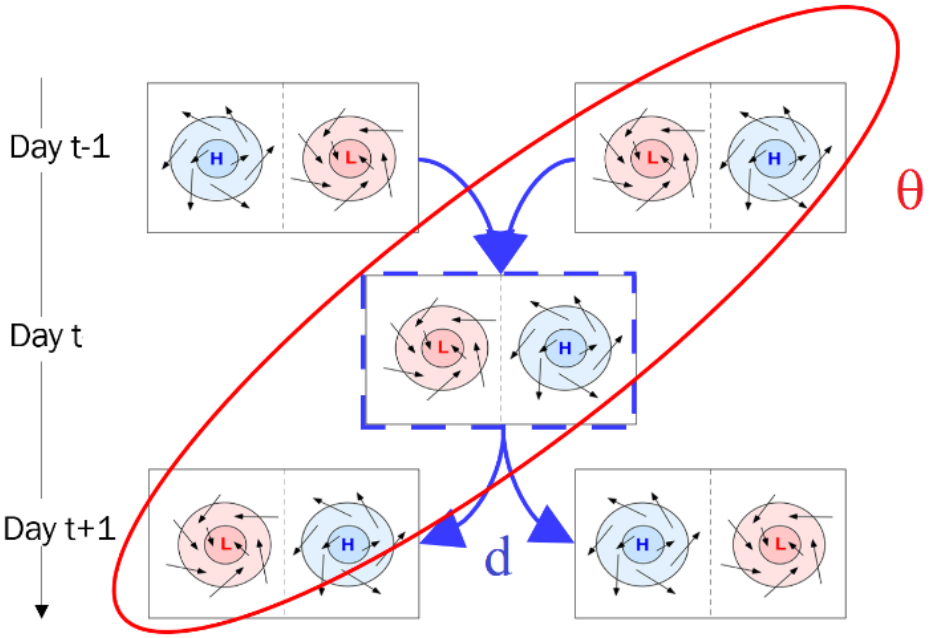

Figure 6.9: Illustration of local indicators d and θ of the atmospheric circulation for high (H) and low (L) pressures. The local dimension d helps to detect the possible states of the system from day $t-1$ to day $t+1$. d is proportional to the number of possible configurations. While θ quantifies the persistence of the states H and L over time. The Figure is taken from Rodrigues et al. (2018).

6.3.1 Local Dimension and the extremal index

The local dimension d measures the density of neighbouring points (Faranda et al., 2017b). The distribution of d gives information about the predictability of the observed variable (Faranda et al., 2022). θ, so-called extremal index, is the inverse of the mean time of persistence of the trajectories around the attractor. For a state ζ, one can define the observable $g(x(t))$, from the

log-distance between ζ and the other observations in the trajectory (Faranda et al., 2017b):

$$g(x(t)) = -\log(\text{dist}(x(t), \zeta)). \tag{6.11}$$

The logarithmic weight is applied to the time series of the distance to increase the discrimination of small values. This is an application of the Poincaré recurrence theorem (Poincaré, 1900) which has an exponential return time.

The idea is for a given point ζ in the attractor, the probability that the system returns within a ball of radius centred on ζ is computed. This probability converges to a Generalized extreme value distribution defined as (Lucarini et al., 2012; Caby et al., 2020):

$$\Pr(g(x(t)) > q; \zeta) \simeq \exp\left[-\theta(\zeta)\left(\frac{x-\mu(\zeta)}{\sigma(\zeta)}\right)\right], \tag{6.12}$$

the parameters μ and σ, namely the location and scale parameter of the distribution, depend on the point ζ in phase space. q is a threshold that is usually chosen to be the 98th percentile.

The local dimension $d = d(\zeta)$ is defined by the following relation (Faranda et al., 2017b):

$$d = \frac{1}{\sigma}. \tag{6.13}$$

The persistence of the state ζ is measured via the extremal index quantified by θ. θ values varies between $[0, 1]$. For all points which are not fixed points $\theta = 1$. With a finite dataset, θ values are neither 0 nor 1.

6.3.2 Application

This study aims **to evaluate the local indicators of meteorological variables (one-dimensional and multidimensional)**. I aim to study the local indicators of the geopotential height and those of European precipitation and **explain the relationship between the forecast skill of the European precipitation with the analogs and the SWG** presented in Chapter 2 and **the local indicators of Z500** in order to assess the relationship between the two variables.

Data

I used the geopotential height at 500 hPa from ERA5 (Hersbach et al., 2020). Daily data are available from 1979 to 2020 with a spatial resolution of 0.25°x0.25°. We also used Z500 data from NCEP (Kistler et al., 2001). The Z500 from NCEP, is available from 1948 to 2020 with a spatial resolution of 2.5°x2.5°. For verification and comparison purposes, I collected data over different regions: Large Euro-Atlantic domain (80°W – 50°E ; 22.5° – 70°N) with the same coordinates as Faranda et al. (2017b), Large domain (80°W – 20°E ; 30° – 70°N) and a small region (30°W–20°E ; 40°N – 60°N) which is the same as the domain of computation of analogs Krouma et al. (2022) as illustrated in Figure 6.10. The daily precipitation data are collected from the ECA&D project (Klein Tank et al., 2002). While the CRPS values are computed from the forecast of the precipitation by the Analog-SWG (Krouma et al., 2022). The CRPS was computed between the simulated precipitation and the observed precipitation at each station 6.10 as explained in chapter 2.

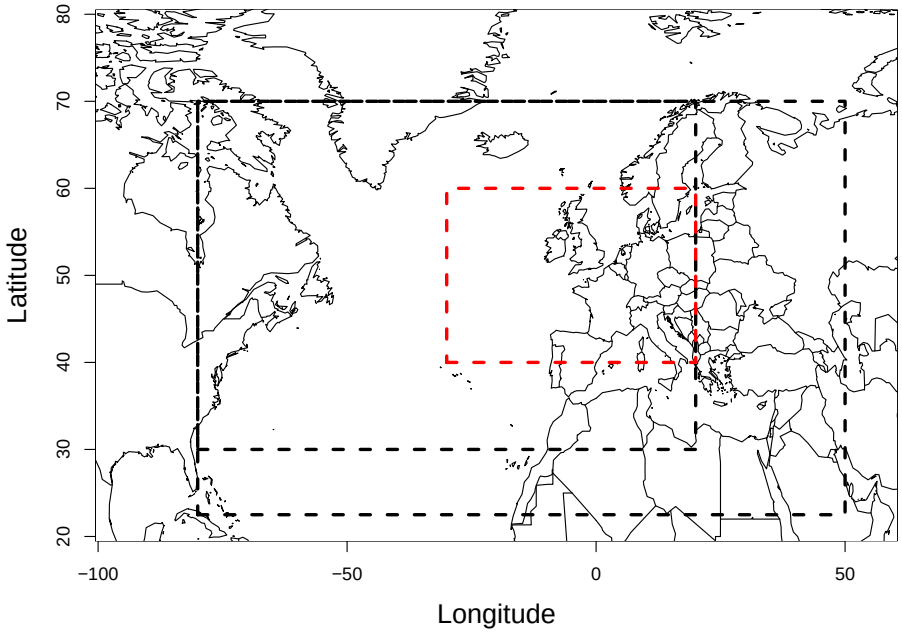

Figure 6.10: Domains of computation of d and θ for geopotential Z500 and precipitation for Berlin, Orly and Madrid.

Protocol

I start by computing the local indicators of the geopotential height at 500 hPa from the different sources (ERA5 (Hersbach et al., 2020) and NCEP (Kistler et al., 2001)) and at different geographical regions (Figure 6.10), and the observed precipitation at each area (Orly, Berlin and Madrid) (Klein Tank et al., 2002). To compute the local indicators, the Süveges estimator (Süveges, 2007; Caby et al., 2020) was adopted to compute θ. As a second step, I quantified the relationship between the local indicators of Z500 and precipitation. I looked at the dependence of the local indicators of precipitation and Z500 on the daily CRPS as well as the euclidean distance of the analogs.

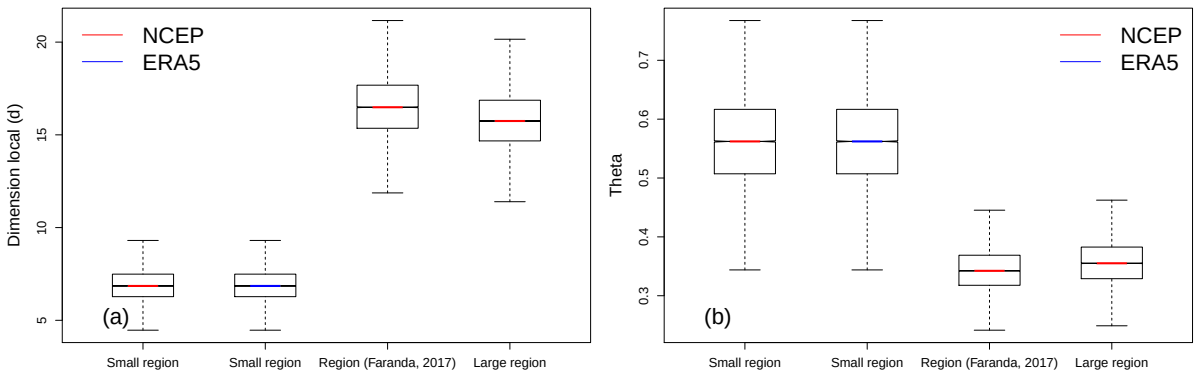

Figure 6.11: Comparison of the local indicators d (a) and θ (b) of Z500 over different geographical domains and using reanalyses of NCEP (red) and ERA5 (blue). Small region indicates the domain with coordinates (30°W–20°E ; 40°N – 60°N) and Large region indicates the domain with (80°W – 20°E ; 30° – 70°N).

6.3.3 Results

To start, I compared the local indicators computed from different regions and for the two reanalyses (ERA5 and NCEP) for Z500. I notice that the values of θ and d are different from one region to another (Figure 6.11). The median of θ for the Z500 is smaller over the large domains, while the median of d is higher over the large domains 6.11. Comparing the values of d and θ from NCEP and ERA5 values 6.11, I find that the median of d and θ are slightly higher with Z500 from ERA5. However, they correspond to what was found by Faranda et al. (2017b). The difference between the local indicators of ERA5 and NCEP can be related to the resolution of the two datasets. For the rest of the analysis, I keep the values of d and θ for Z500 computed from NCEP reanalysis over the region with coordinates (30°W–20°E ; 40°N – 60°N) as I compare them to the CRPS of the SWG precipitation forecast (Krouma et al., 2022) computed over this region and with NCEP.

The mean value of the local dimension D for Z500 is small with respect to what Faranda et al. (2017a) found, (Figure 6.11) which indicates that the state of Z500 at t and $t+1$ are close. The θ values are higher which indicates a persistent state of the Z500 from t to $t+1$. D and θ indicate that the state of Z500 is predictable and less chaotic over time. Further, I check the dependence of d and θ of Z500 on the European weather regimes in winter and summer. The idea is to verify whether the predictability of Z500 is related to a specific weather regime (Figure 6.12). I find that the Z500 is more persistent (high values of θ) and less chaotic (small values of d) during the NAO+ in winter. It is less predictable during the Atlantic ridge either in summer or winter with low values of θ and high values of d. This same result was found by Faranda et al. (2017b) for the mean sea level pressure.

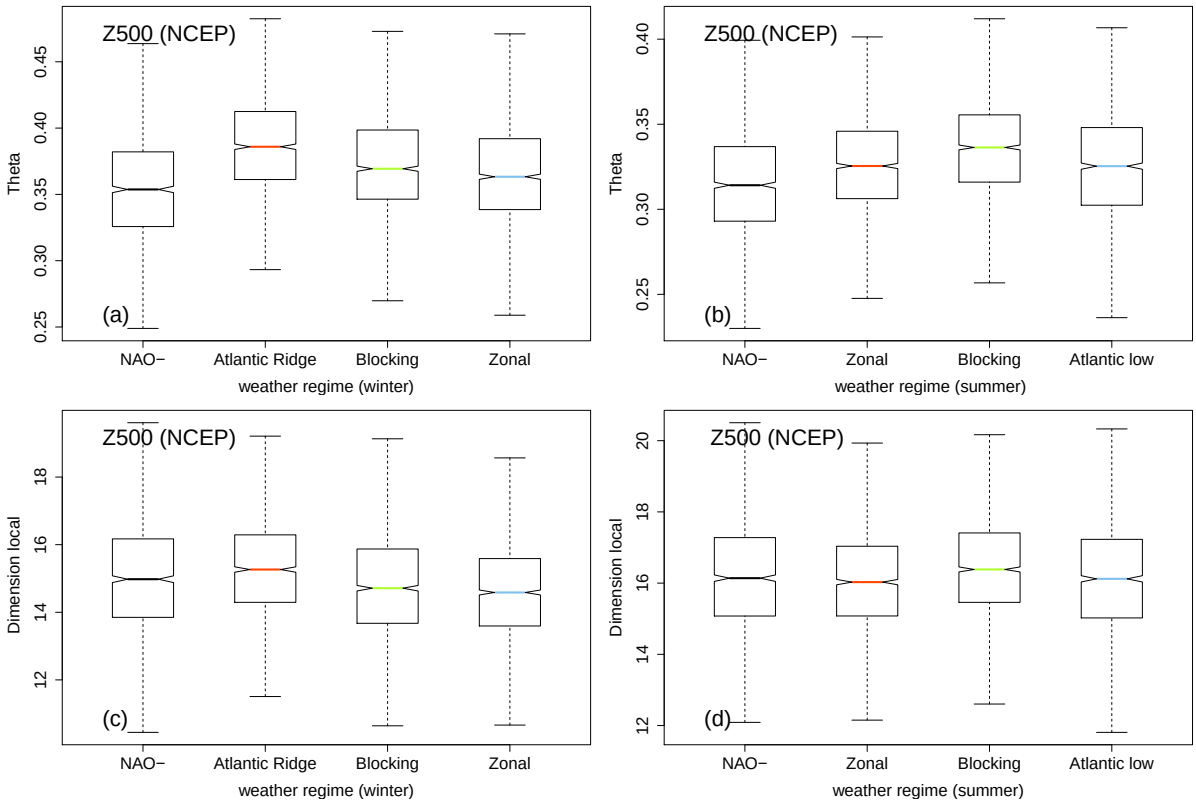

Figure 6.12: Distribution of (d,θ) of geopotential according to European weather regimes in winter and summer.

For precipitation, D (mean of d) is mostly equal to one for the different studied areas and the values of θ are around $[0.5, 0.65]$. D and θ indicate predictable daily precipitation from 1948 to 2020. In addition, I checked the relationship between, Z500 and CRPS of the predicted

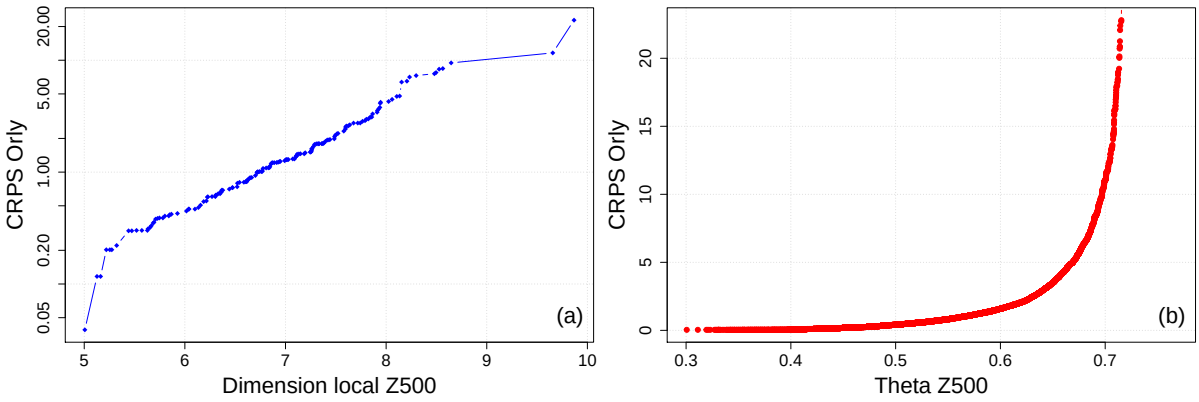

Figure 6.13: QQplot between the forecast skill (CRPS) of the SWG for the precipitation over Orly for a lead time of 5 days and the local indicators d (a) and θ (b) of geopotential height at 500hPa.

precipitation with SWG, using local indicators (d, θ) (Figure 6.13). However, no clear relation was found between Z500 and observed precipitation as well as Z500 and the skill of the forecast (CRPS) precipitation (Figure 6.13). At the moment of the study, I related that to the fact that I consider the forecast skill and the Z500 at a lead time of 5 days. This means that at 5 days the uncertainties in both variables are higher and impact the local indicators. Actually, I think that is more related to the fact that local indicators are not adapted to study relationships between meteorological variables as we showed with the work done in Chapter 3, that Z500 5 days ahead is still a good candidate to forecast European precipitation. However, the non-ability of the local indicators to detect such kind of relationship may be related to the fact that the two variables are spatially different. This hypothesis needs to be confirmed in future works.

6.3.4 Conclusion

This study shows that there is no obvious relation between the (d, θ) indicators and probability forecast scores like CRPS. This conclusion is not specific to precipitation as we found the same result using the Lorenz system and other meteorological variables. However, local indicators are still a useful tool to study the predictability of meteorological variables as shown in previous studies (Faranda et al., 2017a; Messori et al., 2017) and this one for precipitation as well as high dimensional systems such as the geopotential height. Using local indicators, I showed that precipitation over Berlin, Orly and Madrid is predictable at daily lead time. θ values for precipitation showed a persistence state.

Comparing those results to the work of Faranda et al. (2017b), I showed the sensitivity of the local indicators metrics to the size of the geographical domain, which should be adapted to the studied variable (Figure 6.11). As Faranda et al. (2017b), I found that Z500 is persistent and less chaotic during NAO+, especially in the winter. However, it is less predictable during the Atlantic ridge. What is new in this study compared to Faranda et al. (2017b), is the assessment of the relationship between two meteorological variables using d and θ.

6.4 Discussion and Additional work

In this chapter, I showed two non-linear tools to study the behaviour of a dynamical system. Both **recurrence plot** (Marwan, 2020) and **local indicators** (Caby et al., 2020; Faranda et al., 2017b) are methods to study the dynamics and predictability of the atmosphere. The two approaches show some differences in the shape of the final result. Both methods propose metrics, even if they are computed and named differently, but they lead to a similar interpretation (configuration and evolution of states of a system over time). Both methods indicate that European precipitation is predictable on a daily and monthly scale. RQA and local indicators showed that the European precipitation at three different locations (Berlin, Orly and Madrid) from 1948 to 2019 showed changes in the state from periodic to stochastic behaviour.

Both methods have some limitations and specificities. Indeed, RPs are more applicable to time series, while local indicators can be applied to high-dimensional systems such as atmospheric fields. The final result of the RP depends a lot on time embedding value. On the other side, local indicators can not be used to define or explain the relationship between climate variables.

Several studies have used those nonlinear approaches, for instance, the local indicators were also applied in a study by Faranda et al. (2022), in which I participated, about the predictability of extreme events in 2021. In this work, we used d and θ to study the predictability and the persistence of extreme events such as the Mediterranean heatwave that occurred over the Mediterranean basin from 11 to 14 August 2021. This Heatwave induces a new European temperature record over Sicily (Mazzoleni, 2021). It causes a lot of fires over France, Italy, Spain and North Africa (WMO, 2021; CEMS, 2021; AEMET, 2021). in this study, for the Mediterranean heatwave, we defined 33 analogs from Sea level pressure (SLP), the temperature (t2m) and the precipitation (tp) for JJAS (June-July- August and September) for two periods defined as the counterfactual period (1950-1979) and the factual period (1992-2021) as shown in Figure 6.14. Then, we compared the local indicators (d and θ) at the two mentioned climatological periods as well as the quality of the analogs. Comparing the d of the event between past (1950-1979) and actual (1992-2021) periods (Figure 6.14) showed that the Mediterranean heatwave is unpredictable in the actual climatological period (Faranda et al., 2022, Figure 5).

This paper is included in Appendix D (Faranda et al., 2022).

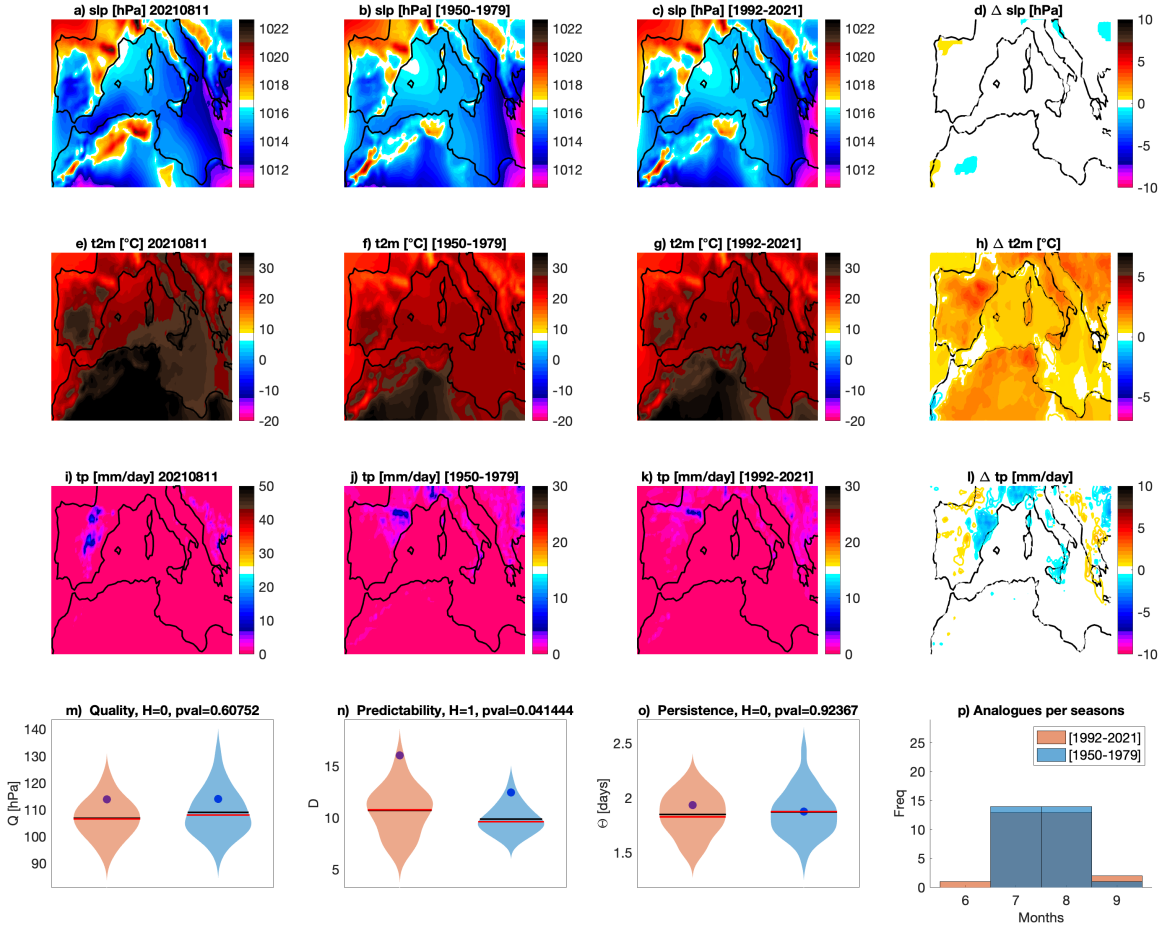

Figure 6.14: Attribution for the Mediterranean Heat Peak on 11-08-2021. Daily mean sea-level pressure slp (a), 2-meter temperatures $t2m$ (e) and total precipitation tp (i) on the day of the event. Average of the 33 sea-level pressure analogues found for the counterfactual [1950-1979] (b) and factual [1992-2021] (c) periods and corresponding 2-meter temperatures (f,g) and daily precipitation rate (j,k). Δslp (d), $\Delta t2m$ (h) and Δtp (i) between factual and counterfactual periods: colored-filled areas show significant anomalies with respect to the bootstrap procedure. Violin plots for counterfactual (blue) and factual (orange) periods for the analogues Quality Q (m) the Predictability index D (n), the Persistence index Θ (o) and the distribution of analogues in each month (p).

Résumé

Contexte et objectifs
Des méthodes de la dynamique non-linéaires ont montré leur capacité à étudier les propriétés des systèmes naturels à différentes échelles. L'atmosphère représente un système chaotique et dynamique ayant des états récurrents. L'étude des propriétés de l'atmosphère a fait l'objet de plusieurs études. Dans ce chapitre, nous avons appliqué des méthodes non-linéaires telles que **les dimensions locales** et **les graphiques de récurrences** pour étudier la prévisibilité des variables météorologiques principalement les précipitations.

Méthodes
La méthode des graphiques de récurrences consiste à chercher des états similaires dans le système dynamique. Les graphiques de récurrences sont des matrices (graphiques) représentant des points et des traits intereprétables. Un point noir indique un état récurrent, et un point blanc indique un état non récurrent. Comme l'interprétation des graphiques de récurrence peut être subjective, des outils de quantifications des récurrences ont été développés. Dans cette étude, on utilise les graphiques de récurrence ainsi que les outils de quantification pour étudier le comportement des précipitations en Europe ainsi que les états de transition depuis 1948 jusqu'à 2019.
D'autres méthodes non-linéaires comme les dimensions locales sont utilisées pour étudier la dynamique de l'atmosphère. Les dimensions locales étudient l'évolution d'un état de l'atmosphère au cours du temps. Les dimensions locales sont définies par deux paramètres d qui étudie la prévisibilité et θ qui étudie la persistance des trajectoires de chaque état. Nous avons utilisé d et θ pour étudier la prévisibilité des précipitations et le géopoteniel en Europe ainsi que la relation entre eux.

Résultats
Les graphiques de récurrences ont montré que les précipitations en Europe de 1948 à 2019 ont un comportement stochastique stationnaire. Ils ont indiqué que les précipitations européennes sont passées d'un système périodique (1948 à 1969) à un système à comportement plus stochastique dans la période de 2000 à 2019. En utilisant les outils de quantification, nous avons trouvé que la moyenne mensuelle des précipitations (SPI) en Europe est prévisible. Cette étude nous a permis de mettre en avant l'importance de bien choisir les paramètres des graphiques de récurrences. Nous avons ainsi proposé une méthode pour mieux les sélectionner. Les propriétés locales sont utiles pour étudier la prévisibilité des précipitations ainsi que le géopotentiel. Ils donnent une idée sur l'évolution de chaque état de l'espace des phases. Avec les propriétés locales, nous avons montré que les précipitations à Berlin, Orly et Madrid sont prévisibles à l'échelle journalière. Les propriétés locales ne sont pas appropriées pour étudier la relation entre différentes variables météorologiques.
Nous avons constaté l'importance des deux méthodes pour étudier la dynamique des précipitations.

Chapter 7

Conclusion & perspectives

In this chapter, the main results of this thesis will be recalled in the following subsection. I will then explore research directions resulting from the body of work presented in this manuscript.

7.1 Conclusions

Accurate weather forecasts at different time scales are crucial to predict usual and particularly unusual weather events in order to anticipate extreme socio-economic and environmental impacts. **The objective of this thesis was to assess whether and how the use of statistical and probabilistic approaches can contribute to provide convenient ensemble forecast at the sub-seasonal lead time, for different meteorological variables and in different locations**. This thesis focused on developing a weather ensemble forecasting tool for European precipitation and other climate variables and assessing the performance of the ensemble forecast at the sub-seasonal lead time. These specific topics were briefly introduced in Chapter 1 and 2.

My work has first focused on forecasting European precipitation at a local scale using a stochastic weather generator and analogs circulation (Chapter 3). In this first work, I used analogs from the geopotential height at 500 hPa over the Euro-Atlantic regions as input to the SWG to forecast precipitation. The SWG showed skill in forecasting precipitation over different local stations in Europe, going from Madrid, Orly (Paris) to Berlin. This has been evaluated using forecast verification scores such as the continuous rank probability skill score (CRPSS) and the correlation between observations and simulations. The performance of the SWG has been evaluated over climatology and persistence and, on the other hand, against precipitation forecasts from meteorological centers such as the ECMWF forecast. In general, this chapter concludes that **the SWG has the ability to simulate European precipitation with reasonable skills over climatology and persistence. As well as a good skill forecast over the ECMWF precipitation forecast within 10 days.** This first part of my thesis work, showed the importance of large-scale circulation in forecasting local weather, as well as the need to adjust well the forecast parameters (e.g the domain of computation of analogs, the number of analogs to keep..) to get a reasonable forecast skill as well as the capacity of the SWG to perform with different source of reanalyses. Although the SWG showed a skill to forecast the European precipitation, the work carried out still shows some limitations. Indeed, the SWG forecast does not give information about the forecasted precipitation type (if it is snow

or rain..). In addition, it has not been applied under specific extreme weather conditions such as floods or drought. Therefore, more work is still needed to test the SWG forecast capacity with analogs circulation in those specific situations. Finally, making the SWG forecast of precipitation operational would help to assess its real added value compared to other operational forecasts. I launched an operational forecast of the SWG for two stations Berlin and Orly during my thesis, but more years of data are still needed to obtain a fair skill score.

Among the perspectives arising from Chapter 4 is the need for improving the SWG forecasts in order to reach the sub-seasonal lead time. I then proposed two approaches to improve precipitation forecasts with the SWG (Chapter 4). The first approach led to develop the **HC-SWG**, which is a new version of the SWG. The HC-SWG is a combination of the SWG with dynamical models hindcasts. I used the outputs of the dynamical models days ahead as input to the SWG in order to forecast European precipitation. For that, analogs circulation were computed from the 5-day forecasted Z500 from European meteorological dynamical models such as the ECMWF and the CNRM. The second approach was based on the use of the **multi-analogs** to forecast European precipitation. The motivation behind this approach is to use different atmospheric fields, such as the relative humidity and the geopotential hight at 1000 hPa, as drivers of European precipitation. The results obtained in this chapter suggest that **either the HC-SWG or the multi-analogs approaches can help to reach the sub-seasonal lead time**. The two proposed approaches provide a better forecast skill of the European precipitation within 30 days. Skill scores of the HC-SWG and the multi-analogs SWG forecasts were assessed over climatology and persistence, as well as against the ECMWF precipitation forecasts. The HC-SWG showed capacities to distinguish between different precipitation events, this has been quantified using the Area under the ROC curve. The HC-SWG was able to provide forecasts of precipitation at a large scale (over Europe) and local scale (over defined local stations). The HC-SWG led to significant improvements over ECMWF and Météo-France forecasts. The work carried out in this chapter has allowed to draw general recommendations to help end users to choose which forecasting approaches to use depending on their needs and available data in their regions.

The work carried out in chapters 3 & 4 encouraged us to expand the SWG forecast applications to other climate variables in other regions. The idea was to forecast one of the most known sources of predictability of the sub-seasonal lead time, the Madden Julian oscillation. The goal was to evaluate the capacity of the SWG under other meteorological conditions context and at the same time to propose a new forecasting approach based on probabilistic methods for the MJO at the sub-seasonal lead time. Hence, the challenge started by defining the analogs circulation of the MJO. Several geographical areas and atmospheric fields have been tested for this purpose. That led to conclude that **the Z500 analogs over the Indian Ocean were the best candidates to drive the MJO**. I argued this choice in Chapter 5 and in our paper (Krouma et al., 2023). The MJO was forecasted from the index of the MJO RMM1 and RMM2 as well as directly from the amplitude. The forecast skill of the SWG has been evaluated using probabilistic skill scores and scalar skill scores. **The SWG ensemble forecast of the MJO provides a good forecast skill of the MJO (by respect to the skill scores thresholds) up to 40 days in advance and yields competitive skills compared to numerical weather predictions and machine learning forecasts**. The results also highlight the gained properties of the SWG. Indeed, the SWG conserved its capacity to distinguish between MJO events and also **its sensitivity to seasons**.

In this thesis, I was interested in studying the predictability of climate variables. Indeed, the predictability helps to better understand the dynamical behaviour of the atmosphere as well

as the relationship between climate variables as explained in Chapter 6. To do so, non-linear approaches have been applied. I have used mainly **the recurrence plots** technique to study the predictability and precipitation's behaviour in Europe and **local properties** to define the relationship between precipitation and geopotential height at 500 hPa. Results showed that using the two different techniques, **European precipitation is predictable on a daily and monthly scale**. However, no significant relationship was found using local properties. This led to conclude that either the approach is not adapted to define such a relationship or more sophisticated processing should be done before using the local properties. This could be kept as a scope for my future research work.

7.2 Utility to Society

Our weather forecasting tool showed its capacity to improve existing techniques by allowing a focus on a smaller area for a longer period in advance. In fact, the SWG forecasts can improve the prediction of precipitation and temperature (Yiou and Déandréis, 2019; Krouma et al., 2022) up to three or four weeks in advance at very local scales. This can be particularly valuable for providing information to decision-makers in different sectors. For instance, that can be useful for the agriculture sector in planning fertilization campaigns or crop rotation. As well as for the energy sector's management such as the wind energy sector. Indeed, sub-seasonal forecasts can help to plan the maintenance schedule for wind farm engines. Some applications in this direction are under consideration with ARIA Technologies in Europe and South America to explore our forecasting method for other variables, such as the wind. Having weeks in advance, information about the MJO activity could help to mitigate the impacts of heavy convective precipitation over very populated areas such as India. That can help humanitarian agencies also to plan and organise their activities.

Our forecasting method also has significantly lower computational costs than current methods. This can be a solution for small companies, agencies, or farmers that do not have high computational capacities but need to provide or carry out forecasts of some potential meteorological variables important to their activities. But not only SWG forecasts can be considered eco-friendly forecasting tool. Indeed, it is recommended today, particularly in the context of climate change, to use tools in research with lower computational costs. That can somehow help to reduce emissions. The work carried out in this thesis can serve as a starting point for using such statistical forecasting tools for this purpose.

During my thesis, I have been interested in disseminating my work either in scientific workshops and seminars and more to the general public whenever the opportunity arises. Indeed, I believe that it is part of my work to keep society updated and to exchange with them about their needs. Among the many outreach activities that I did during my thesis, I participated in explaining what I am doing in my PhD work to children in Spanish in the framework of the researchers' Nights 2020 for Spain and Uruguay, as well as in 1C1M (un chercheur, une manip) to explain to a large public how we do attribution of climate events to climate change and the role of statistics in that. I have been preparing and participating actively in the weekly weather discussions at the LSCE. I also wrote two blogs one about my participation in Reasearcher's night 2020 and another about IPCC report that are available on the CAFE Project website. And I made some explainer videos about my PhD work for the general public (See more Video 1, video 2).

7.3 Perspectives

Throughout the manuscript, specific perspectives for each of the presented studies have been discussed in Chapters 3, 4 and 5. In this section, I will not repeat the same perspectives that have already been mentioned, but rather discuss new perspectives emerging from all the work carried out on the European precipitation ensemble forecast (Chapters 3 and 4) and the Madden Julian oscillation ensemble forecast (Chapter 5). Indeed, all the work carried out in this thesis and presented in this manuscript represents a drop in a much larger amount of work that can be done. This provides insight into its fertility, opening up new avenues for future research.

One of the perspectives, that had arisen in my mind all along my thesis, is the use of **machine learning**. Indeed the analogs of circulation and the stochastic weather forecast can be considered as a primitive and simple version of machine learning techniques. However, I think combining the forecasting approach represented in this thesis with some machine learning, especially in the sight of analogs SWG can be helpful:

- For instance, in the context of a multi-analog forecast, machine learning techniques can be used as a pre-processing method to choose variables of interest and drivers of European precipitation. It can also be useful to combine atmospheric and oceanic fields over different geographical regions, as in the case of inducing SST to compute analogs. Machine learning could be especially useful in selecting computing areas for analogs, as for phenomena like the MJO where different trials should be run to define the optimized area. Some work has been done in this context, such as the work by Sonnewald et al. (2021) where they have used machine learning techniques known as **model tuning** to optimise automatic detection of ocean regimes. Such a technique of tuning could be applied to optimize the SWG forecasts.

- Machine learning can be applied as a post-processing approach to select or adjust the number of members to consider and keep. Indeed, in my thesis work, I have been generating an ensemble of 100 members. This, of course, helps to (i) provide a statistical distribution of the precipitation or in general any climate variables, (ii) also to catch all the uncertainties. However, 100-members would be too much as other models are generating smaller ensembles. The use of machine learning would help to optimize the number of members to consider. This could at least reduce the computational time.

Apart from the use of machine learning, another perspective is related to the data used to compute analogs. In my thesis work, I used reanalyses and reforecasts to compute analogs. The analog method is often criticised and qualified as a limited approach as the research of analogs is limited to "small" databases (70 years for reanalyses, or reforecasts of 20 years). However, we actually dispose of large databases such as the CMIP6 data, which offer a large ensemble of data that can help to find analogs of higher quality.

Another point that can be interesting is to apply the SWG to other variables. The SWG has been applied to forecast the North Atlantic oscillation, temperature (Yiou and Déandréis, 2019), precipitation (Krouma et al., 2022) and the Madden Julian oscillation (Krouma et al., 2023). The SWG showed its capacity to forecast different variables, at different time scales and in different regions (tropics and extratropics). Of course, there are some limitations and more other work is needed to overcome those limitations. But it can be extended to other variables of big interest such as wind speed. The wind represents one of the drivers of rain in Europe as

well it plays an important role in the energy sector either in Europe or in South America, like in Brazil.

Bibliography

AEMET: Spanish State Meteorological Agency:La ola de calor del puente de agosto'21 y los récords de temperaturas en España, URL https://aemetblog.es/2021/08/18/la-ola-de-calor-del-puente-de-agosto21-y-los-records-de-temperaturas-en-espana/, accessed: 2022-01-27, 2021.

Ahn, M.-S., Kim, D., Ham, Y.-G., and Park, S.: Role of Maritime Continent land convection on the mean state and MJO propagation, Journal of Climate, 33, 1659–1675, 2020.

Ailliot, P., Allard, D., Monbet, V., and Naveau, P.: Stochastic weather generators: an overview of weather type models, 156, 101–113, 2015.

Alexander, R., Zhao, Z., Székely, E., and Giannakis, D.: Kernel analog forecasting of tropical intraseasonal oscillations, Journal of the Atmospheric Sciences, 74, 1321–1342, 2017.

Anderson, J. L. and van den Dool, H. M.: Skill and return of skill in dynamic extended-range forecasts, Monthly weather review, 122, 507–516, 1994.

Anderson, N., Bischof, W., Laidlaw, K., Risko, E., and Kingstone, A.: Recurrence quantification analysis of eye movements, Behavior research methods, 45, https://doi.org/10.3758/s13428-012-0299-5, 2013.

Ardilouze, C., Specq, D., Batté, L., and Cassou, C.: Flow dependence of wintertime subseasonal prediction skill over Europe, Weather and Climate Dynamics, 2, 1033–1049, https://doi.org/10.5194/wcd-2-1033-2021, 2021.

Arias, P., Bellouin, N., Coppola, E., Jones, R., Krinner, G., Marotzke, J., Naik, V., Palmer, M., Plattner, G.-K., Rogelj, J., Rojas, M., Sillmann, J., Storelvmo, T., Thorne, P., Trewin, B., Achuta Rao, K., Adhikary, B., Allan, R., Armour, K., Bala, G., Barimalala, R., Berger, S., Canadell, J., Cassou, C., Cherchi, A., Collins, W., Collins, W., Connors, S., Corti, S., Cruz, F., Dentener, F., Dereczynski, C., Di Luca, A., Diongue Niang, A., Doblas-Reyes, F., Dosio, A., Douville, H., Engelbrecht, F., Eyring, V., Fischer, E., Forster, P., Fox-Kemper, B., Fuglestvedt, J., Fyfe, J., Gillett, N., Goldfarb, L., Gorodetskaya, I., Gutierrez, J., Hamdi, R., Hawkins, E., Hewitt, H., Hope, P., Islam, A., Jones, C., Kaufman, D., Kopp, R., Kosaka, Y., Kossin, J., Krakovska, S., Lee, J.-Y., Li, J., Mauritsen, T., Maycock, T., Meinshausen, M., Min, S.-K., Monteiro, P., Ngo-Duc, T., Otto, F., Pinto, I., Pirani, A., Raghavan, K., Ranasinghe, R., Ruane, A., Ruiz, L., Sallée, J.-B., Samset, B., Sathyendranath, S., Seneviratne, S., Sörensson, A., Szopa, S., Takayabu, I., Tréguier, A.-M., van den Hurk, B., Vautard, R., von Schuckmann, K., Zaehle, S., Zhang, X., and Zickfeld, K.: Technical Summary, p. 33144, Cambridge University Press, Cambridge, United Kingdom and New York, NY, USA, https://doi.org/10.1017/9781009157896.002, 2021.

Arroyo, J. and Maté, C.: Forecasting histogram time series with k-nearest neighbours methods, International Journal of Forecasting, 25, 192–207, 2009.

Atencia, A. and Zawadzki, I.: A comparison of two techniques for generating nowcasting ensembles. Part I: Lagrangian ensemble technique, Monthly Weather Review, 142, 4036–4052, 2014.

Atencia, A. and Zawadzki, I.: Analogs on the Lorenz attractor and ensemble spread, Monthly Weather Review, 145, 1381–1400, 2017.

Baldwin, M. P., Stephenson, D. B., Thompson, D. W., Dunkerton, T. J., Charlton, A. J., and O'Neill, A.: Stratospheric memory and skill of extended-range weather forecasts, Science, 301, 636–640, 2003.

Bartholy, J., Bogardi, I., and Matyasovszky, I.: Effect of climate change on regional precipitation in Lake Balaton watershed, Theoretical and applied climatology, 51, 237–250, 1995.

Batté, L. and Déqué, M.: Randomly correcting model errors in the ARPEGE-Climate v6.1 component of CNRM-CM: applications for seasonal forecasts, Geoscientific Model Development, 9, 2055–2076, https://doi.org/10.5194/gmd-9-2055-2016, 2016.

Bauer, P., Ohring, G., Kummerow, C., and Auligne, T.: Assimilating satellite observations of clouds and precipitation into NWP models, Bulletin of the American Meteorological Society, 92, ES25–ES28, 2011.

Bazo, J., Singh, R., Destrooper, M., and de Perez, E. C.: Pilot experiences in using seamless forecasts for early action: The "ready-set-go!" approach in the Red Cross, in: Sub-seasonal to seasonal prediction, pp. 387–398, Elsevier, 2019.

Bessafi, M. and Wheeler, M. C.: Modulation of south Indian Ocean tropical cyclones by the Madden–Julian oscillation and convectively coupled equatorial waves, Monthly Weather Review, 134, 638–656, 2006.

Blanchet, J., Stalla, S., and Creutin, J.-D.: Analogy of multiday sequences of atmospheric circulation favoring large rainfall accumulation over the French Alps, Atmos. Sci. Lett., 19, e809, https://doi.org/10.1002/asl.809, 2018.

Board, O. S., National Academies of Sciences, E., Medicine, et al.: Next generation earth system prediction: strategies for subseasonal to seasonal forecasts, National Academies Press, 2016.

Boeing, G.: Chaos theory and the logistic map, at UC Berkeley, 2015.

Brunet, G., Shapiro, M., Hoskins, B., Moncrieff, M., Dole, R., Kiladis, G. N., Kirtman, B., Lorenc, A., Mills, B., Morss, R., et al.: Collaboration of the weather and climate communities to advance subseasonal-to-seasonal prediction, Bulletin of the American Meteorological Society, 91, 1397–1406, 2010.

Caby, T., Faranda, D., Vaienti, S., and Yiou, P.: On the computation of the extremal index for time series, Journal of Statistical Physics, 179, 1666–1697, 2020.

Casati, B., Wilson, L., Stephenson, D., Nurmi, P., Ghelli, A., Pocernich, M., Damrath, U., Ebert, E., Brown, B., and Mason, S.: Forecast verification: current status and future directions, Meteorological Applications: A journal of forecasting, practical applications, training techniques and modelling, 15, 3–18, 2008.

Cassou, C.: Intraseasonal interaction between the Madden–Julian Oscillation and the North Atlantic Oscillation, Nature, 455, 523–527, https://doi.org/10.1038/nature07286, 2008.

Cattiaux, J., Vautard, R., Cassou, C., Yiou, P., Masson-Delmotte, V., and Codron, F.: Winter 2010 in Europe: A cold extreme in a warming climate, Geophysical Research Letters, 37, 2010.

CEMS: COPERNICUS Emergency Management Service: Fire in Var, France, URL https://emergency.copernicus.eu/mapping/list-of-components/EMSR541, accessed: 2022-01-31, 2021.

Cheng, F. and Zhao, J.: Root cause diagnosis of disturbances propagation paths by using improved convergent cross mapping, in: Computer Aided Chemical Engineering, vol. 40, pp. 1693–1698, Elsevier, 2017.

Dayon, G., Boé, J., and Martin, E.: Transferability in the future climate of a statistical downscaling method for precipitation in France, Journal of Geophysical Research: Atmospheres, 120, 1023–1043, 2015.

Delle Monache, L., Eckel, F. A., Rife, D. L., Nagarajan, B., and Searight, K.: Probabilistic Weather Prediction with an Analog Ensemble, Monthly Weather Review, 141, 3498–3516, https://doi.org/10.1175/MWR-D-12-00281.1, 2019.

Déqué, M. and Royer, J.: The skill of extended-range extratropical winter dynamical forecasts, Journal of climate, 5, 1346–1356, 1992.

Eckmann, J.: Kamphorst SO, Ruelle D, Recurrence plots of dynamical systems. Europhys Lett, 4, 973–977, 1987.

Eroglu, D., Marwan, N., Prasad, S., and Kurths, J.: Finding recurrence networks' threshold adaptively for a specific time series, Nonlinear Processes in Geophysics, 21, 1085–1092, 2014.

Faranda, D., Messori, G., Alvarez-Castro, M. C., and Yiou, P.: Dynamical properties and extremes of Northern Hemisphere climate fields over the past 60 years, Nonlinear Processes in Geophysics, 24, 713–725, 2017a.

Faranda, D., Messori, G., and Yiou, P.: Dynamical proxies of North Atlantic predictability and extremes, Scientific reports, 7, 41 278, URL https://www.nature.com/articles/srep41278.pdf, 2017b.

Faranda, D., Bourdin, S., Ginesta, M., Krouma, M., Noyelle, R., Pons, F., Yiou, P., and Messori, G.: A climate-change attribution retrospective of some impactful weather extremes of 2021, Weather and Climate Dynamics, 3, 1311–1340, 2022.

Fawcett, T.: An introduction to ROC analysis, Pattern Recognition Letters, 27, 861–874, https://doi.org/10.1016/j.patrec.2005.10.010, 2006.

Fealy, R. and Mills, G.: Deriving Lamb weather types suited to regional climate studies: A case study on the synoptic origins of precipitation over Ireland, International Journal of Climatology, 38, 3439–3448, 2018.

Ferro, C. A. T.: A probability model for verifying deterministic forecasts of extreme events, Weather and Forecasting, 22, 1089–1100, URL <GotoISI>://000250413300011, 2007.

Ferro, C. A. T.: Fair scores for ensemble forecasts, Quarterly Journal of the Royal Meteorological Society, 140, 1917–1923, https://doi.org/https://doi.org/10.1002/qj.2270, 2014.

Foley, A. M., Leahy, P. G., Marvuglia, A., and McKeogh, E. J.: Current methods and advances in forecasting of wind power generation, Renewable energy, 37, 1–8, 2012.

Fraedrich, K. and Rückert, B.: Metric adaption for analog forecasting, Physica A: Statistical Mechanics and its Applications, 253, 379–393, 1998.

Fraser, A. M. and Swinney, H. L.: Independent coordinates for strange attractors from mutual information, Physical review A, 33, 1134, 1986.

Gascón, E., Magnusson, L., and Barroso, J. A.: Unusual snowfall in Madrid in January. ECMWF Newsletter 167, Spring 2021., URL https://www.ecmwf.int/sites/default/files/elibrary/042021/19991-newsletter-no-167-spring-2021_1.pdf, accessed: 2022-10-22, 2021.

Goddard, L., Mason, S. J., Zebiak, S. E., Ropelewski, C. F., Basher, R., and Cane, M. A.: Current approaches to seasonal to interannual climate predictions, International Journal of Climatology: A Journal of the Royal Meteorological Society, 21, 1111–1152, 2001.

Goswami, B., Marwan, N., Feulner, G., and Kurths, J.: How do global temperature drivers influence each other?, The European Physical Journal Special Topics, 222, 861–873, 2013.

Goswami, B., Boers, N., Rheinwalt, A., Marwan, N., Heitzig, J., Breitenbach, S. F., and Kurths, J.: Abrupt transitions in time series with uncertainties, Nature communications, 9, 1–10, 2018.

Goulet, L. and Duvel, J.-P.: A new approach to detect and characterize intermittent atmospheric oscillations: Application to the intraseasonal oscillation, Journal of the atmospheric sciences, 57, 2397–2416, 2000.

Grassberger, P., Schreiber, T., and Schaffrath, C.: Nonlinear time sequence analysis, International Journal of Bifurcation and Chaos, 1, 521–547, 1991.

Hamill, T. M. and Whitaker, J. S.: Probabilistic quantitative precipitation forecasts based on reforecast analogs: Theory and application, Monthly Weather Review, 134, 3209–3229, 2006.

Harrison, R. L.: Introduction to monte carlo simulation, in: AIP conference proceedings, vol. 1204, pp. 17–21, American Institute of Physics, 2010.

Haylock, M. R., Hofstra, N., Tank, A. M. G. K., Klok, E. J., Jones, P. D., and New, M.: A European daily high-resolution gridded data set of surface temperature and precipitation for 1950-2006, J. Geophys. Res. - Atmospheres, 113, doi:10.1029/2008JD010 201, URL <GotoISI>://000260598000009, 2008.

Hendon, H. H. and Liebmann, B.: The intraseasonal (30–50 day) oscillation of the Australian summer monsoon, Journal of Atmospheric Sciences, 47, 2909–2924, 1990.

Hendon, H. H., Zhang, C., and Glick, J. D.: Interannual Variation of the Madden–Julian Oscillation during Austral Summer, Journal of Climate, 12, 2538 – 2550, https://doi.org/10.1175/1520-0442(1999)012<2538:IVOTMJ>2.0.CO;2, 1999.

Hersbach, H.: Decomposition of the Continuous Ranked Probability Score for Ensemble Prediction Systems, WEATHER AND FORECASTING, 15, 12, 2000.

Hersbach, H., Bell, B., Berrisford, P., Hirahara, S., Horányi, A., Muñoz-Sabater, J., Nicolas, J., Peubey, C., Radu, R., and Schepers, D.: The ERA5 global reanalysis, Quat. J. Roy. Met. Soc., 146, 1999–2049, 2020.

Horton, P.: AtmoSwing: Analog Technique Model for Statistical Weather forecastING and downscalING (v2.1.0), Geosci. Model Dev., 12, 2915–2940, https://doi.org/10.5194/gmd-12-2915-2019, 2019.

Hsu, H.-H. and Lee, M.-Y.: Topographic effects on the eastward propagation and initiation of the Madden–Julian oscillation, Journal of Climate, 18, 795–809, 2005.

Hsu, H.-H. and Weng, C.-H.: Northwestward propagation of the intraseasonal oscillation in the western North Pacific during the boreal summer: Structure and mechanism, Journal of climate, 14, 3834–3850, 2001.

IPCC: Climate Change 2021: The Physical Science Basis. Contribution of Working Group I to the Sixth Assessment Report of the Intergovernmental Panel on Climate Change, vol. In Press, Cambridge University Press, Cambridge, United Kingdom and New York, NY, USA, https://doi.org/10.1017/9781009157896, 2021.

Jolliffe, I. T. and Stephenson, D. B.: Forecast verification: a practitioner's guide in atmospheric science, John Wiley & Sons, 2011.

Jolliffe, I. T. and Stephenson, D. B.: Forecast verification: a practitioner's guide in atmospheric science, John Wiley & Sons, 2012.

Jones, A. and Morse, A.: Skill of ENSEMBLES seasonal re-forecasts for malaria prediction in West Africa, Geophysical Research Letters, 39, 2012.

Jones, P., Osborn, T., Harpham, C., and Briffa, K. R.: The development of Lamb weather types: from subjective analysis of weather charts to objective approaches using reanalyses, Weather, 69, 128–132, 2014.

Jézéquel, A., Yiou, P., and Radanovics, S.: Role of circulation in European heatwaves using flow analogues, Climate Dynamics, 50, 1145–1159, 2018a.

Jézéquel, A., Yiou, P., Radanovics, S., and Vautard, R.: Analysis of the exceptionally warm December 2015 in France using flow analogues, Bulletin of the American Meteorological Society, 99, S76–S79, 2018b.

Kantz, H. and Schreiber, T.: Nonlinear time series analysis, vol. 7, Cambridge university press, 2004.

Karl, T. R., Wang, W.-C., Schlesinger, M. E., Knight, R. W., and Portman, D.: A Method of Relating General Circulation Model Simulated Climate to the Observed Local Climate. Part I: Seasonal Statistics, Journal of Climate, 3, 1053 – 1079, https://doi.org/10.1175/1520-0442(1990)003<1053:AMORGC>2.0.CO;2, place: Boston MA, USA, 1990.

Kennel, M. B., Brown, R., and Abarbanel, H. D.: Determining embedding dimension for phase-space reconstruction using a geometrical construction, Physical review A, 45, 3403, 1992.

Khalsa, S. J. S. and Steiner, E. J.: A TOVS dataset for study of the tropical atmosphere, Journal of Applied Meteorology and Climatology, 27, 851–862, 1988.

Kim, H., Vitart, F., and Waliser, D. E.: Prediction of the Madden–Julian Oscillation: A Review, J. Climate, 31, 9425–9443, https://doi.org/10.1175/JCLI-D-18-0210.1, 2018.

Kim, H.-M., Hoyos, C. D., Webster, P. J., and Kang, I.-S.: Sensitivity of MJO simulation and predictability to sea surface temperature variability, Journal of climate, 21, 5304–5317, 2008.

Kim, H.-M., Webster, P. J., Toma, V. E., and Kim, D.: Predictability and prediction skill of the MJO in two operational forecasting systems, Journal of Climate, 27, 5364–5378, 2014.

Kim, H.-M., Kim, D., Vitart, F., Toma, V. E., Kug, J.-S., and Webster, P. J.: MJO propagation across the Maritime Continent in the ECMWF ensemble prediction system, Journal of Climate, 29, 3973–3988, 2016.

Kistler, R., Kalnay, E., Collins, W., Saha, S., White, G., Woollen, J., Chelliah, M., Ebisuzaki, W., Kanamitsu, M., Kousky, V., van den Dool, H., Jenne, R., and Fiorino, M.: The NCEP-NCAR 50-year reanalysis: Monthly means CD-ROM and documentation, Bulletin of the American Meteorological Society, 82, 247–267, URL <GotoISI>://000166742900003, 2001.

Klein Tank, A. M. G., Wijngaard, J. B., Können, G. P., Böhm, R., Demarée, G., Gocheva, A., Mileta, M., Pashiardis, S., Hejkrlik, L., Kern-Hansen, C., Heino, R., Bessemoulin, P., Müller-Westermeier, G., Tzanakou, M., Szalai, S., Pálsdóttir, T., Fitzgerald, D., Rubin, S., Capaldo, M., Maugeri, M., Leitass, A., Bukantis, A., Aberfeld, R., van Engelen, A. F. V., Forland, E., Mietus, M., Coelho, F., Mares, C., Razuvaev, V., Nieplova, E., Cegnar, T., Antonio López, J., Dahlström, B., Moberg, A., Kirchhofer, W., Ceylan, A., Pachaliuk, O., Alexander, L. V., and Petrovic, P.: Daily dataset of 20th-century surface air temperature and precipitation series for the European Climate Assessment, International Journal of Climatology, 22, 1441–1453, https://doi.org/10.1002/joc.773, 2002.

Koster, R. D., Mahanama, S., Yamada, T., Balsamo, G., Berg, A., Boisserie, M., Dirmeyer, P., Doblas-Reyes, F., Drewitt, G., Gordon, C., et al.: Contribution of land surface initialization to subseasonal forecast skill: First results from a multi-model experiment, Geophysical Research Letters, 37, 2010.

Krouma, M., Yiou, P., Déandreis, C., and Thao, S.: Assessment of stochastic weather forecast of precipitation near European cities, based on analogs of circulation, Geoscientific Model Development, 15, 4941–4958, https://doi.org/10.5194/gmd-15-4941-2022, 2022.

Krouma, M., Silini, R., and Yiou, P.: Ensemble forecast of an index of the Madden–Julian Oscillation using a stochastic weather generator based on circulation analogs, Earth System Dynamics, 14, 273–290, https://doi.org/10.5194/esd-14-273-2023, 2023.

Lafleur, D. M., Barrett, B. S., and Henderson, G. R.: Some Climatological Aspects of the Madden–Julian Oscillation (MJO), Journal of Climate, 28, 6039–6053, https://doi.org/10.1175/JCLI-D-14-00744.1, 2015.

Lau, W. K.-M. and Waliser, D. E.: Intraseasonal variability in the atmosphere-ocean climate system, Springer Science & Business Media, 2011.

Lawrence, D. M. and Webster, P. J.: The boreal summer intraseasonal oscillation: Relationship between northward and eastward movement of convection, Journal of the atmospheric sciences, 59, 1593–1606, 2002.

Lguensat, R., Tandeo, P., Ailliot, P., Pulido, M., and Fablet, R.: The analog data assimilation, Monthly Weather Review, 145, 4093–4107, 2017.

Liess, S., Waliser, D. E., and Schubert, S. D.: Predictability Studies of the Intraseasonal Oscillation with the ECHAM5 GCM, Journal of the Atmospheric Sciences, 62, 3320–3336, https://doi.org/10.1175/JAS3542.1, 2005.

Lim, Y., Son, S.-W., and Kim, D.: MJO Prediction Skill of the Subseasonal-to-Seasonal Prediction Models, Journal of Climate, 31, 4075–4094, https://doi.org/10.1175/JCLI-D-17-0545.1, 2018.

Lin, H. and Wu, Z.: Contribution of the autumn Tibetan Plateau snow cover to seasonal prediction of North American winter temperature, Journal of Climate, 24, 2801–2813, 2011.

Lin, J.-L., Kiladis, G. N., Mapes, B. E., Weickmann, K. M., Sperber, K. R., Lin, W., Wheeler, M. C., Schubert, S. D., Del Genio, A., Donner, L. J., et al.: Tropical intraseasonal variability in 14 IPCC AR4 climate models. Part I: Convective signals, Journal of climate, 19, 2665–2690, 2006.

Livada, I. and Assimakopoulos, V.: Spatial and temporal analysis of drought in Greece using the Standardized Precipitation Index (SPI), Theoretical and applied climatology, 89, 143–153, 2007.

Lorenz, E. N.: The statistical prediction of solutions of dynamical equations, in: Proceedings of the International Symposium on Numerical Weather Prediction, 1962, Meteor. Soc. Japan, 1962.

Lorenz, E. N.: Deterministic nonperiodic flow, Journal of atmospheric sciences, 20, 130–141, 1963.

Lorenz, E. N.: Atmospheric predictability as revealed by naturally occurring analogues, Journal of Atmospheric Sciences, 26, 636–646, 1969.

Lucarini, V. and Gritsun, A.: A new mathematical framework for atmospheric blocking events, Climate Dynamics, 54, 575–598, 2020.

Lucarini, V., Faranda, D., and Wouters, J.: Universal behaviour of extreme value statistics for selected observables of dynamical systems, Journal of statistical physics, 147, 63–73, 2012.

Lynch, P.: The emergence of numerical weather prediction: Richardson's dream, Cambridge University Press, 2006.

MacLeod, D. A., Jones, A., Di Giuseppe, F., Caminade, C., and Morse, A. P.: Demonstration of successful malaria forecasts for Botswana using an operational seasonal climate model, Environmental Research Letters, 10, 044 005, 2015.

Madden, R. A. and Julian, P. R.: Description of Global-Scale Circulation Cells in the Tropics with a 40–50 Day Period, Journal of Atmospheric Sciences, 29, 1109 – 1123, https://doi.org/10.1175/1520-0469(1972)029<1109:DOGSCC>2.0.CO;2, 1972.

Magnusson, L., Simmons, A., Harrigan, S., and Pappenberger, F.: Extreme rain in Germany and Belgium in July 2021. ECMWF Newsletter 169, Autumn 2021., URL https://www.ecmwf.int/sites/default/files/elibrary/102021/20225-newsletter-no-169-autumn-2021_1.pdf, accessed: 2022-10-22, 2021.

Magnusson, L., Tsonevsky, I., Gascon, E., Emerton, R., and Rouges, E.: Predicting the heat over western Europe in the summer of 2022. ECMWF Newsletter 173, Autumn 2022., URL https://www.ecmwf.int/sites/default/files/elibrary/102022/20502-newsletter-no-173-autumn-2022_0.pdf, accessed: 2022-10-22, 2022.

Maraun, D. and Widmann, M.: Weather Generators, p. 201–219, Cambridge University Press, https://doi.org/10.1017/9781107588783.014, 2018.

Marshall, A. G., Hendon, H. H., and Hudson, D.: Visualizing and verifying probabilistic forecasts of the Madden-Julian Oscillation: PROBABILISTIC MJO FORECASTS, Geophys. Res. Lett., 43, 12,278–12,286, https://doi.org/10.1002/2016GL071423, 2016.

Marwan, N.: A historical review of recurrence plots, The European Physical Journal Special Topics, 164, 3–12, 2008.

Marwan, N.: Recurrence-Plot-Techniken zur Untersuchung wiederkehrender Phänomene im System ErdeRecurrence plot techniques for the investigation of recurring phenomena in the system earth, Universität Potsdam, https://doi.org/10.25932/PUBLISHUP-44197, artwork Size: 120001 KB, 695513 KB, ix, 254 pages, 2020.

Marwan, N., Wessel, N., Meyerfeldt, U., Schirdewan, A., and Kurths, J.: Recurrence-plot-based measures of complexity and their application to heart-rate-variability data, Physical review E, 66, 026 702, 2002.

Marwan, N., Carmenromano, M., Thiel, M., and Kurths, J.: Recurrence plots for the analysis of complex systems, Physics Reports, 438, 237–329, https://doi.org/10.1016/j.physrep.2006.11.001, 2007.

Marwan, N., Donges, J. F., Zou, Y., Donner, R. V., and Kurths, J.: Complex network approach for recurrence analysis of time series, Physics Letters A, 373, 4246–4254, https://doi.org/10.1016/j.physleta.2009.09.042, 2009.

Marwan, N., Kurths, J., and Foerster, S.: Analysing spatially extended high-dimensional dynamics by recurrence plots, Physics Letters A, 379, 894–900, 2015.

Mazzoleni, M.: Cronaca meteo 3Bmeteo - Caldo storico in Sicilia, raggiunti i 49°C: è il nuovo record Europeo, URL https://www.3bmeteo.com/giornale-meteo/cronaca-meteo---caldo-storico-in-sicilia--raggiunti-i-49-c----il-nuovo-record-europeo-504610, accessed: 2022-10-21, 2021.

Messori, G., Caballero, R., and Faranda, D.: A dynamical systems approach to studying midlatitude weather extremes, Geophysical Research Letters, 44, 3346–3354, 2017.

Miyakoda, K., Gordon, T., Caverly, R., Stern, W., Sirutis, J., and Bourke, W.: Simulation of a blocking event in January 1977, Monthly Weather Review, 111, 846–869, 1983.

Miyakoda, K., Sirutis, J., and Ploshay, J.: One-month forecast experiments—Without anomaly boundary forcings, Monthly weather review, 114, 2363–2401, 1986.

Molteni, F., Cubasch, U., and Tibaldi, S.: 30-and 60-day forecast experiments with the ECMWF spectral models, in: Proc. ECMWF Workshop on Predictability in the Medium and Extended Range, pp. 51–107, ECMWF Reading, United Kingdom, 1986.

Molteni, F., Stockdale, T. N., and Vitart, F.: Understanding and modelling extra-tropical teleconnections with the Indo-Pacific region during the northern winter, Clim Dyn, 45, 3119–3140, https://doi.org/10.1007/s00382-015-2528-y, 2015.

Morse, A. P., Doblas-Reyes, F. J., Hoshen, M. B., Hagedorn, R., and Palmer, T. N.: A forecast quality assessment of an end-to-end probabilistic multi-model seasonal forecast system using a malaria model, Tellus A: Dynamic Meteorology and Oceanography, 57, 464–475, 2005.

Neena, J. M., Lee, J. Y., Waliser, D., Wang, B., and Jiang, X.: Predictability of the Madden–Julian Oscillation in the Intraseasonal Variability Hindcast Experiment (ISVHE)*, Journal of Climate, 27, 4531–4543, https://doi.org/10.1175/JCLI-D-13-00624.1, 2014.

Newman, M., Sardeshmukh, P. D., Winkler, C. R., and Whitaker, J. S.: A study of subseasonal predictability, Monthly weather review, 131, 1715–1732, 2003.

Nicolis, G. and Daems, D.: Probabilistic and thermodynamic aspects of dynamical systems, Chaos: An Interdisciplinary Journal of Nonlinear Science, 8, 311–320, 1998.

Nihan, N. L. and Holmesland, K. O.: Use of the Box and Jenkins time series technique in traffic forecasting, Transportation, 9, 125–143, 1980.

Paegle, J. N., Byerle, L. A., and Mo, K. C.: Intraseasonal modulation of South American summer precipitation, Monthly Weather Review, 128, 837–850, 2000.

Palmer, T., Brankovic, C., Molteni, F., Tibaldi, S., Ferranti, L., Hollingsworth, A., Cubasch, U., and Klinker, E.: The European Centre for Medium-range Weather Forecasts (ECMWF) program on extended-range prediction, Bulletin of the American Meteorological Society, 71, 1317–1330, 1990.

Palmer, T. N.: Predicting uncertainty in forecasts of weather and climate, Reports on Progress in Physics, 63, 71–116, URL <GotoISI>://000085479700001, 2000.

Pegion, K. and Kirtman, B. P.: The Impact of Air–Sea Interactions on the Predictability of the Tropical Intraseasonal Oscillation, Journal of Climate, 21, 5870–5886, https://doi.org/10.1175/2008JCLI2209.1, 2008.

Platzer, P.: Forecasts of dynamical systems from analogs : applications to geophysical variables with a focus on ocean waves., Ecole nationale supérieure Mines-Télécom Atlantique, 2020. English. ⟨NNT : 2020IMTA0221, 2020.

Platzer, P., Yiou, P., Naveau, P., Filipot, J.-F., Thiebaut, M., and Tandeo, P.: Probability distributions for analog-to-target distances, Journal of the Atmospheric Sciences, 78, 3317–3335, 2021a.

Platzer, P., Yiou, P., Naveau, P., Filipot, J.-F., Thiébaut, M., and Tandeo, P.: Probability Distributions for Analog-To-Target Distances, Journal of the Atmospheric Sciences, 78, 3317 – 3335, https://doi.org/10.1175/JAS-D-20-0382.1, 2021b.

Poincaré, H.: Introduction, Acta Mathematica, 13, 5 – 7, https://doi.org/10.1007/BF02392506, 1900.

Rajagopalan, B. and Lall, U.: A k-nearest-neighbor simulator for daily precipitation and other weather variables, Water resources research, 35, 3089–3101, 1999.

Rashid, H. A., Hendon, H. H., Wheeler, M. C., and Alves, O.: Prediction of the Madden–Julian oscillation with the POAMA dynamical prediction system, Clim Dyn, 36, 649–661, https://doi.org/10.1007/s00382-010-0754-x, 2011.

Reichler, T. and Roads, J. O.: Long-range predictability in the tropics. Part II: 30–60-day variability, Journal of climate, 18, 634–650, 2005.

Richardson, C. W.: Stochastic simulation of daily precipitation, temperature, and solar radiation, Water Resour. Res., 17, 182–190, https://doi.org/10.1029/WR017i001p00182, 1981.

Robertson, A. W. and Vitart, F.: SUB-SEASONAL TO SEASONAL PREDICTION: The Gap Between Weather and Climate Forecasting, vol. 569, Elsevier, 2019.

Robin, Y., Yiou, P., and Naveau, P.: Detecting changes in forced climate attractors with Wasserstein distance, Nonlinear Processes in Geophysics, 24, 393–405, 2017.

Rodrigues, D., Alvarez-Castro, M. C., Messori, G., Yiou, P., Robin, Y., and Faranda, D.: Dynamical properties of the North Atlantic atmospheric circulation in the past 150 years in CMIP5 models and the 20CRv2c reanalysis, Journal of Climate, 31, 6097–6111, 2018.

Rodwell, M. and Palmer, T.: Using NWP to assess climate models., p. 26, https://doi.org/10.21957/74cdjc70y, 2007.

Rogers, D. P., Shapiro, M. A., Brunet, G., Cohen, J.-C., Connor, S. J., Diallo, A. A., Elliott, W., Haidong, K., Hales, S., Hemming, D., et al.: Health and climate–opportunities, Procedia Environmental Sciences, 1, 37–54, 2010.

Roulston, M. S., Kaplan, D. T., Hardenberg, J., and Smith, L. A.: Using medium-range weather forcasts to improve the value of wind energy production, Renewable Energy, 28, 585–602, 2003.

Rousseau, D.-D., Bagniewski, W., and Lucarini, V.: A Punctuated Equilibrium Analysis of the Climate Evolution of Cenozoic: Hierarchy of Abrupt Transitions, 2022.

Ruelle, D. and Takens, F.: On the nature of turbulence, Les rencontres physiciens-mathématiciens de Strasbourg-RCP25, 12, 1–44, 1971.

Sankarasubramanian, A., Lall, U., Souza Filho, F. A., and Sharma, A.: Improved water allocation utilizing probabilistic climate forecasts: Short-term water contracts in a risk management framework, Water Resources Research, 45, 2009.

Schepen, A., Wang, Q., and Robertson, D. E.: Combining the strengths of statistical and dynamical modeling approaches for forecasting Australian seasonal rainfall, Journal of Geophysical Research: Atmospheres, 117, 2012.

Schultz, D., Spiegel, S., Marwan, N., and Albayrak, S.: Approximation of diagonal line based measures in recurrence quantification analysis, Physics Letters A, 379, 997–1011, https://doi.org/https://doi.org/10.1016/j.physleta.2015.01.033, 2015.

Semmlow, J.: Chapter 10 - Stochastic, Nonstationary, and Nonlinear Systems and Signals, in: Circuits, Signals and Systems for Bioengineers (Third Edition), edited by Semmlow, J., Biomedical Engineering, pp. 449–489, Academic Press, third edition edn., https://doi.org/https://doi.org/10.1016/B978-0-12-809395-5.00010-2, 2018.

Shukla, J.: Predictability in the midst of chaos: A scientific basis for climate forecasting, science, 282, 728–731, 1998.

Shukla, J., DelSole, T., Fennessy, M., Kinter, J., and Paolino, D.: Climate model fidelity and projections of climate change, Geophysical Research Letters, 33, 2006.

Silini, R., Barreiro, M., and Masoller, C.: Machine learning prediction of the Madden-Julian oscillation, npj Clim Atmos Sci, 4, 57, https://doi.org/10.1038/s41612-021-00214-6, 2021.

Silini, R., Lerch, S., Mastrantonas, N., Kantz, H., Barreiro, M., and Masoller, C.: Improving the prediction of the Madden-Julian Oscillation of the ECMWF model by post-processing, EGUsphere, 2022, 1–15, https://doi.org/10.5194/egusphere-2022-2, 2022.

Sonnewald, M., Lguensat, R., Jones, D. C., Dueben, P., Brajard, J., and Balaji, V.: Bridging observations, theory and numerical simulation of the ocean using machine learning, Environmental Research Letters, 2021.

Specq, D. and Batté, L.: Do subseasonal forecasts take advantage of Madden–Julian oscillation windows of opportunity?, Atmospheric Science Letters, 2020a.

Specq, D. and Batté, L.: Improving subseasonal precipitation forecasts through a statistical–dynamical approach : application to the southwest tropical Pacific, Clim Dyn, p. 15, 2020b.

Specq, D., Bellon, G., and Peltier, A.: Influence of Subseasonal Variability on the Diurnal Cycle of Precipitation on a Mountainous Island: The Case of New Caledonia, MONTHLY WEATHER REVIEW, 148, 19, 2022.

Stott, P. A., Christidis, N., Otto, F. E., Sun, Y., Vanderlinden, J.-P., van Oldenborgh, G. J., Vautard, R., von Storch, H., Walton, P., Yiou, P., et al.: Attribution of extreme weather and climate-related events, Wiley Interdisciplinary Reviews: Climate Change, 7, 23–41, 2016.

Straub, K. H.: MJO Initiation in the Real-Time Multivariate MJO Index, Journal of Climate, 26, 1130–1151, https://doi.org/10.1175/JCLI-D-12-00074.1, 2013.

Süveges, M.: Likelihood estimation of the extremal index, Extremes, 10, 41–55, 2007.

Thorpe, M., Park, S., Kolouri, S., Rohde, G. K., and Slepčev, D.: A Transportation Lˆ p L p Distance for Signal Analysis, Journal of mathematical imaging and vision, 59, 187–210, 2017.

Toth, Z.: Intercomparison of Circulation Similarity Measures, Mon. Wea. Rev., 119, 55–64, URL <GotoISI>://A1991FA68200003, 1991.

Tracton, M. S., Mo, K., Chen, W., Kalnay, E., Kistler, R., and White, G.: Dynamical extended range forecasting (DERF) at the National Meteorological Center, Monthly weather review, 117, 1604–1635, 1989.

Tripathi, O. P., Baldwin, M., Charlton-Perez, A., Charron, M., Eckermann, S. D., Gerber, E., Harrison, R. G., Jackson, D. R., Kim, B.-M., Kuroda, Y., et al.: The predictability of the extratropical stratosphere on monthly time-scales and its impact on the skill of tropospheric forecasts, Quarterly Journal of the Royal Meteorological Society, 141, 987–1003, 2015.

Türkes, M., Sümer, U., and Kiliç, G.: Persistence and periodicity in the precipitation series of Turkey and associations with 500 hPa geopotential heights, Clim. Res., 21, 59–81, https://doi.org/10.3354/cr021059, 2002.

Vaittinada Ayar, P., Vrac, M., Bastin, S., Carreau, J., Déqué, M., and Gallardo, C.: Intercomparison of statistical and dynamical downscaling models under the EURO-and MED-CORDEX initiative framework: present climate evaluations, Climate dynamics, 46, 1301–1329, 2016.

Van den Dool, H.: Searching for analogues, how long must we wait?, Tellus A, 46, 314–324, 1994.

van den Dool, H. M.: Empirical Methods in Short-Term Climate Prediction, Oxford University Press, 2007.

Vannitsem, S., Wilks, D. S., and Messner, J.: Statistical postprocessing of ensemble forecasts, Elsevier, 2018.

Vitart, F.: Evolution of ECMWF sub-seasonal forecast skill scores, Quarterly Journal of the Royal Meteorological Society, 140, 1889–1899, 2014.

Vitart, F.: Madden—Julian Oscillation prediction and teleconnections in the S2S database, Quarterly Journal of the Royal Meteorological Society, 143, 2210–2220, https://doi.org/https://doi.org/10.1002/qj.3079, 2017a.

Vitart, F.: Madden—Julian Oscillation prediction and teleconnections in the S2S database, Quarterly Journal of the Royal Meteorological Society, 143, 2210–2220, https://doi.org/https://doi.org/10.1002/qj.3079, _eprint: https://rmets.onlinelibrary.wiley.com/doi/pdf/10.1002/qj.3079, 2017b.

Vitart, F. and Molteni, F.: Simulation of the Madden- Julian Oscillation and its teleconnections in the ECMWF forecast system: Simulation of the Madden- Julian Oscillation, Q.J.R. Meteorol. Soc., 136, 842–855, https://doi.org/10.1002/qj.623, 2010.

Vitart, F. and Robertson, A. W.: The sub-seasonal to seasonal prediction project (S2S) and the prediction of extreme events, npj Climate and Atmospheric Science, 1, 3, https://doi.org/10.1038/s41612-018-0013-0, 2018.

Vitart, F., Ardilouze, C., Bonet, A., Brookshaw, A., Chen, M., Codorean, C., Déqué, M., Ferranti, L., Fucile, E., Fuentes, M., Hendon, H., Hodgson, J., Kang, H.-S., Kumar, A., Lin, H., Liu, G., Liu, X., Malguzzi, P., Mallas, I., Manoussakis, M., Mastrangelo, D., MacLachlan, C., McLean, P., Minami, A., Mladek, R., Nakazawa, T., Najm, S., Nie, Y., Rixen, M., Robertson, A. W., Ruti, P., Sun, C., Takaya, Y., Tolstykh, M., Venuti, F., Waliser, D., Woolnough, S., Wu, T., Won, D.-J., Xiao, H., Zaripov, R., and Zhang, L.: The Subseasonal to Seasonal (S2S) Prediction Project Database, Bulletin of the American Meteorological Society, 98, 163–173, https://doi.org/10.1175/BAMS-D-16-0017.1, 2017.

Waliser, D., Lau, K., Stern, W., and Jones, C.: Potential predictability of the Madden–Julian oscillation, Bulletin of the American Meteorological Society, 84, 33–50, 2003.

Webber Jr, C. L. and Zbilut, J. P.: Recurrence quantification analysis of nonlinear dynamical systems, Tutorials in contemporary nonlinear methods for the behavioral sciences, 94, 26–94, 2005.

Weisstein, E. W.: Lorenz attractor, https://mathworld. wolfram. com/, 2002.

Weisstein, E. W.: Strange attractor, https://mathworld. wolfram. com/, 2003.

Wetterhall, F., Halldin, S., and Xu, C.-y.: Statistical precipitation downscaling in central Sweden with the analogue method, Journal of Hydrology, 306, 174–190, 2005.

Wheeler, M. C. and Hendon, H. H.: An All-Season Real-Time Multivariate MJO Index: Development of an Index for Monitoring and Prediction, MONTHLY WEATHER REVIEW, 132, 16, 2004.

Whitaker, J. S. and Weickmann, K. M.: Subseasonal variations of tropical convection and week-2 prediction of wintertime western North American rainfall, Journal of climate, 14, 3279–3288, 2001.

Wilks, D. S.: Statistical methods in the atmospheric sciences, vol. 100, Academic press, 2011.

Wilks, D. S. and Wilby, R. L.: The weather generation game: a review of stochastic weather models, Progress in Physical Geography: Earth and Environment, 23, 329–357, https://doi.org/10.1177/030913339902300302, 1999.

WMO: World Mteorological Organisation: SUBSEASONAL TO SEASONAL PREDICTION - RESEARCH IMPLEMENTATION PLAN, URL https://ane4bf-datap1.s3-eu-west-1.amazonaws.com/wmocms/s3fs-public/article_bulletin/related_docs/Implementation_plan_V6.4_nolinenos.pdf, accessed: 2022-10-22, 2012.

WMO: World meteorological organisation:État du climat en 2021: des phénomènes météorologiques extrêmes et de lourdes conséquences, URL https://public.wmo.int/fr/medias/communiquÃĺs-de-presse/Ãľtat-du-climat-en-2021-des-phÃĺnomÃĺnes-mÃľtÃľorologiques-extrÃłmes-et-de, accessed: 2022-10-22, 2021.

Wu, C.-H. and Hsu, H.-H.: Topographic influence on the MJO in the Maritime Continent, Journal of Climate, 22, 5433–5448, 2009.

Wu, H., Hayes, M. J., Wilhite, D. A., and Svoboda, M. D.: The effect of the length of record on the standardized precipitation index calculation, International Journal of Climatology: A Journal of the Royal Meteorological Society, 25, 505–520, 2005.

Wu, J., Ren, H.-L., Zuo, J., Zhao, C., Chen, L., and Li, Q.: MJO prediction skill, predictability, and teleconnection impacts in the Beijing Climate Center Atmospheric General Circulation Model, Dynamics of Atmospheres and Oceans, 75, 78–90, https://doi.org/https://doi.org/10.1016/j.dynatmoce.2016.06.001, 2016.

Wu, M.-L. C., Schubert, S. D., Suarez, M. J., Pegion, P. J., and Waliser, D. E.: Seasonality and meridional propagation of the MJO, Journal of climate, 19, 1901–1921, 2006.

Xoplaki, E., Luterbacher, J., Burkard, R., Patrikas, I., and Maheras, P.: Connection between the large-scale 500 hPa geopotential height fields and precipitation over Greece during wintertime, Clim. Res., 14, 129–146, https://doi.org/10.3354/cr014129, 2000.

Yang, D. and Ingersoll, A. P.: Triggered convection, gravity waves, and the MJO: A shallow-water model, Journal of the atmospheric sciences, 70, 2476–2486, 2013.

Yiou, P.: AnaWEGE: a weather generator based on analogues of atmospheric circulation, Geosci. Model Dev., 7, 531–543, https://doi.org/10.5194/gmd-7-531-2014, 2014.

Yiou, P. and Déandréis, C.: Stochastic ensemble climate forecast with an analogue model, Geosci. Model Dev., 12, 723–734, https://doi.org/10.5194/gmd-12-723-2019, 2019.

Yiou, P., Goubanova, K., Li, Z. X., and Nogaj, M.: Weather regime dependence of extreme value statistics for summer temperature and precipitation, Nonlinear Processes in Geophysics, 15, 365–378, 2008.

Yiou, P., Salameh, T., Drobinski, P., Menut, L., Vautard, R., and Vrac, M.: Ensemble reconstruction of the atmospheric column from surface pressure using analogues, Climate Dynamics, 41, 1333–1344, https://doi.org/10.1007/s00382-012-1626-3, 2013.

Zamo, M. and Naveau, P.: Estimation of the Continuous Ranked Probability Score with Limited Information and Applications to Ensemble Weather Forecasts, Mathematical Geosciences, 50, 209–234, 2018.

Zhang, C.: Madden-julian oscillation, Reviews of Geophysics, 43, 2005.

Zhang, C.: Madden–Julian Oscillation: Bridging Weather and Climate, Bull. Amer. Meteor. Soc., 94, 1849–1870, https://doi.org/10.1175/BAMS-D-12-00026.1, 2013.

Zhang, C. and Hendon, H. H.: Propagating and standing components of the intraseasonal oscillation in tropical convection, Journal of the atmospheric sciences, 54, 741–752, 1997.

Zhang, C., Adames, Á., Khouider, B., Wang, B., and Yang, D.: Four theories of the Madden-Julian oscillation, Reviews of Geophysics, 58, e2019RG000 685, 2020a.

Zhang, C., Adames, F., Khouider, B., Wang, B., and Yang, D.: Four Theories of the Madden-Julian Oscillation, Rev. Geophys., 58, https://doi.org/10.1029/2019RG000685, 2020b.

Zhao, J., Guo, Z.-H., Su, Z.-Y., Zhao, Z.-Y., Xiao, X., and Liu, F.: An improved multi-step forecasting model based on WRF ensembles and creative fuzzy systems for wind speed, Applied Energy, 162, 808–826, 2016.

Zhen, Y., Tandeo, P., Leroux, S., Metref, S., Penduff, T., and Le Sommer, J.: An adaptive optimal interpolation based on analog forecasting: application to SSH in the Gulf of Mexico, Journal of Atmospheric and Oceanic Technology, 37, 1697–1711, 2020.

Zuo, J., Ren, H.-L., Li, W., and Wang, L.: Interdecadal variations in the relationship between the winter North Atlantic Oscillation and temperature in south-central China, Journal of Climate, 29, 7477–7493, 2016.

Appendix

Appendix A

Supplement of the article "Assessment of stochastic weather forecast of precipitation near European cities, based on analogs of circulation"

Geosci. Model Dev., 15, 4941–4958, 2022
https://doi.org/10.5194/gmd-15-4941-2022

Geoscientific Model Development
Open Access
EGU

Assessment of stochastic weather forecast of precipitation near European cities, based on analogs of circulation

Meriem Krouma[1,2], **Pascal Yiou**[2], **Céline Déandreis**[1], **and Soulivanh Thao**[2]

[1]ARIA Technologies, 8 Rue de la Ferme, 92100 Boulogne-Billancourt, France
[2]Laboratoire des Sciences du Climat et de l'Environnement, UMR 8212 CEA-CNRS-UVSQ, IPSL & Université Paris-Saclay, 91191 Gif-sur-Yvette, France

Correspondence: Meriem Krouma (meriem.krouma@lsce.ipsl.fr)

Received: 9 February 2021 – Discussion started: 24 March 2021
Revised: 13 May 2022 – Accepted: 20 May 2022 – Published: 28 June 2022

Abstract. In this study, we assess the skill of a stochastic weather generator (SWG) to forecast precipitation in several cities in western Europe. The SWG is based on a random sampling of analogs of the geopotential height at 500 hPa ($Z500$). The SWG is evaluated for two reanalyses (NCEP and ERA5). We simulate 100-member ensemble forecasts on a daily time increment. We evaluate the performance of SWG with forecast skill scores and we compare it to ECMWF forecasts.

Results show significant positive skill score (continuous rank probability skill score and correlation) compared with persistence and climatology forecasts for lead times of 5 and 10 d for different areas in Europe. We find that the low predictability episodes of our model are related to specific weather regimes, depending on the European region. Comparing the SWG forecasts to ECMWF forecasts, we find that the SWG shows a good performance for 5 d. This performance varies from one region to another. This paper is a proof of concept for a stochastic regional ensemble precipitation forecast. Its parameters (e.g., region for analogs) must be tuned for each region in order to optimize its performance.

1 Introduction

Ensemble weather forecasts were designed to overcome the issues of meteorological chaos, from which small uncertainties in initial conditions can lead to a wide range of possible trajectories (Sivillo et al., 1997; Palmer, 2000). Hence, from a sufficiently large ensemble of initial conditions, it is in principle possible to sample the probability distribution of future states of the system.

Forecasts issued by meteorological centers are obtained by computing several simulations with perturbed initial conditions, in order to sample uncertainties. Those experiments are rather costly in terms of computing resources and are generally limited to a few tens of members (Hersbach et al., 2020; Toth and Kalnay, 1997), which can hinder a proper estimate of probability distributions of trajectories. Moreover, obtaining information at local spatial scales can be difficult because the horizontal resolution of the atmospheric models is around 18 km, e.g., for the European Centre for Medium-Range Weather Forecasts (ECMWF) ensemble forecast system.

From a mathematical point of view, computing the probability distribution of the trajectories of a (deterministic) system makes the underlying assumption that the system behaves like a stochastic process, for which statistical properties are defined naturally (Ruelle, 1979; Eckmann and Ruelle, 1985). This has justified the development of stochastic weather generators (SWG), which are stochastic processes that emulate the behavior of key climate variables (Ailliot et al., 2015). The advantages of stochastic models are a relative simplicity of implementation and a low computing cost. The challenge of their development is to verify that the behavior of the simulations is realistic, according to well-defined criteria (van den Dool, 2007; Jolliffe and Stephenson, 2012).

The first stochastic weather generators were devised to simulate rainfall occurrence (Gabriel and Neumann, 1962) and to simulate rainfall amounts (Todorovic and Woolhiser,

Published by Copernicus Publications on behalf of the European Geosciences Union.

Appendix A. Supplement of the article "Assessment of stochastic weather forecast of precipitation near European cities, based on analogs of circulation"

1975). SWGs were developed and used to estimate the probability distributions of climate variables such as temperature, solar radiation, and precipitation through extensive simulations (Richardson, 1981).

Stochastic weather generators can be useful complements to atmospheric circulation models, in order to simulate large ensembles of local variables, as they can be calibrated for small spatial scales compared with numerical models (Ailliot et al., 2015). This explains their wide applications in impact studies.

A successful simulation with a SWG relies on the choice of inputs. The atmospheric circulation can be chosen a predictor for other local variables. The (loose) rationale for this choice is that the circulation is modeled by prognostic equations (Peixoto and Oort, 1992), which drive the other physical variables. Therefore, the primitive equations of the atmosphere (Peixoto and Oort, 1992, Chap. 3) suggest that reproducing temporal variability on daily time scales requires considering circulation variables. The influence of large-scale circulation on local climate variables has been proven in previous studies such as the influence of atmospheric circulation on the Mediterranean Basin (Mastrantonas et al., 2021) and Greece's precipitation (Xoplaki et al., 2000; Türkes et al., 2002). Similar influences have been found on precipitation and temperature over the North Atlantic region (Jézéquel et al., 2018).

Analogs of circulation were initially designed to provide "model-free" forecasts by assuming that similar situations in atmospheric circulation may lead to similar local weather conditions (Lorenz, 1969). The potential to simulate large ensembles of forecast temperature with circulation analogs was explored by Yiou and Déandréis (2019) by considering random resamplings of K best analogs (rather than only considering the best analog). This has led to the development of an SWG in "predictive" mode, which uses updates of reanalysis datasets as input.

Alternative systems of analogs to forecast precipitation have been proposed by Atencia and Zawadzki (2014). Those systems are based on analogs of precipitation itself. Such systems are very efficient for nowcasting, i.e., forecasting precipitation within the next few hours. Considering the atmospheric circulation analogs allows focusing on longer time scales.

Yiou and Déandréis (2019) evaluated ensemble forecasts of the analog SWG for temperature and the NAO index with classical probability scores against climatology and persistence. Reasonable scores were obtained up to 20 d. Through this study, we aim to assess the skill of this SWG to forecast precipitation in different areas of Europe and for different lead times. The previous study on this forecasting tool was a proof of concept for temperature. In this study, we will adapt the parameters of the analog SWG to optimize the simulation of European precipitations. We then analyze the performance of this SWG for lead times of 5–20 d, with the forecast skill scores used by Yiou and Déandréis (2019).

We will evaluate the seasonal dependence of the forecast skills of precipitation and the conditional dependence on weather regimes. Finally, comparisons with medium-range precipitation forecasts from the ECMWF will be performed.

The paper is divided as follows: Section 2 is dedicated to describing the data used for the experiments. Section 3 explains the methodology (analogs, stochastic weather generator, and forecast skill scores). Section 4 details the experimental setup and justifies the choice of parameters that we made for the forecast parameters. Section 5 details the results of simulations and the evaluation of the ensemble forecast. Section 6 contains the main conclusions of the analyses.

2 Data

Daily precipitation data were obtained from the European Climate Assessment and Data (ECAD) project (Klein Tank et al., 2002) for four locations in western Europe (Berlin, Madrid, Orly, and Toulouse), which are subject to contrasted meteorological influences (Fig. 1). The ECAD provides station data that are available at a daily time step from 1948 to 2019. The choice of those stations was based on the availability of a large and common period of observations with a low rate of missing data (less than 10 %). For verification purposes, we used also the E-Obs data (Haylock et al., 2008), which are a daily gridded data available from 1979 to the present with a horizontal resolution of $0.25° \times 0.25°$. E-Obs data are spatial interpolations of ECAD data.

We recovered the geopotential height at 500 hPa ($Z500$) and sea level pressure (SLP) fields from the reanalysis of the National Centers for Environmental Prediction (NCEP: Kistler et al., 2001) with a spatial resolution of $2.5° \times 2.5°$ from 1 January 1948 to 31 December 2019.

We also used the atmospheric reanalysis (version 5) of the European Centre for Medium-Range Weather Forecasts (ECMWF) (ERA5; Hersbach et al., 2020). ERA5 data are available from 1950 to the present with a horizontal resolution of $0.25° \times 0.25°$. The two reanalyses have fundamental differences in terms of atmospheric models, assimilated data, and assimilation scheme.

We considered the daily averages of $Z500$ from NCEP and ERA5, over the region covering 30° W–20° E and 40–60° N, to compute circulation analogs. Daily averages of SLP were used over the region covering 80° W–20° E and 30–70° N to define weather regimes.

In order to assess the predictive skill of our precipitation forecast model, a comparison with another forecast was made. Many available datasets can be used for deriving this information. We considered the ECMWF ensemble forecast dataset system 5 (Vitart et al., 2017). It is a daily gridded dataset interpolated over Europe that provides information covering all the domains. Data are available through the Copernicus Climate Data Store. They include forecasts created in real time (since 2017) and hindcast forecasts

from 1993 to 2019 (Vitart et al., 2017). The data are provided at an hourly time step with a horizontal resolution of $0.25° \times 0.25°$. We considered the grid points that include Berlin, Madrid, Orly, and Toulouse, which were identified in the ECAD database.

3 Methodology

3.1 Analogs

The first step is to build a database of analogs of the atmospheric circulation. We outline the procedure of Yiou and Déandréis (2019), summarized in Fig. 1a. For a given day t, we determine the similarity of $Z500$ for all days t' that are within 30 calendar days of t but in a different year from t. The similarity is quantified by a Euclidean distance (or root mean square error) between the daily $Z500$ maps. Other types of similarity measures are possible (Blanchet et al., 2018), but the expected impact on the results is often marginal (Toth, 1991). We believe that the simplicity of the Euclidean distance makes it more robust to changes in horizontal resolution (e.g., from NCEP to ERA5), compared with more sophisticated distances that include local spatial gradients, which would require adjustments and additional tuning. This choice can be left open for future fine-tuning, depending on the region.

For each day t, we consider the K best analogs, i.e., for which the distances are the smallest. We compute the spatial rank correlation between the $Z500$ best analogs and the $Z500$ at time t for posterior verification purposes.

As a refinement over the study of Yiou and Déandréis (2019), a time embedding of τ days was used for the search of the analogs dates. This means that the field $X(t)$ for which we compute analogs is $X(t) = (Z500(t), Z500(t+1), \ldots, Z500(t+\tau))$. This ensures that temporal derivatives of the atmospheric field are preserved (Yiou et al., 2013). Hence, the distance that is optimized to find analogs of the $Z500(x,t)$ field is

$$D(t,t') = \left[\sum_x \left(\sum_{i=0}^{\tau} \left|Z500(x,t+i) - Z500(x,t'+i)\right|^2\right)\right]^{\frac{1}{2}}, \quad (1)$$

where x is a spatial index and τ is the embedding time.

We consider different geographic domains as shown in Fig. 1 for the computation of analogs and weather regimes. The computation of circulation analogs was performed with the "blackswan" Web Processing Service (WPS; Hempelmann et al., 2018). The "blackswan" WPS is an online tool that helps compute circulation analogs on various datasets (e.g., reanalyses and climate model simulations) with a user-friendly interface.

3.2 Configuration of stochastic weather generator

We use a stochastic weather generator (SWG) based on a random sampling of the circulation analogs. The operation of the SWG and its design are detailed by Yiou and Déandréis (2019). The aim is to generate random trajectories from the previously computed analogs. Therefore, to generate a trajectory, we proceed as follows: for a given day t_0 in year y_0, we generate a set of $N = 100$ simulations until a time t_0+T, with a lead time $T \in \{5, 10, 20\}$ d. We start at day t_0 and randomly select an analog (out of K analogs) of day $t_0 + 1$. The random selection of analogs of the day $t_0 + 1$ is performed with weights that are proportional to the calendar difference between t_0 and analog dates, to ensure that time goes forward. We also exclude analog dates with years that are equal to y_0. This rule is important for the next iterations. We then replace t_0 by the selected analog of $t_0 + 1$ and repeat the operation T times. Excluding analogs in year y_0 from the selection ensures that we do not use information from the T days that follow t_0. Hence, we obtain a hindcast trajectory between t_0 and $t_0 + T$.

The procedure presented above is repeated $N = 100$ times to simulate $N = 100$ trajectories from t_0 to $t_0 + T_0$. The daily precipitation of each trajectory is time averaged between t_0 and $t_0 + T$. Hence, we obtain an ensemble of $N = 100$ forecasts of the average precipitation for day t_0 and lead time T.

Then t_0 is shifted by $\Delta t \geq 1$ d, and the ensemble simulation procedure is repeated. This provides a set of ensemble forecasts with analogs.

We made a hindcast exercise, where the forecasts of precipitations based on analogs of atmospheric circulation ($Z500$), are started every $\Delta t \approx T/2$ d between 1 January 1948 and 31 December 2019. This yields a stochastic ensemble hindcast of precipitation and atmospheric circulation ($Z500$). In this paper, therefore, we analyze the properties of an ensemble forecast of mean precipitation between t_0 and $t_0 + T$. To evaluate our forecasts, the predictions made with the SWG are compared with the persistence and climatological forecasts. The persistence forecast consists of using the average value between $t_0 - T$ and t_0 for a given year. The climatological forecast takes the climatological mean between t_0 and $t_0 + T$. The two "reference" forecasts are randomized by adding a small Gaussian noise, whose standard deviation is estimated by bootstrapping over T long intervals. We thus generate sets of persistence forecasts and climatological forecasts that are consistent with the observations (Yiou and Déandréis, 2019).

The simulations of this stochastic model will be called "SWG forecasts", as opposed to ECMWF forecasts.

3.3 Forecast verification

Forecast verification is the process of determining the statistical quality of forecasts. A wide variety of ensemble forecast verification procedures exists (Jolliffe and Stephenson, 2012;

Appendix A. Supplement of the article "Assessment of stochastic weather forecast of precipitation near European cities, based on analogs of circulation"

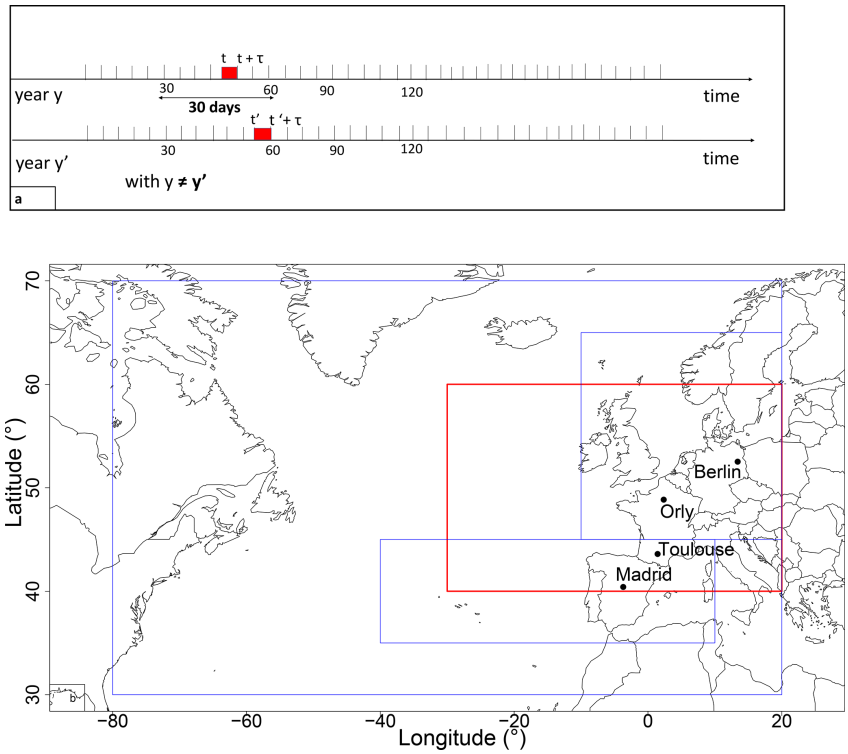

Figure 1. Parameters of the analog computation. **(a)** For each day t in year y, we chose an analog day t' with a similar sequence of τ consecutive day $Z500$ patterns. t_0 is selected within 30 calendar days of t and in a year $y' \neq y$. **(b)** Domains of computation of analogs. We computed analogs over different domains, each one including a part of the Atlantic and focusing on a part of western Europe, in order to test the sensitivity of our model to different geographic areas. The optimizing area was [30° W–20° E; 40–60° N], indicated by the red rectangle.

Wilks, 1995). They involve measures of the relationship between a set of forecasts and corresponding observations. To assess the quality of precipitation forecasts, we compute indicators such as the correlation and continuous rank probability skill score (CRPSS) for each lead time T, for different seasons and months.

The temporal rank correlation (referred to as correlation skill) is calculated between the precipitation observations and the median of 100 simulations. This simple diagnostic is often used to assess forecast skills of indices (Scaife et al., 2014).

The continuous ranked probability score (CRPS) is widely used for probabilistic forecast verification (Ferro, 2007). It is sensitive to the distance between forecast and observation probability distributions.

If the ensemble forecast x yields a probability distribution $P(x)$ for a value x_a, the CRPS measures how the probability distribution of x compares with x_a (Hersbach, 2000).

The CRPS is computed as

$$\mathrm{CRPS}(P, x_a) = \int_{-\infty}^{+\infty} (P(x) - \mathcal{H}(x - x_a))^2 \mathrm{d}x, \quad (2)$$

where x_a is the observation and $\mathcal{H}$ is the Heaviside function of the occurrence of x_a ($\mathcal{H}(y) = 1$ if $y \geq 0$, and $\mathcal{H}(y) = 0$ otherwise). The decomposition and properties of the CRPS have been investigated by Ferro (2007), Hersbach (2000), and Zamo and Naveau (2018). A perfect forecast would have a CRPS equal to 0, but the CRPS value obviously depends on the units of the variable to forecast, so quantifying what is a "good" forecast requires a normalization. It is hence difficult to compare CRPS values for temperature and precipitation, within the same ensemble forecast. This issue is also acute for non-Gaussian variables with heavy tails (Zamo and Naveau, 2018) so that the interpretation of a given CRPS value might not be informative.

One way of circumventing this difficulty is to compare CRPS values to reference forecasts, such as persistence or climatology. The continuous rank probability skill score (CRPSS) is a normalization of Eq. (2) with respect to such a reference.

The CRPSS is hence computed by

$$\mathrm{CRPSS} = 1 - \frac{\overline{\mathrm{CRPS}}}{\overline{\mathrm{CRPS}_{\mathrm{ref}}}}, \quad (3)$$

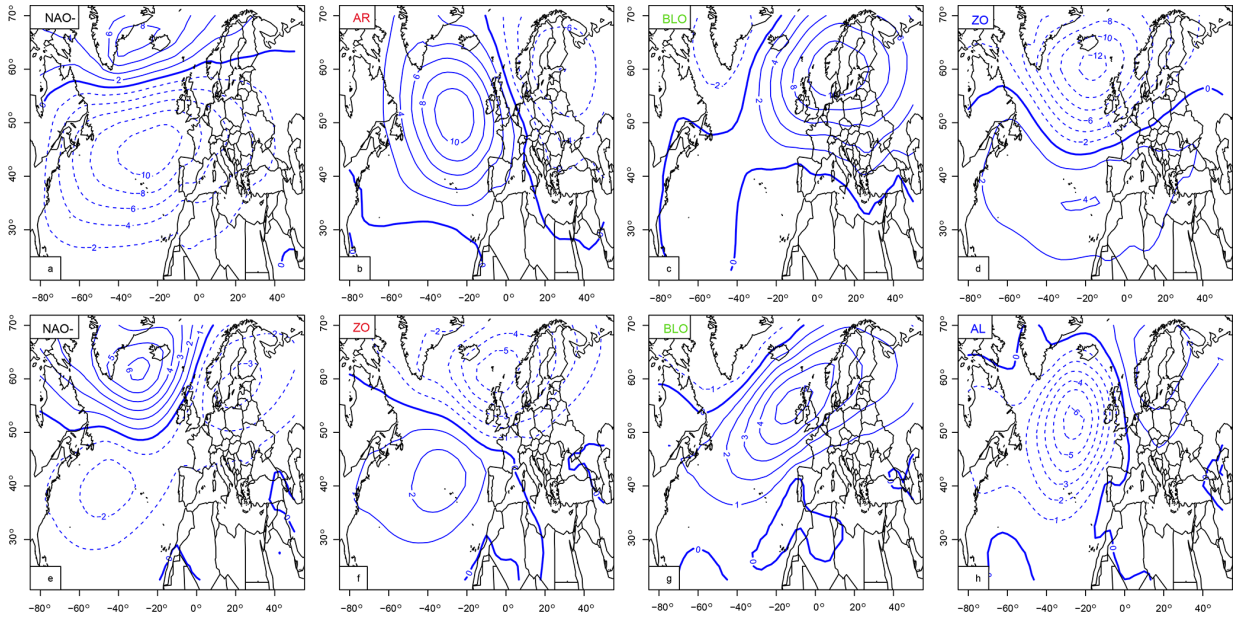

Figure 2. Weather regimes over Europe from SLP fields. Upper panels **(a)**–**(d)** contain winter (December–January–February: DJF) regimes: negative phase of the North Atlantic oscillation (NAO−), Atlantic Ridge (AR), Scandinavian blocking (BLO), and Zonal regime (ZO). Lower panels **(e)**–**(h)** contain summer (June–July–August: JJA) weather regimes: negative phase of the North Atlantic oscillation (NAO−), Zonal (ZO), Scandinavian blocking (BLO) and Atlantic low (AL). The isolines show seasonal anomalies with respect to a DJF and JJA, in hPa with 2 hPa increments.

where $\overline{\text{CRPS}}$ is the time average of the CRPS of the SWG forecast and $\overline{\text{CRPS}_{\text{ref}}}$ is the time average of the CRPS of the reference (either climatology or persistence). The CRPSS is interpreted as a fraction of improvement over a reference forecast.

The values of the CRPSS vary between $-\infty$ and 1. The forecast is considered to be an improvement over the reference when the CRPSS value is positive. Values of CRPSS equal to 0 indicate no improvement over the reference. Values inferior to 0 mean that the forecast is worse than the reference.

We use the CRPSS values to determine the maximum lead time T for which the SWG forecast is better than references. Then the SWG assessments will use the CRPS and directly compare the probability distributions of precipitation ensemble forecasts.

3.4 Dependence of forecast on weather regimes

We investigated the role of North Atlantic weather patterns on the forecast quality by attributing CRPS values of the SWG precipitation simulations to weather regimes. Weather regimes are defined as large-scale quasi-stationary atmospheric states. They are characterized by their recurrence, persistence, and stationarity (Michelangeli et al., 1995). They help in describing the features of the atmospheric circulation. Surface variables like temperature and precipitation are largely correlated with weather regimes (van der Wiel et al., 2019).

The North Atlantic weather regimes were computed with the procedure of Yiou et al. (2008), with the NCEP reanalysis. The first 10 principal components of SLP (large region in Fig. 1b) were classified with a k-means algorithm onto four classes over a reference period between 1970 and 2010. The procedure was repeated 100 times with random k-means initialization. Then we classified the resulting 100×4 k-means weather regimes in order to determine the most probable classification. This heuristic procedure increases the robustness of the obtained weather regimes. Figure 2 shows four weather regimes for each season (winter and summer) that are coherent with the literature (Cassou et al., 2011; Ghil et al., 2008; Kimoto, 2001; Michelangeli et al., 1995).

The winter weather regimes are the negative phase of the North Atlantic oscillation (NAO−), Atlantic Ridge (AR), Scandinavian blocking (BLO), and Zonal (ZO). The summer weather regimes are the negative phase of the NAO (NAO−), Zonal (ZO), Scandinavian blocking (BLO), and Atlantic low (AL). The regimes are not the same in both seasons due to the seasonality of the large-scale atmospheric circulation.

For each day (in winter and summer) between 1948 and 2019, we classified the SLP by minimizing the root mean square to four reference (1970–2010) weather regimes.

For each day t (within a given season), we considered the analog dates of all $N = 100$ simulations between t and $t +$

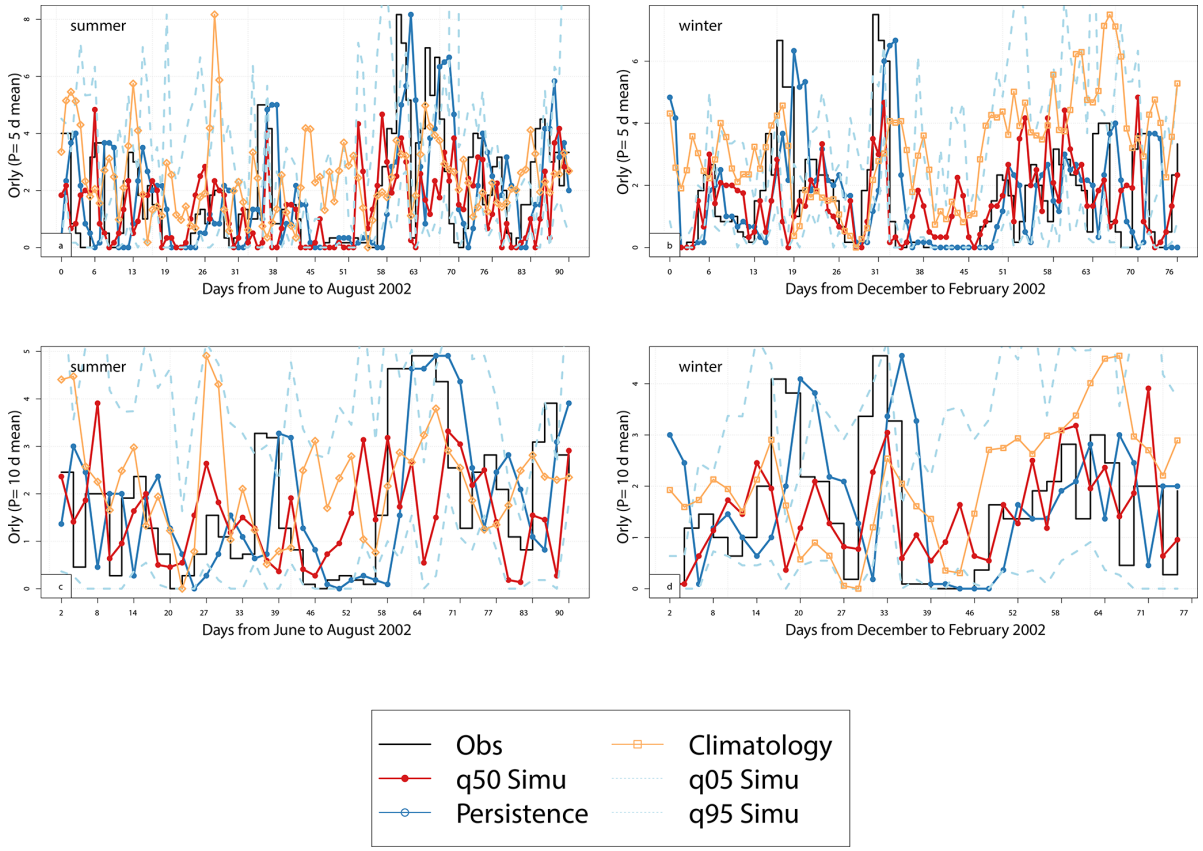

Figure 3. Time series of analog ensemble forecasts for 2002, for lead times of 5 d **(a, b)** and 10 d **(c, d)** for summer (June to August) **(a)** and **(c)** and winter (December to February) **(b)** and **(d)** for Orly. The median of 100 simulations is represented by the red line. The black line represents observation values. Dashed lines represent the 5th and 95th quantiles. The blue line represents the persistence forecasts and the orange line represents the climatology forecasts. The y-axis represents the average precipitation over $T = 5, 10$ d.

T and the corresponding classification into weather regimes. Then we determined the most frequent weather regime of the N member ensemble forecast between t and $t+T$. We hence obtained time series on the most likely weather pattern that dominates in the ensemble forecast between t and $t+T$.

We evaluated the influence of the dominating weather regimes on the SWG forecast quality by plotting the probability distribution of CRPS values *conditioned* on the weather regimes. This is done separately for "good" forecasts (low CRPS values) and "poor" forecasts (high CRPS values).

We identified two classes of predictability from CRPS values:

- Low predictability is related to high values of CRPS that exceed the 75th quantile.
- High predictability is linked to low values of CRPS, below the 25th quantile.

Then we associated the dominating weather regimes computed above with classes of high or low predictability. This procedure helps in identifying atmospheric patterns that could lead to low or high predictability with the SWG model.

4 Stochastic weather generator parameter optimization

We started by verifying the relationship between $Z500$ over the Euro-Atlantic region and the precipitation in the four studied areas to ensure that $Z500$ analogs would be reasonable predictors of precipitation. We show the maps of the temporal rank correlation between the daily average of $Z500$ and the precipitation in Appendix B1. We found a significant negative correlation between $Z500$ and the precipitation with p values ≤ 0.05.

Then we empirically adjusted the parameters of the SWG simulations to optimize the forecast scores. The first parameter is the geographic area. We computed sample trajectories of the SWG for the four domains outlined in Fig. 1b. We used different domains in order to find an optimal region that

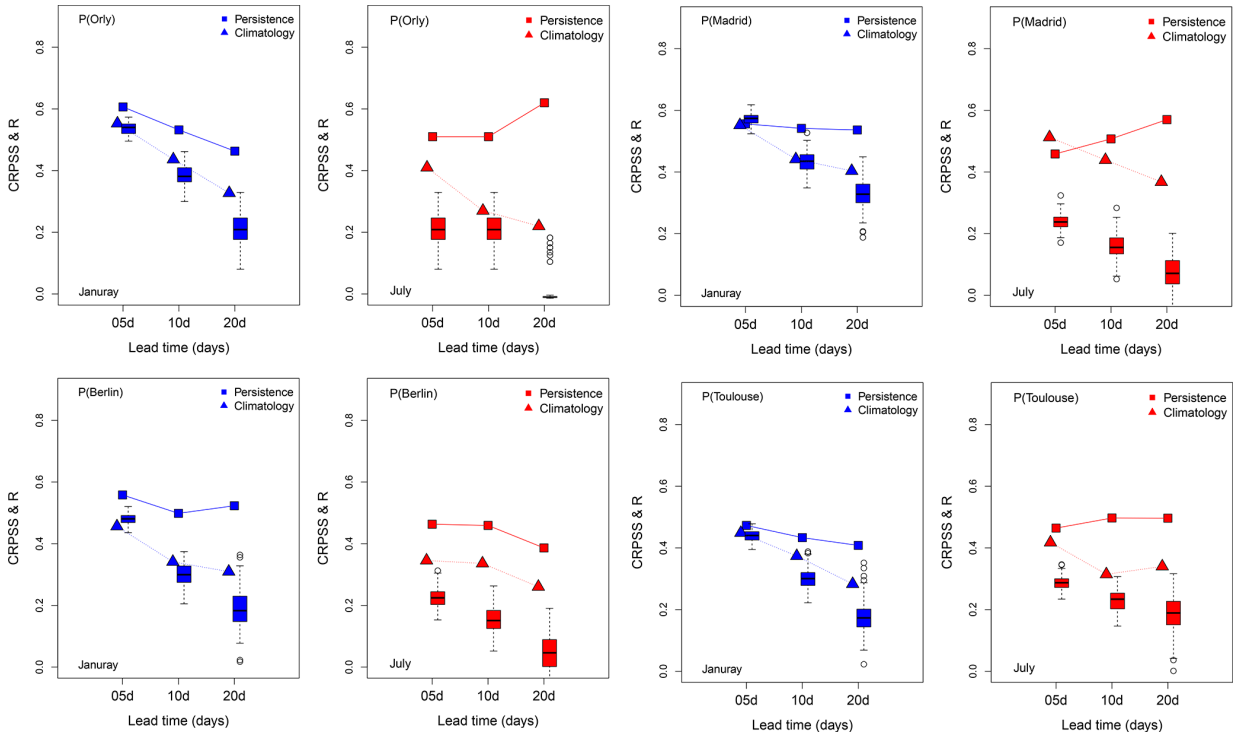

Figure 4. Skill scores for the precipitation of Orly, Madrid, Berlin, and Toulouse for lead times of 5, 10, 20 d for January (blue) and July (red) for analogs computed from reanalyses of NCEP. Squares indicate CRPSS where the persistence is the baseline, triangles indicate CRPSS where the climatology is the reference, and boxplots indicate the probability distribution of correlation between observation and the median of 100 simulations for all days. The boxplot upper whisker is: $\min\{1.5(q_{75}-q_{50})+q_{50}, \max(\text{CRPSS})\}$. The boxplot lower whisker is: $\max\{q_{50}-1.5(q_{75}-q_{50}), \min(\text{CRPSS})\}$.

allows verifying the relationship between precipitation and $Z500$ for the four studied areas. Each domain included a part of the Atlantic and a part of western Europe. We chose the widest domain with the coordinates 80° W–20° E and 30–70° N in order to catch the variability in the whole Euro-Atlantic region; however, this large domain gave the poorest skill scores for precipitation forecasting for the studied areas as shown in Table 1. Then we focused on two smaller domains (outlined in blue in Fig. 1b): one centered over northern Europe and the other centered over southern Europe. We found better forecast skills for specific locations. The same level of performance was found for the domain (outlined in red in Fig. 1b) with coordinates 30° W–20° E and 40–60° N. Therefore, we kept this domain for the subsequent analyses, because it allows optimizing the correlations between $Z500$ and precipitation for the four studied areas and the time of computation of analogs at the same time. We compared the skill scores over the geographic domain with the coordinates [80° W–20° E; 30–70° N] and [30° W–20° E; 40–60° N]. We determined that the SWG simulations showed a better skill for the geographic domain (outlined in red in Fig. 1b) and the skill scores remained the highest ones as represented in Table 1.

The second parameter is the number K of the best analogs that we use to simulate the precipitation. Our choice was based on numerical experiments. We performed different SWG simulations where we varied the number of analogs ($K = 5,\ 10,\ 20$). We noticed an improvement in the skill scores by increasing the number of analogs as shown in Table 2. Therefore, we considered $K = 20$ analogs to ensure that we had enough analog dates for the simulations. It appears that the Euclidean distance of analogs grows rather slowly after $K = 20$. Our choice was also supported by a theoretical study by (Platzer et al., 2021) who showed that, for complex systems, the use of a large number of analogs ($K > 30$ analogs) does not change the prediction properties with analogs. Thus, we kept $K = 20$ best analogs for the rest of the analyses.

We quantified the dependence of the forecast on the time embedding for the analogs τ by calculating the analogs based on different embedding values from $\tau = 1$– 4 d. We found that an embedding of 4 d helped to better catch the persistence and improve the skill scores for the forecast compared

Appendix A. Supplement of the article "Assessment of stochastic weather forecast of precipitation near European cities, based on analogs of circulation"

Table 1. Correlation between observations and the median of 100 simulations for the winter (DJF) for the different studied domains represented in Fig. 1b, with the coordinates [80° W–20° E; 30–70° N] for the largest one (blue) and [30° W–20° E; 40°–60° N] for the red rectangle for a lead time of 5 d.

Location	[80° W–20° E; 30–70° N] domain		[30° W–20° E; 40–60° N] domain	
	Correlation	95 % confidence interval	Correlation	95 % confidence interval
Berlin	0.32	0.30–0.35	0.50	0.48–0.56
Madrid	0.35	0.33–0.39	0.53	0.51–0.55
Orly	0.39	0.37–0.41	0.58	0.56–0.59
Toulouse	0.34	0.31–0.36	0.40	0.39–0.44

Table 2. CRPSS versus persistence and climatology for SWG simulations with 5, 10, and 20 analogs for the [30° W–20° E; 40–60° N] domain and for a lead time of 5 d.

Location	$K = 5$ analogs		$K = 10$ analogs		$K = 20$ analogs	
	Persistence	Climatology	Persistence	Climatology	Persistence	Climatology
Berlin	0.29	0.20	0.39	0.31	0.56	0.50
Madrid	0.32	0.31	0. 40	0.39	0.57	0.57
Orly	0.34	0.12	0. 40	0.23	0.60	0.53
Toulouse	0.34	0.24	0.38	0.45	0.41	0.48

with 1 d, as shown in Table 3. Therefore, we kept the forecast based on a 4 d embedding. This choice was based on the numerical experiments performed for the studied locations. This is also supported by the study of Yiou et al. (2013), where the analog computation with time embedding was argued to improve the temporal smoothness of simulations. With such an embedding, forecasts for lead times of $T = 5$ d yield at least two time increments.

For comparison purposes, SWG simulations are obtained using analogs computed from reanalyses on the NCEP and ERA5 reanalyses. By comparing their skill scores, we found that CRPSS and correlations between observations and simulations are positive in both cases, and show positive improvement compared with persistence and climatology forecasts. The CRPSS and correlation for simulations with analogs of NCEP are almost identical to those with ERA5, as shown in Table 4. Therefore, we focused on SWG simulations with analogs from the NCEP reanalysis in the sequel as both NCEP and ERA5 (1950–2019) have the same skill, as shown in Table 4, and because NCEP is easier to handle due to its lower horizontal resolution. The computations were made using observations of precipitation from the ECAD (Klein Tank et al., 2002) and E-Obs (Haylock et al., 2008) databases. We found the same results because the ECAD and E-Obs are highly correlated (by the construction of E-Obs).

In summary, we made the forecast of the precipitation using $K = 20$ analogs computed from $Z500$ over the [30° W–20° E; 40–60° N] domain (red rectangle in Fig. 1b). To compute analogs, we used NCEP reanalyses and an embedding of $\tau = 4$ d. The computations were based on ECAD observations (Klein Tank et al., 2002).

5 Results

5.1 Sample forecast

As an example, we illustrate the behavior of the trajectories in Orly for the summer and winter of 2002. Figure 3 shows the observed and simulated values of precipitation for lead times of 5 and 10 d for summer (June–July–August: JJA) and winter (December–January–February: DJF), for Orly precipitation data. We observe significantly positive correlations between observed values and the median of the forecasts for the four data sets as represented in Table 5. The correlation is generally smaller in the summer than in the winter. The correlation skill is low for some extreme values of precipitation. For a lead time of 10 d, SWG simulation still shows a capacity to predict precipitation, in particular for winter with a correlation equal to 0.23 (Orly), 0.30 (Berlin), 0.43 (Madrid), and 0.31 (Toulouse).

We observe that the 5th and 95th quantiles of the simulations include the different values of observations. This heuristically confirms the good skill of SWG to forecast precipitation from $Z500$ for various seasons (winter and summer) in several locations for $T = 5$ and $T = 10$ d lead times.

The difference in the forecast correlation skills between the four studied locations may be related to the variation of the local climate from one region to another. The studied areas are in different climate types according to the Köppen–Geiger climate classification (Peel et al., 2007). From the southwestern side of Europe, Madrid is in the arid zone of the classification (Peel et al., 2007), which indicates that convective rains are less frequent, and the origin of precipitation

Table 3. Correlation between observations and the median of 100 simulations for the winter (DJF) based on analogs computed with an embedding of 1 and 4 d for the geographic domain with the coordinates [30° W–20° E; 40–60° N] for a lead time of 5 d.

Location	$\tau = 1$ d time embedding		$\tau = 4$ d time embedding	
	Correlation	95 % confidence interval	Correlation	95 % confidence interval
Berlin	0.39	0.37–0.43	0.50	0.48–0.56
Madrid	0.40	0.38–0.42	0.53	0.51–0.55
Orly	0.42	0.39–0.45	0.58	0.56–0.59
Toulouse	0.35	0.34–0.37	0.40	0.39–0.44

Table 4. Comparison between the values of the CRPSS of SWG computed using different reanalysis datasets for NCEP and ERA5 from 1979 to 2019 for a lead time of $T = 5$ d for winter (DJF).

Location	CRPSS DJF (ERA5)	CRPSS DJF (NCEP)
Berlin	0.50	0.50
Madrid	0.55	0.57
Orly	0.53	0.53
Toulouse	0.41	0.41

might be the result of humidity coming from the Atlantic. Conversely, Berlin is located in a cold zone characterized by warm summer and the absence of a dry season (Peel et al., 2007); the precipitation could be the result of both, convective rains and Atlantic humidity.

In this paper, we decided (for simplicity) to use the same analogs to forecast precipitation for those four stations as discussed in Sect. 4. A refinement of the analog regions would be necessary when focusing on Madrid vs. Berlin.

5.2 Forecast probability skill

The CRPSS and correlation skill scores are computed for the four studied stations (Berlin, Madrid, Orly, and Toulouse), as shown in Fig. 4 and for lead times from 5 to 20 d.

In this paper, we chose to present the results for summer and winter to highlight the capacity of the SWG to forecast the precipitation in extreme seasons. We focus on January and July in order to show the skill of the SWG in predicting precipitation in different conditions.

The CRPSS against the persistence and climatology references show positive values for lead times of up to 20 d (Fig. 4). The values of CRPSS against the persistence reference (represented by squares) decrease with lead times in winter for the different studied areas, showing high values over 5 d. However, for summer, we notice that the values of CRPSS against persistence increase with lead time, with high values over 20 d except for Berlin. This indicates that the SWG forecast is still better than the persistence forecast (the average of the CRPS of SWG is smaller than the average of the CRPS of the persistence) for lead times of 20 d in the summer. This could be explained by the fact that summer precipitation in Orly (51 % of the time, on average) comes in clusters contrary to precipitation in Berlin. Indeed, we computed the seasonal frequency of precipitation (defined as the number of days when precipitation exceeds 0.5 mm d^{-1}). We found that for Berlin, precipitation exceeding 0.5 mm d^{-1} is more frequent than in the other stations (close to 50 % of the time for both seasons).

This means that a persistence forecast for Orly is likely to be skillful, even for longer lead times, especially in the summer. Therefore, the trends in CRPSS values for different lead times are probably due to the intrinsic time persistence of local precipitation.

The CRPSS against the climatology reference (triangles in Fig. 4) shows lower values compared with the CRPSS against persistence reference, although they are positive for all lead times and for both seasons. However, we notice that for a short lead time the SWG is better than the climatology.

The correlation skill is positive for both seasons but higher in winter (January) than in summer (July). For a lead time of 5 d, the correlation is equal to 0.59 for Madrid, 0.50 for Berlin, and 0.40 for Toulouse. For a lead time of 10 d, it is equal to 0.42 for Madrid, 0.30 for Berlin, and 0.41 for Toulouse.

The SWG was tested by Yiou and Déandréis (2019) to forecast temperature in western Europe. Comparing the performance of the SWG to forecast those different meteorologic variables, we noticed that the model shows good performance to forecast the temperature in the winter; also the best performance of the model is at a lead time of 5 d. We find that the skill scores (CRPSS and correlation) decrease with lead times. The forecast skill of the SWG shows variability from one location to another. However, the model was able to forecast temperature until 40 d in Berlin, Orly, and Toulouse with positive skill scores.

From a visual inspection of the CRPSS and correlations, we chose to focus on lead times of $T = 5$ d, for which the correlation exceeds 0.5 in the winter. It is rather low in the summer, due to convective events leading to a high precipitation variability (from no rain to very high values). Correlation scores become barely significant for lead times of 20 d, so that, like temperature, the SWG should not be used beyond that horizon.

Table 5. Correlation between observations and the median of 100 simulations for both seasons, winter (DJF) and summer (JJA), for a lead time of 5 d.

Location	Correlation DJF	95 % confidence interval	Correlation JJA	95 % confidence interval
Berlin	0.50	0.48–0.56	0.22	0.21–0.23
Madrid	0.53	0.51–0.55	0.29	0.27–0.30
Orly	0.58	0.56–0.59	0.23	0.20–0.24
Toulouse	0.40	0.39–0.44	0.18	0.15–0.19

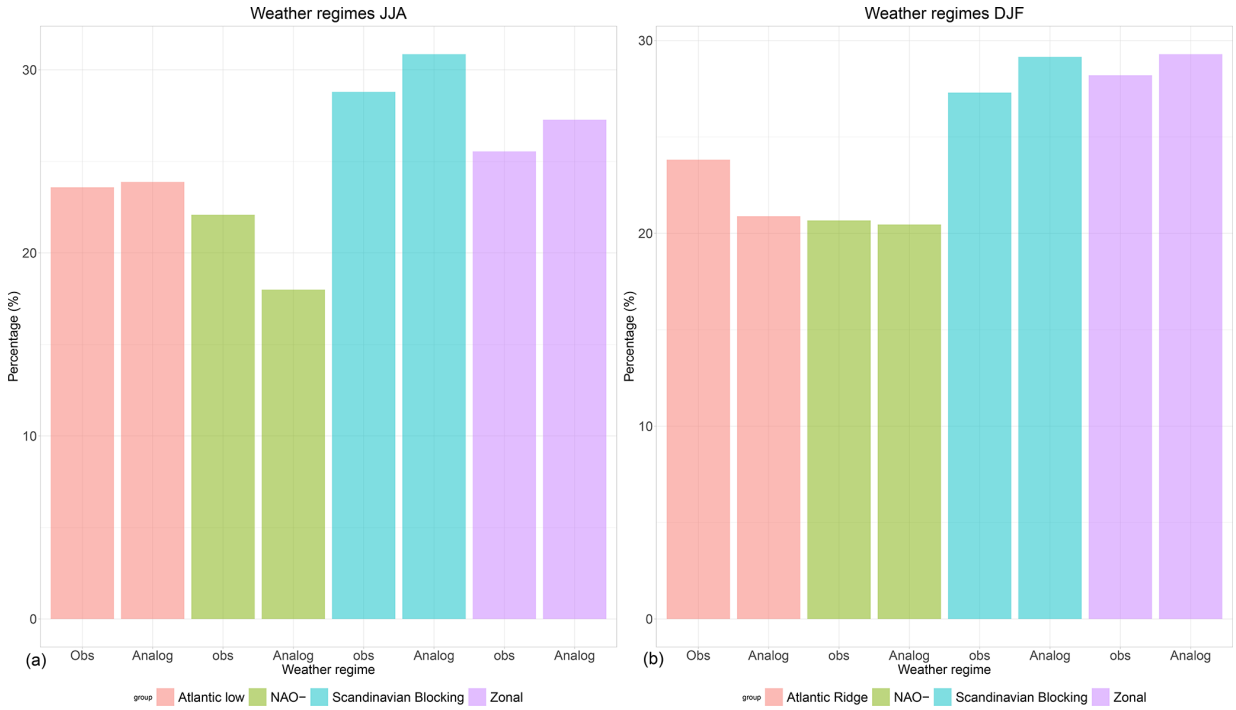

Figure 5. Percentage of each weather regime for observations dates (Obs) and the most frequent weather regime from SWG simulations between t_0 and $t_0 + T = 5$ d (Analog) over the period from 1948 to 2019 for summer (JJA: **a**) and winter (DJF: **b**). The percentage of weather regime is the same in Obs and Analog.

5.3 Relation between weather regimes and CRPS

We investigated the role of North Atlantic weather patterns defined in Sect. 3.4 (Fig. 2) on the forecast skill of the SWG precipitation simulations.

We started by comparing the frequencies of the weather regimes from the observations and the most frequent weather regime found in SWG simulations for a given lead time $T =$ 5 d. We found that the percentages are very similar (Fig. 5). This means that the weather regimes of the simulated trajectories do not yield major biases for the summer or winter seasons.

Then we looked at the relation between weather regimes and CRPS values by using the most frequent weather regime within T days and the two classes of quantiles of the CRPS that related to good quality of forecast (attributed to low values of CRPS $\leq q_{25}$) and poor quality of forecast (attributed to high values of CRPS $\geq q_{75}$). This relation is represented in Fig. 6 for Orly and for the rest of the studied stations in Fig. A1. We found a small influence of specific weather regimes on the CRPS distribution for summer.

The weather regime signal for "good" forecasts depends on the season and the considered station. When the forecast has a low CRPS value (for Orly), we find that the Scandinavian blocking regime slightly dominates (green bar in Fig. 6a, b). This is also the case for Berlin (in winter) and Toulouse (Fig. A1b, j). The low CRPS values in Madrid are obtained for the Atlantic Ridge regime (Fig. A1f).

The weather regime signal for "poor" forecasts also yields a dependence on the season and station. Higher CRPS values are obtained with the Zonal regime in the summer for Orly (red line in Fig. 6c) and Toulouse. The Atlantic Ridge regime

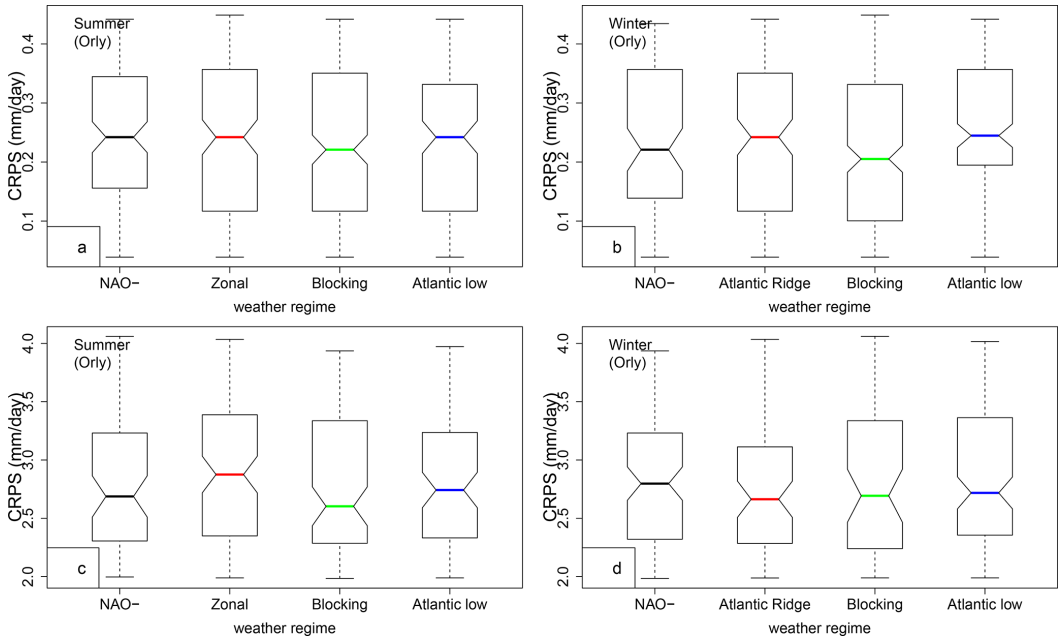

Figure 6. Relation between CRPS and weather regimes for Orly, for SWG forecasts with lead time $T = 5$ d. Panels **(a)** and **(b)** show CRPS value distribution conditioned on four weather regimes, when CRPS is lower than q_{25}. Panels **(c)** and **(d)** show that CRPS is higher than q_{75}. The boxplots indicate the median (q_{50}) of the distribution (thick bar). The 25th (q_{25}) and 75th (q_{75}) quartiles (lower and upper segments of each boxplot). The boxplot upper whisker is $\min\{1.5(q_{75} - q_{50}) + q_{50}, \max(\text{CRPS})\}$. The boxplot lower whisker is $\max\{q_{50} - 1.5(q_{75} - q_{50}), \min(\text{CRPS})\}$.

favors high CRPS values (i.e., poor forecasts) for Madrid in winter Fig. A1h. The Scandinavian blocking favors high CRPS values for Berlin in winter and summer (green line in Fig. A1c and d). The different impacts of the weather regimes on the studied areas are related to the position of the high- and low-pressure regions of each weather regime in the studied areas.

This relation between predictability (or the CRPS distribution) and weather regimes, albeit weak, is consistent with previous work of Faranda et al. (2017). Similar relations were found between weather regimes over Europe and the temperature in a recent study by Ardilouze et al. (2021). We found that the sensitivity of the forecast to weather regime is larger for low values of CRPS and in winter. The sensitivity of forecast skill to weather regimes is rather small on average, even for small lead times ($T = 5$ d).

5.4 Comparison with ECMWF forecast

We first compared the CRPSS of SWG forecasts for winter and summer with the CRPSS of ECMWF forecasts.

The CRPSS of the ECMWF forecast is computed for different lead times going from 1 to 10 d for precipitation (Haiden et al., 2018) over the region 12.5° W–42.5° E; 35.0–75.0° N (ECMWF, 2020). It uses the climatology as a reference (Haiden et al., 2018). The values of CRPSS for Europe for 2020 decrease in accordance with lead times (Haiden et al., 2018). The CRPSS of ECMWF is about 0.16 in summer (JJA) and 0.25 in winter (DJF) for a lead time of $T = 5$ d (ECMWF, 2020). The CRPSS of SWG simulations for a lead time of $T = 5$ d is shown in Table 4. The values suggest that the predictive skill of SWG is qualitatively promising for short lead times, compared with ECMWF forecasts. However, we have to mention that the values of CRPSS for ECMWF are computed over all of Europe for both seasons (Haiden et al., 2018), while with the SWG we are doing a forecast for local stations.

We made a quantitative comparison between the two forecasts for the different lead times. We computed the CRPS for the ECMWF forecast. Then we used the Kolmogorov–Smirnov (KS) test (von Storch and Zwiers, 2001, chap. 1) to compare the probability distributions of the CRPS of SWG and ECMWF forecasts. The null hypothesis supposes that the CRPS of ECMWF and SWG forecasts have the same distribution. The null hypothesis of the KS test was rejected; this means that the two time series do not have the same distribution, with a p value $= 0.11$. A similar result was found by Ardilouze et al. (2021), where they compared the efficiency between ECMWF and CNRM forecasts.

We found that 80 %, 39 %, 50 %, and 40 % of the CRPS of SWG forecast are equal to zero for, respectively, Orly, Berlin, Madrid, and Toulouse, for a lead time of $T = 5$ d

Appendix A. Supplement of the article "Assessment of stochastic weather forecast of precipitation near European cities, based on analogs of circulation"

Table 6. CRPSS of ECMWF forecasts using as a reference the CRPS of SWG, for lead times of $T = 5$, 10, and 20 d. The forecasts show that the SWG has a positive improvement compared with the ECMWF forecast as the CRPSS scores are above zero, except for that of Toulouse.

Location	Orly	Berlin	Madrid	Toulouse
CRPSS $T = 5$ d	−0.09	−0.02	−0.2	0.25
CRPSS $T = 10$ d	−0.17	−0.54	−0.33	0.23
CRPSS $T = 20$ d	−0.50	−0.36	−0.1	−0.08

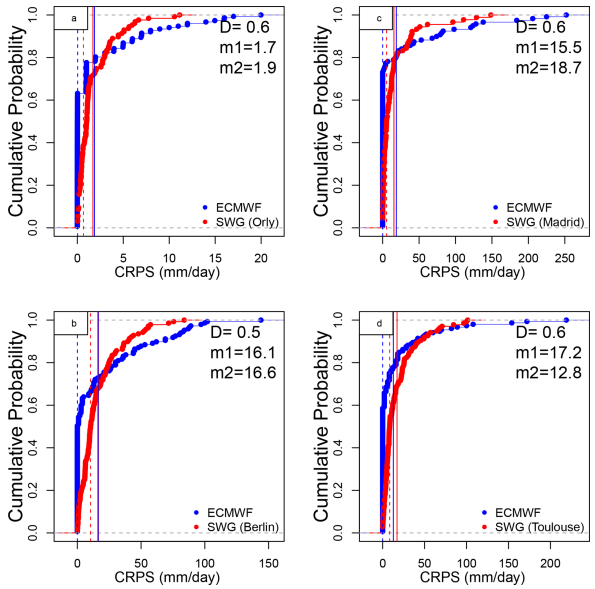

Figure 7. Empirical cumulative distribution function of the CRPS of ECMWF (blue) and SWG (red) forecasts for 5 d, for Orly **(a)**, Berlin **(b)**, Madrid **(c)**, and Toulouse **(d)**. D is the maximum distance between both ECDFs (value of Kolmogorov–Smirnov test). $m1$ is the value of the time average of CRPS of SWG and $m2$ is the value of the time average of CRPS of ECMWF. The dashed vertical lines represent the median of CRPS of ECMWF (blue) and SWG (red).

Fig. 7, which shows the capacity of the SWG to simulate rain events well. One notable difference between SWG and ECMWF forecasts is that although the proportion of CRPS values close to zero is higher for ECMWF, the CRPS for the worst forecasts is much higher than those of SWG. Indeed, we noticed that the time average of CRPS of ECMWF (vertical blue lines) and SWG (red vertical lines) for $T = 5$ d are close, with higher values for ECMWF (Fig. 7). However, the median CRPS of ECMWF is smaller compared with the SWG (dashed vertical lines in Fig. 7). Finally, we computed the CRPSS for ECMWF forecasts taking as a reference the CRPS of SWG (Table 6). We hence computed the CRPSS of ECMWF forecast by normalizing the CRPS by the CRPS of the SWG forecast in Eq. (C1).

This new ECMWF CRPSS evaluates the added value of the ECMWF forecast over the SWG forecast. We found that the ECMWF forecast has no improvement over the SWG forecast for the different lead times because the CRPSS values are negative. At $T = 5$ d, we noticed that the improvement is negligible for Orly and Berlin, while it is much better for Madrid. However, for Toulouse, the ECMWF forecast still has better skills for lead times of $T = 5$ and 10 d. For a lead time of $T = 10$ d, the improvement of the SWG forecast over the ECMWF is significant, particularly for Berlin and Madrid. There is a major improvement for a lead time of $T = 20$ d for Orly and Berlin.

This confirms the relatively good skill of the SWG to forecast precipitation, compared with ECMWF. This could be explained by the difference in the average of the CRPS of the two forecasts. Indeed, as we mentioned before, the ECMWF forecast yields the best skill scores for small values of precipitations (< 2 mm d^{-1}). We further illustrate those comparisons in Fig. C1 and Table C1.

6 Conclusions

In this work, we have shown the performance of a stochastic weather generator (SWG) to simulate precipitation over different locations in western Europe and for various time scales from 5 to 20 d. The input of our model was analogs of geopotential heights at 500 hPa ($Z500$). The choice of such input was made in order to evaluate the impact of large-scale circulation on local weather variables. The SWG showed a good skill in predicting precipitation for a lead time of 5 and 10 d from analogs of $Z500$.

This study of precipitation forecast complements the work of Yiou and Déandréis (2019) initially made to forecast temperature and the NAO index. We explored the sensitivity of the SWG model on analogs computed from different geographic areas and from different reanalyses (ERA5 and NCEP). We found that both NCEP and ERA5 reanalyses perform well for simulations.

We evaluated the relation between the quality of the forecast and weather regimes over Europe. We found that low and high predictability were related to specific weather regimes. This dependence is more significant in winter than in summer. We found that good predictability is mainly related to blocking.

A comparison with the ECMWF forecast system over western Europe confirmed quantitatively and qualitatively the skill forecast of the SWG , for lead times of $T \leq 10$ d. Of course, the SWG model cannot replace a numerical weather prediction, as the SWG parameters (e.g., region of analogs) need to be tuned to local variables and rely on the existence of a fairly large database to compute analogs. Here we used the same domain of circulation analogs for stations from Madrid to Berlin. Obviously, this region should be optimized for each individual station. Therefore, the main utility of the SWG forecast system is to make local ensemble simulations, where its performances can challenge a numerical weather prediction if the parameters are well tuned.

This paper hence confirms the proof of concept to generate ensembles of (local) precipitation forecasts from analogs of circulation. The SWG ensemble forecast performance relies on the relation between precipitation and the synoptic atmospheric circulation, which is verified for western Europe. Transposing this SWG to other regions of the globe requires observations covering several decades. Numerical weather models obviously do not yield this constraint.

Appendix A. Supplement of the article "Assessment of stochastic weather forecast of precipitation near European cities, based on analogs of circulation"

Appendix A: CRPS and weather regimes

To avoid a tedious redundancy we deferred the figures of evaluation of the forecast quality by weather regimes to this appendix section.

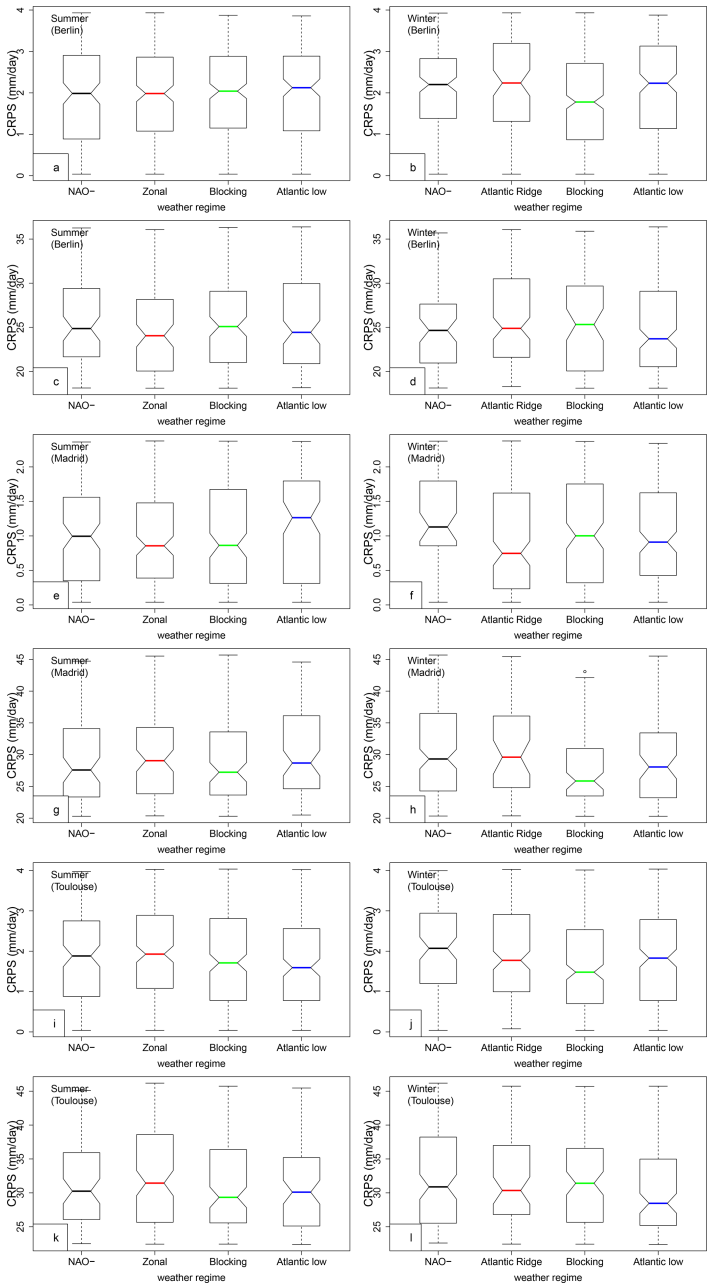

Figure A1. Relation between CRPS and weather regimes for Berlin **(a–d)**, Madrid **(e–h)**, and Toulouse **(i–l)**, for SWG forecasts with lead time $T = 5$ d. Panels **(a)**, **(b)**, **(e)**, **(f)**, **(i)**, and **(j)** correspond to CRPS value distribution conditioned on four weather regimes, when CRPS is lower than q_{25}. Panels **(c)**, **(d)**, **(g)**, **(h)**, **(k)**, and **(l)** correspond to a higher CRPS value (CRPS $\geq q_{75}$). The boxplots indicate the median (q_{50}) of the distribution (thick bar).

Appendix B: Relation between Z500 and precipitation

In order to justify the use of the $Z500$ as a driver of precipitation, we computed the rank spatial correlation between the daily average of $Z500$ over the Euro-Atlantic region and the precipitation in each studied station (Berlin, Madrid, Orly, and Toulouse). We did the analysis for different seasons (DJF and JJA). We found a maximum correlation amplitude of -0.5 for Madrid and Orly, and a correlation of -0.4 and -0.3, respectively, for Toulouse and Berlin. The correlation is significant as we have a p value < 0.05 for the different grid points. This indicates the relation between $Z500$ patterns and precipitation, in particular in western Europe, and that a decrease in $Z500$ is linked with precipitation.

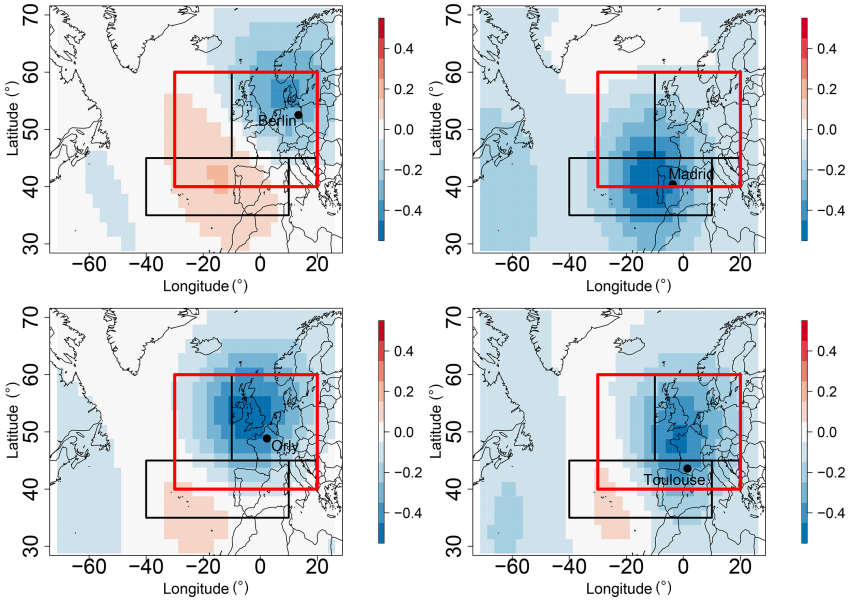

Figure B1. Maps of correlation between $Z500$ and precipitation in Berlin, Madrid, Orly, and Toulouse for the period from 1948 to 2019 over the Euro-Atlantic region. The rectangles represent the domains of computation of analogs. The optimized area [30° W–20° E; 40–60° N] is highlighted by the red rectangle.

Appendix C: CRPSS of ECMWF vs. SWG

We explain further the comparison that we made between the ECMWF forecast and the SWG forecast. As mentioned we found that the SWG has improved compared with the ECMWF forecast. This is related to the difference in the time average of the CRPS of the two forecasts. We computed the CRPSS as follows:

$$\mathrm{CRPSS} = 1 - \frac{\overline{\mathrm{CRPS}_{\mathrm{ECMWF}}}}{\overline{\mathrm{CRPS}_{\mathrm{SWG}}}}, \tag{C1}$$

where $\overline{\mathrm{CRPS}_{\mathrm{ECMWF}}}$ is the time average of the CRPS of the ECMWF forecast and $\overline{\mathrm{CRPS}_{\mathrm{SWG}}}$ is the time average of the CRPS of the SWG.

Appendix A. Supplement of the article "Assessment of stochastic weather forecast of precipitation near European cities, based on analogs of circulation"

Table C1. Average and median values of CRPS, average CRPSS (in bold) of the ECMWF and SWG forecasts for lead times of $T = 5$, 10, and 20 d. The table shows that the CRPS of the SWG forecast has a smaller average than the CRPS of the ECMWF forecast, which explains the values of CRPSS for the different studied areas and the positive improvement of the SWG compared with the ECMWF.

Location	Orly	Berlin	Madrid	Toulouse
$\overline{\text{CRPS}_{\text{ECMWF}}}$; median	1.87; 0.04	16.56; 0.05	18.73; 0.003	12.76; 0.01
$\overline{\text{CRPS}_{\text{SWG}}}$; median	1.70; 0.67	16.10; 10.37	15.49; 5.45	17.16; 8.39
CRPSS for $T = 5$ d	**−0.09**	**−0.02**	**−0.2**	**0.25**
$\overline{\text{CRPS}_{\text{ECMWF}}}$	1.70; 0.05	18.1; 0.06	20.03; 0.1	14.87; 0.09
$\overline{\text{CRPS}_{\text{SWG}}}$	1.44; 0.78	11.67; 5.45	15.04; 6.13	19.45; 7.89
CRPSS for $T = 10$ d	**−0.17**	**−0.54**	**−0.33**	**0.23**
$\overline{\text{CRPS}_{\text{ECMWF}}}$	1.67; 0.1	13.54; 0.09	17.89; 0.1	17.8; 0.08
$\overline{\text{CRPS}_{\text{SWG}}}$	1.11; 0.9	9.91; 6.3	16.23; 5.89	16.41; 8.34
CRPSS for $T = 20$ d	**−0.50**	**−0.36**	**−0.1**	**−0.08**

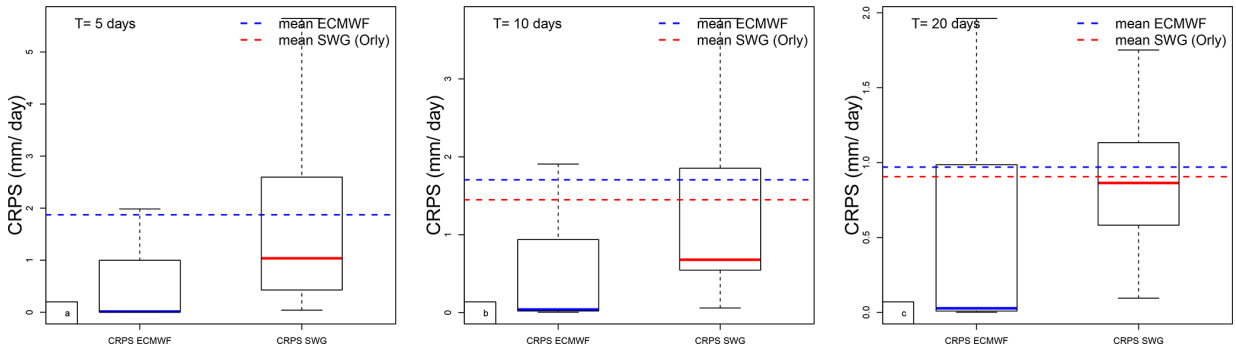

Figure C1. Boxplots of CRPS of ECMWF and CRPS of SWG for Orly, with lead time $T = 5$, 10, and 20 d. The boxplots indicate the median (q_{50}) of the distribution (thick blue bar for ECMWF and red for SWG). The 25th (q_{25}) and 75th (q_{75}) quartiles are, respectively, the lower and upper segments of each boxes. The upper whisker is $\min\{\max(X), q_{50} + 1.5(q_{75} - q_{25})\}$. The average CRPS of the ECMWF and SWG forecasts are indicated with dashed horizontal lines. Note that the distribution is asymmetric as the median and the average are unequal. The average CRPS for the SWG forecast is lower than the average CRPS for the ECMWF forecast. The outliers that are above the upper whiskers are not shown.

Code and data availability. The code and data files are available at https://doi.org/10.5281/zenodo.4524562 (Krouma, 2021).

Author contributions. MK performed the analyses. PY co-designed the analyses. CD and ST participated in the manuscript preparation.

Competing interests. The contact author has declared that neither they nor their co-authors have any competing interests.

Disclaimer. Publisher's note: Copernicus Publications remains neutral with regard to jurisdictional claims in published maps and institutional affiliations.

Acknowledgements. This work is part of the EU International Training Network (ITN) Climate Advanced Forecasting of subseasonal Extremes (CAFE). We thank Linus Magnusson and Florian Pappenberger for helpful discussions on the ECMWF data.

Financial support. This work is part of the EU International Training Network (ITN) "Climate Advanced Forecasting of subseasonal Extremes" (CAFE). The project receives funding from the European Union's Horizon 2020 research and innovation program under the Marie Skłodowska-Curie Grant (agreement no. 813844).

Review statement. This paper was edited by Chiel van Heerwaarden and reviewed by two anonymous referees.

References

Ailliot, P., Allard, D., Monbet, V., and Naveau, P.: Stochastic weather generators: an overview of weather type models, Journal de la Société Française de Statistique, 156, 101–113, 2015.

Ardilouze, C., Specq, D., Batté, L., and Cassou, C.: Flow dependence of wintertime subseasonal prediction skill over Europe, Weather Clim. Dynam., 2, 1033–1049, https://doi.org/10.5194/wcd-2-1033-2021, 2021.

Atencia, A. and Zawadzki, I.: A comparison of two techniques for generating nowcasting ensembles. Part I: Lagrangian ensemble technique, Mon. Weather Rev., 142, 4036–4052, 2014.

Blanchet, J., Stalla, S., and Creutin, J.-D.: Analogy of multiday sequences of atmospheric circulation favoring large rainfall accumulation over the French Alps, Atmos. Sci. Lett., 19, e809, https://doi.org/10.1002/asl.809, 2018.

Cassou, C., Minvielle, M., Terray, L., and Périgaud, C.: A statistical–dynamical scheme for reconstructing ocean forcing in the Atlantic. Part I: weather regimes as predictors for ocean surface variables, Clim. Dynam., 36, 19–39, https://doi.org/10.1007/s00382-010-0781-7, 2011.

Eckmann, J.-P. and Ruelle, D.: Ergodic theory of chaos and strange attractors, in: The Theory of Chaotic Attractors, pp. 273–312, Springer Nature, ISBN 978-1-4419-2330-1, https://doi.org/10.1007/978-0-387-21830-4_17, 1985.

ECMWF: European Centre for Medium-Range Weather Forecasts, https://apps.ecmwf.int/webapps/opencharts/products/plwww_3m_ens_tigge_wp_mean?area=Europe&parameter=24h%20precipitation&score=CRPSS (last access: 2 March 2022), 2020.

Faranda, D., Messori, G., and Yiou, P.: Dynamical proxies of North Atlantic predictability and extremes, Sci. Rep., 7, 41278, https://doi.org/10.1038/srep41278, 2017.

Ferro, C. A. T.: A probability model for verifying deterministic forecasts of extreme events, Weather Forecast., 22, 1089–1100, https://doi.org/10.1175/WAF1036.1, 2007.

Gabriel, K. R. and Neumann, J.: A Markov chain model for daily rainfall occurrence at Tel Aviv, Q. J. Roy. Meteor. Soc., 88, 90–95, 1962.

Ghil, M., Chekroun, M., and Simonnet, E.: Climate dynamics and fluid mechanics: Natural variability and related uncertainties, Physica D, 237, 2111–2126, https://doi.org/10.1016/j.physd.2008.03.036, 2008.

Haiden, T., Janousek, M., Bidlot, J., Buizza, R., Ferranti, L., Prates, F., and Vitart, F.: Evaluation of ECMWF forecasts, including the 2018 upgrade, European Centre for Medium Range Weather Forecasts, https://doi.org/10.21957/ldw15ckqi, 2018.

Haylock, M. R., Hofstra, N., Klein Tank, A. M. G., Klok, E. J., Jones, P. D., and New, M.: A European daily high-resolution gridded data set of surface temperature and precipitation for 1950–2006, J. Geophys. Res., 113, D20119, https://doi.org/10.1029/2008JD010201, 2008.

Hempelmann, N., Ehbrecht, C., Alvarez-Castro, C., Brockmann, P., Falk, W., Hoffmann, J., Kindermann, S., Koziol, B., Nangini, C., Radanovics, S., Vautard, R., and Yiou, P.: Web processing service for climate impact and extreme weather event analyses. Flyingpigeon (Version 1.0), Comput. Geosci., 110, 65–72, https://doi.org/10.1016/j.cageo.2017.10.004, 2018.

Hersbach, H.: Decomposition of the Continuous Ranked Probability Score for Ensemble Prediction Systems, Weather Forecast., 15, 559–570, https://doi.org/10.1175/1520-0434(2000)015<0559:DOTCRP>2.0.CO;2, 2000.

Hersbach, H., Bell, B., Berrisford, P., Hirahara, S., Horányi, A., Muñoz-Sabater, J., Nicolas, J., Peubey, C., Radu, R., and Schepers, D.: The ERA5 global reanalysis, Q. J. Roy. Meteor. Soc., 146, 1999–2049, 2020.

Jolliffe, I. T. and Stephenson, D. B.: Forecast Verificaton: A Practitioner's Guide in Atmospheric Science, 2nd edn., Wiley-Blackwell, Oxford, ISBN 978-0-470-66071-3, 2012.

Jézéquel, A., Yiou, P., Radanovics, S., and Vautard, R.: Analysis of the exceptionally warm December 2015 in France using flow analogues, B. Am. Meteorol. Soc., 99, S76–S79, 2018.

Kimoto, M.: Studies of Climate Variability Using General Circulation Models, in: Earth Planets and Space, TERRAPUB, http://citeseerx.ist.psu.edu/viewdoc/summary?doi=10.1.1.534.3517&rank=1 (last access: 18 March 2021), 2001.

Kistler, R., Kalnay, E., Collins, W., Saha, S., White, G., Woollen, J., Chelliah, M., Ebisuzaki, W., Kanamitsu, M., Kousky, V., van den Dool, H., Jenne, R., and Fiorino, M.: The NCEP–NCAR 50-Year Reanalysis: Monthly Means CD-ROM and Documentation, B. Am. Meteorol. Soc., 82, 247–268, http://www.jstor.org/stable/26215517 (last access: 27 February 2022), 2001.

Klein Tank, A. M. G., Wijngaard, J. B., Können, G. P., Böhm, R., Demarée, G., Gocheva, A., Mileta, M., Pashiardis, S., Hejkrlik, L., Kern-Hansen, C., Heino, R., Bessemoulin, P., Müller-Westermeier, G., Tzanakou, M., Szalai, S., Pálsdóttir, T., Fitzgerald, D., Rubin, S., Capaldo, M., Maugeri, M., Leitass, A., Bukantis, A., Aberfeld, R., van Engelen, A. F. V., Forland, E., Mietus, M., Coelho, F., Mares, C., Razuvaev, V., Nieplova, E., Cegnar, T., Antonio López, J., Dahlström, B., Moberg, A., Kirchhofer, W., Ceylan, A., Pachaliuk, O., Alexander, L. V., and Petrovic, P.: Daily dataset of 20th-century surface air temperature and precipitation series for the European Climate Assessment, Int. J. Climatol., 22, 1441–1453, https://doi.org/10.1002/joc.773, 2002.

Krouma, M.: Assessment of stochastic weather forecast based on analogs of circulation, Zenodo [code and data set], https://doi.org/10.5281/zenodo.4524562, 2021.

Lorenz, E. N.: Atmospheric Predictability as Revealed by Naturally Occurring Analogues, J. Atmos. Sci., 26, 636–646, 1969.

Mastrantonas, N., Herrera-Lormendez, P., Magnusson, L., Pappenberger, F., and Matschullat, J.: Extreme precipitation events in the Mediterranean: Spatiotemporal characteristics and connection to large-scale atmospheric flow patterns, Int. J. Climatol., 41, 2710–2728, https://doi.org/10.1002/joc.6985, 2021.

Michelangeli, P., Vautard, R., and Legras, B.: Weather regimes: Recurrence and quasi-stationarity, J. Atmos. Sci., 52, 1237–1256, 1995.

Palmer, T. N.: Predicting uncertainty in forecasts of weather and climate, Rep. Prog. Phys., 63, 71–116, https://doi.org/10.1088/0034-4885/63/2/201, 2000.

Peel, M. C., Finlayson, B. L., and McMahon, T. A.: Updated world map of the Köppen-Geiger climate classification, Hydrol. Earth Syst. Sci., 11, 1633–1644, https://doi.org/10.5194/hess-11-1633-2007, 2007.

Peixoto, J. P. and Oort, A. H.: Physics of climate, American Institute of Physics, New York, ISBN 978-0-88318-712-8, 1992.

Platzer, P., Yiou, P., Naveau, P., Filipot, J.-F., Thiébaut, M., and Tandeo, P.: Probability Distributions for Analog-

Appendix A. Supplement of the article "Assessment of stochastic weather forecast of precipitation near European cities, based on analogs of circulation"

To-Target Distances, J. Atmos. Sci., 78, 3317–3335, https://doi.org/10.1175/JAS-D-20-0382.1, 2021.

Richardson, C. W.: Stochastic simulation of daily precipitation, temperature, and solar radiation, Water Resour. Res., 17, 182–190, https://doi.org/10.1029/WR017i001p00182, 1981.

Ruelle, D.: Ergodic theory of differentiable dynamical systems, Publications Mathématiques de l'IHÉS, Tome, 50, 27–58, http://www.numdam.org/item/PMIHES_1979__50__27_0/ (last access: 19 June 2022), 1979.

Scaife, A. A., Arribas, A., Blockley, E., Brookshaw, A., Clark, R. T., Dunstone, N., Eade, R., Fereday, D., Folland, C. K., and Gordon, M.: Skillful long-range prediction of European and North American winters, Geophys. Res. Lett., 41, 2514–2519, 2014.

Sivillo, J. K., Ahlquist, J. E., and Toth, Z.: An ensemble forecasting primer, Weather Forecast., 12, 809–818, https://doi.org/10.1175/1520-0434(1997)012<0809:AEFP>2.0.CO;2, 1997.

Todorovic, P. and Woolhiser, D. A.: A stochastic model of n-day precipitation, J. Appl. Meteorol., 14, 17–24, 1975.

Toth, Z.: Intercomparison of Circulation Similarity Measures, Mon. Weather Rev., 119, 55–64, https://doi.org/10.1175/1520-0493(1991)119<0055:IOCSM>2.0.CO;2, 1991.

Toth, Z. and Kalnay, E.: Ensemble forecasting at NCEP and the breeding method, Mon. Weather Rev., 125, 3297–3319, https://doi.org/10.1175/1520-0493(1997)125<3297:EFANAT>2.0.CO;2, 1997.

Türkes, M., Sümer, U., and Kiliç, G.: Persistence and periodicity in the precipitation series of Turkey and associations with 500 hPa geopotential heights, Clim. Res., 21, 59–81, https://doi.org/10.3354/cr021059, 2002.

van den Dool, H. M.: Empirical Methods in Short-Term Climate Prediction, Oxford University Press, Oxford, ISBN-13 9780199202782, https://doi.org/10.1093/oso/9780199202782.001.0001, 2007.

van der Wiel, K., Bloomfield, H. C., Lee, R. W., Stoop, L. P., Blackport, R., Screen, J. A., and Selten, F. M.: The influence of weather regimes on European renewable energy production and demand, Environ. Res. Lett., 14, 094010, https://doi.org/10.1088/1748-9326/ab38d3, 2019.

Vitart, F., Ardilouze, C., Bonet, A., Brookshaw, A., Chen, M., Codorean, C., Déqué, M., Ferranti, L., Fucile, E., Fuentes, M., Hendon, H., Hodgson, J., Kang, H.-S., Kumar, A., Lin, H., Liu, G., Liu, X., Malguzzi, P., Mallas, I., Manoussakis, M., Mastrangelo, D., MacLachlan, C., McLean, P., Minami, A., Mladek, R., Nakazawa, T., Najm, S., Nie, Y., Rixen, M., Robertson, A. W., Ruti, P., Sun, C., Takaya, Y., Tolstykh, M., Venuti, F., Waliser, D., Woolnough, S., Wu, T., Won, D.-J., Xiao, H., Zaripov, R., and Zhang, L.: The Subseasonal to Seasonal (S2S) Prediction Project Database, B. Am. Meteorol. Soc., 98, 163–173, https://doi.org/10.1175/BAMS-D-16-0017.1, 2017.

von Storch, H. and Zwiers, F. W.: Statistical Analysis in Climate Research, Cambridge University Press, Cambridge, ISBN 9780511612336, https://doi.org/10.1017/CBO9780511612336, 2001.

Wilks, D.: Statistical Methods in the Atmospheric Sciences: An Introduction, Elsevier's Science & Technology Rights Department in Oxford, UK, ISBN 978-0-12-751966-1, 1995.

Xoplaki, E., Luterbacher, J., Burkard, R., Patrikas, I., and Maheras, P.: Connection between the large-scale 500 hPa geopotential height fields and precipitation over Greece during wintertime, Clim. Res., 14, 129–146, https://doi.org/10.3354/cr014129, 2000.

Yiou, P. and Déandréis, C.: Stochastic ensemble climate forecast with an analogue model, Geosci. Model Dev., 12, 723–734, https://doi.org/10.5194/gmd-12-723-2019, 2019.

Yiou, P., Goubanova, K., Li, Z. X., and Nogaj, M.: Weather regime dependence of extreme value statistics for summer temperature and precipitation, Nonlin. Processes Geophys., 15, 365–378, https://doi.org/10.5194/npg-15-365-2008, 2008.

Yiou, P., Salameh, T., Drobinski, P., Menut, L., Vautard, R., and Vrac, M.: Ensemble reconstruction of the atmospheric column from surface pressure using analogues, Clim. Dynam., 41, 1333–1344, https://doi.org/10.1007/s00382-012-1626-3, 2013.

Zamo, M. and Naveau, P.: Estimation of the Continuous Ranked Probability Score with Limited Information and Applications to Ensemble Weather Forecasts, Math. Geosci., 50, 209–234, 2018.

Appendix B

Supplement of the (submitted) article "Improving the ensemble forecast of precipitation in Europe by combining a stochastic weather generator with dynamical models"

Received <day> <Month>, <year>; | Revised <day> <Month>, <year>; | Accepted <day> <Month>, <year>

DOI: xxx/xxxx

RESEARCH ARTICLE

Improving subseasonal forecast of precipitation in Europe by combining a stochastic weather generator with dynamical models

Meriem Krouma[1,2] | Damien Specq[3] | Linus Magnusson[5] | Constantin Ardilouze[3] | Lauriane Batté[3,4] | Pascal Yiou[2]

[1]ARIA Technologies, Boulogne-Billancourt, France
[2]Laboratoire des Sciences du Climat et de l'Environnement, UMR 8212 CEA-CNRS-UVSQ, IPSL & Université Paris-Saclay, 91191 Gif-sur-Yvette, France
[3]CNRM, Université de Toulouse, Météo-France, CNRS, Toulouse, France
[4]Direction de la Climatologie et des Services Climatiques, Météo-France, Toulouse, France
[5]European Centre for Medium-Range Weather Forecast, Reading, UK

Correspondence
Meriem Krouma
Laboratoire des Sciences du Climat et de l'Environnement - CEA - CNRS - UVSQ - Université Paris-Saclay, Orme des Merisiers, Bat 714, 91190 Saint-Aubin, France
Email: meriem.krouma@lsce.ipsl.fr

Funding Information
H2020 Marie Skłodowska-Curie Actions,Grant/Award Number: 813844; EUInternational Training Network (ITN)Climate Advanced Forecasting of sub-seasonal Extremes (CAFE).

Abstract

We propose a forecasting tool for precipitation based on analogs of circulation defined from hindcasts and a stochastic weather generator that we call "HC-SWG". In this study, we aim to improve the forecast of European precipitation for subseasonal lead times (from 2 to 4 weeks) using the HC-SWG. We designed the HC-SWG to generate an ensemble precipitation forecast from the ECMWF and CNRM S2S ensemble reforecasts. We define analogs from the ensemble reforecast of Z500 from the ECMWF (11 members) and CNRM (10 members) models. Then, we generate a 100-member ensemble for precipitation over Europe. We evaluate the skill of the ensemble forecast using probabilistic skill scores such as the continuous probabilistic skill score (CRPSS) and ROC curve. We obtain reasonable forecast skill scores within 35 days for different locations in Europe. The CRPSS shows positive improvement with respect to climatology and persistence at the station level. The HC-SWG shows a capacity to distinguish between events and non-events of precipitation within 15 days at the different stations. We compare the HC-SWG forecast with other precipitation forecasts to further confirm the benefits of our method. We found that the HC-SWG shows improvement against the ECMWF precipitation forecast until 25 days.

KEYWORDS:
Ensemble forecast; European precipitation; subseasonal; dynamical models

1 | INTRODUCTION

Making accurate subseasonal forecasts remains a challenge for the scientific community (White et al., 2022). The subseasonal time range lies between the medium-term daily weather forecast and the seasonal forecasting (Vitart et al., 2017). The subseasonal predictability is linked to atmospheric, oceanic, and land processes (Robertson and Vitart, 2019). The most important sources of predictability of the subseasonal range are the Madden Julian oscillation (Lau and Waliser, 2011), soil moisture (Koster et al., 2010), snow cover (Lin and Wu, 2011) and ocean conditions (Woolnough et al., 2007). Considerable efforts have been made to understand those different processes in order to improve models, the initialisation and the generation of ensemble forecasts at the subseasonal range (Merryfield et al., 2020; Newman et al., 2003; Rashid et al., 2011; Vitart, 2014).

Appendix B. Supplement of the (submitted) article "Improving the ensemble forecast of precipitation in Europe by combining a stochastic weather generator with dynamical models"

Subseasonal forecasts have been more accurate with the improvement of numerical weather prediction (NWP) models (Robertson and Vitart, 2019). NWP forecasting has improved over the past decades due to model improvements and the availability of better data and forecast initialisation (Magnusson and Källén, 2013). NWP models have shifted in the past decades from a deterministic to a probabilistic approach. Indeed, ensemble (probabilistic) forecasts help to catch atmospheric chaos by producing a set of probabilities for the predicted variable (Palmer, 2000). Hence, a probabilistic forecast provides both the most likely scenario as well as the uncertainties associated with it. For instance, ensemble NWP predictions showed a good forecast skill for atmospheric fields such as the geopotential height at 500 hPa for up to 1 month (Robertson and Vitart, 2019). Nevertheless, the NWP forecast skill is still insufficient for some weather variables such as precipitation, particularly for the subseasonal lead times. There are at least two reasons for this shortcoming. Precipitation results from complex non-linear and multiscale processes that are not well resolved in NWP models. Errors related to the physical parametrization assumptions combined to a lack of resolution explain the poor predictability of precipitation (Karl et al., 1990). In addition, small-scale effects such as topography or orography are not well resolved by NWP models. However, those parameters are important for local weather (Wilks, 2011, chap.6).

Forecasts for the subseasonal lead time can be obtained by combining statistical techniques with numerical or dynamical weather prediction models, which can also contribute to improve the forecast information on a small scale. Indeed, statistical forecasts based on NWP information tend to correct forecast biases (Klein et al., 1959; Specq and Batté, 2020).

Stochastic weather generators (SWGs) have been used to generate ensemble weather forecasts for different climate/weather variables (Wilks and Wilby, 1999). SWGs have a good capacity to simulate the behaviour of the climate variables (Ailliot et al., 2015). They have been used to forecast weather and climate variables such as temperature (Yiou and Déandréis, 2019), precipitation (Krouma et al., 2022), the Madden Julian oscillation (Krouma et al., 2023) and the North Atlantic oscillation. SWGs have a low computing cost compared to numerical models. Combining stochastic weather generators with analogs of atmospheric circulation is a promising approach to simulate the weather. Indeed, the circulation analog method assumes that the future evolution of the atmosphere will be similar to the flows that followed the historical analogs (Atencia and Zawadzki, 2014; Blanchet et al., 2018; Lorenz, 1969; Yiou et al., 2013).

The aim of this work is to improve the forecast skill of precipitation averages over Europe using a stochastic weather generator based on analog circulation for subseasonal lead times ($\approx$ 2 to 4 weeks). The SWG developed by (Yiou, 2014) showed the capacity to forecast average precipitation (Krouma et al., 2022) within 5-10 days and temperature within 40 days (Yiou and Déandréis, 2019) with promising probabilistic scores. In this work, we revisit the SWG described by Krouma et al. (2022) to optimize the simulation of European precipitation from ensemble dynamical reforecasts of the European Center of Medium-range Weather Forecast (ECMWF) and the Centre National de la Recherche Météorologique (CNRM) of Météo France. The idea is to use the forecast of the Z500 from dynamical models as input to the SWG to have an ensemble forecast of precipitation at different lead times up to 1 month. Then, we evaluate the skill of the ensemble forecast using skill scores such as the continuous probabilistic score (CRPS) and ROC curve. We also compare our forecasts of precipitation with the ECMWF precipitation forecast.

The paper is structured as follows: Section 2 specifies the data used for running our forecast. Section 3 explains the methodology: circulation analogs computation, stochastic weather generator and the verification metrics that we used to evaluate the forecast skill. Section 4 details the results of the simulations and the evaluation of the ensemble forecast, as well as the comparison of the SWG forecast with the ECMWF precipitation forecast. Section 5 contains the main conclusions of the analyses.

2 | DATA

We use daily geopotential at 500 hPa (Z500) data from dynamical reforecasts. Reforecasts (also known as hindcast) are forecast runs using the same model version as the real-time forecast for past periods. Two configurations are mainly used to produce reforecasts. The first configuration, so called "fixed configuration", consists in producing reforecasts for all past dates once during the lifetime of a given model version. In this case, a new set of reforecasts is produced with each new model version. The second configuration, known as "on-the-fly configuration", consists in producing reforecasts at the same time as the real-time forecasts, which means that each reforecast refers to a real-time forecast.

The reforecasts of Z500 were collected from the subseasonal to seasonal (S2S) database for two models: CNRM and ECMWF (Vitart et al., 2017). The ECMWF reforecast is produced "on the fly" and it is composed of an 11-member ensemble covering the past 20 years (Vitart et al., 2019). As initial conditions, the ECMWF reforecast uses ERA5 (Hersbach et al., 2020) and ORAS5

ocean initial conditions (Hersbach et al., 2020). The CNRM reforecasts are produced with the fixed configuration (Ardilouze et al., 2021; Batté and Déqué, 2016). The CNRM reforecast ensemble is composed of 10 members initialized each week over the 1993-2017 period. The CNRM model uses as initial conditions ERA5 for atmosphere and land surface and MERCATOR-OCEAN ocean reanalyses. Both reforecasts feed the S2S database weekly. We considered two models produced with similar properties coupled with ocean and sea ice models. The main characteristics of the ECMWF and CNRM models are shown in the following table 1 .

TABLE 1 Characteristics of the ECMWF and CNRM S2S ensemble reforecasts

	Model version	**Period**	**Horizontal resolution**	**Size**	**Ocean resolution**	**Sea ice**
ECMWF	CY47R2	2001 – 2021	15 to 31 km	11	0.25° 75 levels	Active
CNRM	CNRM-CM 6.1	1993 – 2017	50 km	10	0.25° 75 levels	Active

We used two different precipitation databases for verification purposes. Daily observation data (i) at the station scale from ECA&D (Klein Tank et al., 2002) served as a reference for four different stations in Europe (Berlin, Orly, Toulouse, Madrid), and (ii) data from E-OBS (Cornes et al., 2018) in order to test the forecast skill of our model over Europe. E-OBS data is available in a daily range from 1950 to 2022. We re-gridded the E-OBS data to a resolution of $1.5° \times 1.5°$ to comply with the reforecast horizontal resolution.

3 | METHODOLOGY

The goal of this study is to simulate forecast ensembles of $N = 100$ members for European precipitation at the subseasonal lead time (from 2 to 4 weeks). Our methodology enhances the available hindcast ensembles to $N = 100$ members through a random sampling of circulation analogs selected separately from the ECMWF and CNRM reforecasts ensembles. The following subsections explain how the circulation analogs are computed from reforecasts of the ECMWF and CNRM, and how the random sampling (or Stochastic Weather Generator) is performed.

3.1 | Data processing and analog dataset

The first step in our forecasting process is to define the analogs of Z500. An analog is a date where the configuration of the atmospheric circulation is similar to a selected day t (Krouma et al., 2022; Yiou, 2014). To define an analog, we apply mainly two rules: the calendar distance between t and its analogs should not exceed 30 calendar days, and an analog of t should be in a different year than t. Our selection criterion is the Euclidean distance, which we compute between Z500 at a day t and its analog day t'. Then, for each day, we keep the K analogs that have the minimum Euclidean distance.

To define analogs, some parameters need to be adjusted such as the geographical region. We determined analogs over the region with coordinates 30°W –- 20°E, 40° –- 60°N defined by Krouma et al. (2022) as an optimal region to compute analogs for precipitation forecast in Europe. In this study, we keep $K = 20$ best analogs as in Krouma et al. (2022).

Before defining the analogs, we start by assessing the quality of the reforecast ensemble of ECMWF and CNRM on the 5^{th} day. The aim is to verify the spread of the ensemble and check whether we can use the whole ensemble to compute analogs. We computed the Euclidean distance between the members of each ensemble. Then, we compared it separately to the distance between the analogs of each model (Figure 1). We computed analogs from the 1st and 11th (or 10th) members, and the ensemble mean (figure 1 (a)). The analogs were computed for the 11 (or 10) members, but for brevity's sake and as the conclusion is the same, we choose to show the comparison between the analogs of the ensemble mean and, the 1st and last members.

The distance between the 11 members of the ECMWF reforecast of Z500 for 5 days ahead varies between 169 m and 175 m (figure 1 (b)). The analogs of the ensemble mean are closer than the analogs of the 1st and last members. For the ensemble reforecast of the CNRM, the maximum distance between the 10 members is 184 m (Figure 1 (d)). The analogs of the ensemble mean show an average distance of 259 m compared to the analogs of the 1st and 10th members. We conclude that the maximum distance between the members of the ensembles of ECMWF or CNRM is smaller compared to the average distance between the analogs, as shown in Figure 1 .

The ensemble spread is small enough compared to the distance between the analogs, hence, we decided to use the ensemble mean at the 5^{th} day to compute the analogs as illustrated in Figure 2 instead of using the ensemble members seperately.

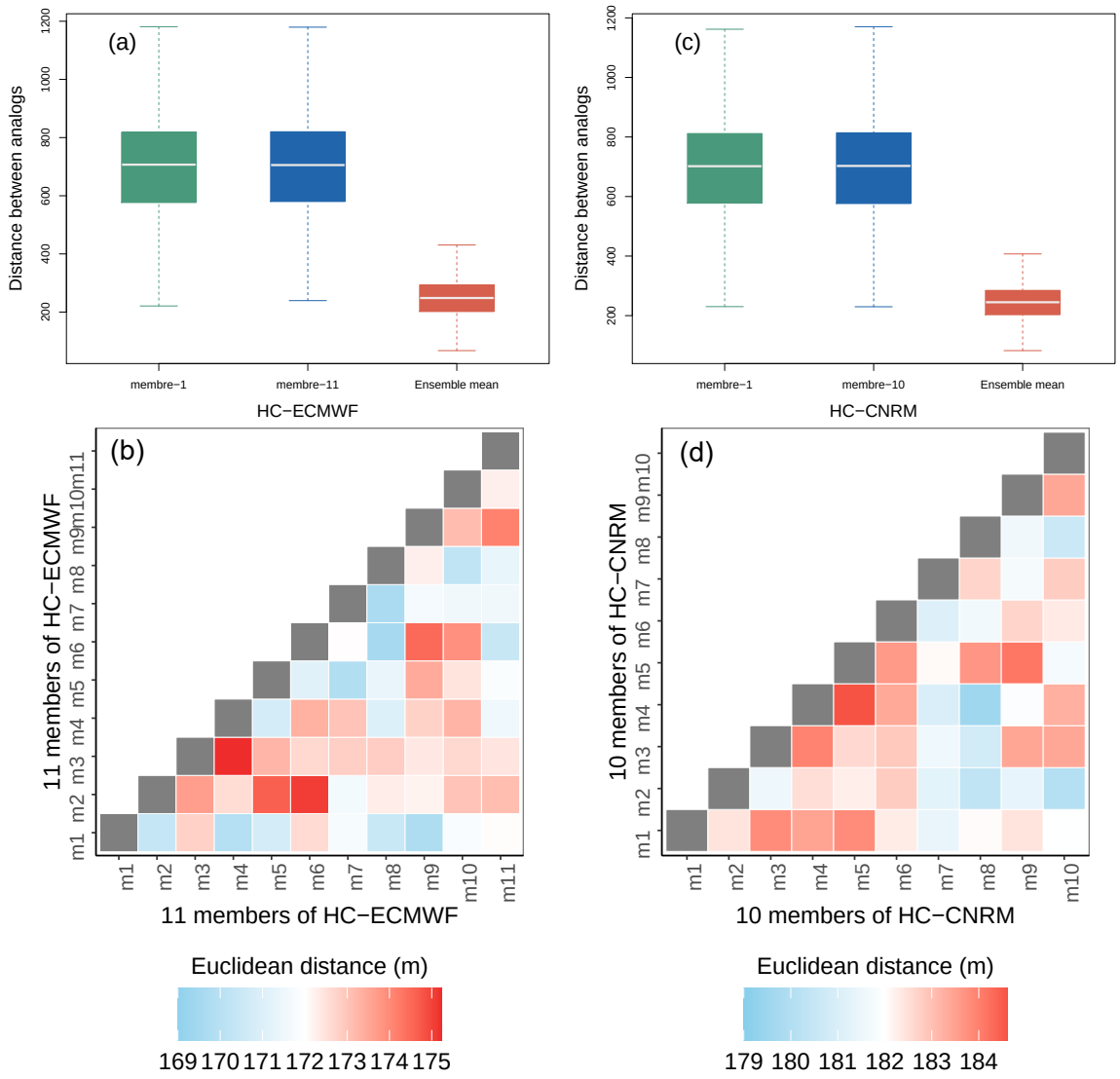

FIGURE 1 Comparison between the distance between the analogs computed from the 1^{st}, last members and the ensemble mean of the (a) ECMWF and (c) CNRM reforecasts and the distance between the members of the ensembles of (b) ECMWF and (d) CNRM ensemble members at 5 days ahead.

3.2 | Stochastic Weather Generator configuration

The role of the analog stochastic weather generator (SWG) is to generate random trajectories from the previously computed analogs (Yiou, 2014). To generate a trajectory for a given day t_0 in year y_0, we generate a set of $N = 100$ simulations until a time $t_0 + T$, with a lead time $T \in \{10, 15, 25, 35\}$ days. In this paper, we make a forecast for $t_0 = t + \delta$. Here, we assume $\delta = 5$ days to refer to the analogs of the atmospheric circulation computed from the ECMWF and CNRM reforecasts 5 days ahead

that are used as input to forecast the average of precipitation between t_0 and $t_0 + T$. In this work, for conciseness, we call T a lead time because $T > 0$ and we consider averages ahead of t_0. However, T is a different quantity from δ.

To generate one trajectory, we proceed as described in Krouma et al. (2022) as follow: we start at day t_0 and randomly select an analog t'_k (out of the $K = 20$ best analogs) of day $t_0 + 1$. The random selection of analogs of the day $t_0 + 1$ is performed with weights that are proportional to the calendar difference between t_0 and analog dates, to ensure that time goes forward (Yiou, 2014). We also exclude analog dates with years that are equal to y_0. This rule is important for the next iterations, in order to produce a hindcast simulation. We then replace t_0 with the selected analog of t'_k and repeat the operation T times. Excluding analogs in year y_0 from the selection ensures that we do not use information from the T days that follow t_0. Next, the simulated precipitation is the next selected analog $t'_k + 1$. Hence, we obtain one hindcast random trajectory between t_0 and $t_0 + T$. Then t_0 is shifted by $\Delta t \approx T/2$ days, and the ensemble simulation procedure is repeated. This provides a set of ensemble forecasts with analogs.

The procedure presented above is repeated $N = 100$ times to simulate $N = 100$ trajectories from t_0 to $t_0 + T$. The daily precipitation of each trajectory is time-averaged between t_0 and $t_0 + T$. Hence, we obtain an ensemble of $N = 100$ forecasts of the average precipitation for a day t_0 and lead time T.

The forecasts of precipitations based on analogs of atmospheric circulation Z500 from the ensemble mean of the CNRM and ECMWF reforecasts, are started every $\Delta t \approx T/2$ day between January 1, 1993 and December 31, 2017 using the CNRM reforecast and between January 1, 2002 and December 31, 2021 using the ECMWF reforecast. This yields a stochastic ensemble hindcast of precipitation and atmospheric circulation (Z500) for the ECMWF and CNRM reforecasts.

The added value of this study compared to the previous study (Krouma et al., 2022) where the atmospheric circulation from reanalyses was used, is that we consider Z500 from the reforecasts of S2S models and at $\delta = 5$ days ahead instead of $\delta = 0$ days as in Krouma et al. (2022), to forecast precipitation beyond 5 days. This means that the circulation analogs calculated in this study are analogs of 5 days ahead (Figure 2). Consequently, the simulations will be called **HC-SWG** forecasts.

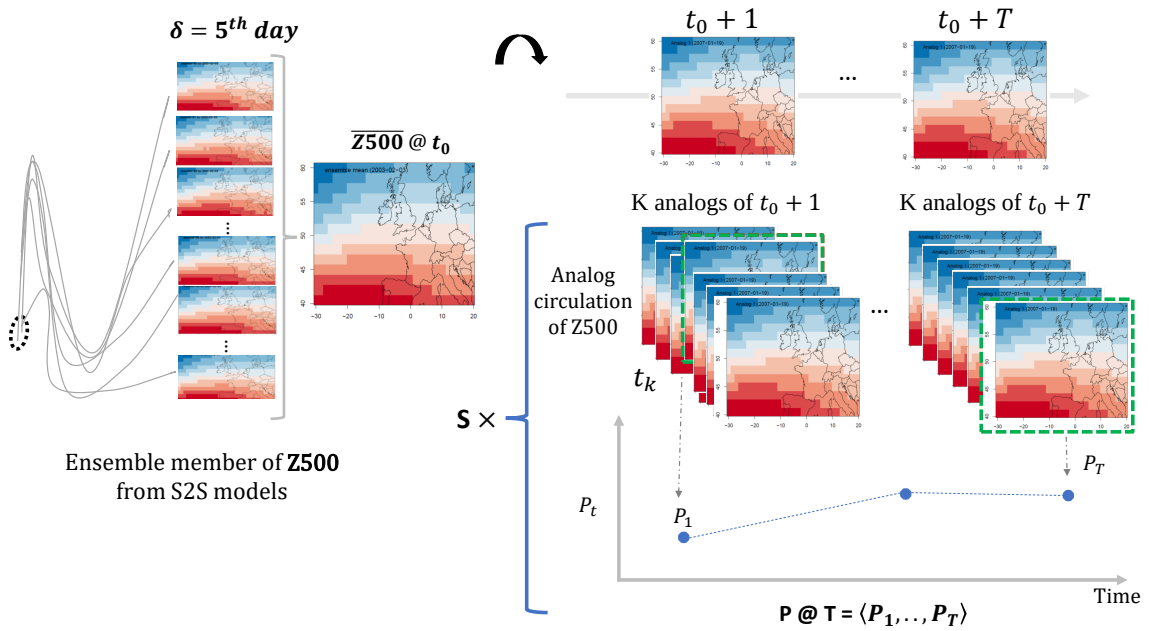

FIGURE 2 Schematic to illustrate the HC-SWG forecast procedure at a day t_0 for a lead time of T days. The starting point is the ECMWF or CNRM reforecasts ensemble members of Z500 at $\delta = 5$ days and the output is the ensemble members of precipitation at a lead time T. This illustration shows the HC-SWG process to generate one trajectory for a day t_0.

Example

To illustrate the procedure, we start from the 11 (or 10) reforecast members of Z500, $\delta = 5$ days ahead to get an ensemble forecast of precipitation, as shown in Figure 2 . For a given day $t_0 = 02/03/2003$, we compute the ensemble average of the Z500 reforecast (either ECMWF or CNRM). Then, we compute analogs from the ensemble average at a day $t_0 = 02/03/2003$, and we keep $K = 20$ best analogs of Z500. For a lead time $T = 3$ days, we randomly select an analog from the 20 analogs of Z500 at $t_0 + 1$. For instance, the first best analog for $t_0 = 02/03/2003$ is $t'_k = 01/19/2007$. We repeat this operation $T = 3$ times. Then, for each analog, we consider the corresponding amount of precipitation. This way, we construct the first trajectory of precipitation as shown in Figure 2 . We generate 100 trajectories of precipitation using the same procedure. Hence, we obtain 100 samples of average precipitation between t_0 and $t_0 + T$ for the defined day t_0 and at $T = 3$ days.

As an example, we show the time series of the simulations and observations of precipitation over Madrid within 15 days for 2003 in Figure 3 . It shows the mean of the 100 simulations (forecast of precipitation) and the observations for lead times of $T = 15$ days for the whole year. We notice that the HC-SWG reproduces precipitation fluctuations within 15 days as it gets the high and low values of precipitation for the whole year. We can also see that all the values are covered, as shown by the 5th and 95th quantiles (dash grey lines in the figure 3).

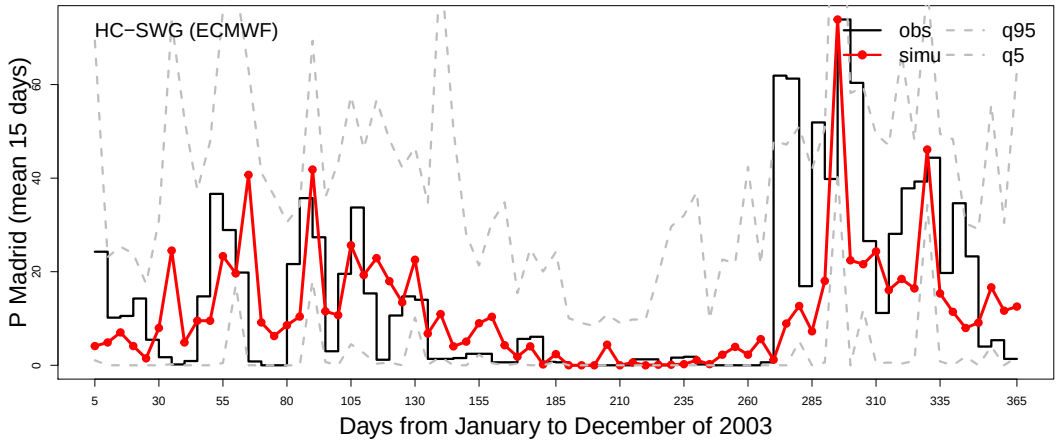

FIGURE 3 Time series of the simulations (red line), observations (black line), and the 5th and 95 the quantiles of simulations (dash grey lines) for precipitation over Madrid at a lead time $T = 15$ days for 2003 using the HC-SWG with hindcast of the ECMWF.

3.3 | Forecast verification

To assess the forecast skill of our model, we used skill scores such as the rank correlation, the Continuous Rank Probability Score (CRPS) and ROC curve (Wilks, 2011). The temporal rank correlation is calculated between the precipitation observations and the median of 100 simulations. The CRPS is a quadratic measure of the difference between the forecast cumulative distribution function and the empirical cumulative distribution function of the observation (Wilks, 2011; Zamo and Naveau, 2018). The CRPS is defined by:

$$CRPS(P, x_a) = \int_{-\infty}^{+\infty} (P(x) - \mathcal{H}(x - x_a))^2 dx, \tag{1}$$

where x_a is the observed precipitation between $[t_0\ ,\ t_0 + T]$, P is the cumulative distribution function of x of the ensemble forecast and $\mathcal{H}$ represents the Heaviside function, ($\mathcal{H}(y) = 1$ if $y \geq 0$, and $\mathcal{H}(y) = 0$ otherwise). A perfect forecast yields a CRPS value equal to 0.

As the CRPS value depends on the unit of the variable to be predicted, it is useful to normalize it with the CRPS value of a reference forecast, which can be obtained by a persistence or climatology hypothesis. The Continuous Rank Probability Skill Score (CRPSS) is defined as a percentage of improvement over such a reference forecast (Hersbach, 2000). We compute the CRPSS with reference values of the CRPS.

$$CRPSS = 1 - \frac{\overline{CRPS}}{\overline{CRPS_{ref}}}, \tag{2}$$

where $\overline{CRPS}$ is the average of the $CRPS$ of the SWG forecast and $\overline{CRPS_{ref}}$ is the average of the $CRPS$ of a reference.

As a reference we used climatology, persistence and model forecasts. The persistence forecast consists of using the average value between $t_0 - T$ and t_0 for a given year. The climatological forecast takes the climatological mean between t_0 and $t_0 + T$. The persistence and climatological forecasts are randomized by adding a small white Gaussian noise, whose standard deviation is estimated by bootstrapping over T long intervals. We also consider the precipitation forecast from the ECMWF model for a third CRPS reference.

The CRPSS values vary between $-\infty$ and 1. The forecast has improvement over the reference when the CRPSS value is above 0. For the comparison of the HC-SWG forecasts with the ECMWF precipitation forecast, we used the "fair CRPSS" (Ferro, 2007, 2014). Indeed, the fair CRPSS takes into account the difference in ensemble sizes as we are generating 100 members versus 51 members from the ECMWF.

The CRPS can be decomposed into three parts: reliability (Re), resolution (Res), and uncertainty (U) (Hersbach, 2000).

$$CRPS = Re - Res + U. \tag{3}$$

The Reliability (Re) tests the capacity of the ensemble to generate a cumulative distribution function that has on average the desired statistical property (Wilks, 2011). The reliability is sensitive to the average spread of the ensemble. The model is perfectly reliable when Re is equal to 0 (Hersbach, 2000). The uncertainty (U) is the CRPS based only on the sample climatology (Wilks, 2011). Resolution (Res) represents the difference with climatology. A positive resolution indicates that the model's performance is better than the climatology. Resolution and uncertainty are related to the average spread within the ensemble and the behaviour of the outliers (Wilks, 2011). In our analysis, we focus more on the interpretation of Re. Indeed, that helps to understand the spread of the ensemble forecast.

The ROC curve is a plot that represents the false rate versus the positive rate. The diagonal line of the ROC curve represents the random classifier obtained when the forecast has no skill. If the ROC curve is below the diagonal line, then the forecast has a poor skill; otherwise, it has a good skill, i.e. the forecast has the potential to distinguish between success and false alarm (Fawcett, 2006). The ROC curve helps to measure the discrimination skill, which defines the ability of the model to distinguish between binary classes (Fawcett, 2006; Krouma et al., 2023). The Area Under the Curve (AUC) can quantify the discrimination skill. The AUC explains how much the forecast model can distinguish events and non-events of precipitation (Fawcett, 2006; Toth et al., 2003). In our case, we consider that:

- Precipitation < 1 mm as a non-event,
- and P > 1 mm as an event of precipitation.

We also evaluate the capacity of our model to detect extreme events of precipitation. We define the extreme event of precipitation as the precipitation that exceeds the 90^{th} percentile. And our binary classification for extremes is defined as follows:

- P $< q_{90}$ as a non-event,
- P $> q_{90}$ as an extreme event of precipitation.

4 | RESULTS

4.1 | Evaluation of the forecast of the precipitation using HC-SWG in Europe

We first evaluate the HC-SWG forecast of the precipitation over Europe using the CRPSS with respect to persistence and climatology. We make two separate forecasts using the HC-SWG based on analogs of Z500 computed from the ensemble mean of the ECWMF and CNRM S2S reforecast for 5 days ahead for the period between respectively 2002-2021 and 1993-2017. In this paper, we choose to show skill scores for DJF (December, January and February) and JJA (June, July, and August) for the sake of brevity. The computations of the CRPS were made using observations of precipitation from E-Obs (Haylock et al., 2008).

We find that the HC-SWG forecasts show positive improvement against persistence and climatology in different European locations in DJF and JJA (positive values of CRPSS). We notice that the CRPSS for the HC-SWG forecasts using analogs from the ECMWF reforecast has higher scores against persistence and climatology than using analogs from the CNRM reforecast. The CRPSS against persistence is higher in the summer in particular in July in southwest Europe (Figure 4). However, for the winter, the CRPSS against persistence is higher for northern Europe, mainly in France and Germany. The CRPSS for the HC-SWG forecasts using analogs of the CNRM reforecast still shows a positive improvement for the different locations with smaller values of 0.2 to 0.3 (Figure 4). The higher skill values are also obtained in southern Europe. The difference in the HC-SWG forecast skill using the ECMWF and CNRM reforecast could be mainly related to the difference in the configuration of the two dynamic models and the resolution of each model. Similar results have been found by Ardilouze et al. (2021) for 2-meter temperature over Europe, where scores highlighted a better performance of the ECMWF over CNRM for every lead time (weeks).

4.2 | Evaluation of the forecast at the station level

We evaluate the forecast of precipitation using the HC-SWG at the station level for Orly, Berlin, Toulouse, Madrid. The motivation behind choosing those particular stations despite the availability of precipitation observations all over Europe is to ensure a comparison with the previous work Krouma et al. (2022). The computations of the CRPS were made using observations of precipitation from ECA&D databases.

At a local scale, we find that the CRPSS shows a positive improvement for $T \leq 35$ days for the different studied locations for both winter (DJF) and summer (JJA) seasons as shown in Figure 5 for the HC-SWG forecast using analogs of the ECMWF reforecast. We notice that the CRPSS against persistence is higher for Madrid and Toulouse, in particular for JJA, which is consistent with the result of in section 4.1. We notice that the CRPSS against persistence is stable for the four stations in DJF. However, the CRPSS against the climatology decreases with lead time but is still positive within 35 days. This indicates that the HC-SWG performs better than persistence for the different lead times. We argue the increasing of the CRPSS at a lead time of 35 days using the decomposition of the CRPS represented in Appendix (Figure 9). Indeed, we find that the HC-SWG forecast has small reliability values for the different lead times and stations. This confirms the good performance of the HC-SWG. However, we notice that the reliability increases from $T = 25$ days in Madrid as well as Berlin compared to the rest of the studied areas which can explain the highest CRPSS with respect to persistence. This could be related to a larger spread of the ensemble forecast of the HC-SWG from $T = 25$ days. Similar results were found for the HC-SWG forecast using analogs of the CNRM reforecasts Appendix Figure A1 .

4.3 | Comparison of HC-SWG forecasts derived from CNRM or ECMWF

We compare the performance of the HC-SWG using analogs of the ECMWF and CNRM ensemble reforecasts at the station level. We notice that the CRPSS for both sets of HC-SWG forecasts and for the four studied areas is showing a positive improvement over the climatology and the persistence (Appendix Figure A1).

Although the performance of the HC-SWG using analogs computed from ECMWF or CNRM ensemble mean reforecasts of Z500 hPa for $\delta = 5$ days ahead is different at the European level, we found a comparable performance and skill scores when we compare them at the station level. That may be related to some reasons related to the configuration of the models or even to specific regions where the models performs differently from one region to another, as shown by Hewson and Pillosu (2021).

The HC-SWG shows stable CRPSS values against the persistence (Appendix Figure A1 e – h). It is still higher for Madrid in JJA and for Berlin in DJF. However, it decreases with T against climatology (Appendix Figure A1 e – h). Comparing the correlation between the average of the 100 simulations of the HC-SWG and the observations (ECA&D), we notice a tiny difference in the correlation between the two forecasts as illustrated in Figure 6 .

When comparing the forecast skill of the HC-SWG to that of the SWG in Krouma et al. (2022), we find that considering Z500 analogs from the ECMWF and CNRM S2S ensemble mean reforecast for 5 days ahead helped to improve the precipitation forecast for T up to 35 days in different locations in Europe. The forecast at the station level with the SWG in Krouma et al. (2022, e.g. Figure 4) gave a good forecast skill with respect to climatology and persistence for T up to 10 days, and the CRPSS was higher during the DJF with values of CRPSS with respect to climatology and persistence ranges respectively between [0.57 , 0.48] and [0.6 , 0.42] (Krouma et al., 2022). However, the CRPSS decreases considerably during JJA with the SWG as shown in Table 2 . With the HC-SWG, the CRPSS with respect to the climatology and the persistence shows a positive improvement

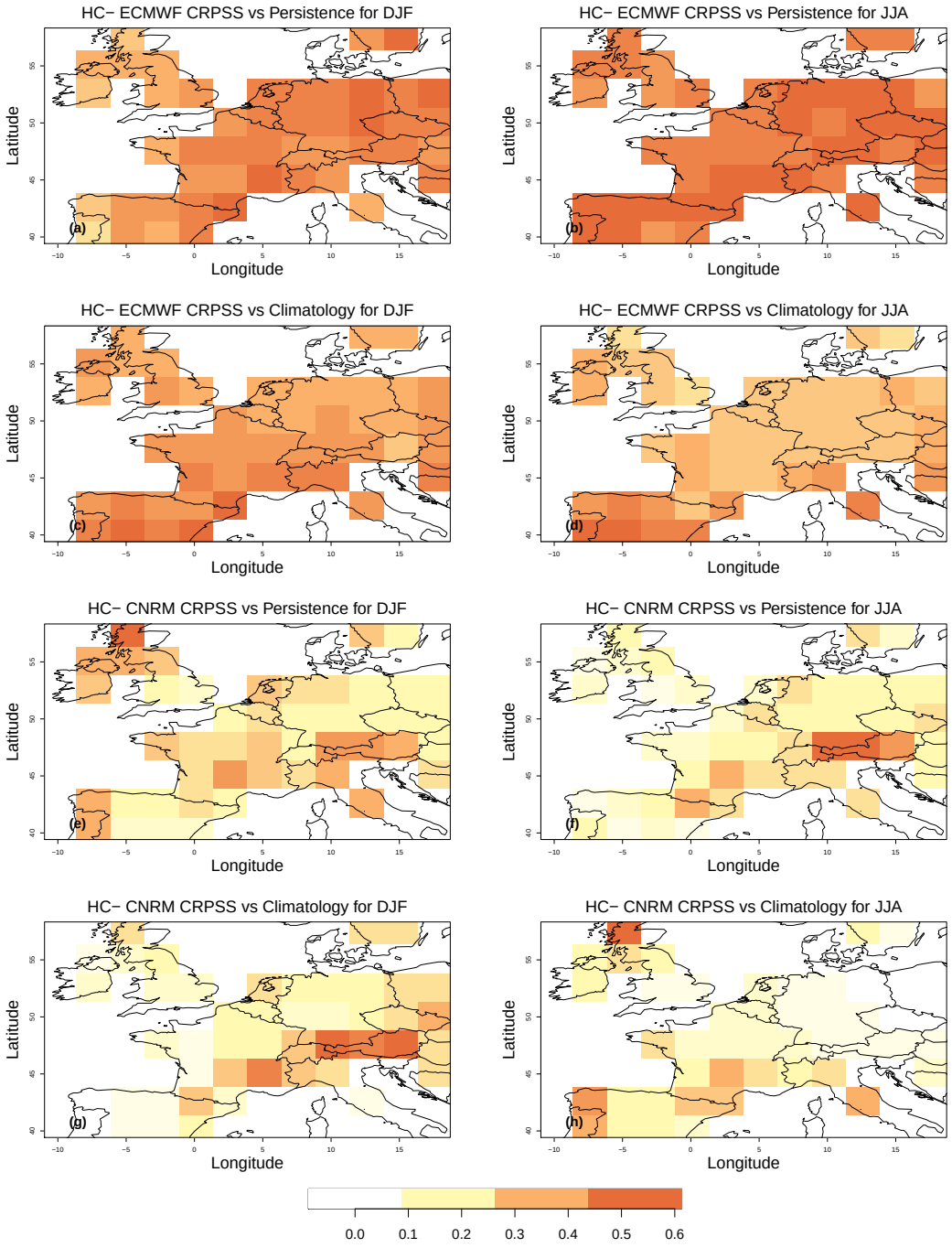

FIGURE 4 CRPSS with respect to persistence and climatology for the forecast of the European precipitation with HC-SWG forecast using analogs of ECMWF and CNRM dynamical models for DJF and JJA for a lead time of 10 days.

for both seasons DJF and JJA, and stays stable for the different lead times (Appendix Figure A1 and Table 2). For instance, the HC-SWG forecasts for Berlin are showing good skill (CRPSS against persistence and climatology) for the different lead times using analogs of Z500 from ECMWF and CNRM reforecasts compared to the SWG forecast of precipitation in Berlin based on analogs of Z500 computed from reanalyses (Table 2) (Krouma et al., 2022, Figure 4).

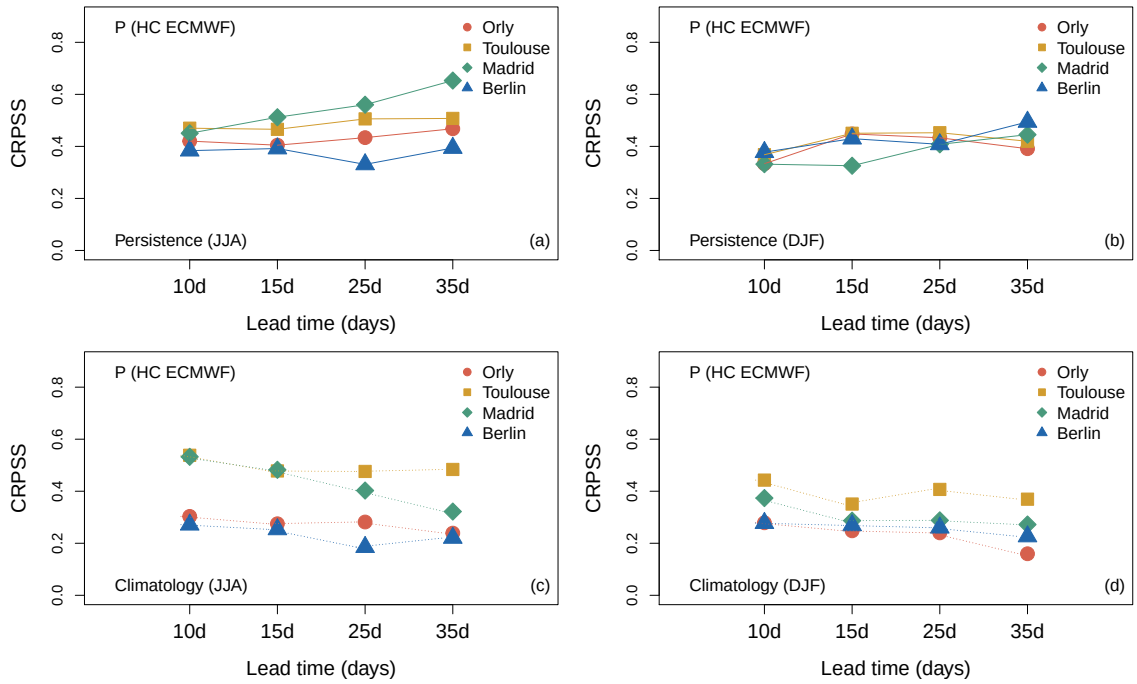

FIGURE 5 CRPSS with respect to climatology in Europe for HC-SWG forecast using ECMWF and CNRM dynamical models for DJF and JJA.

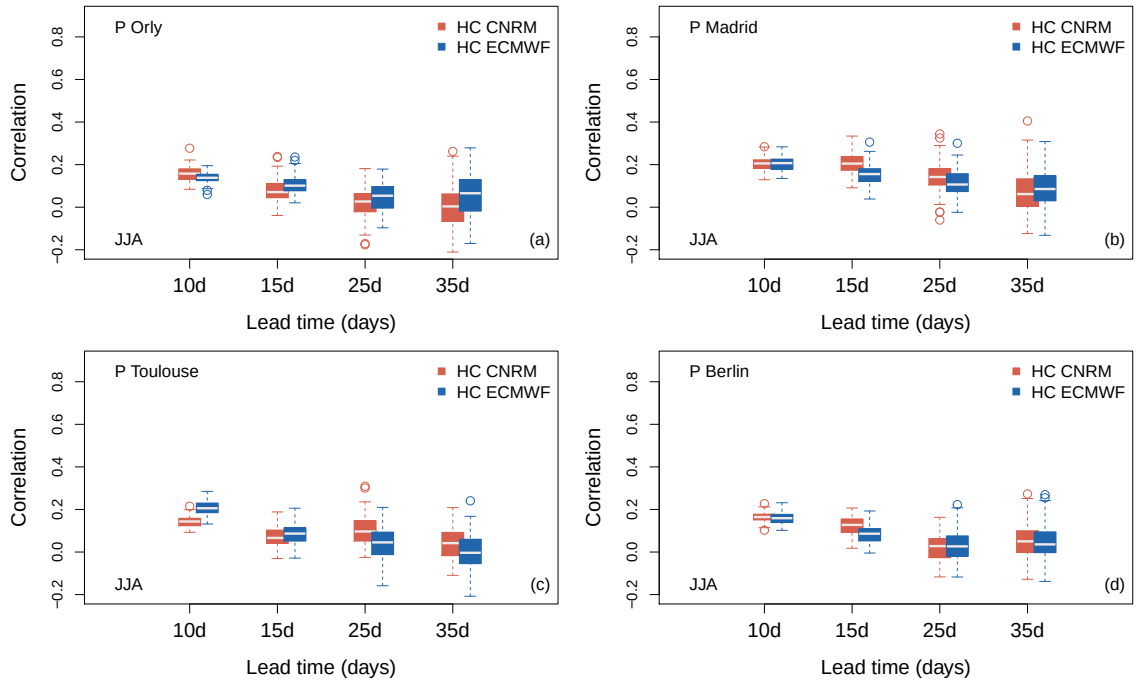

FIGURE 6 Comparison of the rank Correlation between the HC-SWG forecast using analogs of the ECMWF and CNRM reforecasts for all lead times, and for the different studied stations for DJF and JJA.

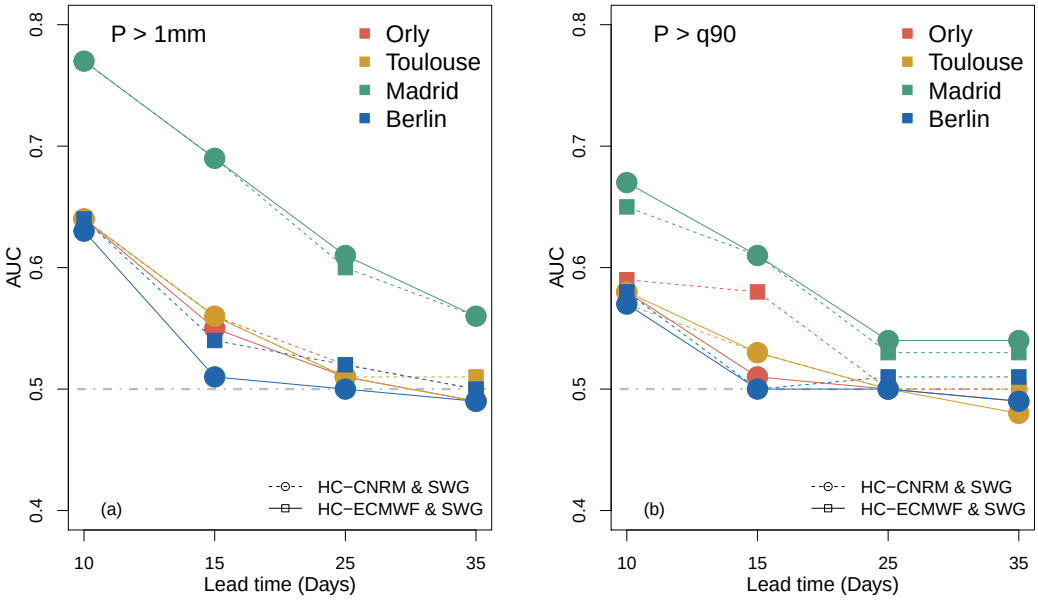

FIGURE 7 AUC for Orly, Madrid, Toulouse, and Berlin for HC-SWG precipitation forecast based on ECMWF (solid line with square) and CNRM (dash line with circle) reforecasts. (a) AUC for precipitation considering 1 mm as a threshold, (b) AUC for extreme precipitation that exceeds the 90th quantile. The dashed grey line represents the diagonal of the ROC curve ($AUC = 0.5$).

TABLE 2 Comparison between the CRPSS with respect to the climatology of the HC-SWG and the SWG in Krouma et al. (2022) in JJA for $T = 10, 20$ days.

	$T = 10$ days		$T = 20$ days	
	HC-SWG	SWG	HC-SWG	SWG
Orly	**0.38**	0.28	**0.38**	0.2
Madrid	**0.58**	0.42	**0.55**	0.38
Berlin	**0.35**	32	**0.30**	0.22
Toulouse	**0.30**	0.58	**0.50**	0.31

Next, we compared the ROC curves for the HC-SWG forecasts based on analogs of Z500 from ECMWF and CNRM dynamical models for the different studied areas (Berlin, Madrid, Orly, Toulouse) and for lead times going from 10 to 35 days. The ROC curve helps to determine the discrimination skill of the HC-SWG. We considered an event of precipitation when the daily amount of precipitation is above 1 mm; otherwise, there is a non-event (Figure 7 -a). We noticed that the HC-SWG is able to distinguish between events and non-events of precipitation for the different studied areas until $T = 15$ days (Figure 7 -a). For Madrid, we notice that the HC-SWG is able to distinguish between precipitation events and non-events until 35 days. We found that the HC-SWG forecasts from analogs of ECMWF or CNRM dynamical models show the same behaviour except for Berlin where we noticed that the discrimination skill persists until 25 days using analogs of ECMWF model. The AUC values range between 0.77 and 0.58 at $T = 15$ days (Figure 7 -a). The HC-SWG keep its skill to distinguish between events and non-events of precipitation as the AUC values are over 0.5 i.e. above the diagonal of ROC curve. We notice that the positive rate is 0.85 for 10 days for Madrid, Orly, Toulouse, and Berlin using analogs of ECMWF or CNRM, but it decreases differently with lead time and from one station to the other.

In addition, we verified the discrimination skill of the HC-SWG using the analogs of both ECMWF and CNRM models for extreme precipitation (Figure 7 -b). For $T = 10$ days, the AUC values range between 0.67 (Madrid) and 0.57 (Berlin) that

indicates that the HC-SWG conserves its capacity to distinguish between non-events of extreme precipitation ($<q_{90}$) and events of extreme precipitation ($> q_{90}$).

We assessed the statistical significance of the AUC in both cases using the Mann-Whitney test (Wilks, 2011) that we describe in Appendix B. We found that the AUC of the HC-SWG using the ECMWF reforecast is significant until $T = 25$ days for Madrid, Orly and Berlin (Table B1). For extreme precipitation, the discrimination skill is significant until 10 days for all stations and until $T = 15$ days with ECMWF reforecast for Madrid and Orly as highlighted in Table B1 .

4.4 | Comparison of HC-SWG and ECMWF precipitation forecast

We compared the HC-SWG precipitation forecasts to the ECMWF precipitation forecast by computing the fair CRPSS as shown in equation (2). We used the ECMWF precipitation forecast as a reference to the HC-SWG forecasts. Positive values indicate an improvement of the HC-SWG forecast over the ECMWF or the CNRM precipitation forecasts. We choose to compare the HC-SWG forecast to the ECMWF precipitation forecast up to 25 days as the AUC values are mainly significant until $T = 25$ days as shown earlier (see also Appendix B).

The comparison shows that the HC-SWG improves the precipitation forecast up to 25 days with respect to the ECMWF precipitation forecast by using either the CNRM or ECMWF analogs of Z500. As shown in figure 8 , we found that the HC-SWG forecast of precipitation based on analogs of ECMWF (figure 8 -a) and CNRM (figure 8 -b) reforecasts of Z500 is more skillful than the ECMWF precipitation forecast for different lead times and for the studied locations, except for Toulouse and Madrid respectively at a lead time of 10 and 25 days. The HC-SWG forecasts based on analogs of the CNRM reforecasts of Z500 show no improvement for Berlin for $T < 15$ days. The ECMWF precipitation forecast shows a better skill for Madrid at 25 days compared to the HC-SWG forecast. Moreover, we notice that the improvement of the HC-SWG using analogs of Z500 of the ECMWF reforecasts is higher than by using CNRM reforecasts.

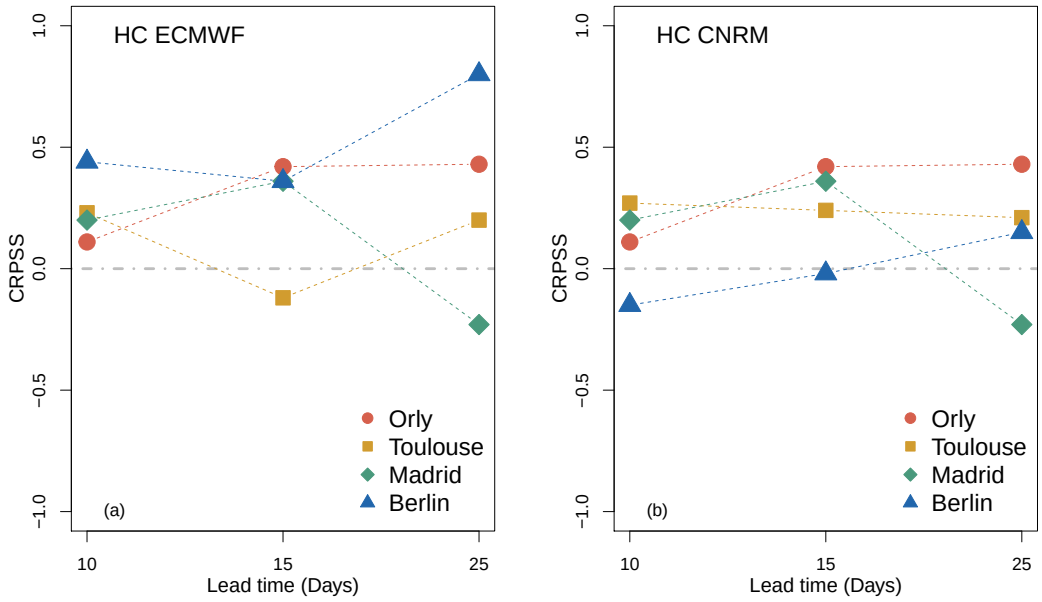

FIGURE 8 CRPSS between the ECMWF precipitation forecast and the HC-SWG forecasts based on the ECMWF and CNRM reforecasts. The CRPSS is computed between the HC-SWG and as a reference, we considered the ECMWF precipitation forecast.

To better explain these results, we compared the CRPS reliability of the HC-SWG forecasts of precipitation using the ECMWF and CNRM reforecasts to the CRPS reliability of the ECMWF precipitation forecast as shown in Figure 9 . We found that the HC-SWG forecast is more reliable for the different lead times and stations compared to the ECMWF precipitation forecast. This confirms the good performance of the HC-SWG compared to the numerical model. However, we notice that the reliability of

the ECMWF precipitation forecast is lower than that of the HC-SWG forecast in Madrid at $T = 25$ days, which can explain the negative CRPSS of the HC-SWG at 25 days for Madrid with respect to the ECMWF precipitation forecast.

Both the HC-SWG and the SWG in (Krouma et al., 2022, Table 6) show comparable improvement in the forecast of precipitation compared to the ECMWF precipitation forecast. The added value of the HC-SWG is that the forecast is initiated at $\delta = 5$ days ahead compared to the SWG in Krouma et al. (2022) where reanalyses were used to define analogs at $\delta = 0$. As well as the HC-SWG can forecast precipitation for further lead times T and with better skill (Table 2) compared to the SWG in Krouma et al. (2022).

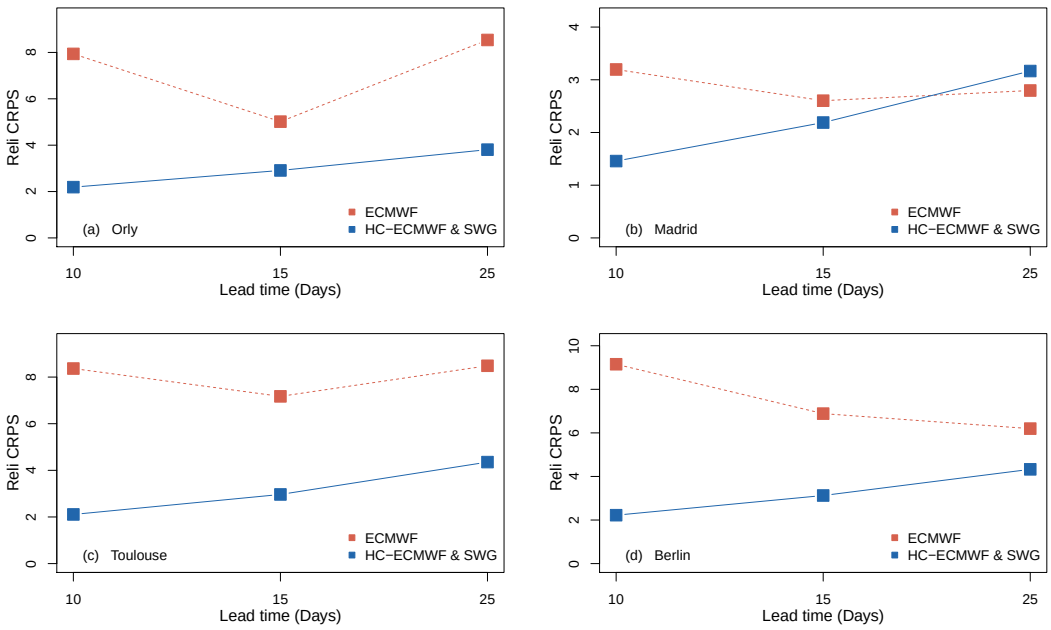

FIGURE 9 Comparison between the CRPS reliability of the HC-SWG forecasts based on ECMWF reforecasts and the CRPS reliability of the ECMWF precipitation forecast.

5 | CONCLUSION

The use of the S2S ECMWF and CNRM ensemble mean reforecasts of the geopotential height at 500 hPa for 5 days ahead helped to improve statistical features of the precipitation forecast over Europe with a stochastic weather generator. The HC-SWG confirmed its capacity to forecast precipitation for up to 35 days in Europe and at the station level. However, the forecast skill differs from one region to another and remains higher over southernmost locations for either summer or winter. The SWG based on analogs circulation has been used in previous studies (Krouma et al., 2022, 2023; Yiou and Déandréis, 2019) to forecast temperature, precipitation and Madden-Julian oscillation. In this version, the HC-SWG confirmed the capacity of the SWG and analogs circulation to forecast precipitation at a local scale as the SWG in Krouma et al. (2022), by showing good skill scores in different regions despite the variety of the local weather and for longer lead time 35 days compared to 10 days in Krouma et al. (2022). The HC-SWG confirmed its capacity to distinguish between events and non-events of precipitation as well as extreme precipitation at least for a lead time of 10 days. In addition, the comparison with the ECMWF precipitation forecast confirmed the performance of the HC-SWG forecasts for $T = 25$ days.

Comparing the HC-SWG precipitation forecast to the SWG precipitation forecast in Krouma et al. (2022), we also noticed the added value of using the analogs computed from reforecasts of Z500 from dynamical models at $\delta = 5$ days instead of using reanalyses of the atmospheric circulation with a $\delta = 0$.

Combining dynamical models with the SWG allowed the improvement of the precipitation forecast to the subseasonal lead time. This work highlights the contribution of dynamical models with a correct initialisation (Zuo et al., 2016) to get a skilful forecast. These results can be considered as a starting point to implement an operational forecast from the HC-SWG at the subseasonal lead time. This can help to verify the forecast skill of the HC-SWG in a real-time. The HC-SWG can also be tested to forecast other meteorological variables and in different regions of the globe. This can help to improve forecasts and verify the capacity of our forecasting tool.

We used the ensemble mean of the Z500 for 5 days ahead to forecast the precipitation. This approach showed a capacity to improve the European precipitation forecast. However, this approach must be verified and adjusted while using the atmospheric circulation for more δ days ahead like for 10 or even more. The verification would depend on the atmospheric circulation field, its forecast skill at different lead times and on the quality of the ensemble member that would help to avoid smoothing data and get wrong analogs.

6 | ACKNOWLEDGEMENTS

This work is part of the EU International Training Network (ITN) Climate Advanced Forecasting of subseasonal Extremes (CAFE). The project receives funding from the European Union's Horizon 2020 research and innovation programme under the Marie Skłodowska-Curie Grant Agreement No 813844.

References

Ailliot, P., Allard, D., Monbet, V., and Naveau, P.: Stochastic weather generators: an overview of weather type models, Journal de la Société Française de Statistique, 156, 101–113, 2015.

Ardilouze, C., Specq, D., Batté, L., and Cassou, C.: Flow dependence of wintertime subseasonal prediction skill over Europe, Weather and Climate Dynamics, 2, 1033–1049, , 2021.

Atencia, A. and Zawadzki, I.: A comparison of two techniques for generating nowcasting ensembles. Part I: Lagrangian ensemble technique, Monthly Weather Review, 142, 4036–4052, 2014.

Batté, L. and Déqué, M.: Randomly correcting model errors in the ARPEGE-Climate v6.1 component of CNRM-CM: applications for seasonal forecasts, Geoscientific Model Development, 9, 2055–2076, , 2016.

Blanchet, J., Stalla, S., and Creutin, J.-D.: Analogy of multiday sequences of atmospheric circulation favoring large rainfall accumulation over the French Alps, Atmospheric Science Letters, 19, e809, , 2018.

Cornes, R. C., van der Schrier, G., van den Besselaar, E. J. M., and Jones, P. D.: An Ensemble Version of the E-OBS Temperature and Precipitation Data Sets, Journal of Geophysical Research: Atmospheres, 123, 9391–9409, , 2018.

Fawcett, T.: An introduction to ROC analysis, Pattern Recognition Letters, 27, 861–874, , 2006.

Ferro, C. A. T.: A probability model for verifying deterministic forecasts of extreme events, Weather and Forecasting, 22, 1089–1100, , 2007.

Ferro, C. A. T.: Fair scores for ensemble forecasts, Quarterly Journal of the Royal Meteorological Society, 140, 1917–1923, , 2014.

Haylock, M. R., Hofstra, N., Tank, A. M. G. K., Klok, E. J., Jones, P. D., and New, M.: A European daily high-resolution gridded data set of surface temperature and precipitation for 1950-2006, J. Geophys. Res. - Atmospheres, 113, , 2008.

Hersbach, H.: Decomposition of the Continuous Ranked Probability Score for Ensemble Prediction Systems, WEATHER AND FORECASTING, 15, 559–570, , 2000.

Hersbach, H., Bell, B., Berrisford, P., Hirahara, S., Horányi, A., Muñoz-Sabater, J., Nicolas, J., Peubey, C., Radu, R., and Schepers, D.: The ERA5 global reanalysis, Quat. J. Roy. Met. Soc., 146, 1999–2049, 2020.

Hewson, T. D. and Pillosu, F. M.: A low-cost post-processing technique improves weather forecasts around the world, Communications Earth & Environment, 2, 132, 2021.

Karl, T. R., Wang, W.-C., Schlesinger, M. E., Knight, R. W., and Portman, D.: A Method of Relating General Circulation Model Simulated Climate to the Observed Local Climate. Part I: Seasonal Statistics, Journal of Climate, 3, 1053 – 1079, , 1990.

Klein, W. H., Lewis, B. M., and Enger, I.: OBJECTIVE PREDICTION OF FIVE-DAY MEAN TEMPERATURES DURING WINTER, Journal of Atmospheric Sciences, 16, 672 – 682, , 1959.

Klein Tank, A. M. G., Wijngaard, J. B., Können, G. P., Böhm, R., Demarée, G., Gocheva, A., Mileta, M., Pashiardis, S., Hejkrlik, L., Kern-Hansen, C., Heino, R., Bessemoulin, P., Müller-Westermeier, G., Tzanakou, M., Szalai, S., Pálsdóttir, T., Fitzgerald, D., Rubin, S., Capaldo, M., Maugeri, M., Leitass, A., Bukantis, A., Aberfeld, R., van Engelen, A. F. V., Forland, E., Mietus, M., Coelho, F., Mares, C., Razuvaev, V., Nieplova, E., Cegnar, T., Antonio López, J., Dahlström, B., Moberg, A., Kirchhofer, W., Ceylan, A., Pachaliuk, O., Alexander, L. V., and Petrovic, P.: Daily dataset of 20th-century surface air temperature and precipitation series for the European Climate Assessment, International Journal of Climatology, 22, 1441–1453, , 2002.

Koster, R. D., Mahanama, S., Yamada, T., Balsamo, G., Berg, A., Boisserie, M., Dirmeyer, P., Doblas-Reyes, F., Drewitt, G., Gordon, C., et al.: Contribution of land surface initialization to subseasonal forecast skill: First results from a multi-model experiment, Geophysical Research Letters, 37, 2010.

Krouma, M., Yiou, P., Déandreis, C., and Thao, S.: Assessment of stochastic weather forecast of precipitation near European cities, based on analogs of circulation, Geoscientific Model Development, 15, 4941–4958, , 2022.

Krouma, M., Silini, R., and Yiou, P.: Ensemble forecast of an index of the Madden–Julian Oscillation using a stochastic weather generator based on circulation analogs, Earth System Dynamics, 14, 273–290, , 2023.

Lau, W. K.-M. and Waliser, D. E.: Intraseasonal variability in the atmosphere-ocean climate system, Springer Science & Business Media, 2011.

Lin, H. and Wu, Z.: Contribution of the autumn Tibetan Plateau snow cover to seasonal prediction of North American winter temperature, Journal of Climate, 24, 2801–2813, 2011.

Lorenz, E. N.: Atmospheric Predictability as Revealed by Naturally Occurring Analogues, J. Atmos. Sci., 26, 636–646, 1969.

Magnusson, L. and Källén, E.: Factors Influencing Skill Improvements in the ECMWF Forecasting System, Monthly Weather Review, 141, 3142 – 3153, , 2013.

Merryfield, W. J., Baehr, J., Batté, L., Becker, E. J., Butler, A. H., Coelho, C. A., Danabasoglu, G., Dirmeyer, P. A., Doblas-Reyes, F. J., Domeisen, D. I., et al.: Current and emerging developments in subseasonal to decadal prediction, Bulletin of the American Meteorological Society, 101, E869–E896, 2020.

Newman, M., Sardeshmukh, P. D., Winkler, C. R., and Whitaker, J. S.: A study of subseasonal predictability, Monthly weather review, 131, 1715–1732, 2003.

Palmer, T. N.: Predicting uncertainty in forecasts of weather and climate, Reports on Progress in Physics, 63, 71–116, , 2000.

Rashid, H. A., Hendon, H. H., Wheeler, M. C., and Alves, O.: Prediction of the Madden–Julian oscillation with the POAMA dynamical prediction system, Climate Dynamics, 36, 649–661, 2011.

Robertson, A. W. and Vitart, F.: SUB-SEASONAL TO SEASONAL PREDICTION The Gap Between Weather and Climate Forecasting, vol. 569, Elsevier, 2019.

Specq, D. and Batté, L.: Improving subseasonal precipitation forecasts through a statistical–dynamical approach : application to the southwest tropical Pacific, Climate Dynamics, p. 15, 2020.

Toth, Z., Talagrand, O., Candille, G., and Zhu, Y.: Probability and ensemble forecasts, Forecast verification: A practitioner's guide in atmospheric science, 137, 163, 2003.

Vitart, F.: Evolution of ECMWF sub-seasonal forecast skill scores, Quarterly Journal of the Royal Meteorological Society, 140, 1889–1899, 2014.

Vitart, F., Ardilouze, C., Bonet, A., Brookshaw, A., Chen, M., Codorean, C., Déqué, M., Ferranti, L., Fucile, E., Fuentes, M., Hendon, H., Hodgson, J., Kang, H.-S., Kumar, A., Lin, H., Liu, G., Liu, X., Malguzzi, P., Mallas, I., Manoussakis, M., Mastrangelo, D., MacLachlan, C., McLean, P., Minami, A., Mladek, R., Nakazawa, T., Najm, S., Nie, Y., Rixen, M., Robertson, A. W., Ruti, P., Sun, C., Takaya, Y., Tolstykh, M., Venuti, F., Waliser, D., Woolnough, S., Wu, T., Won, D.-J., Xiao, H., Zaripov, R., and Zhang, L.: The Subseasonal to Seasonal (S2S) Prediction Project Database, Bulletin of the American Meteorological Society, 98, 163–173, , 2017.

Vitart, F., Balsamo, G., Bidlot, J.-R., Lang, S., Tsonevsky, I., Richardson, D., and Alonso-Balmaseda, M.: Use of ERA5 to Initialize Ensemble Re-forecasts, 841, ECMWF Technical Memoranda, , 2019.

White, C. J., Domeisen, D. I., Acharya, N., Adefisan, E. A., Anderson, M. L., Aura, S., Balogun, A. A., Bertram, D., Bluhm, S., Brayshaw, D. J., et al.: Advances in the application and utility of subseasonal-to-seasonal predictions, Bulletin of the American Meteorological Society, pp. 1–57, 2022.

Wilks, D. S.: Statistical methods in the atmospheric sciences, vol. 100, Academic press, 2011.

Wilks, D. S. and Wilby, R. L.: The weather generation game: a review of stochastic weather models, Progress in Physical Geography: Earth and Environment, 23, 329–357, , 1999.

Woolnough, S., Vitart, F., and Balmaseda, M.: The role of the ocean in the Madden–Julian Oscillation: Implications for MJO prediction, Quarterly Journal of the Royal Meteorological Society: A journal of the atmospheric sciences, applied meteorology and physical oceanography, 133, 117–128, 2007.

Yiou, P.: AnaWEGE: a weather generator based on analogues of atmospheric circulation, Geoscientific Model Development, 7, 531–543, , 2014.

Yiou, P. and Déandréis, C.: Stochastic ensemble climate forecast with an analogue model, Geoscientific Model Development, 12, 723–734, , 2019.

Yiou, P., Salameh, T., Drobinski, P., Menut, L., Vautard, R., and Vrac, M.: Ensemble reconstruction of the atmospheric column from surface pressure using analogues, Climate Dynamics, 41, 1333–1344, , 2013.

Zamo, M. and Naveau, P.: Estimation of the Continuous Ranked Probability Score with Limited Information and Applications to Ensemble Weather Forecasts, Mathematical Geosciences, 50, 209–234, 2018.

Zuo, J., Ren, H.-L., Li, W., and Wang, L.: Interdecadal variations in the relationship between the winter North Atlantic Oscillation and temperature in south-central China, Journal of Climate, 29, 7477–7493, 2016.

How to cite this article: Krouma M., Specq D., Magunsson L., Ardilouze C., Batté L. and Yiou P. (2023), Improving subseasonal forecast of precipitation in Europe by combining a stochastic weather generator with dynamical models, *Q.J.R. Meteorol. Soc.*, .

APPENDIX

A COMPARISON BETWEEN THE FORECAST USING ANALOGS OF THE CNRM ECMWF REFORECASTS

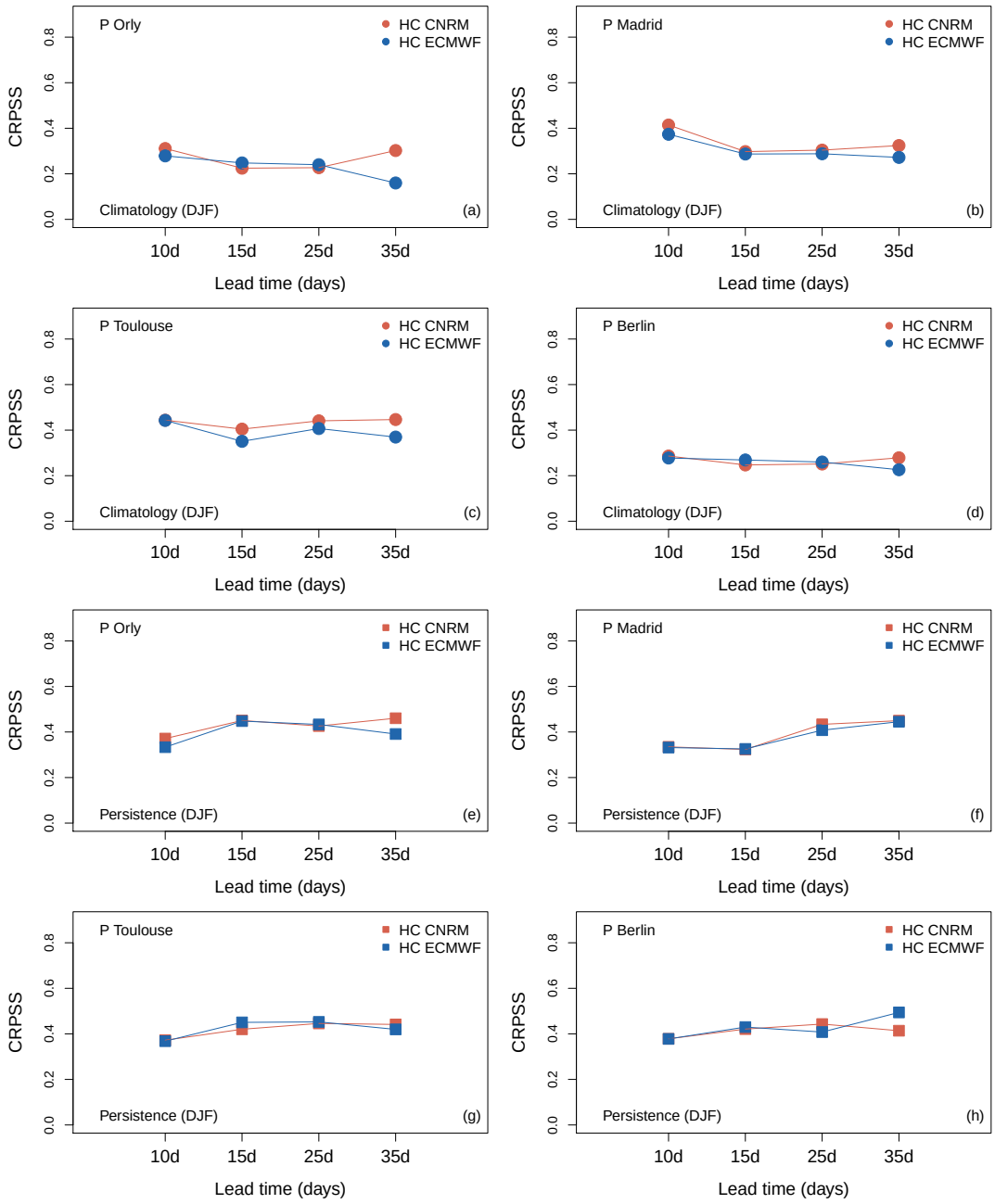

FIGURE A1 Comparison of the CRPSS with respect to the climatology (a – d) and the persistence (e – h) of the HC-SWG forecast using analogs of the ECMWF and CNRM reforecasts for all lead times and for the different studied areas at winter DJF.

B STATISTICAL SIGNIFICANCE OF THE AREA UNDER THE ROC CURVE (AUC) FOR HC-SWG PRECIPITATION FORECAST FOR DIFFERENT LEAD TIMES

We evaluated the discrimination skill of the HC-SWG forecast of European precipitation using the AUC as described in section 3. We assessed the statistical significance of the AUC of the HC-SWG forecasts with the ECMWF and CNRM reforecasts against the AUC_{obs}. The AUC_{obs} depends on the event and non-event of precipitation in the observations.

To define the AUC_{obs} is computed as follows (Wilks, 2011, Chap.7):

$$AUC_{obs} = \frac{1 - U}{n1 * n2} \tag{B1}$$

Where $n1$ is the event of precipitation on the observations and $n2$ is the non-event of precipitation. and U is the Mann-Whitney variable defined from $n1$ and $n2$ (Wilks, 2011, Chap.7). The interpretation of this significance test is as follows: If $AUC_{SWG} > AUC_{obs}$, the AUC value of the SWG is significant otherwise it is not significant.

We applied this test for the event and non-event of precipitation where (precipitation events are above 1mm and non-event with precipitation below 1mm) as shown in Table B1 and extreme precipitation (where extreme precipitation events are above q_{90} and non-event with precipitation below q_{90}) as illustrated in Table B2 .

TABLE B1 Significant test for AUC of Orly, Madrid, Toulouse, and Berlin for HC-SWG forecast for non-event of precipitation (< 1 mm) and event of precipitation (> 1 mm) based on ECMWF (AUC_{ECMWF}) and CNRM reforecasts (AUC_{CNRM}) for different lead times

		Madrid	Orly	Berlin	Toulouse
T=10	AUC_{ECMWF}	**0.77**	**0.64**	**0.64**	**0.64**
	AUC_{CNRM}	**0.77**	**0.64**	**0.63**	**0.64**
	AUC_{obs}	0.52	0.51	0.52	0.51
T=15	AUC_{ECMWF}	**0.69**	**0.56**	**0.54**	**0.56**
	AUC_{CNRM}	**0.69**	**0.55**	0.51	**0.56**
	AUC_{obs}	0.53	0.52	0.52	0.52
T=25	AUC_{ECMWF}	**0.6**	**0.53**	**0.53**	0.51
	AUC_{CNRM}	**0.61**	0.51	0.50	0.51
	AUC_{obs}	0.54	0.53	0.53	0.53
T=35	AUC_{ECMWF}	**0.56**	0.50	0.50	0.51
	AUC_{CNRM}	**0.56**	0.49	0.49	0.49
	AUC_{obs}	0.55	0.54	0.54	0.53

TABLE B2 Significant test for AUC of Orly, Madrid, Toulouse, and Berlin for HC-SWG extreme precipitation forecast based on ECMWF and CNRM reforecasts for different lead times.

		Madrid	Orly	Berlin	Toulouse
T=10	AUC_{ECMWF}	**0.65**	**0.59**	**0.58**	**0.57**
	AUC_{CNRM}	**0.67**	**0.58**	**0.57**	**0.58**
	AUC_{obs}	0.52	0.51	0.52	0.52
T=15	AUC_{ECMWF}	**0.61**	**0.58**	0.50	0.53
	AUC_{CNRM}	**0.61**	0.51	0.50	0.53
	AUC_{obs}	0.54	0.54	0.54	0.54
T=25	AUC_{ECMWF}	0.53	0.50	0.51	0.50
	AUC_{CNRM}	0.54	0.50	0.50	0.50
	AUC_{obs}	0.55	0.55	0.55	0.56
T=35	AUC_{ECMWF}	0.53	0.50	0.51	0.50
	AUC_{CNRM}	0.54	0.49	0.49	0.48
	AUC_{obs}	0.57	0.57	0.57	0.57

Appendix C

Supplement of the article "Ensemble forecast of an index of the Madden Julian Oscillation using a stochastic weather generator based on circulation analogs"

Earth Syst. Dynam., 14, 273–290, 2023
https://doi.org/10.5194/esd-14-273-2023

Earth System Dynamics
Open Access
EGU

Ensemble forecast of an index of the Madden–Julian Oscillation using a stochastic weather generator based on circulation analogs

Meriem Krouma[1,2], **Riccardo Silini**[3], **and Pascal Yiou**[2]

[1]ARIA Technologies, 8 Rue de la Ferme, 92100 Boulogne-Billancourt, France
[2]Laboratoire des Sciences du Climat et de l'Environnement, UMR 8212 CEA-CNRS-UVSQ, IPSL, Université Paris-Saclay, 91191 Gif-sur-Yvette, France
[3]Departament de Fisica, Universitat Politècnica de Catalunya, Edifici Gaia, Rambla Sant Nebridi 22, 08222 Terrassa, Barcelona, Spain

Correspondence: Meriem Krouma (meriem.krouma@lsce.ipsl.fr)

Received: 21 June 2022 – Discussion started: 27 June 2022
Revised: 20 December 2022 – Accepted: 2 February 2023 – Published: 1 March 2023

Abstract. The Madden–Julian Oscillation (MJO) is one of the main sources of sub-seasonal atmospheric predictability in the tropical region. The MJO affects precipitation over highly populated areas, especially around southern India. Therefore, predicting its phase and intensity is important as it has a high societal impact. Indices of the MJO can be derived from the first principal components of zonal wind and outgoing longwave radiation (OLR) in the tropics (RMM1 and RMM2 indices). The amplitude and phase of the MJO are derived from those indices. Our goal is to forecast these two indices on a sub-seasonal timescale. This study aims to provide an ensemble forecast of MJO indices from analogs of the atmospheric circulation, computed from the geopotential at 500 hPa (Z500) by using a stochastic weather generator (SWG). We generate an ensemble of 100 members for the MJO amplitude for sub-seasonal lead times (from 2 to 4 weeks). Then we evaluate the skill of the ensemble forecast and the ensemble mean using probabilistic scores and deterministic skill scores. According to score-based criteria, we find that a reasonable forecast of the MJO index could be achieved within 40 d lead times for the different seasons. We compare our SWG forecast with other forecasts of the MJO. The comparison shows that the SWG forecast has skill compared to ECMWF forecasts for lead times above 20 d and better skill compared to machine learning forecasts for small lead times.

1 Introduction

Forecasting the Madden–Julian Oscillation (MJO) is a crucial scientific endeavor as the MJO represents one of the most important sources of sub-seasonal predictability in the tropics. The Madden–Julian Oscillation controls tropical convection, with a life cycle going from 30 to 60 d (Lin et al., 2008). It is characterized by a dominant eastward propagation over the tropical Indo-Pacific basin, in particular during the boreal winter. The MJO affects the Indian and Australian monsoons (Zhang, 2013) and West African monsoon (Barlow et al., 2016). It was shown that it affects precipitation in East Asia (Zhang et al., 2013) and North America (Becker et al., 2011). The MJO affects the global weather as it impacts the tropics as well as the extratropics due to the atmospheric teleconnections (Zhang, 2013; Cassou, 2008).

The improvement of the forecast skill of the MJO is the subject of several studies. Numerical models have shown an ability to forecast the MJO index (Kim et al., 2018). However, the forecast of the MJO is sensitive to the quality of the initial conditions (Zhang, 2013; Straub, 2013). This motivates probabilistic forecasts to overcome the chaotic nature of climate variability (Sivillo et al., 1997; Palmer, 2000). Indeed, ensemble forecasts have shown improvements over deterministic forecasts for weather and climatic variables in the short and long term (Yiou and Déandréis, 2019; Hersbach

Published by Copernicus Publications on behalf of the European Geosciences Union.

et al., 2020). One of the advantages of ensemble forecasts is that they provide information about the forecast uncertainties, which deterministic forecasts cannot provide. In addition, the use of ensemble means has shown better forecast results than the individual ensemble members in previous works (Toth and Kalnay, 1997; Grimit and Mass, 2002; Xiang et al., 2015).

Statistical models, such as stochastic weather generators (SWGs), have been used for this purpose. SWGs are designed to mimic the behavior of climate variables (Ailliot et al., 2015). They have been used to forecast various weather and climatic variables such as temperature (Yiou and Déandréis, 2019), precipitation (Krouma et al., 2021), and the North Atlantic Oscillation (NAO) (Yiou and Déandréis, 2019). One of the benefits of using stochastic weather generators is that they have a low computing cost compared to numerical models. Combining stochastic weather generators with analogs of the atmospheric circulation is an efficient approach to generate ensemble weather forecasts with consistent atmospheric patterns (Yiou and Déandréis, 2019; Krouma et al., 2021; Blanchet et al., 2018).

Analogs of circulation were designed to provide forecasts assuming that similar situations in the atmospheric circulation could lead to similar local weather conditions (Lorenz, 1969). Recent studies have evaluated the potential of analogs to forecast the probability distribution of climate variables: Yiou and Déandréis (2019) simulated ensemble members of temperature using random sampling of atmospheric circulation analogs; Atencia and Zawadzki (2014) used analogs of precipitation to forecast precipitation.

The goal of this study is to forecast a daily MJO index for a sub-seasonal lead time ($\approx$ 2–4 weeks) with a SWG based on analogs of the atmospheric circulation, described in Sect. 3.2. The SWG approach was evaluated in previous studies by Yiou and Déandréis (2019) and Krouma et al. (2021) for European temperature and precipitation. The SWG was able to forecast the temperature within 40 d and the precipitation within 20 d with reasonable skill scores in western Europe (Krouma et al., 2021; Yiou and Déandréis, 2019). In this paper, we adjust the parameters of the SWG in order to forecast the MJO indices. More precisely, our goals are (i) to forecast the MJO amplitude (directly from the amplitude and using the MJO indices) and (ii) to evaluate the ability of our SWG model to forecast active events of the MJO for the following weeks. We evaluate the sensitivity of the SWG approach to the forecast with different seasons and compare the forecast skill using SWG to other forecast approaches.

The paper is divided as follows: Sect. 2 shows the data used for running our forecast. Section 3 explains the methodology: circulation analogs, stochastic weather generator, and the verification metrics that we used to evaluate the SWG forecast. Section 4 explains the experimental setup. Section 5 details the results of the simulations and the evaluation of the ensemble forecast. Section 6 is devoted to the comparison of the SWG forecast with the literature. Section 7 contains the main conclusions of the analyses.

2 Data

The MJO has been described by various indices that are obtained from different atmospheric variables (Stachnik and Chrisler, 2020). Wheeler and Hendon (2004) defined an MJO index from two so-called real-time multivariate MJO series (RMMs). RMM1 and RMM2 represent the first and second principal components of the empirical orthogonal functions (EOFs), respectively, resulting from the combination of daily fields of the satellite-observed outgoing longwave radiation (OLR) and the zonal wind at 250 and 850 hPa latitudinally averaged between 15° N and 15° S (Rashid et al., 2011). The EOFs are computed from daily normalized fields after applying a filter to remove the long timescale variability (annual mean and the first three harmonics of the seasonal cycle), the previous 120 d of anomaly fields, and the El Niño signal as described by Wheeler and Hendon (2004). Lim et al. (2018) and Ventrice et al. (2013) proposed other indices of the MJO. The main difference between the indices consists of the input fields and the computation of the index. For instance, Ventrice et al. (2013) replace OLR with 200 hPa velocity potential, and Lim et al. (2018) do not remove an El Niño signal.

The RMM1 and RMM2 allow the computation of the amplitude and the phase of the MJO (Wheeler and Hendon, 2004). For this paper, we selected the RMM-based MJO index. One of the reasons is that it is often used for MJO forecast (e.g., Kim et al., 2018; Rashid et al., 2011; Silini et al., 2021).

To simplify notations in the equations, we note that $R_1 =$ RMM1 and $R_2 =$ RMM2. The amplitude (A) and phase (ϕ) are defined as follows:

$$A(t) = \sqrt{R_1(t)^2 + R_2(t)^2}, \tag{1}$$

and

$$\phi(t) = \tan^{-1}\frac{R_2(t)}{R_1(t)}. \tag{2}$$

The amplitude and the phase describe the evolution of the MJO and its position along the Equator, respectively. The amplitude is related to the intensity of the MJO activity. There are different classifications related to the intensity of the active-MJO events (Lafleur et al., 2015). In this paper, we consider that there is an MJO event when $A(t) \geq 1$ (Lafleur et al., 2015). The phase ϕ is decomposed into eight areas known as centers of convection of the MJO over the Equator, starting from the Indian Ocean through the Maritime Continent to the western Pacific Ocean. This leads to a discretization $\hat{\phi}$ of phase ϕ into those eight identified areas (Lafleur et al., 2015). For each day t, we consider the amplitude $A(t)$, which can be above 1 (active MJO) or below 1,

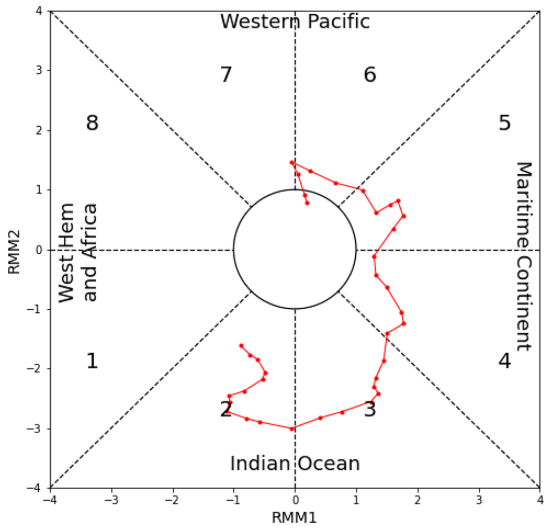

Figure 1. Wheeler–Hendon phase diagram of the MJO event for the period between 3 March and 9 April 1986, for observations. The diagram shows the eight areas of activity of MJO starting from the Indian Ocean.

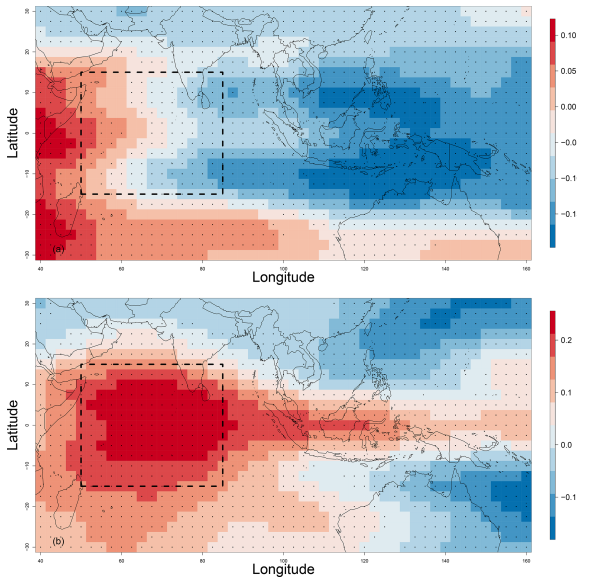

Figure 2. The optimal domain of computation of analogs. We computed analogs over the Indian Ocean, in the geographic areas indicated by the dashed black rectangle with coordinates 15° S–15° N, 50–85° E. The figure shows the temporal correlation between Z500, RMM1 **(a)**, and RMM2 **(b)** for the whole studied period from 1979 to 2020. The correlation is weak, but it is still significant, with p values ≤ 0.05 that we indicate with black dots over each grid of the considered domain (including the optimal region used to compute analogs).

and the phase $\hat{\phi} \in \{1, \ldots, 8\}$. The amplitude and the phase are usually represented in a phase-space diagram (Lafleur et al., 2015), called the Wheeler–Hendon phase diagram. An example of a Wheeler–Hendon phase diagram is shown in Fig. 1.

We obtained daily time series of RMMs, amplitude (A), and phase ($\hat{\phi}$) from January 1979 to December 2020 over the region covering 15° N–15° S from IRI (2022). In this paper, we aim at forecasting RMM variations.

We used the geopotential at 500 hPa (Z500) and 300 hPa (Z300) and outgoing longwave radiation (OLR) daily data to compute the analogs. The data are available from 1948 to 2020 with a horizontal resolution of 2.5° × 2.5°. The data were downloaded from the National Centers for Environmental Prediction (NCEP; Kistler et al., 2001).

In this paper, we predict the daily amplitude A and phase ϕ of the MJO from the daily analogs of Z500, Z300, and OLR.

3 Methodology

3.1 Analog computation

We start by building a database of analogs. For a day t, we define analogs as dates t' within 30 calendar days of t that have a similar Z500 (or Z300 or OLR) configuration to t. We look for analogs in different years from t. We quantify the similarity between daily Z500 maps using the Euclidean distance. The analogs are computed from daily data using a moving time window of $\Delta = 30$ d. This duration Δ corresponds to the life cycle of the MJO. Then, we keep the 20 best analogs. We define "best analog" as dates which have the minimum Euclidean distance between t and $t\prime$. The use of the Euclidean distance and the number of the analogs was explored and justified in previous studies (Krouma et al., 2021; Platzer et al., 2021).

Hence the distance that is optimized to find analogs of the $Z500(x,t)$ field is

$$D(t,t') = \left[\sum_{x}\left(\sum_{i=0}^{\tau}\left|Z500(x,t+i) - Z500(x,t'+i)\right|^2\right)\right]^{\frac{1}{2}}, \quad (3)$$

where x is a spatial index, and τ is a time window size (e.g., $\tau = 3$ d).

We compute separate analogs of Z500, Z300, and OLR following the same procedure over the Indian Ocean as represented in Fig. 2. We adjusted the parameters of computation of the analogs, mainly the search window of the analogs and the geographical domain. We considered different geographical regions to search for analogs. We computed analogs over the Indian Ocean, the Indian and Pacific oceans, and the Indian Ocean–Maritime Continent region for verification purposes (Appendix B1). This led to consideration of an optimal region for the analog search outlined in Fig. 2.

Appendix C. Supplement of the article "Ensemble forecast of an index of the Madden Julian Oscillation using a stochastic weather generator based on circulation analogs"

3.2 Configuration of the stochastic weather generator

The stochastic weather generator (SWG) aims to generate ensembles of random trajectories that yield physically consistent features. Our SWG is based on circulation analogs that are computed in advance with the procedure described in Sect. 3.1 (Yiou, 2014; Krouma et al., 2021). We produce an ensemble hindcast forecast with the circulation analog SWG with the following procedure (see Fig. 3 for a summary).

For a given day t_0 in year y_0, we generate a set of $S = 100$ simulations until a time $t_0 + T$, where T is the lead time, which goes from 3 to 90 d. We start at day t_0 and randomly select an analog (out of $K = 20$) of day $t_0 + 1$. The random selection of analogs of day $t_0 + 1$ among K analogs is performed with a weight w_k that is computed as the products of two weights, w_k^c and w_k^ϕ, defined by the following rules:

1. Weights w_k^c are inversely proportional to the calendar difference between t_0 and analog dates to ensure that time goes "forward". If δ_k is the difference in calendar days between t_0+1 and t_k, where t_k is the date of the kth analog of $t_0 + 1$, then the calendar day sampling weight w_k^c is proportional to $\exp(-|\delta_k|)$.

2. Weights w_k^ϕ are the difference between the phase at t_0 and analog dates. Indeed, we give more weight to analogs that are in the same phase. If δ'_k is the difference between $\hat{\phi}(t_0 + 1)$ and the discrete phase $\hat{\phi}_k$ of t_k, then the phase weight w_k^ϕ is proportional to $\exp(-|\delta'_k|)$.

Then we set $w_k = 0$ when the analog year is y_0. Indeed, excluding analog selection in year y_0 ensures that we do not use information from the T days that follow t_0. Then $w_k = w_k^c \times w_k^\phi$ and the values of w_k are normalized so that their sum is 1. Rule 1 is similar to the SWG used by Krouma et al. (2021). Rule 2 adds a constraint to ensure phase consistency across analogs.

We then replace t_0 with t_k, the selected analog of $t_0 + 1$, and repeat the operation T times. Hence we obtain a hindcast trajectory between t_0 and t_0+T. This operation of trajectory simulation from t_0 to $t_0 + T$ is repeated $S = 100$ times. The daily MJO ($A(t)$ or RMMs) of each trajectory is time-averaged between t_0 and $t_0 + T$. Hence, we obtain an ensemble of $S = 100$ forecasts of the average MJO ($A(t)$ or RMMs) for day t_0 and lead time T. Then t_0 is shifted by $\Delta t \geq 1$ d, and the ensemble simulation procedure is repeated. This provides a set of ensemble forecasts with analogs.

To evaluate our forecasts, the predictions made with the SWG are compared to the persistence and climatological forecasts. The persistence forecast consists of using the average value between $t_0 - T$ and t_0 for a given year. The climatological forecast takes the climatological mean between t_0 and $t_0 + T$. The persistence and climatological forecasts are randomized by adding a small Gaussian noise, whose standard deviation is estimated by bootstrapping over T long intervals. We thus generate sets of persistence forecasts and climatological forecasts that are consistent with the observations (Yiou and Déandréis, 2019).

3.3 Forecast verification metrics

We assess the skill of the SWG to forecast the $A(t)$ and the RMMs using two approaches. We start by evaluating the performance of the SWG to forecast $A(t)$. For that, we use probabilistic scores (Zamo and Naveau, 2018; Hersbach, 2000; Marshall et al., 2016) like the continuous ranked probability score (CRPS) for each lead time T. The CRPS is a quadratic measure of the difference between the forecast cumulative distribution function and the empirical cumulative distribution function of the observation (Zamo and Naveau, 2018). The CRPS is defined by

$$\mathrm{CRPS}(P, x_a) = \int_{-\infty}^{+\infty} (P(x) - \mathcal{H}(x - x_a))^2 \mathrm{d}x, \tag{4}$$

where x_a is the observed $\mathrm{RMM}^{\mathrm{obs}}$ or $A(t)^{\mathrm{obs}}$, P is the cumulative distribution function of x of the ensemble forecast, and $\mathcal{H}$ represents the Heaviside function ($\mathcal{H}(y) = 1$ if $y \geq 0$ and $\mathcal{H}(y) = 0$ otherwise). A perfect forecast yields a CRPS value equal to 0.

As the CRPS value depends on the unit of the variable to be predicted, it is useful to normalize it with the CRPS value of a reference forecast, which can be obtained by a persistence or a climatology hypothesis. The continuous ranked probability skill score (CRPSS) is defined as a percentage of improvement over such a reference forecast (Hersbach, 2000). We compute the CRPSS using as a reference the climatology and the persistence.

$$\mathrm{CRPSS} = 1 - \frac{\overline{\mathrm{CRPS}}}{\overline{\mathrm{CRPS}_{\mathrm{ref}}}}, \tag{5}$$

where $\overline{\mathrm{CRPS}}$ is the average of the CRPS of the SWG forecast, and $\overline{\mathrm{CRPS}_{\mathrm{ref}}}$ is the average of the CRPS of the reference (either climatology or persistence).

The CRPSS values vary between $-\infty$ and 1. The forecast has improvement over the reference when the CRPSS value is above 0.

We also computed the rank (temporal) correlation between the observations and the median of the 100 simulations (Scaife et al., 2014).

A robust forecast requires a good discrimination skill. A discrimination skill represents the ability to distinguish events from non-events. We measure the skill of the SWG in discriminating between situations leading to the occurrence of an MJO event (active MJO) and those leading to the non-occurrence of the event (inactive MJO). To do so, we use the relative operating characteristic (ROC) score. The ROC is used for binary events (Fawcett, 2006). Since we have a probabilistic forecast, we can use a threshold value of 1 to

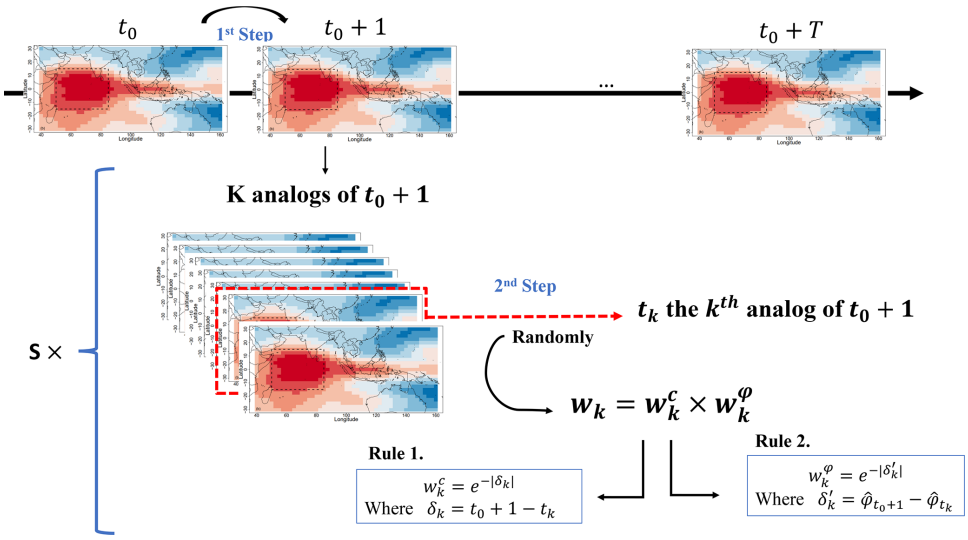

Figure 3. Illustration of the SWG process. The first step goes from a given day to the next day. The second step explains how we randomly select a kth analog with respect to weight w_k.

construct a classifier for the binary event of MJO from the feature $A(t)$:

- If $A(t) \geq 1$ we predict a positive outcome (active MJO).
- If $A(t) < 1$ we predict a negative outcome (inactive MJO).

The ROC curve is a plot of the success rate versus the false alarm rate (Verde, 2006). The ROC curve could also be a plot of the sensitivity versus the specificity (Fawcett, 2006). The sensitivity (true positive rate) is the probability of an active-MJO event, assuming that $A(t) \geq 1$ is really observed. The specificity (true negative rate) refers to the probability of an inactive-MJO event, as long as we have $A(t) \leq 1$. Moreover, the sensitivity is a measure of the ability of the prediction to identify true positives, and the specificity is a measure of the ability to identify true negatives. Both quantities describe the accuracy of a prediction that signals the presence or absence of an MJO event (Fawcett, 2006). Therefore, we define the relationship between sensitivity and specificity as follows:

- Specificity $= 1 -$ sensitivity means that we have a poor prediction because the rate of true negative and the false alarm rate are the same.
- Specificity $> 1 -$ sensitivity means that we have a good prediction.

Another performance measurement that we can infer from the ROC curve is the area under the curve (AUC). The AUC explains how much the forecast model is able to distinguish between binary classes. The AUC is the area in the ROC curve between sensitivity and the false positive rate computed as follows:

$$\mathrm{AUC} = \int_0^1 S(x)\mathrm{d}x\,, \tag{6}$$

where S is the sensitivity, and x is the false positive rate.

An increase in AUC indicates an improvement in discriminatory abilities of the model at predicting a negative outcome as a negative outcome and a positive outcome as a positive outcome. An AUC of 0.5 is non-informative.

Finally, we evaluate the ensemble-mean forecast of RMM1 and RMM2 using the usual scalar metrics for MJO forecasts (Rashid et al., 2011; Silini et al., 2021; Kim et al., 2018). We computed the bivariate anomaly correlation coefficient (COR) and the bivariate root mean square error (RMSE) between the forecasted RMMs (R_i^{pred}) and the observed RMMs (R_i^{obs}) as follows:

$$\mathrm{COR}(T) = \frac{\sum_{t=1}^{t=N}[R_1^{\mathrm{obs}}(t)R_1^{\mathrm{pred}}(t,T) + R_2^{\mathrm{obs}}(t)R_2^{\mathrm{pred}}(t,T)]}{\sqrt{\sum_{t=1}^{t=N}[R_1^{\mathrm{obs}}(t)^2 + R_2^{\mathrm{obs}}(t)^2]}\sqrt{\sum_{t=1}^{N}[R_1^{\mathrm{pred}}(t,T)^2 + R_2^{\mathrm{pred}}(t,T)^2]}}, \tag{7}$$

$$\mathrm{RMSE}(T) = \sqrt{\frac{\sum_{t=1}^{t=N}[|R_1^{\mathrm{obs}}(t) - R_1^{\mathrm{pred}}(t,T)|^2 + |R_2^{\mathrm{obs}}(t) - R_2^{\mathrm{pred}}(t,T)|^2]}{N}}, \tag{8}$$

where t is the time, T is the lead time of the forecast, and N is the length of the time series ($N \sim 10^4$). We interpret the values of COR and RMSE using thresholds fixed by previous studies to define the forecast skill of the SWG. The forecast has skill when the COR value is larger than 0.5, and the

RMSE value is lower than $\sqrt{2}$. Rashid et al. (2011) explain that for a climatological forecast, RMSE $= \sqrt{2}$ because the standard deviation of the observed RMM indices is 1. Hence, forecasts are considered to be skillful for RMSE $< \sqrt{2}$ (i.e., they have lower RMSE than a climatological forecast). We use those thresholds in our analyses.

We compare the RMSE to the ensemble spread in order to evaluate the forecast accuracy. The ensemble spread measures the difference between the members of the ensemble forecast. The ensemble spread ES is obtained by the root mean square difference between the ensemble members and the ensemble mean defined as follows:

$$ES = \sqrt{\frac{\sum_{n=1}^{S}(A_n - \overline{A})^2}{S}}, \tag{9}$$

where S is the size of the ensemble members, A_n is the amplitude of the nth ensemble member of the forecast, and $\hat{A}$ is the ensemble average of A_n over the S members.

We compute the average amplitude error (E_A) and the average phase error (E_ϕ) for the different lead times T. They allow the evaluation of the quality of the forecast. The average amplitude error (E_A) is defined as follows:

$$E_{A(T)} = \frac{1}{N}\sum_{t=1}^{t=N}[A_{\text{pred}}(t,T) - A_{\text{obs}}(t)]. \tag{10}$$

The value of $E_{A(T)}$ indicates how fast the forecast system loses the amplitude of the MJO signal. A positive value indicates an overestimation of the amplitude in predictions compared to the observation. A negative value indicates an underestimated amplitude. Rashid et al. (2011) define the average phase error (E_ϕ) as

$$E_{\phi(T)} = \frac{1}{N}\sum_{t=1}^{t=N}\tan^{-1}\frac{R_1^{\text{obs}}(t)R_2^{\text{pred}}(t,T) - R_2^{\text{obs}}(t)R_1^{\text{pred}}(t,T)}{R_1^{\text{obs}}(t)R_1^{\text{pred}}(t,T) + R_2^{\text{obs}}(t)R_2^{\text{pred}}(t,T)}. \tag{11}$$

This formulation stems from the ratio of the cross product (numerator) and dot product (denominator) of the vectors of forecasts (R_1^{pred}, R_2^{pred}) and observations (R_1^{obs}, R_2^{obs}). Equation (11) is equivalent to the average phase angle difference between the prediction and observations, with a positive angle indicating the forecast leads the observations (Rashid et al., 2011). The negative (positive) value of $E_{\phi(T)}$ indicates a slower (faster) propagation of the phase in predictions compared to the observations.

4 Forecast protocol

We explore the skill of a SWG in forecasting the $A(t)$ and the RMMs (R_1 and R_2) using analogs of the atmospheric circulation. We generate separately an ensemble of 100 members of the $A(t)$ of the MJO and RMMs using the same approach. The goal is to have a probabilistic forecast of the $A(t)$ for a sub-seasonal lead time T ($\approx$ 2 to 4 weeks). As input to the SWG, we use analogs of the atmospheric circulations. We computed analogs separately from Z500, Z300, the wind at 250 and 850 hPa, and the OLR. We choose to keep analogs from the geopotential at height 500 hPa instead of the other atmospheric fields. We explain our choice in Sect. 5.

Then, we adjusted the geographical region and the window search of analogs (Fig. B1). Indeed, the forecast skill of the MJO depends on the geographical region. We choose to compute the analogs over the Indian Ocean with coordinates of 15° S–15° N, 50–85° E. We argue our choice (i) by the fact that the Indian Ocean corresponds to the first phase of the MJO in the phase-space diagram, where the MJO starts; (ii) because different models found good results by initiating their forecast in this region (Kim et al., 2018); and (iii) based on the experiment analyses that we made over different geographical regions (Fig. B2). We explain that in Appendix B.

We search for analogs within 30 calendar days. This duration corresponds to the life cycle of the MJO. In addition, we adjust the SWG in order to select analogs from the same phase, as described in Sect. 3.2.

To evaluate the skill score of our forecasts, we used two approaches. We used the probabilistic scores such as CRPS, correlation, and ROC score (Sect. 3.3) to evaluate the ensemble forecast of the amplitude. Then, we evaluate the ensembles mean of RMM1 and RMM2. For that, we used scalar metrics such as the COR and the RMSE (Sect. 3.3), as they are commonly used to evaluate MJO forecast (Rashid et al., 2011; Lim et al., 2018).

5 Results

We show results of the forecast of $A(t)$ and RMMs (R_1 and R_2) from the analogs of Z500 over the Indian Ocean with a time of search of 30 d. As explained in Sect. 4, we explored the potential of other atmospheric circulations (wind at 250 and 850 hPa, OLR, and Z300) to forecast the MJO amplitude. The forecast skill with analogs of OLR and the zonal wind in the upper and lower troposphere (250 and 850 hPa) was not that satisfying compared to the forecast skill using analogs of Z500 or Z300 (Fig. 4). Indeed, the wind at 250 and 850 hPa and the OLR do not improve the bivariate correlation and RMSE forecast skill of the MJO index for a longer lead time (above 20 d) over Z500 or Z300 (Fig. 4), despite the fact that they are the driver of the MJO. This could be explained by different reasons.

The first reason is related to the composition of the RMM index. Indeed, the OLR is used as a proxy for organized moist convection (Kim et al., 2018). However, the fractional contribution of the convection to the variance of RMMs is considerably lower than the fraction of the zonal wind fields (Kim et al., 2018; Straub, 2013). The second reason is that the MJO predictability can be improved by including atmospheric and

oceanic processes (Pegion and Kirtman, 2008). According to some theories that explain the MJO, the geopotential and the moisture are considered to be drivers of precipitation and convection (Zhang et al., 2020). For instance, in the gravity-wave theory for MJO (Yang and Ingersoll, 2013), the convection and precipitation are triggered by a specific geopotential threshold.

Another reason is related to our forecast approach. The composites of OLR and wind speed highly depend on the phase of the MJO (Kim et al., 2018). As our analog approach is constrained by choice of a geographical region, it misses the spatio-temporal variability in OLR and wind speed during the MJO. We computed analogs from other regions (Fig. B1). However, we obtain better forecast scores by focusing on the "small" area represented by a dashed rectangle (Fig. B1). This is explained by the higher quality of analogs.

Indeed, choosing a "large" region to compute analogs yields rather large distances or low correlations for analogs. This implies that the analog SWG gets lower skill scores because the analogs are not very informative. The OLR or zonal wind analogs were computed on the optimal window obtained for Z500 or Z300 as mentioned in Fig. 2, which is not appropriate for OLR or wind speed, as reflected by Kim et al. (2018). Therefore, we find lower COR and RMSE scores compared to the forecast using Z300 and Z500. This is a potential feature of analogs. The analog geometry needs to be imposed a priori in a rather simplistic way, which does not follow the spatio-temporal features of the MJO, which are known independently.

We tested the forecast of $A(t)$ and RMMs using analogs of Z300. We get a satisfactory forecast skill (i.e., with COR $>$ 0.5 and RMSE $< \sqrt{2}$) up to $T = 60$ d. However, we note that the forecast skill scores based on analogs of Z500 are higher for small lead times (up to 30 d). This is explained by the fact that Z300 analogs are close to where the MJO takes place, even if this does not lead to significant improvement over Z500 analog skill scores. Therefore the geopotential heights, although less physically and dynamically relevant for the MJO, are more appropriate predictors from the statistical and mathematical constraints of the analog-based method. The results of the forecast with analogs of Z300 can be found in Appendix A, where we compare the performance of the SWG forecast based on the analogs of Z500 and Z300 for different seasons (Figs. A1 and A2). For those reasons, we decided to keep the results of the forecast for $A(t)$ and RMMs with analogs of Z500. This analysis highlights the capacity of Z500 to catch the variability in the MJO.

As an illustration, we show the time series of the simulations and observations of the MJO amplitude for 1986. This year yields an unusually large period of RMM amplitude above 1, suggesting an important MJO activity. Figure 5 shows the mean of the 100 simulations and the observations for lead times of 3, 5, and 10 d for the whole year. We find that there is a strong correlation between observed and simulated $A(t)$ for the different lead times represented. Moreover, the SWG was able to distinguish between the active-MJO days ($A(t) \geq 1$) and inactive-MJO events ($A(t) \leq 1$). The same figures for the forecast with the SWG based on analogs of OLR and Z300 are provided in Appendix A.

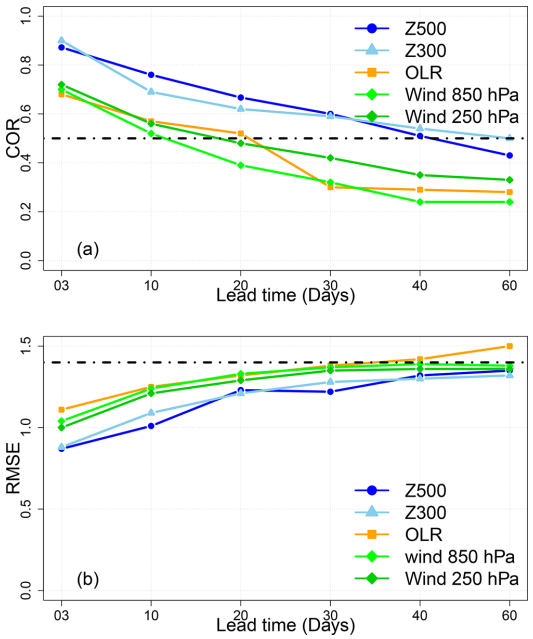

Figure 4. COR **(a)** and RMSE **(b)** values for different lead times of forecasts from 3 to 60 d over the period from 1979 to 2020 for the SWG forecast using analogs of OLR and zonal wind speed at 250 and 850 hPa as well as Z300 and Z500.

5.1 Evaluation of the ensemble forecast of the MJO amplitude

We evaluate the forecast of amplitude $A(t)$ using the probabilistic skill scores (CRPSS, ROC, and correlation) defined in Sect. 3.3. We consider the average of the skill scores up to each lead time T. In Fig. 6, we show the CRPSS and the correlation for DJF (December, January, and February) and JJA (June, July, and August) for different lead times T going from 3 to 40 d.

The CRPSS was computed using as a reference the forecast made from climatology and persistence. We note that the CRPSS vs. persistence reference decreases with time. It has higher values for $T = 3, 5, 10$ d. We note that when the lead time is larger than $T = 15$ d, CRPSS values become stable for both seasons. However, the CRPSS vs. climatology increases with lead time. We note that for small lead times ($T \leq 15$ d), the SWG forecast does better than the persistence, while for big lead times $T \geq 15$ d, the SWG forecast does better than the climatology. We can say that the forecast has a positive improvement compared to climatology

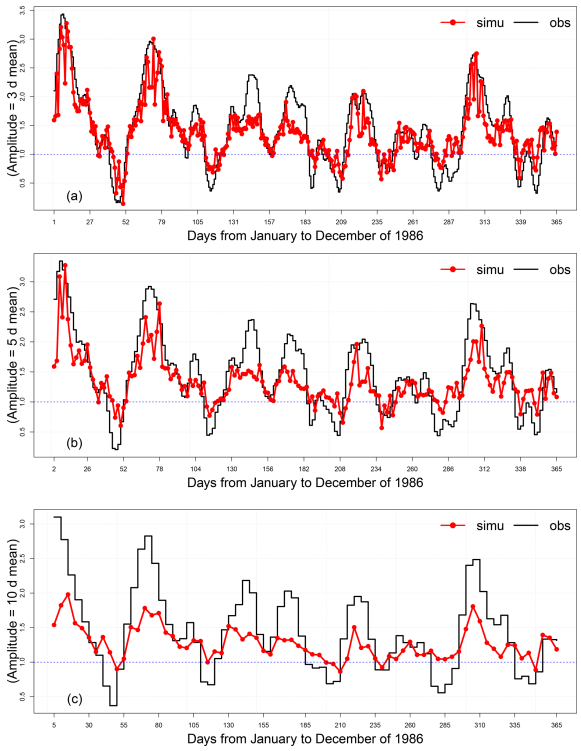

Figure 5. Time series of observations and simulations of the MJO amplitude for lead times of 3 **(a)**, 5 **(b)**, and 10 d **(c)** for the year 1986. The red line represents the mean of the 100 simulations, the black line represents the observations, and the blue line indicates the threshold of the MJO activity (below 1: inactive; above 1: active).

and persistence for DJF and JJA for all the studied lead times. We see that correlation mostly decreases with lead times. The highest correlation is related to small lead times ($T \leq 15$ d).

We used the ROC diagram to determine the discrimination between active and inactive events of the MJO. We associated 1 with an active-MJO event and zero with the inactive-MJO events. In Fig. 7, we show the ROC diagram for the different lead times T from 3 to 40 d. Analyzing the AUC, shown in Table 1, we find that until 40 d, the SWG is able to separate non-events (inactive MJO) from events as the AUC values are between 0.88 and 0.61. It is still significant as it is over the diagonal (random forecast). We note that the sensitivity value is 0.9 for 3 d, and it decreases with lead time to reach 0.7 by 40 d. We also find that the specificity and sensitivity are equal for small lead times. However, the specificity remains above ≈ 0.5 for $T = 40$ d. This value of specificity is still higher than $1 -$ sensitivity $= 0.2$. This indicates that the forecast has skill to distinguish between MJO events until 40 d ahead.

Using three probabilistic metrics (CRPSS, correlation, and ROC), we show that the SWG is able to skillfully forecast the

Table 1. Area under ROC curve (AUC) for the different lead times T from 3 to 40 d.

T	3 d	5 d	10 d	20 d	30 d	40 d
AUC	0.88	0.83	0.74	0.66	0.62	0.61

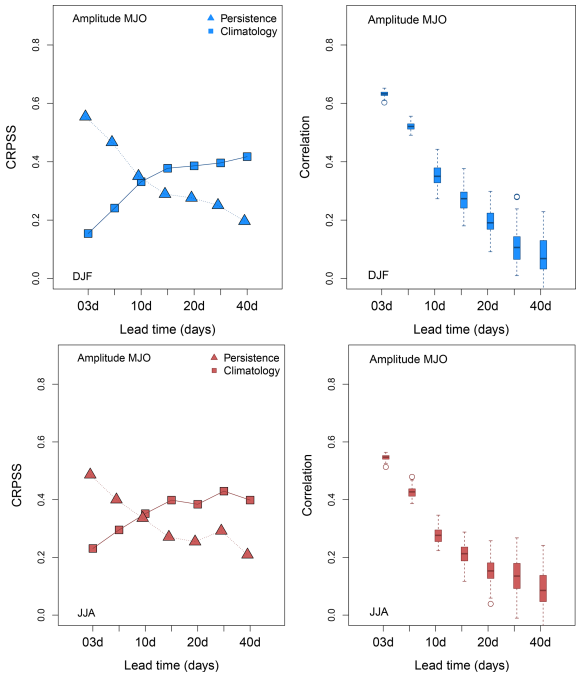

Figure 6. Skill scores for the MJO amplitude for lead times going from 3 to 40 d for DJF (blue) and JJA (red) for analogs computed from Z500. Squares indicate CRPSS where the persistence is the reference, triangles indicate CRPSS where the climatology is the reference, and boxplots indicate the probability distribution of correlation between observation and the median of 100 simulations for the period from 1979 to 2020.

MJO amplitude from analogs of Z500. The CRPSS shows a positive improvement of the forecast until 40 d. However, the correlation is significant until 20 d. By using the ROC curve and the discrimination skill, we show that the forecast still has skill until 40 d.

The difference between the lead times that we found using the CRPSS, correlation, and the ROC result from the difference between the skill scores. In fact, the CRPS is used for different categories of events, while the ROC is used for binary events, which is more suitable with our case of study.

5.2 Evaluation of the ensemble-mean forecast of RMMs

In this part, we evaluate the performance of the SWG in forecasting the RMMs (R_1 and R_2). We simulated R_1 and R_2 using the SWG and analogs of Z500. Then we used the ensem-

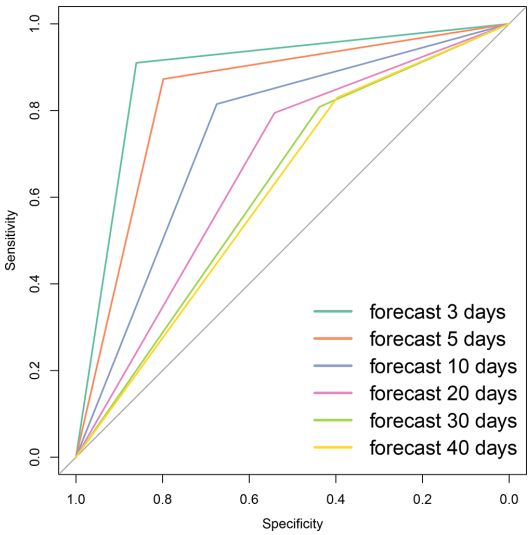

Figure 7. ROC curve for all lead times. The plot represents the sensitivity versus the specificity. The diagonal line represents the random classifier obtained when the forecast has no skill. If the ROC curve is below the diagonal line, then the forecast has a poor skill, otherwise it has a good skill; i.e., the forecast has the potential to distinguish between success and false alarms.

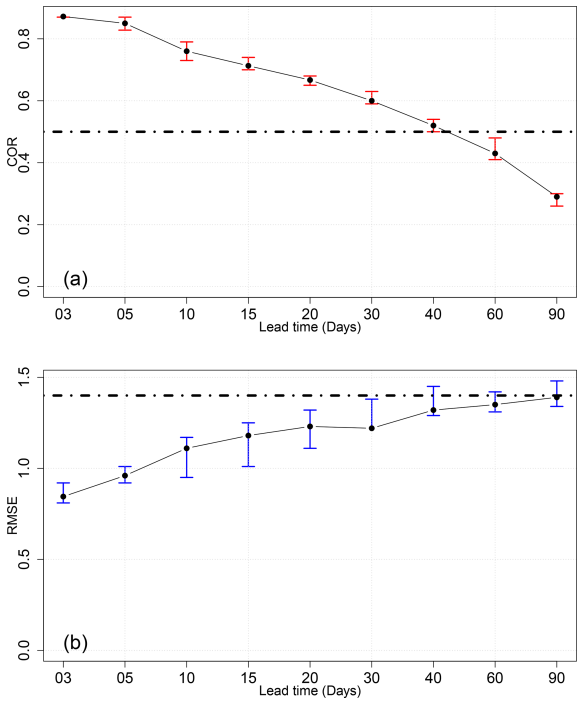

Figure 8. The COR **(a)** and RMSE **(b)** for the different lead times of forecasts from 3 to 90 d over the period from 1979 to 2020. Confidence intervals are obtained with a bootstrap with 1000 samples.

ble mean of R_1 and R_2 to compute the verification metrics, mainly the COR and RMSE (Rashid et al., 2011; Kim et al., 2018; Silini et al., 2021), as shown in Fig. 8. We looked at COR and RMSE averaged up to each lead time T. Respecting the threshold 0.5 for the COR and $\sqrt{2}$ for RMSE, we found that the forecast has skill until $T = 40$ d. We have to mention that T values of 60 and 90 d were used for verification purposes.

In order to verify the forecast skill, we computed the ensemble spread, and we compared it to the RMSE values for the different lead times going from 3 to 40 d (Fig. 9). We found that the difference between the ensemble spread and the RMSE increases with lead time. The RMSE is becoming larger with lead time, which indicates that the distance between the observations and simulations is increasing. In addition, the ensemble spread decreases, which indicates that the uncertainties increase with time. This was verified by computing the bias of the forecast, where we could find that it increases with lead time. The bias represents the average bias of RMM1 and RMM2. It was computed between the ensemble mean of the RMMs and the observations of RMMs.

We explored the sensitivity of the forecast to seasons as shown in Fig. 10. We found that the forecast for DJF and MAM (March, April, May) has a good skill (i.e., with RMSE lower than $\sqrt{2}$) within 30 d. However, for SON (September, October, and November) and JJA, a similar forecast skill was obtained for a lead time of 40 d. The DJF and MAM seasons show the largest RMSE values. This implies that the ensemble forecast in DJFM yields a larger range of values than in SON and JJA, even if the observations and simulations are well correlated. The highest correlation in DJF and MAM could be explained by the fact that the MJO is more active in the boreal winter (DJFM). However, the RMSE values in JJA are more consistent as they represent low distance between simulations and observations. Indeed, even if the MJO events tend to be more intense in DJFM, the amplitude is underestimated. The assessment of the ensemble-mean forecast of RMM1 and RMM2 showed that the forecast has skill until 40 d. However, it is sensitive to seasons, and this is consistent with the previous studies of Wheeler and Hendon (2004), Rashid et al. (2011), and Wu et al. (2016b). Indeed, we found that the SWG forecast of RMM1 and RMM2 has skill, with respect to the thresholds of COR and RMSE, within 40 d for summer (JJA) and 30 d for winter (DJF).

We also computed the amplitude and phase errors (Fig. 11). We found that the $E_{A(t)}$ is negative for all lead times. That indicates a weak amplitude in predictions compared to the observations. The $E_{\phi(t)}$ is positive until 30 d, which indicates fast propagation of the phase in predictions compared to the observations. Then it becomes negative, which means that the phase is slower. We note that the phase is well predicted, while the amplitude is under-

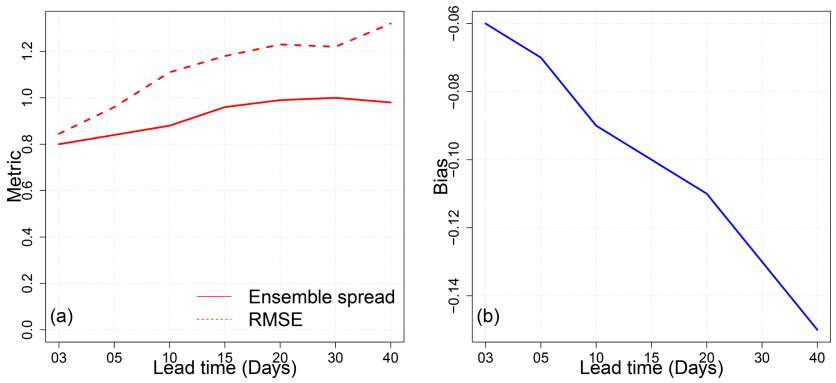

Figure 9. **(a)** Comparison between the ensemble spread and the RMSE. We note that the difference is small for short lead times (≤ 15 d). "Metric" on the vertical axis refers to ensemble spread and RMSE. **(b)** The bias between the simulations and the observations for the lead times going from 3 to 40 d.

estimated (Fig. 11). This is consistent with previous studies (Silini et al., 2021; Rashid et al., 2011).

6 Comparison of the SWG forecast with other forecasts

The assessment of the forecast of MJO amplitude with SWG and analogs of Z500 shows good skill until 40 d using probabilistic scores (CRPSS vs. climatology is 0.2, and CRPSS vs. persistence is 0.4) and scalar scores (COR = 0.54 and RMSE = 1.30) as explained in Sects. 5.1 and 5.2. The SWG forecast shows a positive improvement compared to the climatology and the persistence within 40 d (Fig. 6). In addition, the ROC curve confirmed the ability of the SWG forecast to distinguish between the active and inactive-MJO amplitude as shown in Fig. 7. The same result was obtained using the ensemble mean of RMM1 and RMM2 as represented in Fig. 8. The SWG forecast of RMM1 and RMM2 has good skill within 30–4 d, respecting the threshold of 0.5 for the COR and $\sqrt{2}$ for RMSE. The difference in the lead time of the forecast depends on the seasons as represented in Fig. 10. This is consistent with Wu et al. (2016a), Wheeler and Weickmann (2001), and Rashid et al. (2011), who found significant differences in skill scores between seasons. We find that the forecast has skill until 30 d for DJF and MAM (with RMSE = $\sqrt{2}$) and 40 d for JJA and SON (with COR = 0.5) as shown in Fig. 10. This is different from Rashid et al. (2011) and Silini et al. (2021), who obtain higher forecast skill in the winter. However, it is consistent with the results of Wu et al. (2016b) and Vitart (2017), who found higher skill scores for JJA.

We assessed the forecast skill of the SWG with other forecasts. We selected two models, POAMA (the Australian Bureau of Meteorology coupled ocean–atmosphere seasonal prediction system) and the ECMWF model, which provide probabilistic and deterministic forecast of the MJO, respectively. We compared mainly the maximum lead time of the MJO amplitude forecast. The POAMA model provides a 10-member ensemble. In hindcast mode, the POAMA model has skill up to 21 d (Rashid et al., 2011). The ECMWF reforecasts with Cycle 46r1 have skill to around 40 d. For the error in the amplitude and phase, we found that the ECMWF reforecasts shows lower average amplitude and phase errors

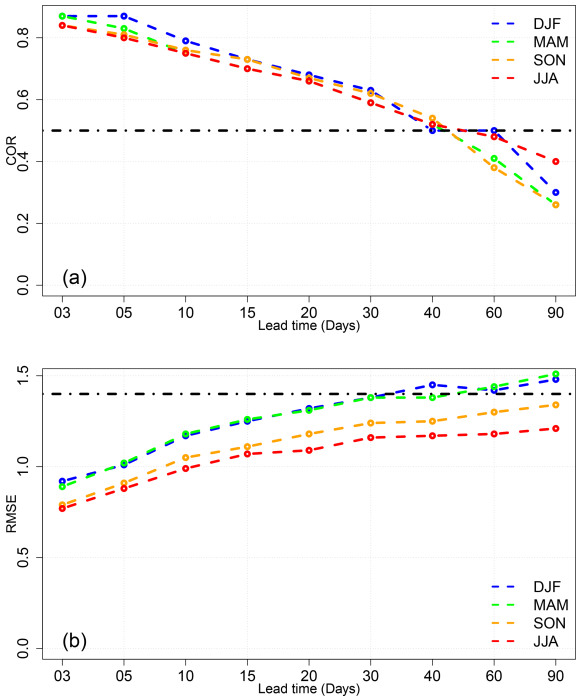

Figure 10. The COR **(a)** and RMSE **(b)** for the different lead times of forecasts from 3 to 90 d over the period from 1979 to 2020 for the different seasons DJF, JJA, MAM, and SON.

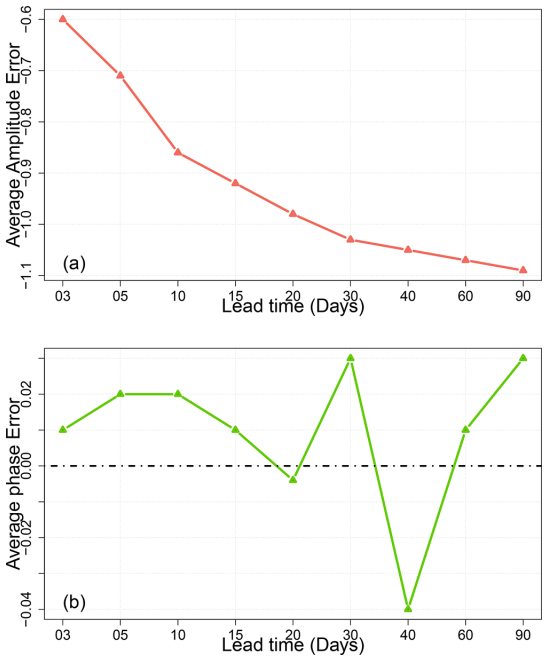

Figure 11. The average amplitude error (E_A) and average phase error (E_ϕ) of the MJO over all seasons for the period from 1979 to 2020. We note that the amplitude is underestimated, and the phase is well predicted by comparing predictions to forecasts.

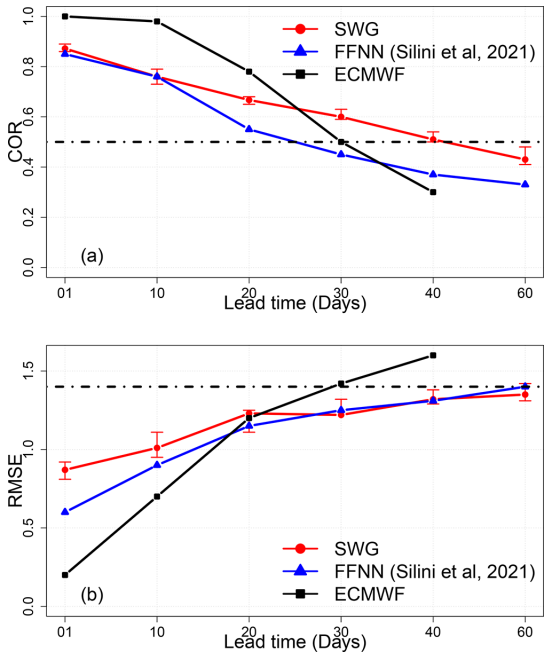

Figure 12. Comparison of the values of COR **(a)** and RMSE **(b)** between the SWG forecast and forecasts of Silini et al. (2021) (blue lines) and the ECMWF (black lines). Confidence intervals for SWG (red lines) were obtained with a bootstrap procedure over the simulations (1000 samples).

compared to those from the SWG forecasts. However, what we found is consistent with other dynamical models (Kim et al., 2018) where they overestimate or underestimate the amplitude and the phase of the MJO.

In addition, we compared quantitatively the SWG forecast with the ECMWF forecast (Fig. 12). The ECMWF reforecasts were taken from Silini et al. (2022). We found that the ECMWF forecast has the highest correlation until 20 d compared to the SWG forecast. The RMSE values of the ECMWF forecast are always small compared to the SWG forecast, which indicates a good reliability skill of the ECMWF forecast for lead times of 5 and 10 d. However, for lead times of 20 d the RMSE of the ECMWF forecast coincides with the RMSE of the SWG, which shows the improvement of the SWG forecast to lead times above 20 d. The skill scores of the ECMWF (COR and RMSE) (Silini et al., 2022) are computed for each lead time, which is different from our way of computing the skill score (considering the average lead time). Of course, this comparison was made to check the performance of our forecast and not to say that the SWG model can replace a numerical prediction.

We also compared the SWG forecast skill with a machine learning forecast of MJO indices (RMM1 and RMM2) (Silini et al., 2021). Silini et al. (2021) explored the skill forecast of two artificial neural network types, FFNN (feed-forward neural network) and AR-RNN (autoregressive recurrent neural network), on MJO indices. Silini et al. (2021) found that the machine learning method gives good skill scores until 26–27 d with respect to the standard thresholds of COR and RMSE. We compared the skill scores (RMSE and COR) of the SWG and Silini et al. (2021) forecasts for all lead times. We found that the two models have the same correlation until 10 d. After 10 d, the correlation of Silini et al. (2021) forecasts decreases rapidly, while the correlation of SWG is still significant. For the RMSE, we found that the SWG has smaller values for a lead time of 10 d. This indicates that the SWG forecast is more reliable. However, from 30 d, the RMSE of the two models starts to be the same.

To sum up, the comparison of SWG forecasts to ECMWF and Silini et al. (2021) forecasts shows that for small lead times (up to 10 d) the ECMWF forecast has better skill. However, the SWG shows a positive improvement for long lead times.

7 Conclusions

We performed an ensemble forecast of the MJO amplitude using analogs of the atmospheric circulation and a stochastic weather generator. We used the Z500 as a driver of the circulation (Fig. 4) over the Indian Ocean (Fig. 2), and we considered analogs from the same phase to provide the fore-

Appendix C. Supplement of the article "Ensemble forecast of an index of the Madden Julian Oscillation using a stochastic weather generator based on circulation analogs"

cast for the sub-seasonal lead time. We explored two ways to forecast the MJO, starting by directly forecasting the daily amplitude, then the daily MJO indices, RMM1 and RMM2, from 1979 to 2020.

We assessed the forecast skill of the MJO forecast by evaluating the ensemble member and the mean of the ensemble member using probabilistic and scalar verification methods, respectively. This allowed us to evaluate the forecast and also to explore the difference between the two verification methods.

We used probabilistic skill scores as the CRPSS and the AUC of the ROC curve (Table 1). We found that the forecast showed positive improvement over the persistence and the climatology within 40 d (CRPSS; Fig. 6). The SWG forecast of the MJO amplitude also showed the capacity to distinguish between active and inactive MJO (ROC curve; Fig. 7) for the different lead times. Using the scalar scores (COR and RMSE) and the ensemble mean of the forecast of RMM1 and RMM2, we found that the SWG is able to forecast the MJO indices (RMM1 and RMM2) within 30–40 d.

We found that the forecast is sensitive to seasons (Fig. 10). The forecast has skill up to 30 d for the boreal winter (DJF and MAM), while it goes to 40 d for the boreal summer (JJA) and SON. That was consistent with previous studies (Silini et al., 2021; Rashid et al., 2011; Vitart et al., 2017). We also note that the forecast of the phase is better than of the amplitude according to the errors for amplitude and phase (Fig. 11). Finally, we found that the SWG had improvement over the ECMWF forecast for long lead times ($T > 30$ d) and a machine learning forecast (Silini et al., 2021) forecast for lead times $T > 20$ d.

This paper hence confirms the skill of the SWG in generating ensembles of MJO index forecasts from analogs of circulation. Such information would be useful to forecast impact variables such as precipitation and temperature.

Appendix A: Comparison of the forecast skill of the MJO using analogs computed from Z500, Z300, and OLR fields

We did the forecast of RMM1 and RMM2 using analogs of Z300 (Fig. A4), OLR (Fig. A3), and the zonal wind at 250 and 850 hPa (Fig. 4). The aim of using different atmospheric fields to compute analogs is to choose the analog circulation for the MJO forecast with the SWG as explained previously in Sect. 4. We found that the SWG based on analogs of Z300 yields good skills (COR > 0.5 and RMSE $< \sqrt{2}$) within $T = 60$ d (Fig. 4). However, the skill of the forecast is better for small lead times ≤ 30 d with analogs of Z500 (Fig. 4). We checked the sensitivity of the forecast to seasons as illustrated in Figs. A1 and A2 using separate analogs of Z500 and Z300. We compared the COR and the RMSE for different lead times (Figs. A1 and A2). We found that the RMSE values for the SWG forecast based on analogs of Z300 are the same as the forecast from analogs of Z500 for the different seasons and at different lead times (Fig. A2). The RMSE for SON and JJA is lower than the threshold for the T from 3 to 90 d for both forecasts (Fig. A2). However, for DJF and MAM the SWG forecast reaches the threshold of $\sqrt{2}$ at 37 d with analogs of Z300, which is slightly higher than the maximum lead time with Z500 (Fig. A2). The COR is slightly higher with analogs of Z500 at different lead times (Fig. A1). However, the threshold of 0.5 is exceeded with forecasts based on analogs of Z300 (Fig. A1).

In this part, we also show the time series for the forecast at different lead times $T = 3, 5, 10$ d for the same year (1986) for the SWG forecast with analog circulation computed from OLR (Fig. A3) and from Z300 (Fig. A4). We note that the correlation between the mean of the simulations (red line) and the observations of the MJO amplitude are better correlated with SWG forecasts based on analogs of Z300 (Fig. A4) than the one based on analogs of OLR (Fig. A3).

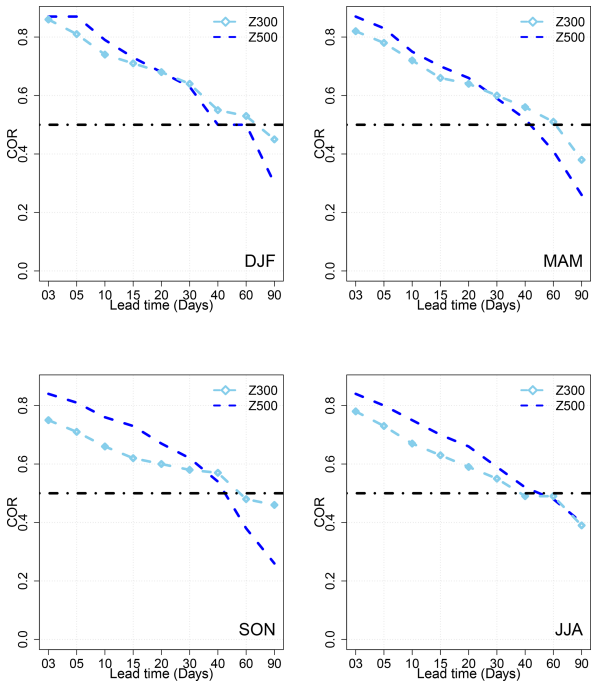

Figure A1. COR values for different lead times of forecasts from 3 to 90 d over the period from 1979 to 2020 for the SWG forecast based on analogs of Z500 and Z300 for different seasons (DJF, JJA, MAM, and SON).

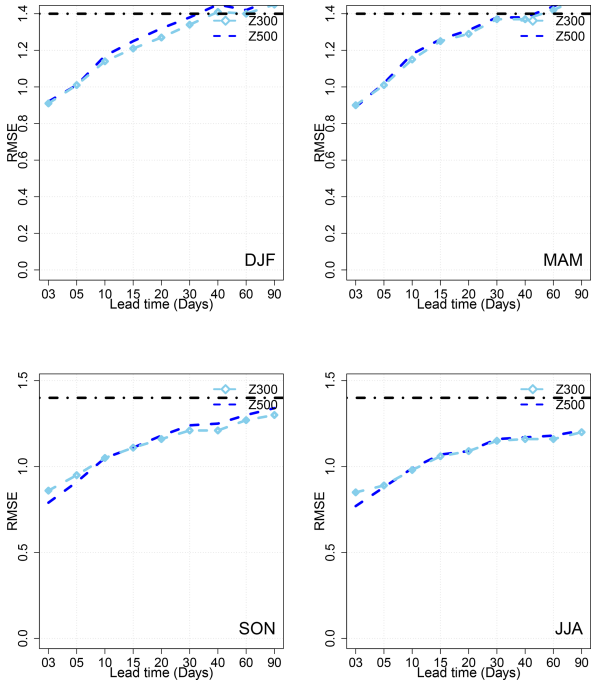

Figure A2. RMSE values for different lead times of forecasts from 3 to 90 d over the period from 1979 to 2020 for the SWG forecast based on analogs of Z500 and Z300 for different seasons (DJF, JJA, MAM, and SON).

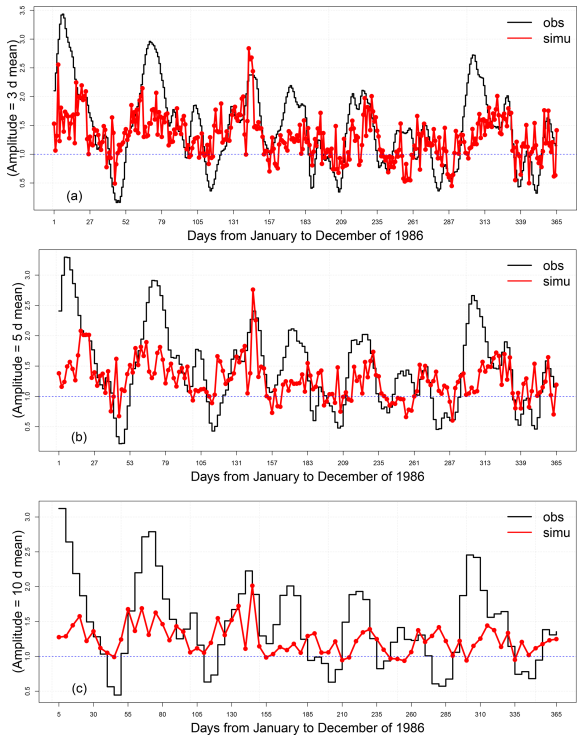

Figure A3. Time series of observations and simulations of the MJO amplitude computed from analogs of OLR for lead times of 3 **(a)**, 5 **(b)**, and 10 d **(c)** for the year 1986. The red line represents the mean of the 100 simulations, the black line represents the observations, and the blue line indicates the threshold of the MJO activity $A(t) > 1$.

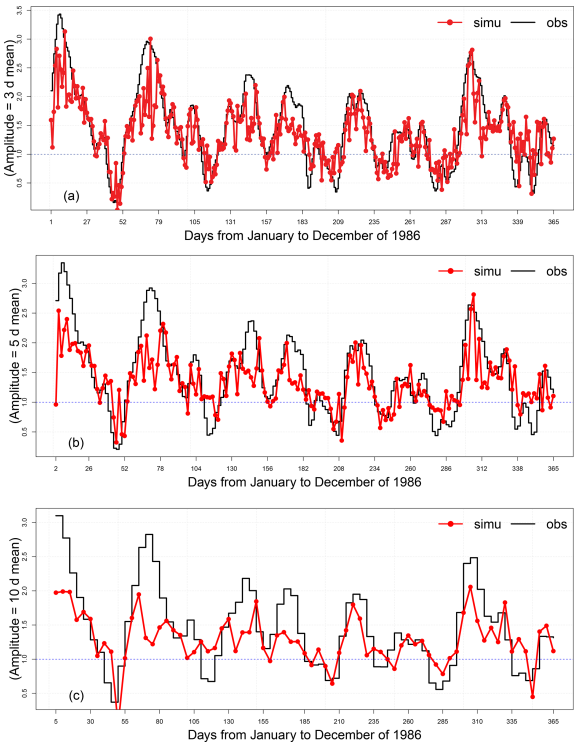

Figure A4. Time series of observations and simulations of the MJO amplitude computed from analogs of Z300 for lead times of 3 **(a)**, 5 **(b)**, and 10 d **(c)** for the year 1986. The red line represents the mean of the 100 simulations, the black line represents the observations, and the blue line indicates the threshold of the MJO activity $A(t) > 1$.

Appendix B: Domains of computation of analogs

We show in Fig. B2 the bivariate correlation (COR) and the RMSE from different geographical regions that we represent in Fig. B1. The different geographical regions shown in Fig. B2 were used to adjust the geographical region to compute analogs.

The COR reaches the threshold of 0.5 at $T = 40$ d for the geographical region with coordinates of 15° S–15° N, 50–85° E (Fig. B2). The same result is found for the region with coordinates of 15° S–15° N, 60–120° E (light-blue line in Fig. B2). However, the COR is lower for the other lead times $T = 3, 10, 20, 30$ d compared to the one for the region (15° S–15° N, 50–85° E). For the region with the coordinates (15° S–15° N, 85–120° E), the threshold of 0.5 for the COR is obtained at a lead time of 34 d (green line in Fig. B2). For the region with coordinates (15° S–15° N, 90–150° E), the forecast skill is significant with COR 0.5, at $T = 30$ d (orange line in Fig. B2), which remains the same results for this region compared to (Silini et al., 2022). The RMSE for the different regions is quite the same (Fig. B2), even if the values for the region (15° S–15° N, 50–85° E) are slightly lower within 30 d. Therefore the skill forecast (using the bivariate correlation and the RMSE) remains higher for the considered geographical region with the coordinates (15° S–15° N, 50–85° E).

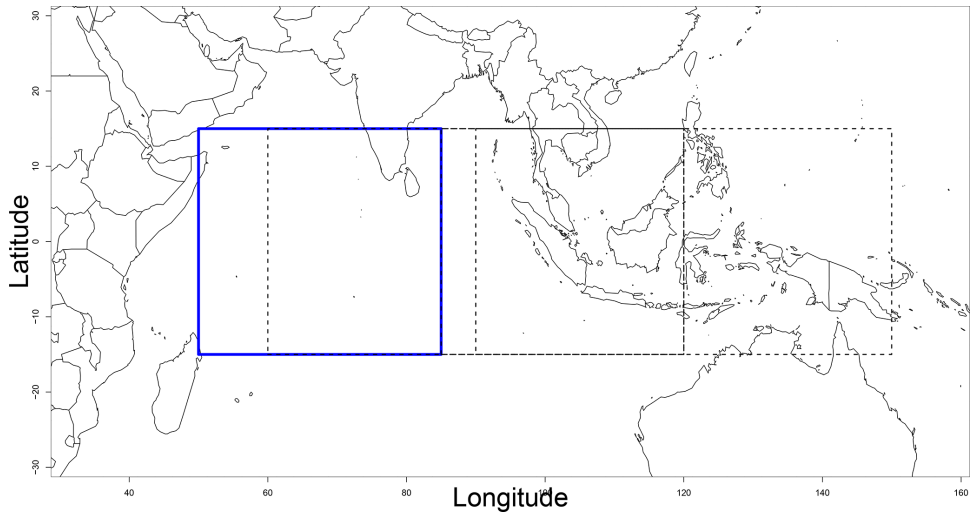

Figure B1. Domains of computation of analogs. We computed analogs over the Indian Ocean with coordinates 15° S–15° N, 50–85° E (blue rectangle); the Indian and Pacific oceans with coordinates 15° S–15° N, 85–120° E; and the Indian Ocean–Maritime Continent region with coordinates 15° S–15° N, 90–150° E.

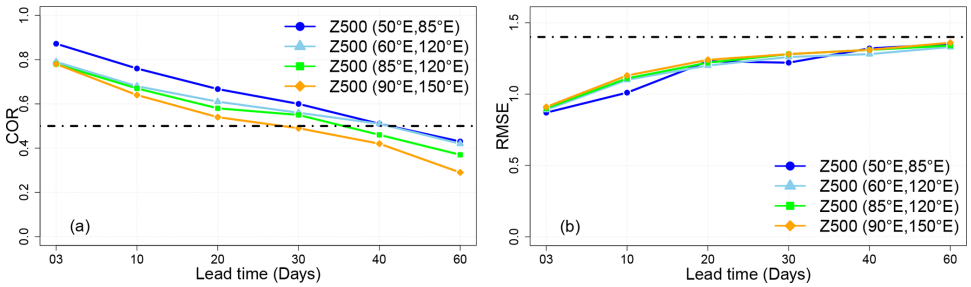

Figure B2. Comparison between the COR **(a)** and RMSE **(b)** of the SWG forecast based on analogs of Z500 computed over different geographical regions, for lead times going from 3 to 60 d over the period from 1979 to 2020. The forecast was made with analogs computed over the Indian Ocean with coordinates 15° S–15° N, 50–85° E, and 15° S–15° N, 60–120° E; the Indian and Pacific oceans with coordinates 15° S–15° N, 85–120° E; and the Indian Ocean–Maritime Continent region with coordinates 15° S–15° N, 90–150° E. As the latitude is the same for the different considered geographical regions, we just mention the longitude of each domain in the legend.

Appendix C: Dependence of the forecast skill on MJO phases

We checked the dependence of the SWG forecast skill of the amplitude of the MJO and the MJO phases. We verified the relationship between the CRPS at $T = 5$ d and the MJO phases (Fig. C1). We divided the CRPS values in two classes:

- CRPS values above the 75th quantile (Fig. C1a),
- CRPS values below the 25th quantile (Fig. C1b).

As shown in Fig. C1 the difference between the boxplots in the two cases is smaller. Hence, we can say that the dependence of the forecast skill of the MJO amplitude with SWG and the MJO phases is small.

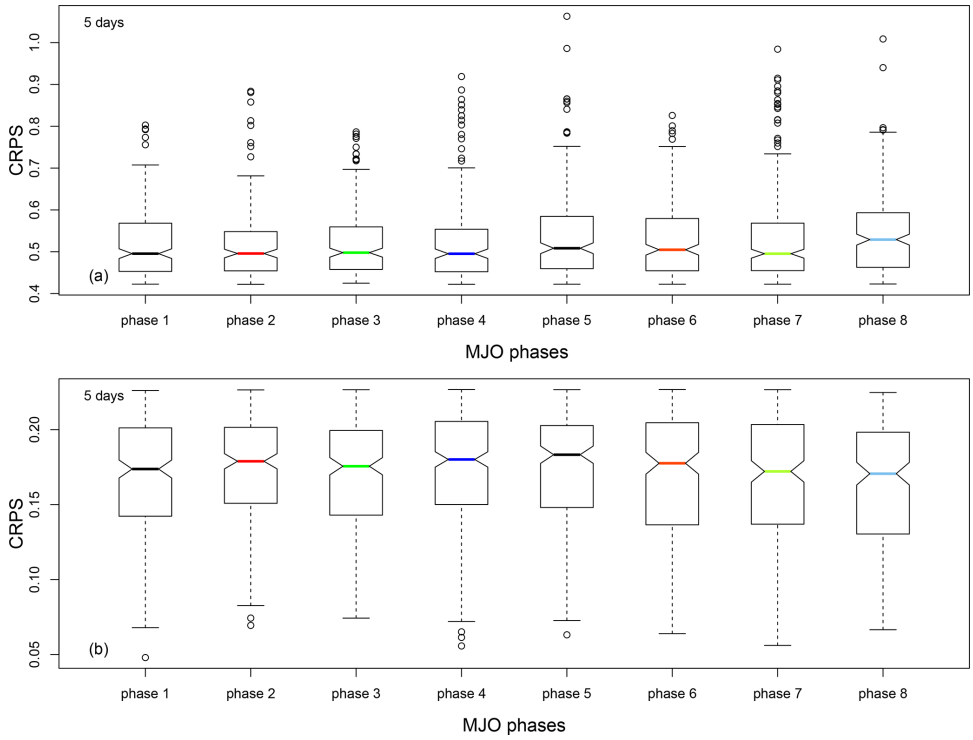

Figure C1. Relationship between CRPS and MJO phases. **(a)** CRPS values above the 75th quantile and **(b)** CRPS values above the 25th quantile.

Code and data availability. The code and data files are available at http://doi.org/10.5281/zenodo.4524562 (Krouma, 2021).

Author contributions. MK designed and performed the analyses and wrote the manuscript. PY co-designed the analyses. RS provided data for comparison.

Competing interests. The contact author has declared that none of the authors has any competing interests.

Disclaimer. Publisher's note: Copernicus Publications remains neutral with regard to jurisdictional claims in published maps and institutional affiliations.

Acknowledgements. This work is part of the EU International Training Network (ITN) Climate Advanced Forecasting of subseasonal Extremes (CAFE). The project receives funding from the European Union's Horizon 2020 research and innovation program under the Marie Skłodowska-Curie Actions (grant agreement no. 813844). The authors would like to thank Alvaro Corral and Monica Minjares for the discussions.

Financial support. This research has been supported by the Horizon 2020.

Review statement. This paper was edited by Yun Liu and reviewed by two anonymous referees.

References

Ailliot, P., Allard, D., Monbet, V., and Naveau, P.: Stochastic weather generators: an overview of weather type models, Journal de la Société Française de Statistique, p. 15, http://www.numdam.org/item/JSFS_2015__156_1_101_0/ (last access: 22 December 2022), 2015.

Atencia, A. and Zawadzki, I.: A comparison of two techniques for generating nowcasting ensembles, Part I: Lagrangian ensemble technique, Month. Weather Rev., 142, 4036–4052, 2014.

Barlow, M., Zaitchik, B., Paz, S., Black, E., Evans, J., and Hoell, A.: A Review of Drought in the Middle East and Southwest Asia, J. Climate, 29, 8547–8574, https://doi.org/10.1175/JCLI-D-13-00692.1, 2016.

Becker, E. J., Berbery, E. H., and Higgins, R. W.: Modulation of Cold-Season U.S. Daily Precipitation by the Madden-Julian Oscillation, J. Climate, 24, 5157–5166, https://doi.org/10.1175/2011JCLI4018.1, 2011.

Blanchet, J., Stalla, S., and Creutin, J.-D.: Analogy of multiday sequences of atmospheric circulation favoring large rainfall accumulation over the French Alps, Atmos. Sci. Lett., 19, e809, https://doi.org/10.1002/asl.809, 2018.

Cassou, C.: Intraseasonal interaction between the Madden-Julian Oscillation and the North Atlantic Oscillation, Nature, 455, 523–527, https://doi.org/10.1038/nature07286, 2008.

Fawcett, T.: An introduction to ROC analysis, Pattern Recogn. Lett., 27, 861–874, https://doi.org/10.1016/j.patrec.2005.10.010, 2006.

Grimit, E. P. and Mass, C. F.: Initial Results of a Mesoscale Short-Range Ensemble Forecasting System over the Pacific Northwest, Weather Forecast., 17, 192–205, https://doi.org/10.1175/1520-0434(2002)017<0192:IROAMS>2.0.CO;2, 2002.

Hersbach, H.: Decomposition of the Continuous Ranked Probability Score for Ensemble Prediction Systems, Weather Forecast., 15, 559–570, https://doi.org/10.1175/1520-0434(2000)015<0559:DOTCRP>2.0.CO;2, 2000.

Hersbach, H., Bell, B., Berrisford, P., Hirahara, S., Horányi, A., Muñoz-Sabater, J., Nicolas, J., Peubey, C., Radu, R., and Schepers, D.: The ERA5 global reanalysis, Q. J. Roy. Meteor. Soc., 146, 1999–2049, 2020.

IRI: The University of Columbia (USA) – RMMs data, https://iridl.ldeo.columbia.edu/SOURCES/.BoM/.MJO/, last access: 19 December 2022.

Kim, H., Vitart, F., and Waliser, D. E.: Prediction of the Madden-Julian Oscillation: A Review, J. Climate, 31, 9425–9443, https://doi.org/10.1175/JCLI-D-18-0210.1, 2018.

Kistler, R., Kalnay, E., Collins, W., Saha, S., White, G., Woollen, J., Chelliah, M., Ebisuzaki, W., Kanamitsu, M., Kousky, V., van den Dool, H., Jenne, R., and Fiorino, M.: The NCEP-NCAR 50-year reanalysis: Monthly means CD-ROM and documentation, B. Am. Meteorol. Soc., 82, 247–267, 2001.

Krouma, M.: Assessment of stochastic weather forecast based on analogs of circulation, Zenodo [code, data set], https://doi.org/10.5281/zenodo.4524562, 2021.

Krouma, M., Yiou, P., Déandreis, C., and Thao, S.: Assessment of stochastic weather forecast of precipitation near European cities, based on analogs of circulation, Geosci. Model Dev., 15, 4941–4958, https://doi.org/10.5194/gmd-15-4941-2022, 2022.

Lafleur, D. M., Barrett, B. S., and Henderson, G. R.: Some Climatological Aspects of the Madden-Julian Oscillation (MJO), J. Climate, 28, 6039–6053, https://doi.org/10.1175/JCLI-D-14-00744.1, 2015.

Lim, Y., Son, S.-W., and Kim, D.: MJO Prediction Skill of the Subseasonal-to-Seasonal Prediction Models, J. Climate, 31, 4075–4094, https://doi.org/10.1175/JCLI-D-17-0545.1, 2018.

Lin, H., Brunet, G., and Derome, J.: Forecast Skill of the Madden-Julian Oscillation in Two Canadian Atmospheric Models, Mon. Weather Rev., 136, 4130–4149, https://doi.org/10.1175/2008MWR2459.1, 2008.

Lorenz, E. N.: Atmospheric Predictability as Revealed by Naturally Occurring Analogues, J. Atmos. Sci., 26, 636–646, 1969.

Marshall, A. G., Hendon, H. H., and Hudson, D.: Visualizing and verifying probabilistic forecasts of the Madden-Julian Oscillation: PROBABILISTIC MJO FORECASTS, Geophys. Res. Lett., 43, 12278–12286, https://doi.org/10.1002/2016GL071423, 2016.

Palmer, T. N.: Predicting uncertainty in forecasts of weather and climate, Rep. Prog. Phys., 63, 71–116, 2000.

Pegion, K. and Kirtman, B. P.: The Impact of Air-Sea Interactions on the Predictability of the Tropical Intraseasonal Oscillation, J. Climate, 21, 5870–5886, https://doi.org/10.1175/2008JCLI2209.1, 2008.

Appendix C. Supplement of the article "Ensemble forecast of an index of the Madden Julian Oscillation using a stochastic weather generator based on circulation analogs"

Platzer, P., Yiou, P., Naveau, P., Filipot, J.-F., Thiébaut, M., and Tandeo, P.: Probability Distributions for Analog-To-Target Distances, J. Atmos. Sci., 78, 3317–3335, https://doi.org/10.1175/JAS-D-20-0382.1, 2021.

Rashid, H. A., Hendon, H. H., Wheeler, M. C., and Alves, O.: Prediction of the Madden-Julian oscillation with the POAMA dynamical prediction system, Clim. Dynam., 36, 649–661, https://doi.org/10.1007/s00382-010-0754-x, 2011.

Scaife, A. A., Arribas, A., Blockley, E., Brookshaw, A., Clark, R. T., Dunstone, N., Eade, R., Fereday, D., Folland, C. K., and Gordon, M.: Skillful long-range prediction of European and North American winters, Geophys. Res. Lett., 41, 2514–2519, 2014.

Silini, R., Barreiro, M., and Masoller, C.: Machine learning prediction of the Madden-Julian oscillation, npj Clim. Atmos. Sci., 4, 57, https://doi.org/10.1038/s41612-021-00214-6, 2021.

Silini, R., Lerch, S., Mastrantonas, N., Kantz, H., Barreiro, M., and Masoller, C.: Improving the prediction of the Madden-Julian Oscillation of the ECMWF model by post-processing, EGUsphere [preprint], https://doi.org/10.5194/egusphere-2022-2, 2022.

Sivillo, J. K., Ahlquist, J. E., and Toth, Z.: An ensemble forecasting primer, Weather Forecast., 12, 809–818, 1997.

Stachnik, J. P. and Chrisler, B.: An index intercomparison for MJO events and termination, J. Geophys. Res.-Atmos., 125, https://doi.org/10.1029/2020JD032507, e2020JD032507, 2020.

Straub, K. H.: MJO Initiation in the Real-Time Multivariate MJO Index, J. Climate, 26, 1130–1151, https://doi.org/10.1175/JCLI-D-12-00074.1, 2013.

Toth, Z. and Kalnay, E.: Ensemble forecasting at NCEP and the breeding method, Mon. Weather Rev., 125, 3297–3319, 1997.

Ventrice, M. J., Wheeler, M. C., Hendon, H. H., Schreck, C. J., Thorncroft, C. D., and Kiladis, G. N.: A Modified Multivariate Madden-Julian Oscillation Index Using Velocity Potential, Mon. Weather Rev., 141, 4197–4210, https://doi.org/10.1175/MWR-D-12-00327.1, 2013.

Verde, M. F.: Measures of sensitivity based on a single hit rate and false alarm rate: The accuracy, precision, and robustness of "A_z, and A", Percept. Psychophys., 68, 643–654, 2006.

Vitart, F.: Madden-Julian Oscillation prediction and teleconnections in the S2S database, Q. J. Roy. Meteor. Soc., 143, 2210–2220, https://doi.org/10.1002/qj.3079, 2017.

Vitart, F., Ardilouze, C., Bonet, A., Brookshaw, A., Chen, M., Codorean, C., Déqué, M., Ferranti, L., Fucile, E., Fuentes, M., Hendon, H., Hodgson, J., Kang, H.-S., Kumar, A., Lin, H., Liu, G., Liu, X., Malguzzi, P., Mallas, I., Manoussakis, M., Mastrangelo, D., MacLachlan, C., McLean, P., Minami, A., Mladek, R., Nakazawa, T., Najm, S., Nie, Y., Rixen, M., Robertson, A. W., Ruti, P., Sun, C., Takaya, Y., Tolstykh, M., Venuti, F., Waliser, D., Woolnough, S., Wu, T., Won, D.-J., Xiao, H., Zaripov, R., and Zhang, L.: The Subseasonal to Seasonal (S2S) Prediction Project Database, B. Am. Meteorol. Soc., 98, 163–173, https://doi.org/10.1175/BAMS-D-16-0017.1, 2017.

Wheeler, M. and Weickmann, K. M.: Real-Time Monitoring and Prediction of Modes of Coherent Synoptic to Intraseasonal Tropical Variability, Mon. Weather Rev., 129, 2677–2694, https://doi.org/10.1175/1520-0493(2001)129<2677:RTMAPO>2.0.CO;2, 2001.

Wheeler, M. C. and Hendon, H. H.: An All-Season Real-Time Multivariate MJO Index: Development of an Index for Monitoring and Prediction, Mon. Weather Rev., 132, 1917–1932, 2004.

Wu, J., Ren, H.-L., Zuo, J., Zhao, C., Chen, L., and Li, Q.: MJO prediction skill, predictability, and teleconnection impacts in the Beijing Climate Center Atmospheric General Circulation Model, Dynam. Atmos. Oceans, 75, 78–90, https://doi.org/10.1016/j.dynatmoce.2016.06.001, 2016a.

Wu, J., Ren, H.-L., Zuo, J., Zhao, C., Chen, L., and Li, Q.: MJO prediction skill, predictability, and teleconnection impacts in the Beijing Climate Center Atmospheric General Circulation Model, Dynam. Atmos. Oceans, 75, 78–90, https://doi.org/10.1016/j.dynatmoce.2016.06.001, 2016b.

Xiang, B., Zhao, M., Jiang, X., Lin, S.-J., Li, T., Fu, X., and Vecchi, G.: The 3–4-Week MJO Prediction Skill in a GFDL Coupled Model, J. Climate, 28, 5351–5364, https://doi.org/10.1175/JCLI-D-15-0102.1, 2015.

Yang, D. and Ingersoll, A. P.: Triggered convection, gravity waves, and the MJO: A shallow-water model, J. Atmos. Sci., 70, 2476–2486, 2013.

Yiou, P.: AnaWEGE: a weather generator based on analogues of atmospheric circulation, Geosci. Model Dev., 7, 531–543, https://doi.org/10.5194/gmd-7-531-2014, 2014.

Yiou, P. and Déandréis, C.: Stochastic ensemble climate forecast with an analogue model, Geosci. Model Dev., 12, 723–734, https://doi.org/10.5194/gmd-12-723-2019, 2019

Zamo, M. and Naveau, P.: Estimation of the Continuous Ranked Probability Score with Limited Information and Applications to Ensemble Weather Forecasts, Math. Geosci., 50, 209–234, 2018.

Zhang, C.: Madden-Julian Oscillation: Bridging Weather and Climate, B. Am. Meteorol. Soc., 94, 1849–1870, https://doi.org/10.1175/BAMS-D-12-00026.1, 2013.

Zhang, C., Gottschalck, J., Maloney, E. D., Moncrieff, M. W., Vitart, F., Waliser, D. E., Wang, B., and Wheeler, M. C.: Cracking the MJO nut, Geophys. Res. Lett., 40, 1223–1230, https://doi.org/10.1002/grl.50244, 2013.

Zhang, C., Adames, Ã. F., Khouider, B., Wang, B., and Yang, D.: Four Theories of the Madden-Julian Oscillation, Rev. Geophys., 58, e2019RG000685, https://doi.org/10.1029/2019RG000685, 2020.

Appendix D

Supplement study about the attribution of extremes events. Article "A climate-change attribution retrospective of some impactful weather extremes of 2021"

https://doi.org/10.5194/wcd-2022-9
Preprint. Discussion started: 17 February 2022

Weather and Climate Dynamics Discussions
Open Access
EGU

A climate-change attribution retrospective of some impactful weather extremes of 2021

Davide Faranda[1,2,3], Stella Bourdin[1], Mireia Ginesta[1], Meriem Krouma[1], Gabriele Messori[4,5], Robin Noyelle[1], Flavio Pons[1], and Pascal Yiou[1]

[1]Laboratoire des Sciences du Climat et de l'Environnement, UMR 8212 CEA-CNRS-UVSQ, Université Paris-Saclay, IPSL, 91191 Gif-sur-Yvette, France
[2]London Mathematical Laboratory, 8 Margravine Gardens London, W6 8RH, UK
[3]LMD/IPSL, Ecole Normale Superieure, PSL research University, Paris, France
[4]Department of Earth Sciences and Centre of Natural Hazards and Disaster Science (CNDS), Uppsala University, Uppsala, Sweden
[5]Department of Meteorology and Bolin Centre for Climate Research, Stockholm University, Stockholm, Sweden

Correspondence: Davide Faranda (davide.faranda@cea.fr)

Abstract. The IPCC report AR6 indicates a general consensus that anthropogenic climate change is modifying frequency and intensity of class of extreme events such as cold spells, heatwaves, storms or floods. A different point of view is to investigate whether a specific extreme event would have been possible in the absence of climate change, or whether climate change may have affected its specific characteristics. Here, we address this question by performing an attribution of some major extreme events that occurred in 2021 over Europe and North America: the winter storm Filomena, the French Spring cold spell, the Westphalia Floods, the Mediterranean summer heatwave, the hurricane Ida, the Po Valley tornadoes outbreak, the medicane Apollo and the late autumn Scandinavian cold-spell. We focus on the role of the atmospheric circulation associated with the events and its likelihood in present (factual world) and past climate conditions (counterfactual world) – defined using the ERA5 dataset 1950 to present. We use an analogs-based methodology whose aim is to find the most similar sea-level pressure patterns to the target events in the factual and counterfactual worlds and compute significant shifts in probability, persistence, predictability and seasonality of the patterns. We also diagnose whether in the present climate the analogs of the studied events lead to warmer/cooler or dryer/wetter conditions than in the past. We find that most of the events are significantly modified in present climate with respect to the past, because of changes in position, persistence and seasonality of cyclonic/anticyclonic patterns. Two of the events, storm Filomena and Medicane Apollo, appears to be a black swan of the atmospheric circulation, with analogs of bad quality. Our approach, complementary to the statistical methods already available in the community, warns that the role of the atmospheric circulation should be taken into account when performing attribution studies.

Appendix D. Supplement study about the attribution of extremes events. Article "A climate-change attribution retrospective of some impactful weather extremes of 2021"

https://doi.org/10.5194/wcd-2022-9
Preprint. Discussion started: 17 February 2022

1 Introduction

One of the main novelties of the latest IPCC AR6 report (Allan et al., 2021) with respect to previous IPCC documents is the increased confidence that anthropogenic climate change is critically affecting the dynamics of weather extremes. For summer, the AR6 report states that we are already observing prolonged periods of extremely warm conditions (Horton et al., 2016) with increased droughts leading to forest fires (Flannigan et al., 2000), species extinctions (Román-Palacios and Wiens, 2020) and health issues for vulnerable populations (Mitchell et al., 2016). In winter, increased persistence of cyclonic and anticyclonic structures leads to extremely wet and dry periods (Ogawa et al., 2018), the latter associated with foggy weather and smog accumulation in urban areas (Sachweh and Koepke, 1995; Hu et al., 2020). Finally, the IPCC also warns that, in the shoulder seasons, we observe a large variability of rains associated with both tropical and extratropical storms and convective events, leading to an alteration of the hydrological cycle (Gordon et al., 2005; Bala et al., 2010; Pendergrass et al., 2017). These trends are expected to accelerate in the coming years, if the global efforts to reduce carbon emissions are not implemented swiftly (Trisos et al., 2020).

While these assessments are meaningful when considering (relatively) large ensembles of extreme events with similar characteristics, it is also important to evaluate whether the probability of occurrence, or physical characteristics, of a single extreme event have been influenced by anthropogenic climate change. This knowledge builds awareness of the consequences of greenhouse gas emissions in the general public, and allows stakeholders to evaluate specific impacts induced by climate change. For these reasons, attributing a single extreme event to climate change has given rise to a wealth of studies, an entire field named attribution (Shepherd, 2016; Jézéquel et al., 2018; Naveau et al., 2020; van Oldenborgh et al., 2021).

Studies in extreme events attribution are conventionally grounded in extreme value theory (Trenberth et al., 2015), which they use to estimate return times of threshold exceedances of particulars observables (e.g. temperatures above or below a target value for a certain number of consecutive days for heatwaves and cold-spells). The main drawback of such statistical attribution is that it does not take into account the physical processes leading to the extreme events. Climate change is likely associated with dynamical changes in the atmosphere (e.g. Stendel et al., 2021), yet the conventional extreme value approach overlooks these entirely. This brought Shepherd (2014) to argue that the atmospheric circulation is a key element of the uncertainty in attribution studies, and in parallel stimulated attempts to incorporate knowledge of the atmospheric circulation into an attribution framework (Shepherd, 2016; Yiou et al., 2017).

Here, we build upon this line of work by performing an attribution of some notable extremes occurring during the 2021 calendar year based on large-scale atmospheric drivers. In particular, we analyze: i) the winter storm Filomena which caused, in January, heavy snowfalls and extremely cold conditions in Spain; ii) the late cold spell that occurred in April 2021 in France with large impacts on vegetation and agriculture; iii) the July floods in Westphalia, Germany, responsible for the destruction of entire villages, infrastructure and heavy loss of lives; iv) the record-breaking temperatures during the August Mediterranean heatwave and the associated wildfires in Greece and Italy; v) the September Po Valley tornado outbreak; vi) Hurricane Ida, which caused heavy damage in Louisiana and New York city; vii) the medicane (Mediterranean Hurricane) Apollo which occurred in Sicily in October; and viii) the November Scandinavian cold spell.

https://doi.org/10.5194/wcd-2022-9
Preprint. Discussion started: 17 February 2022

In order to attribute these events to climate change, we study the concurrent atmospheric circulation patterns and we search for pattern recurrences in the far (1950–1979) and recent past (1992–2021). Our working hypothesis is that the far past acts as a counterfactual world where the Earth's climate was less heavily influenced by anthropogenic forcing when compared to the recent past (the factual world). Additionally, we assume that 30 years is a long enough period to average out the interannual variability of the atmospheric motions (as that caused, for example, by the El Nino–Southern Oscillation) and the climate within these periods can be assumed (quasi)stationary with respect to the climate change signal. We present in Section 2 the methodological aspects of this work, introducing in Section 3 the relevant assessment metrics. The Section 4 contains, for each event: i) a description, ii) a state-of-the art of climate-change aspects related to the event and iii) our attribution analyses. Our conclusions are presented in Section 5.

2 A method for attribution of extreme events to climate change which takes into account changes in atmospheric circulation

We study changes in weather patterns associated with extreme events by leveraging the framework of weather analogs (Yiou et al., 2003). We first identify the peak day of each extreme event. We then perform a semi–objective detection of the concurrent large-scale weather pattern using daily average sea-level pressure (slp) from the ERA5 reanalysis databas eover 1950–2021. The semi-objectivity lies in the exact choice of geographical domain over which the pattern is identified. For cyclones, the domain of the analysis can be easily identified as the low-pressure area associated with the storm. For cold spells and heatwaves, we follow Stefanon et al. (2012), who have shown that these events have a large scale dynamical footprint spanning the size of the European continent. For all cases, we have tested that our method is qualitatively insensitive to modest changes in the domain size. Four our analysis, we split the ERA5 dataset into two periods: 1950–1979 and 1992–2021. We take the first period to represent a counterfactual world with a weaker anthropogenic influence on climate than in the second period, which represents our factual world affected by anthropogenic climate change. For each period, we scan scan all the daily average slp maps and select the best 33 analogs, namely the maps minimizing the euclidean distance with respect to the map of the event itself. The number of 33 corresponds approximately to the smallest 3‰ of euclidean distances in each subset of our data. We have tested extracting between 25 and 50 analogue maps, without finding any qualitatively large differences in our results. Note that for the factual period, as common practise in attribution studies, the event itself is removed. Furthermore, we forbid the analogs search in a window of a week centered around the date of the event. We do not restrict the analogs search to a specific season, which allows us to identify possible seasonality shifts between the counterfactual and factual periods. We then compute the average map for all analogs in each of the two periods, and take the difference between the two averages (Δslp). To determine significant changes between the two periods, we adopt a bootstrap procedure which consists of pooling the dates from the two periods together, randomly extracting 33 dates from this pool 1000 times, creating the corresponding difference maps and marking as significant only grid point changes above two standard deviations of the bootstrap sample. We also plot the 2-meter temperature ($t2m$) and daily precipitation rate fields (tp) on the dates of the closest slp analogs, repeating the same bootstrap procedure to identify significant changes.

Appendix D. Supplement study about the attribution of extremes events. Article "A climate-change attribution retrospective of some impactful weather extremes of 2021"

https://doi.org/10.5194/wcd-2022-9
Preprint. Discussion started: 17 February 2022

3 Evaluation Metrics

Following Faranda et al. (2020), we define some quantities that support our interpretation of the analogs-based attribution. All of these may then be compared between the counterfactual and factual periods.

- Analogue Quality Q: Q is the average euclidean distance of a given day from its closest 33 analogs (Faranda et al., 2020). One can then compare Q for the peak day of the extreme event to Q for each analogue of the extreme event. If the value of Q for the extreme event belongs to the same distribution as, or is smaller than, the values of Q for the analogs, then the extreme event has good analogs and attribution can be performed. If instead the Q for the extreme event is larger than that of the analogue days, then this indicates a highly unusual slp configuration and the results of the attribution analysis must be interpreted with care. Differences between the counterfactual and factual periods indicate whether the the atmosphere is visiting states (analogs) that are more or less similar to the map associated with the extreme (i.e. how large Q for the peak day of the extreme event is), and whether those states are in turn more or less "typical" of the atmospheric variability (i.e. whether the distribution of Q for the 33 analogs shifts towards higher or lower values).

- Seasonality of analogs: We can count the number of analogs in each month to detect whether there has been a shift of the circulation towards earlier or later months of the year. This can have strong thermodynamic implications, for example if a a circulation leading to large positive springtime temperature anomalies becomes more common in summer, when average temperatures are much higher.

- Predictability Index D: Using dynamical systems theory (Freitas et al., 2011, 2016; Lucarini et al., 2016b), we can compute the local dimension D of each daily slp map (Faranda et al. (2017b, 2019b), see Appendix A). The local dimension is a proxy for the number of degrees of freedom of the field, meaning that the higher D, the more unpredictable the temporal evolution of the slp maps will be (Faranda et al., 2017a; Messori et al., 2017). If the dimension D of the chosen day is higher or lower than that of its analogs, then the day will be less or more predictable than the closest dynamical situations identified in the data. We compute two values of D for the event, one using the counterfactual analogs and one using the factual ones. As for Q, we also compute the distribution of D for all the analogs. This informs on how predictable the event is with respect to its analogs.

- Persistence Index Θ: Another quantity derived from the dynamical systems theory is the persistence Θ of a given configuration (Faranda et al. (2017b), see Appendix A). The persistence counts for how many days we are likely to observe a map that is an analogue of the one considered (Moloney et al., 2019). As explained for Q and D, we compute the two values of the persistence for the event in the factual and counterfactual worlds and the corresponding distributions of persistence for the analogs.

https://doi.org/10.5194/wcd-2022-9
Preprint. Discussion started: 17 February 2022

4 Results

Our list of 2021 extreme events is not intended to be exhaustive. We mostly cover Europe and North America, and we try to select events that differ in impacts, season and genesis in order to provide a rich overview of attribution capabilities and difficulties. We provide in Table 1 the list of the events studied, with the date for the analogs search, countries of interest and longitude-latitude box for the analogs search. A graphical representation of the events is provided in Figure 1.

Event	Date	Countries	analogs Box
Winter Storm Filomena	09-01-2021	Spain	[15°W,10°E,30°N,46°N]
French Spring Cold Spell	06-04-2021	France	[10°W,30°E,30°N,70°N]
Westphalia floods	14-07-2021	Benelux/Germany	[5°W,23°E,41°N,59°N]
Mediterranean Heatwave	11-08-2021	Spain/France/Italy	[10°W,25°E,30°N,45°N]
Hurricane Ida	02-09-2021	USA	[80°W,55°W,35°N,55°N]
Po Valley Tornadoes Outbreak	19-09-2021	Italy	[10°W,20°E,35°N,50°N]
Medicane Apollo	29-10-2021	Italy	[10°E,20°E,34°N,40°N]
Scandinavian Cold Spell	28-11-2021	Sweden/Norway	[10°W,30°E,35°N,75°N]

Table 1. List of the events presented in this study, with the date for the analogs search, countries of interest and longitude-latitude box for the analogs search

4.1 Winter Storm Filomena

In early January 2021 the weather regime over the Euro-Atlantic sector was characterized by a negative phase of the North Atlantic Oscillation (NAO, see, e.g. Michelangeli et al. (1995)), with cold air from the Arctic being advected over southern Europe and frontal activity favoured over the Azores. Filomena was named after an extratropical cyclone that moved from the Azores to the Canary Islands and the Iberian Peninsula on the 6th and 7th of January respectively, resulting in strong precipitation and hurricane-force winds. It triggered historic snowfalls in the inland regions of the peninsula and a 14-days long cold spell. This exceptional event caused four casualties between the 9th and the 16th of January and economic losses of up to 2 billion euros (Aon, 2021). The storm formed on January 1st in the northeastern inland of the United States. On January 3rd it entered the North Atlantic and it began a sharp displacement southeastward forced by a high-pressure system in the central North Atlantic and pushed by a strong meridional polar jet. When it reached the Azores on the 5th, despite being weakened, it was finally named Filomena by the AEMET, which emitted a severe weather warning for Canary Islands and Spain for the two following days. The 6th and 7th of January, Filomena strengthened as it moved southeast towards the Canary Islands. The cyclone traveled northeastward towards the Iberian Peninsula on January 7th, bringing relatively warm, humid air for the Winter season. At this time, southern Europe was experiencing cold temperature anomalies because of an anticyclone located west of the UK, resulting in temperature minimums below 0°C in almost the entire Iberian Peninsula. Hence, when the

https://doi.org/10.5194/wcd-2022-9
Preprint. Discussion started: 17 February 2022

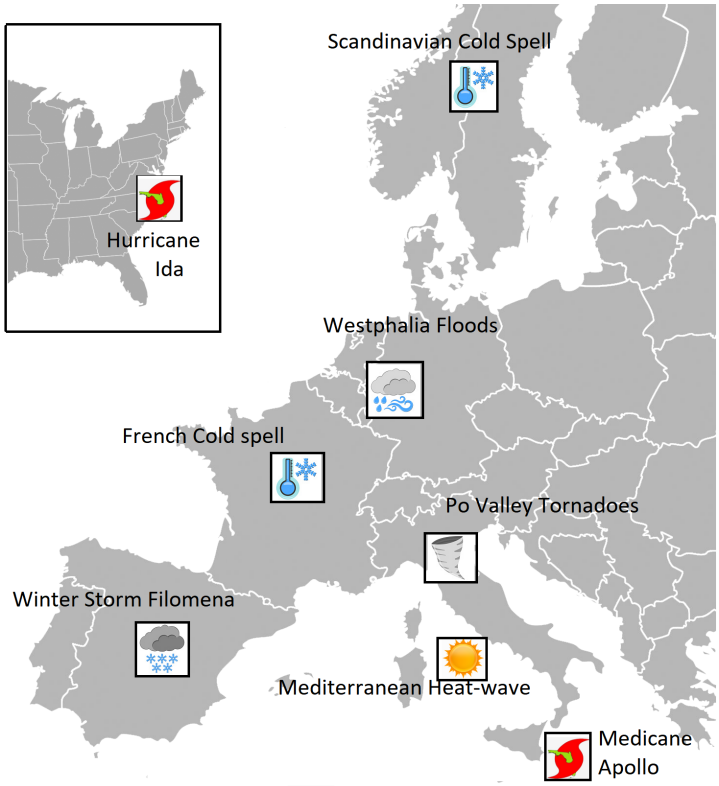

Figure 1. Visual representation of the events studied in this work.

storm arrived in the Gulf of Cadiz on January 8th, its warm front blew over the preexisting cold air, allowing precipitation in the form of snow or sleet throughout most of the Iberian Peninsula, except for some parts of southern Spain. The precipitation lasted for three days, until Filomena dissipated in the Mediterranean sea on January 11th. The most affected regions were central and northeastern Spain, which accumulated an average of 30 to 50 cm of snow (AEMET, 2021b). The accumulated snow favored the persistence of low temperatures in the following days, triggering a cold spell that lasted for about two weeks, from January 5th to 17th, with a temperature average of 2°C in the Iberian peninsula and an anomaly of -3.8° with respect to the 1981-2010 climatology, as recorded by the AEMET (2021b).

4.1.1 Extratropical winter storms and climate change

Numerous studies have addressed the influence of climate change on extratropical cyclones (ECT) due to their impacts on many regions of the planet (e.g. Zappa et al., 2013; Ulbrich et al., 2009). The IPCC report gathers and summarizes some of them (Lee et al., 2021) and it highlights that, by the end of the 21st century, the number of extratropical cyclones will slightly

https://doi.org/10.5194/wcd-2022-9
Preprint. Discussion started: 17 February 2022

Weather and Climate Dynamics Discussions
Open Access
EGU

decrease, especially in the southern flank of storm tracks. In the Southern Hemisphere, storm tracks are likely to shift poleward, while there is low confidence in the response in the Northern Hemisphere. CMIP6 models show a tripolar pattern in the North Atlantic storm track in winter, represented by an increase in storm activity over central Europe and a decrease in Scandinavia, Southern Europe, and the Mediterranean region (Lee et al., 2021). There is high confidence that the average precipitation-rate of ETCs will increase in a future climate in response to the increase in the atmospheric water vapor content. Snowfall associated with ECTs will decrease because of tropospheric temperature increases (Seneviratne et al., 2021). According to Seneviratne et al. (2021), the number of ECT associated with strong winds over the North Atlantic and Europe will decrease. Hence, Filomena-like storms would be less probable in a future climate and would be less likely to produce such amounts of snowfall and strong winds, although they would be associated with more precipitation.

4.1.2 Attribution of Filomena to climate change

We now use the ERA5 data to perform the attribution of the cyclonic circulation associated with Filomena for the 09-01-2021 in the past and present climate (Figure 2). We find a significant decrease of the slp depression up to 3hPa for the factual with respect to the factual period (a-d). Temperatures (e-g) are significantly and considerably warmer (h) in the recent period, specially over land, probably due to a temporal shift of the recurrence of this storm towards warmer months and an increase in surface temperatures in recent years. This warming does not imply a general increase in the precipitation, hence we deduce that the precipitation changes are more dynamically induced. Precipitation (l) is significantly larger over southeastern Cantabrian Sea and Cape Nao, and lower in the Pyrenees, Catalonia and south of the Iberian Peninsula. However, no significant differences are found in the peninsular center, where Filomena had the highest impact. The analogs quality Q (m) shows that this circulation pattern is highly uncommon in both periods because the quality of the event lies at the edge of the violin plots. This suggests that Filomena is somehow a black swan (Taleb, 2005), an event that has not occurred before as its analogs are distributed in a different way. The predictability index D (n) increases slightly in the factual world while the persistence Θ (o) decreases, which means that storms like Filomena are more predictable and less persistent in the current climate. We see an overall decrease in frequency in Spring and an increase in Summer months.

Hence, this event would have been colder and more likely in the counterfactual world, leading to even lower temperatures and higher precipitation on the Pyrenees. We underline that the fact that analogs quality Q is poor for the event and that there are no analogs in the counterfactual nor factual world in January, make Filomena a black swan of the atmospheric circulation, an unprecedented event, emphasizing the exceptional nature of the event and the limitation of this and other attribution studies.

4.2 French Spring Cold Spell

A frost event took place from 6th to 8th April 2021 in France. It was exceptional, with daily minimum temperatures below -5°C recorded in several places. Grapevines and fruit trees were damaged especially in the Loire and Rhône Valleys, as frost management strategies (e.g. as local heating from braseros) could not be implemented in time. The temperatures broke record lows at many French weather stations. This cold event happened one week after an episode of record-breaking high temperatures in March also in many places in France (LaChaineMeteo, 2021) and Western Europe. This sequence (or compound

Appendix D. Supplement study about the attribution of extremes events. Article "A climate-change attribution retrospective of some impactful weather extremes of 2021"

https://doi.org/10.5194/wcd-2022-9
Preprint. Discussion started: 17 February 2022

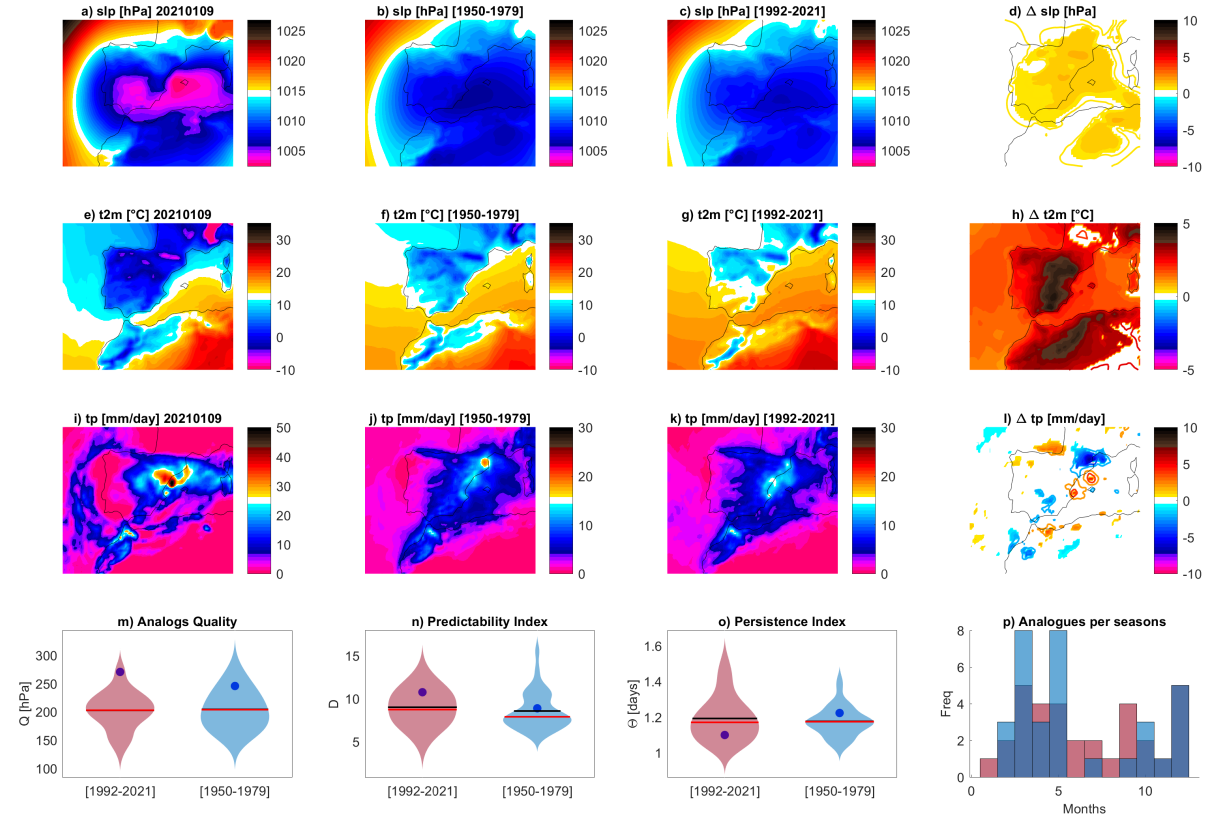

Figure 2. Attribution for Filomena Storm on 09-01-2021. Daily mean sea-level pressure slp (a), 2-meter temperatures $t2m$ (e) and total precipitation tp (i) on the day of the event. Average of the 33 sea-level pressure analogs found for the counterfactual [1950-1979] (b) and factual [1992-2021] (c) periods and corresponding 2-meter temperatures (f,g) and daily precipitation rate (j,k). Δslp (d), $\Delta t2m$ (h) and Δtp (i) between factual and counterfactual periods: colored-filled areas show significant anomalies with respect to the bootstrap procedure. Violin plots for counterfactual (blue) and factual (pink) periods for the Analogs Quality Q (m) the Predictability index D (n), the Persistence index Θ (o) and the distribution of analogs in each month (p). Values for the selected day are marked by a blue dot.

event, according to the definition proposed by Zscheischler et al. (2020)) led the growing season to start early, with bud burst occurring in March and the new leaves and flowers left exposed to the deep frost episode that followed in early April. This cold spell was associated with an advection of cold air from the Arctic into France between April 5th and 7th 2021. A deep low pressure based over Scandinavia and anticyclonic conditions overs Iceland, pumped cold Arctic air into France on April 5-6th 2021, which created the low-temperature anomaly in the subsequent days.

https://doi.org/10.5194/wcd-2022-9
Preprint. Discussion started: 17 February 2022

Weather and Climate Dynamics Discussions
Open Access
EGU

4.2.1 French cold spells and climate change

The IPCC AR6 describes as "virtually certain" that there have been warmer and/or rarer cold spells over most land areas since the 1950s, that this trend is due to anthropogenic climate change and that it is set to continue in the future Allan et al. (2021). Indeed, there is a large consensus the frequency and average duration of such events will eventually decrease (Russo and Sterl, 2011).

While a rapid warming, in general, lowers the probability of cold spell occurrence, projected changes in the temperature distribution imply that regional changes in cold spell frequency and/or intensity may not match changes in the mean temperature (Tamarin-Brodsky et al., 2019). Similarly, Kodra et al. (2011) have shown that long-lasting periods where temperatures drop below an absolute threshold (e.g. frost days) may still be produced locally and occasionally even in future, warmer climates. There has also been a a lively debate in the literature on whether dynamical changes associated with climate change may act to partly counter the thermodynamic changes and favour cold spell occurrence. Faranda (2019) and D'errico et al. (2019) argued that circulation patterns associated with cold spells over Europe have been increasing in frequency in the present climate and will continue to do so under future climate change. Several authors have also argued for or against a link between Arctic Amplification and an increased occurrence of cold spells in some mid-latitude regions (Mori et al., 2014; Cohen et al., 2018; Blackport and Screen, 2020; Ye and Messori, 2020; Jolly et al., 2021).

Cold spells continue to have large detrimental socio-economic effects, with several high-impact events occurring in recent winters, notably during the 2018–2019 and 2020–2021 winters in North America (Lee and Butler, 2020; BBC; Lillo et al., 2021; Doss-Gollin et al., 2021; CNN) and the 2017–2018 winter in Europe (Kautz et al., 2020; LeMonde, 2018). Moreover, even if the absolute severity of cold spells decreases, rapid temperature swings are a hazard in their own right (Kral-O'Brien et al., 2019; Casson et al., 2019).

4.2.2 Attribution of French cold spells to climate change

A statistical analysis of the temperatures during the French cold spell of 2021 was proposed by a team of the World Weather Attribution (Vautard et al., 2021). This report concluded that while climate change has raised the absolute temperatures during cold spells, it has also led to an intensification of growing-period frosts due to earlier bud burst. The 2021 cold outbreak occurred right after a specific weather pattern called the "Atlantic Ridge", identified as one of the four main weather regimes in the North Atlantic region (Michelangeli et al., 1995). The goal of this section is to analyse how the features of this weather pattern have evolved with climate change using the ERA5 reanalyses (Figure 3). This analysis complements the report of Vautard et al. (2021) by examining the atmospheric circulation. We focus on the date of 06-04-2021, the day where the circulation particularly favored the advection of cold air into France. For this day the slp pattern (a) consists of a ridge of high pressure over the Atlantic and a large cyclonic structure over Scandinavia, with cold air advection from Northern latitudes into France. The analogs associated with this circulation in the counterfactual (b) and factual (c) exhibit the same zonal pressure gradient, and their difference (d) shows that the gradient is amplified in factual world, leading to colder advection towards France. The $t2m$ for the 06-04-2021 (e) shows cold conditions over Northern and Western Europe, while the analogs are

https://doi.org/10.5194/wcd-2022-9
Preprint. Discussion started: 17 February 2022

Weather and Climate Dynamics Discussions
Open Access
EGU

milder (f,g) and $\Delta t2m$ is mostly everywhere greater than $0°C$. If we focus over France, we can conclude that this cold spell would have lead to temperature 2-4°C colder without anthropogenic forcing. Looking at the precipitation maps (i,j,k) and the Δtp (l) we see that this pattern corresponds to dry conditions over continental France. There is no change of precipitation patterns over France between the factual and counterfactual conditions. We observe that the atmospheric conditions triggers precipitation over continental and northern Europe. The reinforcement of the pressure gradient leads to an increase of the precipitation over continental Europe and a decrease on the Mediterranean sea. The values of Q (m) suggest that the pattern under examination is rare compared to its analogs, with a tendency to become even rarer in the factual period. The predictability index D (n) tends to decrease in the factual period, While there are not significant shifts in the persistence Θ (o). The monthly distribution of the analogs (p) suggests that there is a significant shift of this circulation pattern towards summer and autumn months and that its occurrence in winter is decreasing in recent times.

To conclude, our analysis suggests, in line with the literature on cold spells and climate change cited in Section 4.2.1, that this event is becoming rare in the current climate and that it would have lead to cooler temperatures in a world without climate change.

4.3 Westphalia floods

On July 11th, 2021 the synoptic situation over Western Europe was characterized by a ridge situated West of Ireland. As this low-pressure system - named "Bernd" by the German Meteorological Service (DWD, see Junghänel et al. (2021)) - gradually moved eastward, it was isolated from the usually westerly flow by a strong anticyclonic system that built up over the Eastern part of the Atlantic and deviated the jet stream north of Scotland. By July 13th, Bernd was completely cut from the main flow and remained stationary over Western and Central Europe until July 16th, before being gradually pushed east. Hot and moist surface air from Northern Europe and the Mediterranean was advected by the cyclonic movement around the cut-off, which led from July 12th to July 15th to recurrent and persistent heavy rains first over mountain ranges due to orographic and dynamic uplift and then over the entire region of Belgium, Luxembourg, Western Germany and Eastern France. The maximum precipitations over the region were centered on the west of Belgium with some locations receiving more than 250mm of rain in 48 hours (e.g. in Jalhay, Belgium, according to what reported by Kreienkamp et al. (2021)). The soils, already humid due to recurring precipitation events during the preceding three weeks, were incapable of absorbing more water which led to runoff and overflow of small watercourses and flash floods. Afterwards, larger rivers such as the Ruhr and the Meuse also overflowed, causing massive casualties mainly in Germany (196 people, according to DieWelt (2021)) and Belgium (42 casualties, according to HotNews.ro (2021)). In addition to the terrible fatalities, the floods severely damaged goods and infrastructures with a total cost estimated around €10 billion (Insurance) for Belgium. It was afterwards found using hydrological data that the flood in the regions affected was significantly higher than any flood since the beginning of the systematic records (Kreienkamp et al., 2021).

https://doi.org/10.5194/wcd-2022-9
Preprint. Discussion started: 17 February 2022

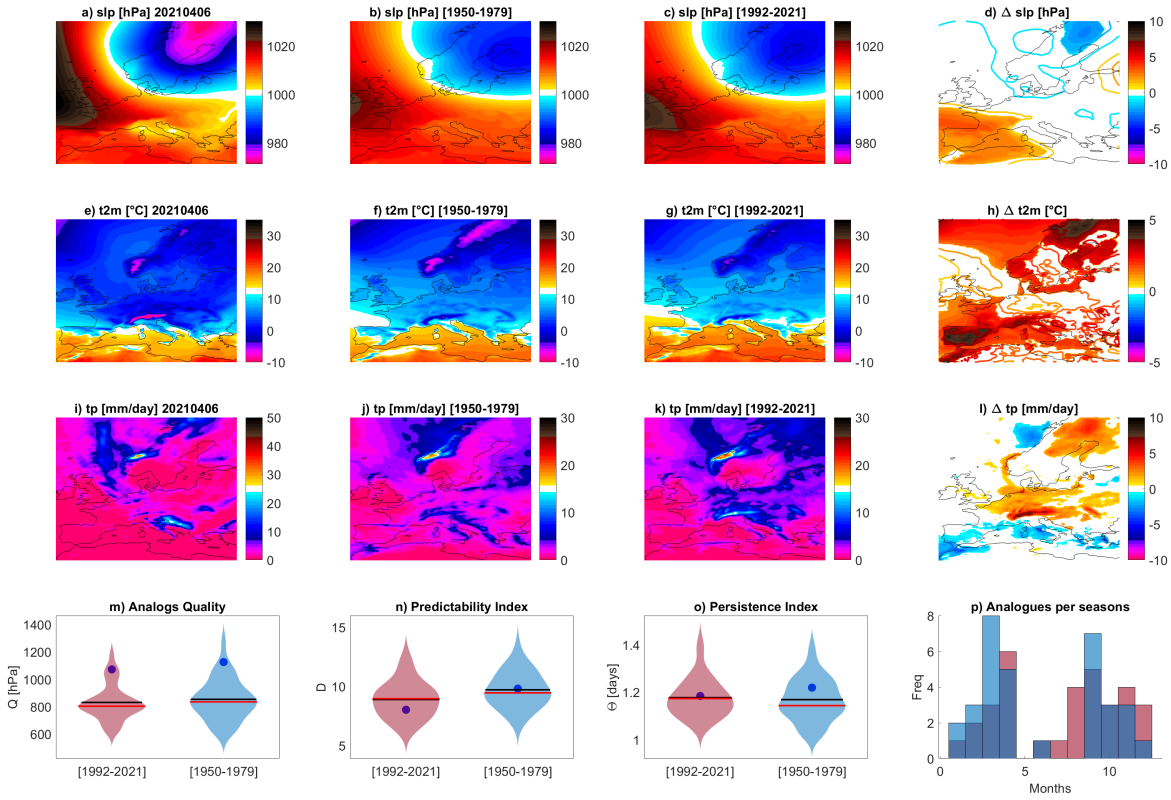

Figure 3. Attribution for the French cold spell on 06-04-2021. Daily mean sea-level pressure slp (a), 2-meter temperatures $t2m$ (e) and total precipitation tp (i) on the day of the event. Average of the 33 sea-level pressure analogs found for the counterfactual [1950-1979] (b) and factual [1992-2021] (c) periods and corresponding 2-meter temperatures (f,g) and daily precipitation rate (j,k). Δslp (d), $\Delta t2m$ (h) and Δtp (i) between factual and counterfactual periods: colored-filled areas show significant anomalies with respect to the bootstrap procedure. Violin plots for counterfactual (blue) and factual (pink) periods for the Analogs Quality Q (m) the Predictability index D (n), the Persistence index Θ (o) and the distribution of analogs in each month (p). Values for the selected day are marked by a blue dot.

4.3.1 Floods and climate change

Rapidly after the event, the potential link between the event and climate change was highlighted by activists and journalists. Indeed, as the atmosphere warms up, it can contain more water - 7% per degree of warming according to the Clausius-Clapeyron relationship - therefore allowing more powerful extreme precipitation events. Several studies (Madsen et al., 2014; Kundzewicz et al., 2018, 2019) investigated the link between climate variability, extreme precipitation and hydrological floods globally and in Europe. As stated in the last IPCC report (Allan et al., 2021) summarising scientific literature on the link between flooding

https://doi.org/10.5194/wcd-2022-9
Preprint. Discussion started: 17 February 2022

Weather and Climate Dynamics Discussions
Open Access
EGU

events and anthropogenic climate change, there is high confidence that "a warmer climate will intensify very wet and very dry weather and climate events and seasons, but the location and frequency of these events depend on projected changes in regional atmospheric circulation." Especially for Europe, there is medium confidence that at 1.5°C of warming, "heavy precipitation and associated flooding are projected to intensify and be more frequent". This result highly depend on the type of water basins, especially if the peak flow is snowmelt-dominated, and more generally heavy precipitation are strongly entangled with natural variability of the climate system. In the end, although flooding usually depend strongly on the local characteristics of the hydrological system - especially artificialization of soils and containment of rivers - more intense flooding can be linked to climate change via the increased intensity of heavy rains.

4.3.2 Attribution of Westphalia floods to climate change

An attribution study of the Westphalia floods has already been published by the World Weather Attribution network, who investigated the influence of climate change on heavy precipitations over a broad region of Western Europe (Kreienkamp et al., 2021). The authors of the study concluded that a climate warming of 1.2°C (current climate) led to an increase of the likelihood of such an event by a factor between 1.2 and 9 with respect to the pre-industrial period. Here we take an approach based on analogs of the atmospheric circulation, which allows to take into account the atmospheric dynamics leading to the occurrence of the event. Results of our attribution analysis are displayed in Figure 4. We found a small significant decrease in the slp of the cut-off low over Germany by 2-3hPa (a-d) but almost no significant changes in the 2m temperatures over the regions of interest (e-h). We found, however, a large and significant increase in precipitation (up to 5mm/day) over south-west Germany, eastern France and western Alps (i-l). This increase is consistent with the increasing amount of water that a hotter atmosphere can carry but can also be explained by the increased advection of most air by the stronger cut-off over Germany. Overall, the analogs quality (m) is good in both periods which reinforce our conclusions and allows us to emphasize that even if intense precipitation events due to cut-off lows over Western Europe in summer are not unusual, this event was particularly intense and climate change made it more intense. While no significant changes are observed for predictability D (n), the persistence index Θ (o) is higher in the recent period, indicating that recent cut-offs are more likely to stay stationary in Western Europe, leading to longer lasting precipitation events and potentially more intense floods. In the factual period, events tend to happen more frequently in the month of July (p), a favorable month for the development of large convective systems in the area.

4.4 Mediterranean Heatwave

During the month of August, an area of high pressure in the upper troposphere affected a large part of the Mediterranean basin. The upper lever tropospheric pressure system caused a downward movement in the atmosphere that simultaneously compressed the air and warmed it, a phenomenon known as heat dome. This atmospheric configuration induced a severe heatwave over the Mediterranean region from August 10th to 15th: south Italy, France, Spain and north Africa were the area mostly affected with wildfires and maxima temperatures record. Indeed, under a high pressure system, the winds tend to be weak, so the heat does not dissipate and help to keep the conditions increasingly warmer especially with the summer sun heat. On August 11th, record-breaking temperatures were recorded at several locations in Italy. The town of Santa Maria Capua Vetere in Campania

https://doi.org/10.5194/wcd-2022-9
Preprint. Discussion started: 17 February 2022

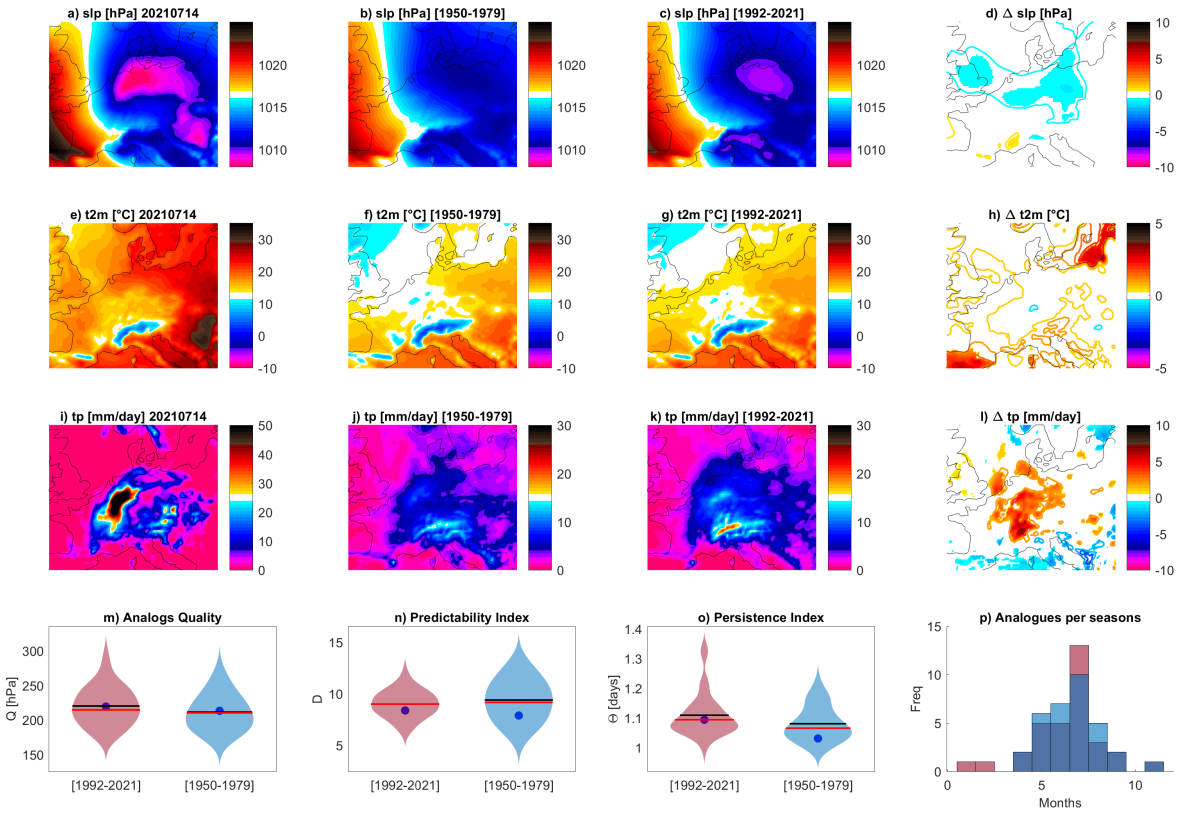

Figure 4. Attribution for the Westphalia Floods on 14-07-2021. Daily mean sea-level pressure slp (a), 2-meter temperatures $t2m$ (e) and total precipitation tp (i) on the day of the event. Average of the 33 sea-level pressure analogs found for the counterfactual [1950-1979] (b) and factual [1992-2021] (c) periods and corresponding 2-meter temperatures (f,g) and daily precipitation rate (j,k). Δslp (d), $\Delta t2m$ (h) and Δtp (i) between factual and counterfactual periods: colored-filled areas show significant anomalies with respect to the bootstrap procedure. Violin plots for counterfactual (blue) and factual (pink) periods for the Analogs Quality Q (m) the Predictability index D (n), the Persistence index Θ (o) and the distribution of analogs in each month (p). Values for the selected day are marked by a blue dot.

reached 42.2°C, 44.5° C at Bova in Calabria and 43.6° C at Ballao in Sardinia (3Bmeteo, 2021). The highest temperature was recorded in eastern Sicily with a peak of 48.8°C recorded by the SIAS (2021) in Floridia in the province of Syracuse. This value represents the highest value recorded in Italy and Europe. From August 12th the heat dome moved towards Spain. The heat peak was reached on August 14th for Spain, establishing a new national record of 47.4° C in Montoro, Andalusia, as recorded by the AEMET (2021a). The heatwave also reached south-east France, where 40.9° C were recorded in Varages in the Var, and in Trets, Bouches-du-Rhône (41.2° C). Same records were broken also in Tunisia, with 47°C in Tunis and 50.3°C in Kairouan (WMO, 2021). The heatwave also triggered a large spread of wildfires in Italy, Spain, France and Greece. During

https://doi.org/10.5194/wcd-2022-9
Preprint. Discussion started: 17 February 2022

the night of August 11th to 12th, more than 500 fires were recorded in Italy, causing 4 casualties (CEMS, 2021c). Spain also faced flames in the area of Navalacruz and Riofrio. A fire of 90 km of perimeter devastated 12 000 hectares of vegetation and led to the evacuation of 1000 inhabitants (CEMS, 2021a). Similarly in the Var (France) wildfires burned 6 300 hectares and resulted in the evacuation of 7000 people and the death of 2 people (CEMS, 2021b).

4.4.1 Mediterranean Heatwaves and climate change

August is known as a hot and dry month in the Mediterranean region. However, the temperatures observed this summer are extreme and are typical of what is expected from climate change. In fact, according to the IPCC's Sixth Assessment Report AR6 (Allan et al., 2021), as a result of climate change, we are experiencing more frequent and severe high temperature events, and that this trend will continue in the future. It indicates that the frequency and intensity of heat extremes, including marine heatwaves, have increased in recent decades and are projected to continue to increase under all greenhouse gas emission scenarios. Temperatures in the Mediterranean region have increased more than the global average (Allan et al., 2021). The IPCC claimed that, for the European Mediterranean, there will be a combination of changes related to climate drivers (e.g. less precipitation and snow, changes in the sea levels mean and extremes) by mid-century and for global warming of at least 2°C and greater (high confidence). For the North African Mediterranean, the IPCC predicts a decrease in mean precipitation and increase in fire-related weather, as well as an observed and projected increase in aridity, meteorological, hydrological, agricultural and ecological droughts (Allan et al., 2021).

4.4.2 Attribution of the Mediterranean Heatwave to climate change

We use the ERA5 dates to perform the attribution of the anticyclonic circulation associated with the Mediterranean heatwave in past and present climate. First, we note that we will select the analogs independently of the extratropical or tropical nature of the depression that produced them. Figure 5 shows the results for the heatwave over Sicily. We do not detect a significant change in the slp for the factual period compared to the counterfactual period (a-d). However, we observe that temperatures (e-g) are significantly warmer (h) in the recent period, especially over the island and the southern Mediterranean basin. This warming is associated with a significant decrease in precipitation in the factual period, especially in southern Europe, that could be explained by the high temperature and stability which suppress convection (i-l). We detect remarkable changes in the predictability index D (n), which means that the slp pattern tends to be more unpredictable in the present time, and we find a slight decrease in the persistence Θ (o). Finally, we notice that the number of analogs per season is increasing in the factual period, in June and September (m).

In summary, our analysis is perfectly in line with the existing literature cited in Section 4.4.1, as it shows the large predominance of the thermodynamic effects of climate change with a clear warming signal, higher on the area than the global average. This signal is associated with dryer conditions over land and an extension of this circulation patterns towards the beginning and the end of summer.

https://doi.org/10.5194/wcd-2022-9
Preprint. Discussion started: 17 February 2022

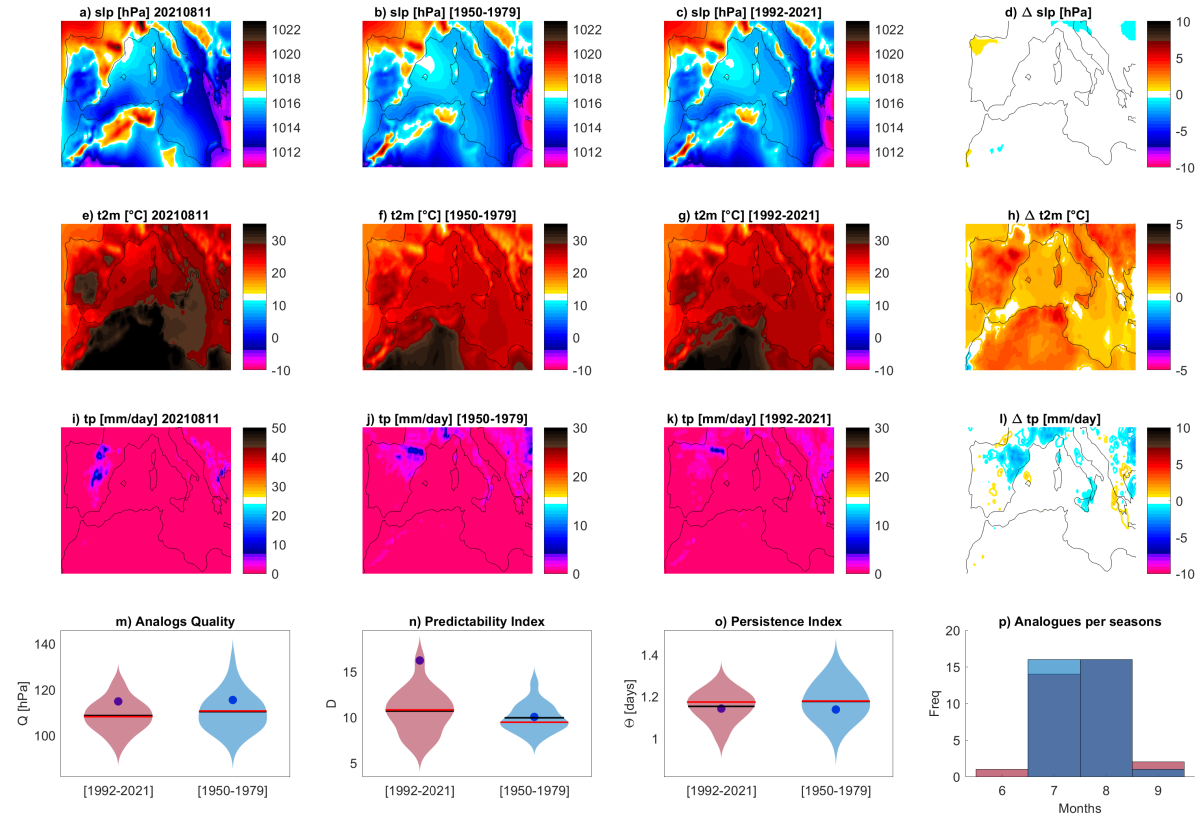

Figure 5. Attribution for the Mediterranean Heat Peak on 11-08-2021. Daily mean sea-level pressure slp (a), 2-meter temperatures $t2m$ (e) and total precipitation tp (i) on the day of the event. Average of the 33 sea-level pressure analogs found for the counterfactual [1950-1979] (b) and factual [1992-2021] (c) periods and corresponding 2-meter temperatures (f,g) and daily precipitation rate (j,k). Δslp (d), $\Delta t2m$ (h) and Δtp (i) between factual and counterfactual periods: colored-filled areas show significant anomalies with respect to the bootstrap procedure. Violin plots for counterfactual (blue) and factual (pink) periods for the Analogs Quality Q (m) the Predictability index D (n), the Persistence index Θ (o) and the distribution of analogs in each month (p). Values for the selected day are marked by a blue dot.

4.5 Hurricane Ida

Hurricane Ida is a tropical and post-tropical cyclone event that occured in the North Atlantic basin (Caribbean Sea Mainland USA) in August-September 2021. Besides being the most intense TC to make landfall in the US this season, it had a very damaging post-tropical stage. Hurricane Ida (track shown in Figure 6) was first detected as a tropical wave on August 23th. It was named as a tropical storm on August 26th and it became a Category 1 Hurricane on the day it made a first landfall over Cuba on August 27th. This landfall did not weaken it, and it underwent rapid intensification as it approached Louisiana's

https://doi.org/10.5194/wcd-2022-9
Preprint. Discussion started: 17 February 2022

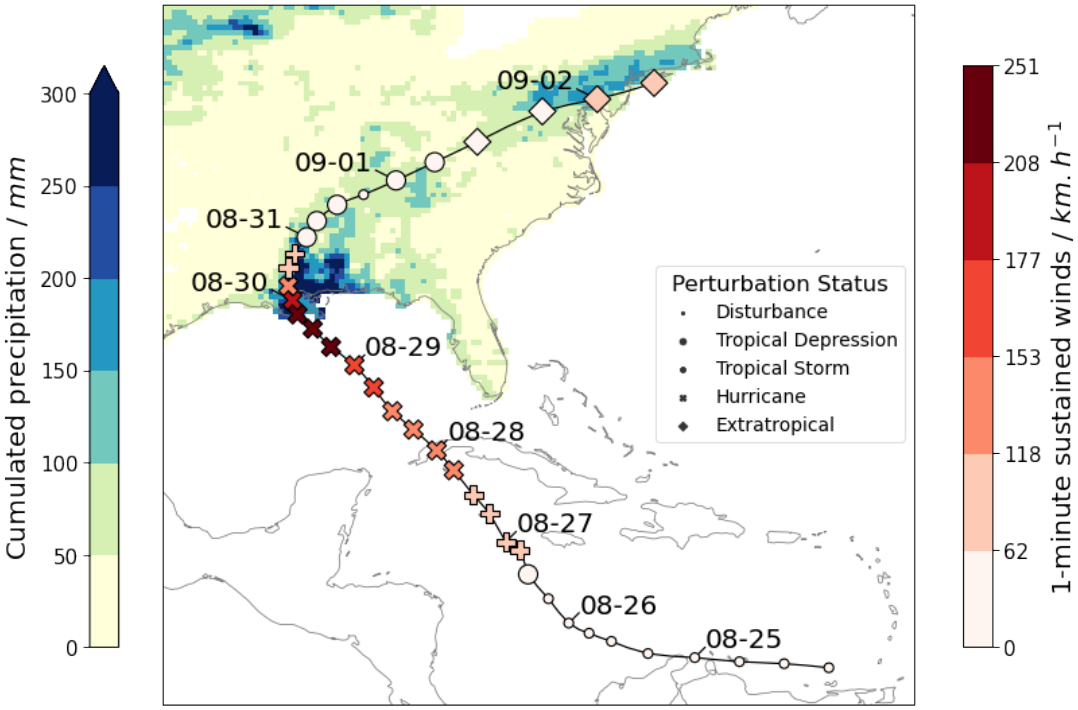

Figure 6. Track and associated precipitation for the Ida hurricane. 6-hourly track position from the IBTrACS (Knapp et al., 2010; Knapp, Kenneth R et al., 2018)) database are provided with their wind speed an status from NHC report. Time stamps are UTC, format mm-dd. Cumulated daily precipitation between 28-08-2021 and 03-09-2021 from the NCEP/CPC US Unified Precipitation are displayed. White color indicates no data in the figure

coast, were it landfell again as a Category 4 hurricane (NHC/NOAA, 2021). At its peak intensity, 1-minute sustained winds reached 240km/h and the minimum central pressure was 929hPa. Notably, it did not rapidly weakened because of the "brown ocean effect", where flat and moist land conditions allow a TC to retain its intensity for a longer period of time. Ida finally dropped below hurricane strength on August 30th. While it was still a tropical wave, Ida triggered floods in Venezuela with 20 casualties. in Cuba, the material damage was important, but no casualties were reported. In Louisiana and Mississippi there were a total of 38 deaths, among which 23 indirect, mostly for CO poisoning (CDC, 2021). A large power outage left more than 1 million people in black-out. Heavy infrastructural damage is estimated around $15 billion (NCDC/NOAA, 2021). These figures can be compared to Katrina's – the costliest hurricane to date, that made landfall on the same date and the same place 16 years before – 1838 deaths and $125 billion damages (NHC/NOAA, 2018). It shows that New Orleans was better prepared, and the forecast improved a lot as well (NHC/NOAA, 2005). While Ida was degenerating into an extratropical low, it combined with a frontal zone regaining tropical-storm force winds, and unleashing large amounts of rainfall over Northeastern US. This

https://doi.org/10.5194/wcd-2022-9
Preprint. Discussion started: 17 February 2022

region was much less prepared, so that the casualties were greater than the tropical stage with 42 deaths, mostly because of the flash floods. Finally, Ida ended its course over Eastern Canada, dissipating in the Gulf of St Lawrence.

4.5.1 Hurricanes and climate change

Among all extreme events, tropical cylones (TC) are among those for which the prediction of the evolution with climate change is the most uncertain. This the reasons for this is threefold: (i) The lack of a satisfying theory for cyclogenesis, (ii) the short-span of reliable observations, and (iii) the difficulty to simulate TC in state-of-the-art global models, because of their too coarse resolution. Despite the relatively short span of observation available, some conclusions can still be drawn from the past record (Knutson et al., 2019). Because of different trends in different regions, it is impossible to conclude on a global trend in TC frequency, but IPCC's AR6 (Allan et al., 2021) note that "it is *likely* that the global proportion of major TC occurrence has increased over the last four decades." Moreover, the latitude of the peak intensity shifted poleward (Kossin et al., 2014). Heavy precipitation associated with TC is also increasing with *high confidence*. Damages have been increasing, because of a larger amount of exposed wealth, but also a decrease in TC translation speed (Kossin, 2018). In the future, modeling studies using different methodologies (large-scale indicators vs. direct TC tracking) disagree on the sign of a global TC frequency trend. But there is confidence in trends of TC-related risks. Knutson et al. (2020) highlight consequences in order of certainty: i) because of sea-level rise, storms surges will become more important; ii) TC precipitation rates will increase, iii) The proportion of intense TC among all TC will continue to rise, and the maximum surface wind speed will increase of about 5%.

There is also growing concern about the increase in windstorm risks associated with post-tropical cyclone (Haarsma, 2021). Indeed, studies in reanalyses showed that despite representing a small number of extra-tropical storms, post-tropical cyclones are among the most intense ones to reach North America and Europe (Baker et al., 2021; Sainsbury et al., 2020). A global climate change projection show that more tropical cyclones are likely to undergo post-tropical transition, especially in the North-Atlantic basin (Michaelis and Lackmann, 2019).

4.5.2 Attribution of Hurricane Ida to climate change

We now focus on the day Ida produced heavy precipitation in New-York city, namely the 02-09-2021 and apply the analogs methodology to perform attribution. First of all, let us note that we will select analogs independently on the extratropical or tropical nature of the depression that have produced them. Figure 7a) shows the daily slp associated with Ida on the chosen date and (b) and (c) the analogs average computed for the counterfactual and the factual periods. We find a significant weakening of the slp depression for the factual with respect to the factual period (d). Furthermore, we observe that temperatures (e-g) are significantly warmer (h) in the recent period especially on the sea grid-points surrounding the North-East US and Nova Scotia. This warming is associated with a significant increase of precipitation in the factual period due to the larger availability of heat and humidity (i-l). We have confidence in these results because the quality of the analogs Q for the event is in the bulk of the distribution of Q for its analogs in both factual and counterfactual periods (m). We do not observe shift in D (n) or in Θ (o) in the factual vs counterfactual period. Finally we do see an increase of analogs in the month of August/September in the factual

https://doi.org/10.5194/wcd-2022-9
Preprint. Discussion started: 17 February 2022

Weather and Climate Dynamics Discussions
Open Access
EGU

period (p): these months are at in the tropical cyclone season in the North Atlantic and therefore similar patterns could trigger deep convection in association with cyclonic depressions, leading to extreme precipitations as observed in the case of Ida.

Ida was already a rare extreme event as a category 4 hurricane, but it will leave a mark especially because of its impactful post-tropical stage. As we have discussed in Section 4.5.1, very intense hurricanes will become more frequent with climate change, and they will be more likely to undergo post-tropical transition. What is particular for Ida, however, is that this transition occurred inland. What allowed the storm to remain intense in between a very strong tropical cyclone stage and the encounter with an extra-tropical perturbation could be the wet and warm condition allowing for the "brown effect". Such conditions are expected to be more likely with climate change. However, no formal study of such inland post-tropical cyclones have been made that we are aware of. While our attribution does not take into account the tropical/extratropical nature or the direction of the storm, we believe that the seasonal shift of the analogs towards late summer together with the temperature increase in the Atlantic in the factual world provides a solid explanation of the potential danger of this kind of events in the present climate.

4.6 Po Valley Tornadoes Outbreak

On September 19, 2021, an outbreak of 7 tornadoes affected the Central Po Valley, in Northern Italy. In particular, 6 of these formed in Lombardy and one, the most intense and damaging, hit a small airport near Carpi, Emilia Romagna. Both mesocyclonic and non-mesocyclonic vortices were observed during the event, making it one the most impressive tornado outbreaks on record for the region. While tornadoes and waterspouts happen regularly in Italy, they are on average much less frequent and less intense than in highly affected areas, such as the Mid-Western and South-Eastern US. However, the structure and location of the Po Valley can lead to the insurgence of environmental conditions conducive for occasionally intense phenomena, including tornadoes reaching EF4+ intensity on the Enhanced Fujita scale (Doswell III et al., 2009). During the summer, the Po Valley can be characterized by the persistence of hot and humid air, and the presence of the Adriatic Sea to the South-East provides an additional source of moisture, which can be advected to the region by low-level jets preceding low pressure areas approaching from the North-West. Moreover, the presence of the Appennini can encourage the formation of dry lines in case of South-Westerly flow due to foehn effect, contributing to supercell development (Alberoni et al., 1996). On September 19th, a high pressure system was elevated from the Central Mediterranean Sea to Scandinavia, while a high-level low pressure was approaching the Po Valley from France, connected to a trough located over North-Western Europe. During the afternoon, the region was affected by a favourable dynamic and thermodynamic setup: a hot and humid low-level jet from the East, a strong wind shear with winds from the South-West at 500 hPa, a jet stream from the West at 200 hPa, and an approaching upper-level low characterized by relatively cold air, and by the entrainment of stratospheric dry air. This led to the formation of strong thunderstorms associated with 6 tornadoes over Lombardy, roughly between the cities of Milan and Brescia. Around 5 pm, an isolated thunderstorm formed to the South-East of this area, closer to the Appenninic range, and assumed markedly supercellular features, with a hook-echo reflectivity signature, a doppler velocity couplet and a deviation to the right w.r.t. the mid-level flow. This supercell produced a well-documented significant tornado which hit a local airport, resulting in possible EF3 damage (Poli and Stanzani, 2022).

https://doi.org/10.5194/wcd-2022-9
Preprint. Discussion started: 17 February 2022

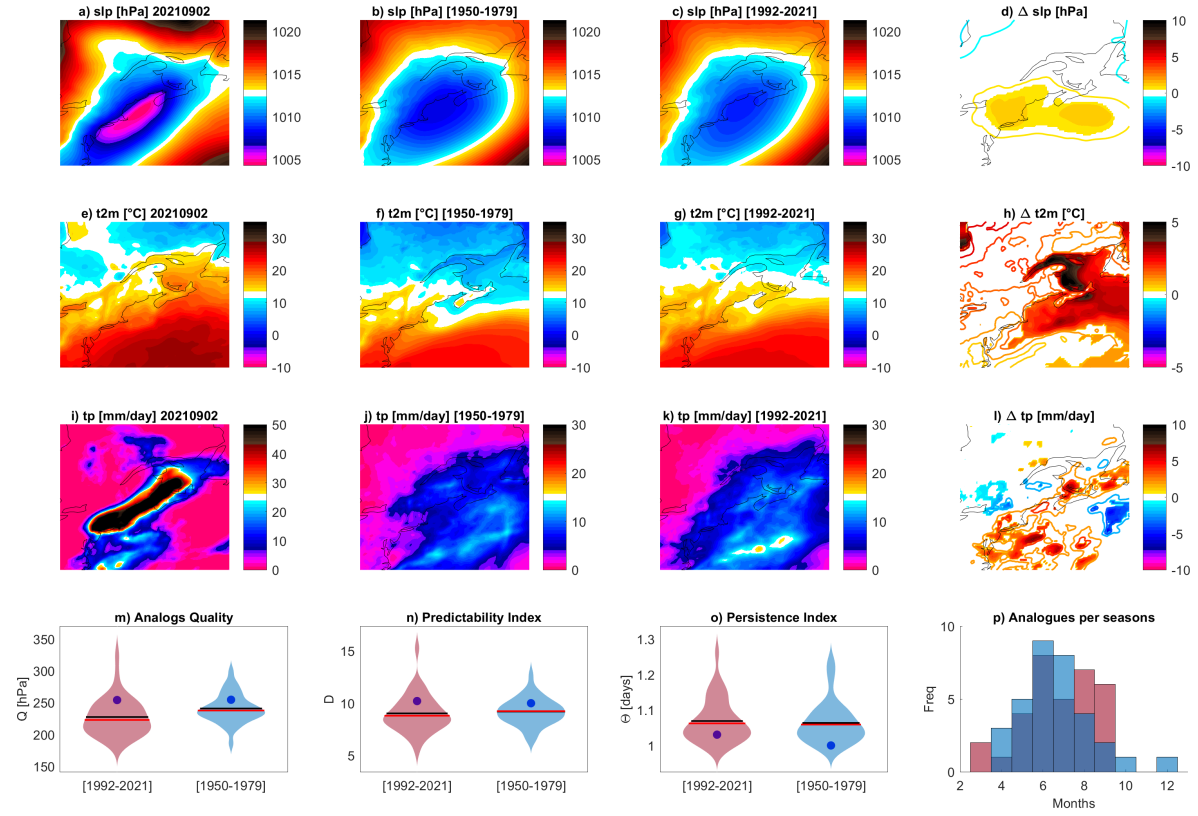

Figure 7. Attribution for the Hurricane Ida passage over New-York City area on 02-09-2021. Daily mean sea-level pressure slp (a), 2-meter temperatures $t2m$ (e) and total precipitation tp (i) on the day of the event. Average of the 33 sea-level pressure analogs found for the counterfactual [1950-1979] (b) and factual [1992-2021] (c) periods and corresponding 2-meter temperatures (f,g) and daily precipitation rate (j,k). Δslp (d), $\Delta t2m$ (h) and Δtp (i) between factual and counterfactual periods: colored-filled areas show significant anomalies with respect to the bootstrap procedure. Violin plots for counterfactual (blue) and factual (pink) periods for the Analogs Quality Q (m) the Predictability index D (n), the Persistence index Θ (o) and the distribution of analogs in each month (p). Values for the selected day are marked by a blue dot.

4.6.1 Tornadoes and Climate Change

Past and future trends in tornado occurrence have been the object of investigation in several studies, summarised in the IPCC AR6 (Allan et al., 2021). In particular, the IPCC reports that observed trends in tornado occurrence are associated with low confidence, due to short time series, reporting inhomogeneity and observation bias; low confidence affects also the estimation of future trends, due to the intrinsic difficulty associated with projections of small-scale convective extremes. However, medium

https://doi.org/10.5194/wcd-2022-9
Preprint. Discussion started: 17 February 2022

confidence is given to a tendency of tornadoes to be clustered in less frequent but more efficient outbreaks, characterized by a higher number of tornadoes per episode, with a total tornado number approximately constant over time. High confidence is given to the projected increase in frequency of environments conducive for the formation of tornadoes. Finally, it is concluded that attribution efforts for this phenomenon are beyond current modelling capabilities (Allan et al., 2021). Most studies are focused on the US, pointing to an increased variability, efficiency and possibly intensity of tornado outbreaks (Brooks et al., 2014; Elsner et al., 2015, 2019); however, tornadoes in Europe remain an underestimated threat (Antonescu et al., 2017), even though they can interest very densely populated areas, as in the case described in this article.

4.6.2 Attribution of the Po-Valley Tornadoes Outbreaks to climate change

We conclude by using the ERA5 dates to perform the attribution of the synoptic configuration associated with the outbreak in the past and present climate. Figure 8 shows the results for the episode. We find a significant but modest and unstructured increase of the slp field for the factual with respect to the counterfactual period (a-d). Instead, we observe that temperatures (e-g) are significantly warmer (h) in the recent period, both over land and the Mediterranean sea. This provides an increased amount of convective potential energy, though the transport of hot and humid air within the low-level jet. Precipitations associated with this configuration are higher over the Alps and Central Europe, while slightly lower over the Italian peninsula (i-l). The analogs quality shows that this circulation pattern is common compared to the rest of the analogs. We do not detect visible changes in the predictability D (n) and persistence Θ (o) of the configuration. Finally, we observe that the seasonal occurrence of analogs (p) is quite consistent with the months of occurrence of tornadoes in the country, with a maximum during summer; however, we do observe a shift of the peak from August to July, when land surface temperatures reach the annual maximum and the probability of low pressure areas entering the Mediterranean basin is higher than in May or June, offering more energy and occasions for convective instability.

Concerning the impact of climate change on the occurrence of tornado outbreaks, our analysis shows a clear increase in temperature associated to the analogs of this event in the factual period 1992-2021. This is compatible with the enhancement of thermodynamic setups due to climate change mentioned in Section 4.6.1, leading to more favourable environments for tornadoes. However, the small spatio-temporal scale of the phenomenon require caution in the interpretation of the attribution results.

4.7 Medicane Apollo

When the relatively cold atmospheric air coming from polar latitudes meets the warm surface of the Mediterranean Sea, extratropical cyclones change their characteristics into near-tropical depressions. These hybrids - termed "medicanes" (crasis for Mediterranean Hurricanes) by climate scientists and meteorologists - can be very damaging because of the strong winds and the intense convective precipitations (thunderstorms) originating around the eye of the storm. Medicane Apollo (named by a consortium of European meteorological services, see Meteoweb (2021)) formed on October 28th in the Jonian sea, offshore Sicily, from a low pressure disturbance which was very active in the days previous the formation of the Medicane. This low pressure system was isolated near the Balearic islands around 22nd of October and then moved on the Central Mediterranean

https://doi.org/10.5194/wcd-2022-9
Preprint. Discussion started: 17 February 2022

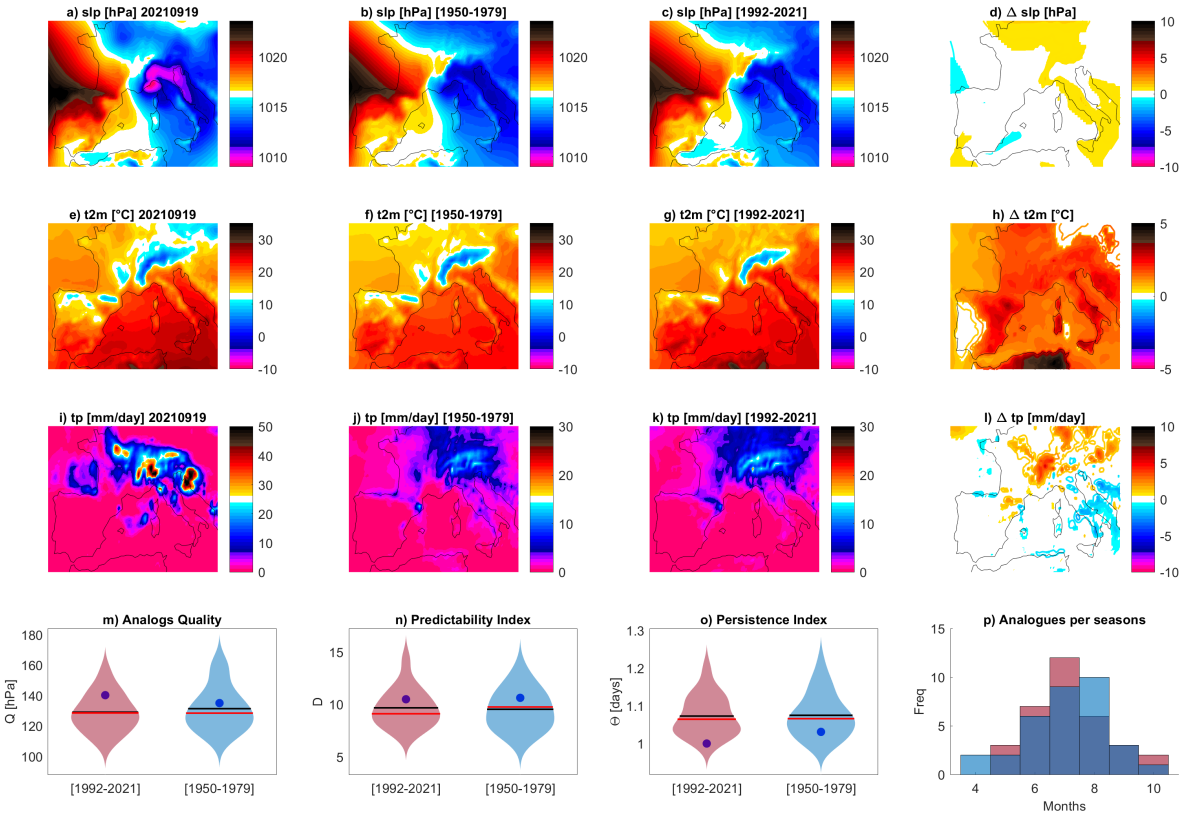

Figure 8. Attribution for the Po Valley Tornadoes Outbreak on 19-09-2021. Daily mean sea-level pressure slp (a), 2-meter temperatures $t2m$ (e) and total precipitation tp (i) on the day of the event. Average of the 33 sea-level pressure analogs found for the counterfactual [1950-1979] (b) and factual [1992-2021] (c) periods and corresponding 2-meter temperatures (f,g) and daily precipitation rate (j,k). Δslp (d), $\Delta t2m$ (h) and Δtp (i) between factual and counterfactual periods: colored-filled areas show significant anomalies with respect to the bootstrap procedure. Violin plots for counterfactual (blue) and factual (pink) periods for the Analogs Quality Q (m) the Predictability index D (n), the Persistence index Θ (o) and the distribution of analogs in each month (p). Values for the selected day are marked by a blue dot.

sea producing self-regenerating thunderstorms in the area of Catania on the 24th of October. Figure 9 displays the track of the cyclone along its life-cycle. These thunderstorms resulted in extreme rain and floods in Catania (>400mm rain in 48h, estimated by SIAS (2021)). During the tropical phase of Apollo, according to the latest report available, at least 10 people were killed by the storm in Sicily, Malta, Algeria and Tunisia (jbarisk, 2021). The highest wind gusts were measured on October 29th (104km/h) and the pressure minimum value was estimated to 999 hPa. From the convective precipitations associated with Apollo, the Sicilian Meteorological service SIAS measured > 200mm rain in the area of Syracuse on the same date. Apollo

https://doi.org/10.5194/wcd-2022-9
Preprint. Discussion started: 17 February 2022

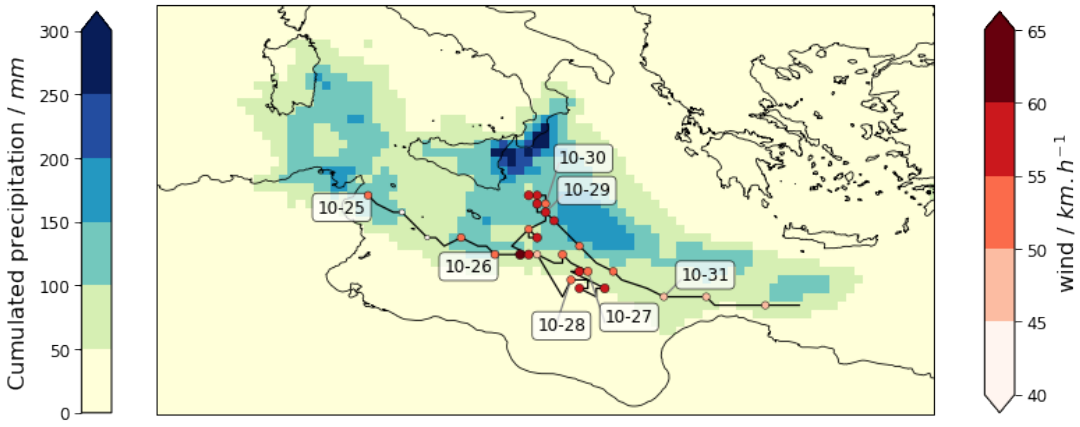

Figure 9. Track and associated precipitation for Apollo. Data from ERA5: Track position is retrieved as the local minimum of *slp*, wind is the maximum wind speed in a 1.5° GCD radius of the slp center, cumulated precipitation between 24-10-2021 and 31-10-2021. Time stamps are UTC, format mm-dd.

weakened on 30th October 2021 landfalling near Bayda and stayed inland until emerging over the Mediterranean a few hours later. Then, on 2nd of November, it dissipated off the coast of Turkey.

4.7.1 Medicanes and climate change

It is difficult to study the modification of frequency and intensity of medicanes in climate change. First of all, our knowledge of historical medicanes is very limited before the satellite era: their frequency is estimated between 1 and 2 events per year (Cavicchia et al., 2014a). Medicanes genesis is favored when an extratropical depression gets isolated from the polar jet stream. This "cut off" becomes quasi-stationary on the Mediterranean sea and can use the large availability of heat and humidity from the sea to produce organized convection. Recent studies of medicanes in climate change have therefore considered two elements: the precursors, namely the cut-off low that get isolated from the jet stream in the Mediterranean sea and the potential for organized convection once the first condition is met (Cavicchia et al., 2014b; Romero and Emanuel, 2017; Tous et al., 2016). On one hand, there is a general consensus that the jet stream will shift northward and therefore cut-off low will become slightly less probable on the Mediterranean sea. On the other hand, the Mediterranean sea is warming faster than oceans, increasing the potential for convection once a depression system is present in the area. We then expect to see less medicanes but more intense ones (González-Alemán et al., 2019).

4.7.2 Attribution of Medicane Apollo to climate change

We now use the ERA5 dataset to perform the attribution of the cyclonic circulation associated with Apollo in the past and present climate. First of all, let us note that we will select analogs independently on the extratropical or tropical nature of the

https://doi.org/10.5194/wcd-2022-9
Preprint. Discussion started: 17 February 2022

depression that have produced them. Figure 10 shows the results for Apollo. We already observe that the analogs average slp for both the periods (b,c) do not reach slp minima comparable to that of Apollo (a) hinting to the uniqueness of this event. The Δslp (d) do not display any interesting structure. Instead, we observe that temperatures (e-g) are significantly warmer (h) the factual world especially on the island of Sicily and on the southern Mediterranean basin. This warming is associated with a significant increase of precipitation in the factual period due to the larger availability of heat and humidity from the sea (i-l). These results must be taken with care because the analogs quality Q>60 hPa (m) clearly shows that this circulation pattern is rarer compared with the rest of its analogs. As in the case of Storm Filomena, Apollo appears to be a black swan event. We do not detect remarkable changes in the predictability index D (n) but we see a slightly increase in the persistence Θ (o) which could also have contributed to enhance the persistence of precipitation on the same areas. Finally we do see an increase of analogs in the month of September in the factual period (p): this is the warmest month for the Mediterranean sea, hence the most favorable for the development of deep convection in association with cyclonic depressions. This factor can greatly enhance precipitations, especially on the mountain ranges exposed to the winds, as in the case of Apollo, for the Etna and the Peloritani mountain ranges.

With respect to the general statements reported in Section 4.7.1, our analysis also highlights the potential intensification of precipitation associated with cyclones around the island of Sicily, supported both by higher temperatures and increased occurrence of cyclones in the month of September, the warmest for the Mediterranean sea. However, we point to the black swan nature of this storm compared to its analogs, and therefore to a careful interpretation of the attribution results obtained above.

4.8 Scandinavian cold spell

During late November 2021, Scandinavia experienced record-low temperatures for the season. On the 28th November, Nikkaluokta weather station in Sweden recorded -37,4 °C, which was the lowest November temperature recorded in the country since 1980. Other stations in northern Sweden recorded their lowest November temperatures since the 1950s (SMHI, a). Comparable records occurred in the first days of December. In Norway, the -36,7 °C recorded in Kautokeino was the lowest November reading since 2002 (SMHI, b). These frigid temperatures were part of a broader area of below-average temperatures, peaking in the last week of November and first days of December, and stretching from North-Western Russia all the way to Spain (which recorded one of the top 10 coldest November months on record (AEMET)). The cold spell impacted transports, including suspension of entire train lines (SVT) and an unusually large number of road accidents in southern Sweden (SVD).

The cold spell was associated with a large ridge forming over the North Atlantic starting from the 23rd November, and drawing cold Arctic and Siberian air over the continent. A pressure dipole with a high over Scandinavia and a low over central Europe further favoured cold air advection. The Atlantic ridge persisted until early December, after which a more zonal circulation occurred, bringing warmer airmasses over large parts of Europe.

https://doi.org/10.5194/wcd-2022-9
Preprint. Discussion started: 17 February 2022

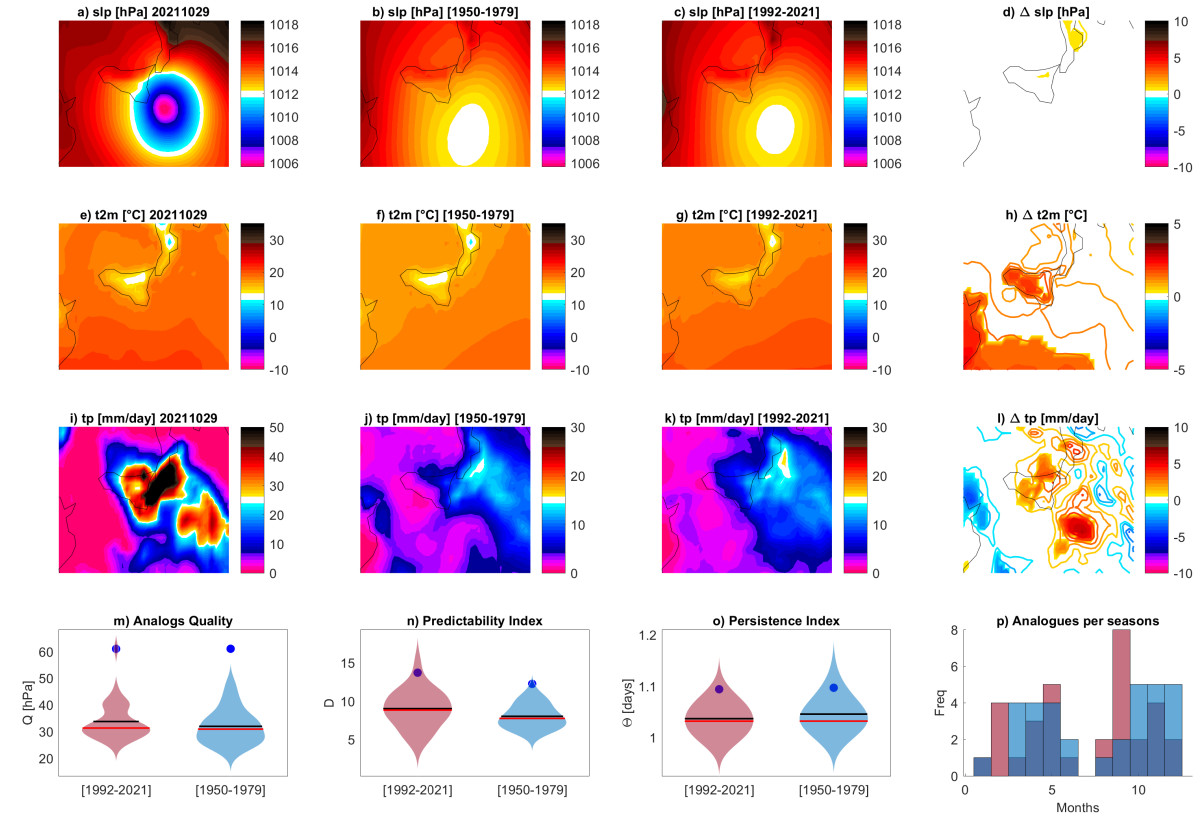

Figure 10. Attribution for the Medicane Apollo on 29-10-2021. Daily mean sea-level pressure slp (a), 2-meter temperatures $t2m$ (e) and total precipitation tp (i) on the day of the event. Average of the 33 sea-level pressure analogs found for the counterfactual [1950-1979] (b) and factual [1992-2021] (c) periods and corresponding 2-meter temperatures (f,g) and daily precipitation rate (j,k). Δslp (d), $\Delta t2m$ (h) and Δtp (i) between factual and counterfactual periods: colored-filled areas show significant anomalies with respect to the bootstrap procedure. Violin plots for counterfactual (blue) and factual (pink) periods for the Analogs Quality Q (m) the Predictability index D (n), the Persistence index Θ (o) and the distribution of analogs in each month (p). Values for the selected day are marked by a blue dot.

4.8.1 Scandinavian Cold Spells and Climate Change

As discussed in Sect. 4.2.1, it is virtually certain that there has been a decrease in severity and/or frequency of cold spells in the last several decades, and the consensus is that at a global level this decrease will continue in the future. Scandinavia fits this trend, and has shown a significant decrease in wintertime cold spell days in recent decades (Matthes et al., 2015). In the future, the decrease in wintertime cold days is expected to be stronger than in several other European regions (Dosio, 2016), as is the

https://doi.org/10.5194/wcd-2022-9
Preprint. Discussion started: 17 February 2022

increase in yearly minimum daily-mean temperature (Bernes, 2017, p. 102).

4.8.2 Attribution of the Scandinavian Cold Spell to Climate Change

Figure 11 shows the results of our attribution analysis for the Scandinavian cold spell. The slp analogs suggest that the pressure dipole over Europe seen during the cold spell is quite an unusual configuration, and that such dipole has typically become weaker i the factual period (a–d). The weaker dipole in the analogs during both periods corresponds to warmer 2-m temperatures compared to the event, but there is no evident increase in the temperatures of the analogs between the two periods over Scandinavia (h). There is instead a strong increase in temperatures over the Norwegian and Barents seas, in keeping with the lower pressure to the North of Scandinavia in the factual period compared to the counterfactual period (d). The lack of a clear warming signal is not coupled to large changes in the seasonality of the analogs (p), nor to notable changes in precipitation and the associated cloudiness (l). We hypothesise that the cold Siberian airmasses contributing to the cold European temperatures during these events have not warmed significantly (Cohen et al., 2013).

The quality of the analogs shows a modest improvement moving from the counterfactual to the factul world (m), and no dramatic change in the persistence of the analogue patterns is observed (o). There is instead a clear shift of the predictability distribution towards lower values (n), in agreement with the long-term trend towards a decrease D in the Euro-Atlantic sector (Faranda et al., 2019a), and the arguments supporting a general increase in wintertime mid-latitude slp predictability in warmer climates (Scher and Messori, 2019). The predictability of the event itself also decreases sharply, suggesting that it is a more predictable occurrence in the context of the atmospheric variability of the factual relative to the counterfactual period. Based on the above, we conclude that the atmospheric configuration driving cold spells such as the November 2021 episode has not become more "unusual" with climate change, and that the intensity of the cold spells engendered by similar atmospheric configurations has not weakened, contrary to the decreasing trends observed in data and model simulations for cold days in Scandinavia 4.8.1. As such, the November 2021 event may be seen as a persistent cold extreme in a warming climate.

5 Conclusions

We have analyzed the atmospheric circulation associated with a selection of high-impact extreme events occurring in 2021 from an attribution perspective. Specifically, we have performed a semi-objective selection of a representative day for each extreme, and have then identified two sets of analogs. The first in the 1950–1979 period, which approximates a counterfactual world; the second in the 1992–2021 period, which approximates a factual world. Regardless the specificity of each event, our analysis allows us to draw some conclusions that may be of relevance to the broader field of extreme event attribution. First, many circulation patterns leading to extremes occur preferentially during a specific season, but are observed with lower frequency during all seasons (e.g. see the attribution of Filomena winter storm or the French spring cold spell). For many events, we have been able to identify seasonal shifts in the occurrence of event analogs with major implications for their surface impacts (e.g.

https://doi.org/10.5194/wcd-2022-9
Preprint. Discussion started: 17 February 2022

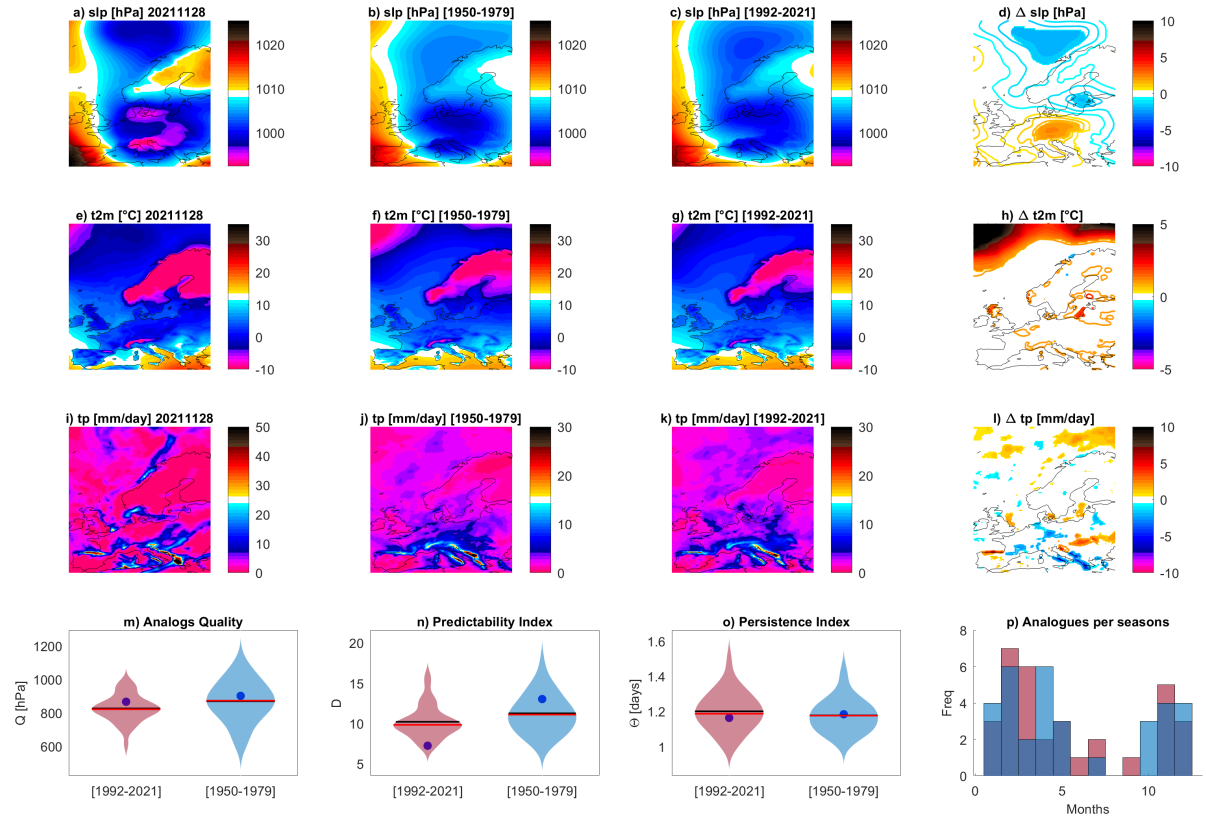

Figure 11. Attribution for the Scandinavian Cold Spell on 28-11-2021. Daily mean sea-level pressure slp (a), 2-meter temperatures $t2m$ (e) and total precipitation tp (i) on the day of the event. Average of the 33 sea-level pressure analogs found for the counterfactual [1950-1979] (b) and factual [1992-2021] (c) periods and corresponding 2-meter temperatures (f,g) and daily precipitation rate (j,k). Δslp (d), $\Delta t2m$ (h) and Δtp (i) between factual and counterfactual periods: colored-filled areas show significant anomalies with respect to the bootstrap procedure. Violin plots for counterfactual (blue) and factual (pink) periods for the Analogs Quality Q (m) the Predictability index D (n), the Persistence index Θ (o) and the distribution of analogs in each month (p). Values for the selected day are marked by a blue dot.

see the attribution of the Scandinavian cold spell). This can occur independently of large changes in the analogue circulation patterns or the thermodynamic effect of global mean surface warming.

A second important outcome of this study is to include, in the attribution framework, the systematic use of the dynamical indicators of persistence and predictability. Persistence is of particular interest, since there has been a lively scientific debate on changes in atmospheric persistence and how this may affect extreme events (Coumou and Rahmstorf, 2012; Hoskins and Woollings, 2015; Wehrli et al., 2020).

https://doi.org/10.5194/wcd-2022-9
Preprint. Discussion started: 17 February 2022

Finally, we have studied the quality of the analogs, the "typicality" of the analogs relative to the atmospheric variability and their changes over time. This brings a third relevant outcome, namely the ability to understand whether both a given circulation and its analogs are becoming more or less "typical" (i.e. have better or worse analogs). The two do not always vary in tandem, meaning that the quality of the analogs for a given extreme may remain unchanged while the analogs of the analogs become better. While not immediate to interpret, this provides some subtle insights into how the configurations conducive to an extreme relate to the broader atmospheric variability typical of a given climate. In the case of the storm Filomena and the medicane Apollo, the lack of analogs of good quality directly points to the emergence of this event as an unprecedented one, a black swan among the weather patterns in Europe. This warns that weather extreme events can appear without belonging to an existing population. It is therefore questionable to attempt any attribution statements in this case.

The main limitations of our framework include the somewhat arbitrary choices of the region used to define the analogs, the time scale for the selection of the analogs and of the number of analogs. We are well aware of these limitations, and have designed the study to minimise their impact. The main advantage of working with analogs of sea-level pressure is the possibility of applying expert judgement to select a region that includes the large-scale cyclonic/anticyclonic structures concurring with the event. The use of daily averages allows to average out the daily cycle. Longer time scales have been tested but they produce worse analogs due to the fact that the synoptic structures move too much and lead to aliased atmospheric patterns. Furthermore, information about the eventual stationarity of the patterns is retained in the persistence metrics. Finally we have tested the dependence on the number of analogs used and found that an optimum performance is reached between 30 and 60 analogs, i.e. a number sufficiently high to have a meaningful statistics but low enough to have authentic analogs. A metric of quality of analogs has been added to control the outcome of the analogs search. Finally we highlight that conventional extreme value attribution shares many of the same limitations, including the choice of the region, thresholds and time scale.

Our approach does not want to substitute extreme value attributions based on the statistical fitting of extreme value distributions: those approaches can be used to provide an immediate answers to stakeholders in changes of return times of extreme events in factual versus counterfactual worlds and have been successfully used by the attribution community in a large number of instances (Trenberth et al., 2015; Van Oldenborgh and Van Ulden, 2003; Vautard and Yiou, 2012; Van Oldenborgh et al., 2012; Trenberth et al., 2015; Vautard et al., 2016, 2018). We rather see our analysis as complementing statistical approaches by providing insights on the possible changes over time of the dynamics underlying an extreme events from a dynamical perspective. Further development of this methodology can include the use of analogs to flag population of events that share the same dynamical origin, on the line of research proposed by Jézéquel et al. (2018b) and Shepherd (2019). This would allow to perform an attribution conditioned to the analogs and the release of an automated package that produces these analyses in matter of minutes as soon as the ERA5 data are available. Other possible extensions include searching for analogs of different observables such as geopotential height, temperature on pressure levels, winds and more. Although valuable, these options must be evaluated with extreme care in the context of attribution because of the non-linear trends already introduced by the anthropogenic forcing on the average of these quantities (Jézéquel et al., 2018a).

To conclude, the analogs approach to extreme event attribution shows that many extreme events are significantly modified in present climate with respect to the past, because of changes in the position, persistence and seasonality of cyclonic/anticyclonic

https://doi.org/10.5194/wcd-2022-9
Preprint. Discussion started: 17 February 2022

patterns. Our approach, complementary to the statistical methods already available in the attribution community, underscore the importance of considering changes in the atmospheric circulation when performing attribution studies.

Code availability. The code to compute the dynamical indicators of predictability D and persistence θ is available at https://fr.mathworks.com/matlabcentral/fileexchange/95768-attractor-local-dimension-and-local-persistence-computation

Data availability. ERA5 is the latest climate reanalysis being produced by ECMWF as part of implementing the EU- funded Copernicus Climate Change Service (C3S), providing hourly data on atmospheric, land-surface and sea-state parameters together with estimates of uncertainty from 1979 to present day. ERA5 data are available on the C3S Climate Data Store on regular latitude-longitude grids at 0.25° x 0.25° resolution at https://cds.climate.copernicus.eu/#!/home, accessed on 2022-01-26

Appendix A: Predictability and Persistence Indices

The attractor of a dynamical system is a geometric object defined in the space hosting all the possible states of the system (phase-space). Each point ζ on the attractor can be characterized by two dynamical indicators: the local dimension D, which indicates the number of degrees of freedom active locally around ζ, and the persistence Θ, a measure of the mean residence time of the system around ζ (Faranda et al., 2017a). To determine D, we exploit recent results from the application of extreme value theory to Poincaré recurrences in dynamical systems. This approach considers long trajectories of a system — in our case successions of daily SLP latitude–longitude maps — corresponding to a sequence of states on the attractor. For a given point ζ in phase space (e.g., a given SLP map), we compute the probability that the system returns within a ball of radius ϵ centered on the point ζ. The Freitas et al. (2010) theorem, modified by Lucarini et al. (2012), states that logarithmic returns:

$$g(x(t)) = -\log(\text{dist}(x(t),\zeta)) \tag{A1}$$

yield a probability distribution such that:

$$\Pr(z > s(q)) \simeq \exp\left[-\vartheta(\zeta)\left(\frac{z-\mu(\zeta)}{\sigma(\zeta)}\right)\right] \tag{A2}$$

where $z = g(x(t))$ and s is a high threshold associated to a quantile q of the series $g(x(t))$. Requiring that the orbit falls within a ball of radius ϵ around the point ζ is equivalent to asking that the series $g(x(t))$ is over the threshold s; therefore, the ball radius ϵ is simply $e^{-s(q)}$. The resulting distribution is the exponential member of the Generalized Pareto Distribution family. The parameters μ and σ, namely the location and the scale parameter of the distribution, depend on the point ζ in phase space. $\mu(\zeta)$ corresponds to the threshold $s(q)$ while the local dimension $d(\zeta)$ can be obtained via the relation $\sigma = 1/D(\zeta)$. This is the metric of predictability introduced in Sect. 3.

https://doi.org/10.5194/wcd-2022-9
Preprint. Discussion started: 17 February 2022

When $x(t)$ contains all the variables of the system, the estimation of D based on extreme value theory has a number of advantages over traditional methods (e.g. the box counting algorithm (Liebovitch and Toth, 1989; Sarkar and Chaudhuri, 1994)). First, it does not require to estimate the volume of different sets in scale-space: the selection of $s(q)$ based on the quantile provides a selection of different scales s which depends on the recurrence rate around the point ζ. Moreover, it does not require the a priori selection of the maximum embedding dimension as the observable g is always a univariate time-series.

The persistence of the state ζ is measured via the extremal index $0 < \vartheta(\zeta) < 1$, an adimensional parameter, from which we extract $\Theta(\zeta) = \Delta t/\vartheta(\zeta)$. $\Theta(\zeta)$ is therefore the average residence time of trajectories around ζ, namely the metric of persistence introduced in Sect. 3, and it has unit of a time (in this study days). If ζ is a fixed point of the attractor $\Theta(\zeta) = \infty$. For a trajectory that leaves the neighborhood of ζ at the next time iteration, $\Theta = 1$. To estimate ϑ, we adopt the Süveges estimator (Süveges, 2007). For further details on the the extremal index, see Lucarini et al. (2016a).

Author contributions. D Faranda conceived the study and performed the attribution analysis for each event, he wrote the section on the medicane Apollo. S Bourdin wrote the section on Hurricane Ida and performed cyclones tracking. M Ginesta wrote the section about storm Filomena. M Krouma wrote the section about the Mediterranean Heatwave. G Messori wrote the section about the Scandinavian Cold Spell. R Noyelle wrote the section about the Westphalia floods. Flavio Pons wrote the section about Tornadoes outbreak. Pascal Yiou wrote the section about the French spring cold-spell. All the authors contributed writing and reviewing the introduction, methods and conclusion of the article.

Competing interests. The authors declare no competing interests

Acknowledgements. The author wishes to thank MC Alvarez-Castro, J Riboldi, M Galfi, M Vrac, A Hisi, E Coppola and R Vautard for the discussions. The authors acknowledge the support of the INSU-CNRS-LEFE-MANU grant (project DINCLIC), as well as the gran ANR-19-ERC7-0003 (BOREAS). This work has received support from the European Union's Horizon 2020 research and innovation programme under grant agreement No. 101003469 (XAIDA), by the European Research Council (ERC) grant agreement No. 948309 (CENÆ), and the Marie Sklodowska-Curie grant agreement No. 956396 (EDIPI).

Appendix D. Supplement study about the attribution of extremes events. Article "A climate-change attribution retrospective of some impactful weather extremes of 2021"

https://doi.org/10.5194/wcd-2022-9
Preprint. Discussion started: 17 February 2022

References

3Bmeteo: Caldo Storico in Sicilia, https://www.3bmeteo.com/giornale-meteo/cronaca-meteo---caldo-storico-in-sicilia--raggiunti-i-49-c---il-nuovo-record-europeo-504610, accessed: 2022-01-31, 2021.

AEMET: Spanish State Meteorological Agency: Noviembre de 2021, un mes muy frío, https://www.aemet.es/es/noticias/2021/12/resumen_clima_noviembre_2021, accessed: 2022-01-14.

AEMET: Spanish State Meteorological Agency, https://aemetblog.es/2021/08/18/la-ola-de-calor-del-puente-de-agosto21-y-los-records-de-temperaturas-en-espana/, accessed: 2022-01-27, 2021a.

AEMET: Spanish State Meteorological Agency: Informe sobre la borrasca Filomena y la ola de frio, http://www.aemet.es/documentos/es/conocermas/recursos_en_linea/publicaciones_y_estudios/estudios/Informe_episodio_filomena.pdf, accessed: 2021, 2021b.

Alberoni, P., Nanni, S., Crespi, M., and Monai, M.: The supercell thunderstorm on 8 June 1990: mesoscale analysis and radar observations, Meteorology and Atmospheric Physics, 58, 123–138, 1996.

Allan, R. P., Hawkins, E., Bellouin, N., and Collins, B.: IPCC, 2021: Summary for Policymakers, 2021.

Antonescu, B., Schultz, D. M., Holzer, A., and Groenemeijer, P.: Tornadoes in Europe: An underestimated threat, Bulletin of the American Meteorological Society, 98, 713–728, 2017.

Aon: Global Catastrophe Recap, http://thoughtleadership.aon.com/documents/20210209_analytics-if-january-global-recap.pdf, accessed: January 2021, 2021.

Baker, A. J., Hodges, K. I., Schiemann, R. K., and Vidale, P. L.: Historical variability and lifecycles of North Atlantic midlatitude cyclones originating in the tropics, Journal of Geophysical Research: Atmospheres, 126, e2020JD033 924, 2021.

Bala, G., Caldeira, K., and Nemani, R.: Fast versus slow response in climate change: implications for the global hydrological cycle, Climate dynamics, 35, 423–434, 2010.

BBC: Polar vortex death toll rises to 21 as US cold snap continues, https://www.bbc.com/news/world-us-canada-47088684, accessed: 2022-01-14.

Bernes, C.: En varmare värld: Växthuseffekten och klimatets förändringar-Tredje upplagan, 2017.

Blackport, R. and Screen, J. A.: Weakened evidence for mid-latitude impacts of Arctic warming, Nature Climate Change, 10, 1065–1066, 2020.

Brooks, H. E., Carbin, G. W., and Marsh, P. T.: Increased variability of tornado occurrence in the United States, Science, 346, 349–352, 2014.

Casson, N., Contosta, A., Burakowski, E., Campbell, J., Crandall, M., Creed, I., Eimers, M., Garlick, S., Lutz, D., Morison, M., et al.: Winter weather whiplash: Impacts of meteorological events misaligned with natural and human Systems in Seasonally Snow-Covered Regions, Earth's Future, 7, 1434–1450, 2019.

Cavicchia, L., von Storch, H., and Gualdi, S.: A long-term climatology of medicanes, Climate dynamics, 43, 1183–1195, 2014a.

Cavicchia, L., von Storch, H., and Gualdi, S.: Mediterranean tropical-like cyclones in present and future climate, Journal of Climate, 27, 7493–7501, 2014b.

CDC: Deaths Related to Hurricane Ida, https://www.cdc.gov/mmwr/volumes/70/wr/mm7039a3.htm, accessed: 2022-01-31, 2021.

CEMS: COPERNICUS Emergency Management Service, https://emergency.copernicus.eu/mapping/list-of-components/EMSR538, accessed: 2022-01-31, 2021a.

CEMS: COPERNICUS Emergency Management Service, https://emergency.copernicus.eu/mapping/list-of-components/EMSR541, accessed: 2022-01-31, 2021b.

https://doi.org/10.5194/wcd-2022-9
Preprint. Discussion started: 17 February 2022

CEMS: COPERNICUS Emergency Management Service, https://emergency.copernicus.eu/mapping/ems/copernicus-emergency-management-service-monitors-fire-events-mediterranean-region, accessed: 2022-01-31, 2021c.

CNN: These US cities had the coldest morning in decades – with some reaching all-time record lows, https://edition.cnn.com/2021/02/16/us/record-cold-weather-us-trnd/index.html, accessed: 2022-01-14.

Cohen, J., Jones, J., Furtado, J. C., and Tziperman, E.: Warm Arctic, cold continents: A common pattern related to Arctic sea ice melt, snow advance, and extreme winter weather, Oceanography, 26, 150–160, 2013.

Cohen, J., Zhang, X., Francis, J., Jung, T., Kwok, R., Overland, J., Tayler, P. C., Lee, S., Laliberte, F., and Feldstein, S.: Arctic change and possible influence on mid-latitude climate and weather: a US CLIVAR White Paper, US CLIVAR, 2018.

Coumou, D. and Rahmstorf, S.: A decade of weather extremes, Nature climate change, 2, 491–496, 2012.

D'errico, M., Yiou, P., Nardini, C., Lunkeit, F., and Faranda, D.: Warmer Mediterranean temperatures do not decrease snowy cold spell intensity over Italy, https://hal.archives-ouvertes.fr/hal-02367559/document, 2019.

DieWelt: "Hochwasser aktuell: Zahl der Toten in Rheinland-Pfalz steigt auf 135 - Mindestens 184 Opfer durch Flut in Deutschland", https://www.welt.de/vermischtes/live232509543/Hochwasser-aktuell-Mindestens-177-Opfer-durch-Flut-in-Deutschland.html, accessed: 2021-07-22, 2021.

Dosio, A.: Projections of climate change indices of temperature and precipitation from an ensemble of bias-adjusted high-resolution EURO-CORDEX regional climate models, Journal of Geophysical Research: Atmospheres, 121, 5488–5511, 2016.

Doss-Gollin, J., Farnham, D. J., Lall, U., and Modi, V.: How unprecedented was the February 2021 Texas cold snap?, Environmental Research Letters, 16, 064 056, 2021.

Doswell III, C. A., Brooks, H. E., and Dotzek, N.: On the implementation of the enhanced Fujita scale in the USA, Atmospheric Research, 93, 554–563, 2009.

Elsner, J. B., Elsner, S. C., and Jagger, T. H.: The increasing efficiency of tornado days in the United States, Climate Dynamics, 45, 651–659, 2015.

Elsner, J. B., Fricker, T., and Schroder, Z.: Increasingly powerful tornadoes in the United States, Geophysical Research Letters, 46, 392–398, 2019.

Faranda, D.: An attempt to explain recent trends in European snowfall extremes, Weather Clim. Dynam. Discuss., 2019, 1–20, https://doi.org/10.5194/wcd-2019-15, 2019.

Faranda, D., Messori, G., and Yiou, P.: Dynamical proxies of North Atlantic predictability and extremes, Scientific reports, 7, 41 278, 2017a.

Faranda, D., Messori, G., and Yiou, P.: Dynamical proxies of North Atlantic predictability and extremes, Scientific reports, 7, 41 278, https://www.nature.com/articles/srep41278.pdf, 2017b.

Faranda, D., Alvarez-Castro, M. C., Messori, G., Rodrigues, D., and Yiou, P.: The hammam effect or how a warm ocean enhances large scale atmospheric predictability, Nature communications, 10, 1–7, 2019a.

Faranda, D., Messori, G., and Vannitsem, S.: Attractor dimension of time-averaged climate observables: insights from a low-order ocean-atmosphere model, Tellus A: Dynamic Meteorology and Oceanography, 71, 1–11, 2019b.

Faranda, D., Vrac, M., Yiou, P., Jézéquel, A., and Thao, S.: Changes in future synoptic circulation patterns: consequences for extreme event attribution, Geophys. Res. Lett., 47, e2020GL088 002, iSBN: 0094-8276 Publisher: Wiley Online Library, 2020.

Flannigan, M. D., Stocks, B. J., and Wotton, B. M.: Climate change and forest fires, Science of the total environment, 262, 221–229, 2000.

Freitas, A. C. M., Freitas, J. M., and Todd, M.: Hitting time statistics and extreme value theory, Probability Theory and Related Fields, 147, 675–710, 2010.

Appendix D. Supplement study about the attribution of extremes events. Article "A climate-change attribution retrospective of some impactful weather extremes of 2021"

https://doi.org/10.5194/wcd-2022-9
Preprint. Discussion started: 17 February 2022

Freitas, A. C. M., Freitas, J. M., and Todd, M.: Extreme value laws in dynamical systems for non-smooth observations, Journal of Statistical Physics, 142, 108–126, 2011.

Freitas, A. C. M., Freitas, J. M., and Vaienti, S.: Extreme Value Laws for sequences of intermittent maps, arXiv preprint arXiv:1605.06287, 2016.

González-Alemán, J. J., Pascale, S., Gutierrez-Fernandez, J., Murakami, H., Gaertner, M. A., and Vecchi, G. A.: Potential increase in hazard from Mediterranean hurricane activity with global warming, Geophysical Research Letters, 46, 1754–1764, 2019.

Gordon, L. J., Steffen, W., Jönsson, B. F., Folke, C., Falkenmark, M., and Johannessen, Å.: Human modification of global water vapor flows from the land surface, Proceedings of the National Academy of Sciences, 102, 7612–7617, 2005.

Haarsma, R.: European Windstorm Risk of Post-Tropical Cyclones and the Impact of Climate Change, Geophysical Research Letters, 48, e2020GL091 483, 2021.

Horton, R. M., Mankin, J. S., Lesk, C., Coffel, E., and Raymond, C.: A review of recent advances in research on extreme heat events, Current Climate Change Reports, 2, 242–259, 2016.

Hoskins, B. and Woollings, T.: Persistent extratropical regimes and climate extremes, Current Climate Change Reports, 1, 115–124, 2015.

HotNews.ro: "Een van de twee laatste vermiste personen na overstromingen in ons land teruggevonden", https://www.hln.be/binnenland/een-van-de-twee-laatste-vermiste-personen-na-overstromingen-in-ons-land-teruggevonden~a4a4c681/, accessed: 2021-07-29, 2021.

Hu, S., Zhang, W., Turner, A. G., and Sun, J.: How does El Niño-Southern Oscillation affect winter fog frequency over eastern China?, Climate Dynamics, 54, 1043–1056, 2020.

Insurance, B.: "Recent floods cause nearly $12 billion damage in Belgium", https://www.businessinsurance.com/article/00010101/STORY/912343432/Recent-floods-cause-nearly-\protect\T1\textdollar12-billion-damage-in-Belgium, accessed: 2022-01-27.

jbarisk: Hurricane-like storm causes flooding in the Mediterranean, October 2021, https://www.jbarisk.com/flood-services/event-response/medicane-apollo, accessed: 2022-02-01, 2021.

Jézéquel, A., Dépoues, V., Guillemot, H., Trolliet, M., Vanderlinden, J.-P., and Yiou, P.: Behind the veil of extreme event attribution, Climatic Change, 149, 367–383, 2018.

Jolly, E., D'Andrea, F., Rivière, G., and Fromang, S.: Linking warm Arctic winters, Rossby waves and Cold Spells: an idealized numerical study, Journal of the Atmospheric Sciences, 2021.

Junghänel, T., Bissolli, P., Daßler, J., Fleckenstein, R., Imbery, F., Janssen, W., Kaspar, F., Lengfeld, K., Leppelt, T., Rauthe, M., et al.: Hydro-klimatologische Einordnung der Stark-und Dauerniederschläge in Teilen Deutschlands im Zusammenhang mit dem Tiefdruckgebiet „Bernd "vom 12. bis 19. Juli 2021, Deutscher Wetterdienst, 2021.

Jézéquel, A., Cattiaux, J., Naveau, P., Radanovics, S., Ribes, A., Vautard, R., Vrac, M., and Yiou, P.: Trends of atmospheric circulation during singular hot days in Europe, Environmental Research Letters, 13, 054 007, https://iopscience.iop.org/article/10.1088/1748-9326/aab5da/pdf, 2018a.

Jézéquel, A., Dépoues, V., Guillemot, H., Trolliet, M., Vanderlinden, J.-P., and Yiou, P.: Behind the veil of extreme event attribution, Climatic Change, https://doi.org/https://doi-org.insu.bib.cnrs.fr/10.1007/s10584-018-2252-9, 2018b.

Kautz, L.-A., Polichtchouk, I., Birner, T., Garny, H., and Pinto, J. G.: Enhanced extended-range predictability of the 2018 late-winter Eurasian cold spell due to the stratosphere, Quarterly Journal of the Royal Meteorological Society, 146, 1040–1055, 2020.

Knapp, K. R., Kruk, M. C., Levinson, D. H., Diamond, H. J., and Neumann, C. J.: The international best track archive for climate stewardship (IBTrACS) unifying tropical cyclone data, Bulletin of the American Meteorological Society, 91, 363–376, 2010.

https://doi.org/10.5194/wcd-2022-9
Preprint. Discussion started: 17 February 2022

Knapp, Kenneth R et al.: International Best Track Archive for Climate Stewardship (IBTrACS) Project, Version 4., https://doi.org/10.25921/82ty-9e16, accessed: 2022-01-26, 2018.

Knutson, T., Camargo, S. J., Chan, J. C., Emanuel, K., Ho, C.-H., Kossin, J., Mohapatra, M., Satoh, M., Sugi, M., Walsh, K., et al.: Tropical cyclones and climate change assessment: Part I: Detection and attribution, Bulletin of the American Meteorological Society, 100, 1987–2007, 2019.

Knutson, T., Camargo, S. J., Chan, J. C., Emanuel, K., Ho, C.-H., Kossin, J., Mohapatra, M., Satoh, M., Sugi, M., Walsh, K., et al.: Tropical cyclones and climate change assessment: Part II: Projected response to anthropogenic warming, Bulletin of the American Meteorological Society, 101, E303–E322, 2020.

Kodra, E., Steinhaeuser, K., and Ganguly, A. R.: Persisting cold extremes under 21st-century warming scenarios, Geophysical research letters, 38, 2011.

Kossin, J. P.: A global slowdown of tropical-cyclone translation speed, Nature, 558, 104–107, 2018.

Kossin, J. P., Emanuel, K. A., and Vecchi, G. A.: The poleward migration of the location of tropical cyclone maximum intensity, Nature, 509, 349–352, 2014.

Kral-O'Brien, K. C., O'Brien, P. L., and Harmon, J. P.: Need for false spring research in the Northern Great Plains, USA, Agricultural & Environmental Letters, 4, 190 025, 2019.

Kreienkamp, F., Philip, S. Y., Tradowsky, J. S., Kew, S. F., Lorenz, P., Arrighi, J., Belleflamme, A., Bettmann, T., Caluwaerts, S., Chan, S. C., et al.: Rapid attribution of heavy rainfall events leading to the severe flooding in Western Europe during July 2021, 2021.

Kundzewicz, Z. W., Pińskwar, I., and Brakenridge, G. R.: Changes in river flood hazard in Europe: a review, Hydrology research, 49, 294–302, 2018.

Kundzewicz, Z. W., Szwed, M., and Pińskwar, I.: Climate variability and floods—A global review, Water, 11, 1399, 2019.

LaChaineMeteo: Bilan climatique d'avril 2021 : entre sécheresse et records de froid, https://actualite.lachainemeteo.com/actualite-meteo/2021-05-05/bilan-climatique-d-avril-2021-entre-secheresse-et-records-de-froid-59270, accessed: 2022-02-01, 2021.

Lee, J.-Y., Marotzke, J., Bala, G., Cao, L., Corti, S., Dunne, J., Engelbrecht, F., Fischer, E., Fyfe, J., Jones, C., Maycock, A., Mutemi, J., Ndiaye, O., Panickal, S., , and Zhou, T.: Future Global Climate: Scenario-Based Projections and Near-Term Information. In Climate Change 2021: The Physical Science Basis. Contribution of Working Group I to the Sixth Assessment Report of the Intergovernmental Panel on Climate Change, 2021.

Lee, S. H. and Butler, A. H.: The 2018–2019 Arctic stratospheric polar vortex, Weather, 75, 52–57, 2020.

LeMonde: La vague de froid se poursuit en Europe et fait des dizaines de morts, https://www.lemonde.fr/climat/article/2018/02/28/la-vague-de-froid-se-poursuit-en-europe-et-fait-des-dizaines-de-morts_5263856_1652612.html, accessed: 2022-01-14, 2018.

Liebovitch, L. S. and Toth, T.: A fast algorithm to determine fractal dimensions by box counting, physics Letters A, 141, 386–390, 1989.

Lillo, S. P., Cavallo, S. M., Parsons, D. B., and Riedel, C.: The Role of a Tropopause Polar Vortex in the Generation of the January 2019 Extreme Arctic Outbreak, Journal of the Atmospheric Sciences, 78, 2801–2821, 2021.

Lucarini, V., Faranda, D., and Wouters, J.: Universal behaviour of extreme value statistics for selected observables of dynamical systems, Journal of statistical physics, 147, 63–73, 2012.

Lucarini, V., Faranda, D., de Freitas, J. M. M., Holland, M., Kuna, T., Nicol, M., Todd, M., Vaienti, S., et al.: Extremes and recurrence in dynamical systems, John Wiley & Sons, 2016a.

Lucarini, V., Faranda, D., Freitas, A. C. M., Freitas, J. M., Holland, M., Kuna, T., Nicol, M., Todd, M., and Vaienti, S.: Extremes and recurrence in dynamical systems, John Wiley & Sons, 2016b.

Appendix D. Supplement study about the attribution of extremes events. Article "A climate-change attribution retrospective of some impactful weather extremes of 2021"

https://doi.org/10.5194/wcd-2022-9
Preprint. Discussion started: 17 February 2022

Madsen, H., Lawrence, D., Lang, M., Martinkova, M., and Kjeldsen, T.: Review of trend analysis and climate change projections of extreme precipitation and floods in Europe, Journal of Hydrology, 519, 3634–3650, 2014.

Matthes, H., Rinke, A., and Dethloff, K.: Recent changes in Arctic temperature extremes: warm and cold spells during winter and summer, Environmental Research Letters, 10, 114 020, 2015.

Messori, G., Caballero, R., and Faranda, D.: A dynamical systems approach to studying midlatitude weather extremes, Geophysical Research Letters, 44, 3346–3354, 2017.

Meteoweb: Medicane Apollo, Aeronautica: per la prima volta un consorzio di Paesi europei ha dato un nome ufficiale ad un evento meteorologico, https://www.meteoweb.eu/2021/10/medicane-apollo-per-la-prima-volta-un-nome-ufficiale/1734332/, accessed: 2022-01-27, 2021.

Michaelis, A. C. and Lackmann, G. M.: Climatological changes in the extratropical transition of tropical cyclones in high-resolution global simulations, Journal of Climate, 32, 8733–8753, 2019.

Michelangeli, P.-A., Vautard, R., and Legras, B.: Weather regimes: Recurrence and quasi stationarity, Journal of the atmospheric sciences, 52, 1237–1256, 1995.

Mitchell, D., Heaviside, C., Vardoulakis, S., Huntingford, C., Masato, G., Guillod, B. P., Frumhoff, P., Bowery, A., Wallom, D., and Allen, M.: Attributing human mortality during extreme heat waves to anthropogenic climate change, Environmental Research Letters, 11, 074 006, 2016.

Moloney, N. R., Faranda, D., and Sato, Y.: An overview of the extremal index, Chaos: An Interdisciplinary Journal of Nonlinear Science, 29, 022 101, 2019.

Mori, M., Watanabe, M., Shiogama, H., Inoue, J., and Kimoto, M.: Robust Arctic sea-ice influence on the frequent Eurasian cold winters in past decades, Nature Geoscience, 7, 869–873, 2014.

Naveau, P., Hannart, A., and Ribes, A.: Statistical methods for extreme event attribution in climate science, Annual Review of Statistics and its Application, 7, 89–110, 2020.

NCDC/NOAA: Billion-Dollar Weather and Climate Disasters, https://www.ncdc.noaa.gov/billions/events/US/2021, accessed: 2022-01-31, 2021.

NCEP/CPC: PSL Data: CPC Unified Gauge-Based Analysis of Daily Precipitation over CONUS RT: NOAA Physical Sciences Laboratory, https://psl.noaa.gov/data/gridded/data.unified.daily.conus.rt.html, accessed: 25-01-2022.

NHC/NOAA: National Hurricane Center - Hurricane KATRINA Advisory Archive, https://www.nhc.noaa.gov/archive/2005/KATRINA.shtml, accessed: 2022-01-31, 2005.

NHC/NOAA: Costliest U.S. tropical cyclones tables updated, https://www.nhc.noaa.gov/news/UpdatedCostliest.pdf, accessed: 2022-01-31, 2018.

NHC/NOAA: National Hurricane Center - Hurricane IDA Advisory Archive, https://www.nhc.noaa.gov/archive/2021/IDA.shtml, accessed: 2022-01-31, 2021.

Ogawa, F., Keenlyside, N., Gao, Y., Koenigk, T., Yang, S., Suo, L., Wang, T., Gastineau, G., Nakamura, T., Cheung, H. N., et al.: Evaluating impacts of recent Arctic sea ice loss on the northern hemisphere winter climate change, Geophysical Research Letters, 45, 3255–3263, 2018.

Pendergrass, A. G., Knutti, R., Lehner, F., Deser, C., and Sanderson, B. M.: Precipitation variability increases in a warmer climate, Scientific reports, 7, 1–9, 2017.

https://doi.org/10.5194/wcd-2022-9
Preprint. Discussion started: 17 February 2022

Poli, V. and Stanzani, R.: Rapporto dell'evento meteorologico del 19 e 20 settembre 2021, Arpae Emilia-Romagna - Struttura Idro-Meteo-Clima. Available online at: https://allertameteo.regione.emilia-romagna.it/documents/20181/437770/Evento+19-20+settembre+2021.pdf/ff3ed88f-773d-06e9-eb02-d0a306ae9121?t=1633503536867 (Accessed January 26, 2022), 2022.

Román-Palacios, C. and Wiens, J. J.: Recent responses to climate change reveal the drivers of species extinction and survival, Proceedings of the National Academy of Sciences, 117, 4211–4217, 2020.

Romero, R. and Emanuel, K.: Climate change and Hurricane-like extratropical cyclones: Projections for North Atlantic polar lows and medicanes based on CMIP5 models, Journal of Climate, 30, 279–299, 2017.

Russo, S. and Sterl, A.: Global changes in indices describing moderate temperature extremes from the daily output of a climate model, Journal of Geophysical Research: Atmospheres, 116, 2011.

Sachweh, M. and Koepke, P.: Radiation fog and urban climate, Geophysical Research Letters, 22, 1073–1076, 1995.

Sainsbury, E. M., Schiemann, R. K., Hodges, K. I., Shaffrey, L. C., Baker, A. J., and Bhatia, K. T.: How important are post-tropical cyclones for European windstorm risk?, Geophysical Research Letters, 47, e2020GL089 853, 2020.

Sarkar, N. and Chaudhuri, B. B.: An efficient differential box-counting approach to compute fractal dimension of image, IEEE Transactions on systems, man, and cybernetics, 24, 115–120, 1994.

Scher, S. and Messori, G.: How global warming changes the difficulty of synoptic weather forecasting, Geophysical Research Letters, 46, 2931–2939, 2019.

Seneviratne, S., Zhang, X., Adnan, M., Badi, W., Dereczynski, C., Luca, A. D., Ghosh, S., Iskandar, I., Kossin, J., Lewis, S., Otto, F., Pinto, I., Satoh, M., Vicente-Serrano, S., Wehner, M., , and Zhou, B.: Weather and Climate Extreme Events in a Changing Climate. In Climate Change 2021: The Physical Science Basis. Contribution of Working Group I to the Sixth Assessment Report of the Intergovernmental Panel on Climate Change, 2021.

Shepherd, T. G.: Atmospheric circulation as a source of uncertainty in climate change projections, Nature Geoscience, 7, 703, 2014.

Shepherd, T. G.: A Common Framework for Approaches to Extreme Event Attribution, Current Climate Change Reports, 2, 28–38, https://doi.org/10.1007/s40641-016-0033-y, 2016.

Shepherd, T. G.: Storyline approach to the construction of regional climate change information, Proceedings of the Royal Society A, 475, 20190 013, 2019.

SIAS: Servizio Informativo Agrometeorologico Siciliano, http://www.sias.regione.sicilia.it/frameset_dati.htm, accessed: 2022-01-27, 2021.

SMHI: November 2021 - Nästan rekordkall avslutning, https://www.smhi.se/klimat/klimatet-da-och-nu/manadens-vader-och-vatten-sverige/manadens-vader-i-sverige/november-2021-nastan-rekordkall-avslutning-1.176606, accessed: 2022-01-14, a.

SMHI: November 2021 - La Niña bidrog till översvämningar i sydvästra Kanada, https://www.smhi.se/klimat/klimatet-da-och-nu/manadens-vader-i-varlden/november-2021-la-nina-bidrog-till-oversvamningar-i-sydvastra-kanada-1.176603, accessed: 2022-01-14, b.

Stefanon, M., D'Andrea, F., and Drobinski, P.: Heatwave classification over Europe and the Mediterranean region, Environmental Research Letters, 7, 014 023, 2012.

Stendel, M., Francis, J., White, R., Williams, P. D., and Woollings, T.: The jet stream and climate change, in: Climate Change, pp. 327–357, Elsevier, 2021.

Süveges, M.: Likelihood estimation of the extremal index, Extremes, 10, 41–55, 2007.

SVD: Oväder drar österut – flera trafikolyckor, https://www.svd.se/fortsatta-snoproblem-i-soder, accessed: 2022-01-14.

SVT: Tågtrafik i Norrbotten ställs in – för kallt att köra, https://www.svt.se/nyheter/lokalt/norrbotten/tagtrafik-i-norrbotten-stalls-in-for-kallt-att-kora, accessed: 2022-01-14.

https://doi.org/10.5194/wcd-2022-9
Preprint. Discussion started: 17 February 2022

Taleb, N.: The black swan: Why don't we learn that we don't learn, NY: Random House, 2005.

Tamarin-Brodsky, T., Hodges, K., Hoskins, B. J., and Shepherd, T. G.: A Dynamical Perspective on Atmospheric Temperature Variability and Its Response to Climate Change, Journal of Climate, 32, 1707–1724, 2019.

Tous, M., Zappa, G., Romero, R., Shaffrey, L., and Vidale, P. L.: Projected changes in medicanes in the HadGEM3 N512 high-resolution global climate model, Climate Dynamics, 47, 1913–1924, 2016.

Trenberth, K. E., Fasullo, J. T., and Shepherd, T. G.: Attribution of climate extreme events, Nature Clim. Change, 5, 725–730, http://dx.doi.org/10.1038/nclimate2657, 2015.

Trisos, C. H., Merow, C., and Pigot, A. L.: The projected timing of abrupt ecological disruption from climate change, Nature, 580, 496–501, 2020.

Ulbrich, U., Leckebusch, G. C., and Pinto, J. G.: Extra-tropical cyclones in the present and future climate: a review, Theoretical and Applied Climatology volume, 96, 117–131, 2009.

Van Oldenborgh, G. J. and Van Ulden, A.: On the relationship between global warming, local warming in the Netherlands and changes in circulation in the 20th century, International Journal of Climatology, 23, 1711–1724, <GotoISI>://000186918700003, 2003.

Van Oldenborgh, G. J., Van Urk, A., and Allen, M.: The absence of a role of climate change in the 2011 Thailand floods, Bull. Amer. Meteor. Soc, 93, 1047–1049, 2012.

van Oldenborgh, G. J., van der Wiel, K., Kew, S., Philip, S., Otto, F., Vautard, R., King, A., Lott, F., Arrighi, J., Singh, R., et al.: Pathways and pitfalls in extreme event attribution, Climatic Change, 166, 1–27, 2021.

Vautard, R. and Yiou, P.: ATTRIBUTION Robustness of warming attribution, Nature Climate Change, 2, 26–27, <GotoISI>://000299495500014, 2012.

Vautard, R., Yiou, P., Otto, F., Stott, P., Christidis, N., Oldenborgh, G. J. v., and Schaller, N.: Attribution of human-induced dynamical and thermodynamical contributions in extreme weather events, Environmental Research Letters, 11, 114 009, http://stacks.iop.org/1748-9326/11/i=11/a=114009, 2016.

Vautard, R., Colette, A., Van Meijgaard, E., Meleux, F., Jan van Oldenborgh, G., Otto, F., Tobin, I., and Yiou, P.: Attribution of Wintertime Anticyclonic Stagnation Contributing to Air Pollution in Western Europe, Bulletin of the American Meteorological Society, 99, S70–S75, 2018.

Vautard, R., van Oldenborg, G., Bonnet, R., Li, S., Robin, Y., Kew, S., Philip, S., Soubeyroux, J., Dubuisson, B., N, V., RIechstein, M., and Otto, F.: Human influence on growing period frosts like the early april 2021 in Central France, https://www.worldweatherattribution.org/wp-content/uploads/GrowingPeriodFrost2021.pdf, accessed: 2022-01-31, 2021.

Wehrli, K., Hauser, M., and Seneviratne, S. I.: Storylines of the 2018 Northern Hemisphere heatwave at pre-industrial and higher global warming levels, Earth System Dynamics, 11, 855–873, 2020.

WMO: world meteorological organisation, https://public.wmo.int/fr/medias/communiqués-de-presse/état-du-climat-en-2021-des-phénomènes-météorologiques-extrêmes-et-de, accessed: 2022-01-27, 2021.

Ye, K. and Messori, G.: Two leading modes of wintertime atmospheric circulation drive the recent warm Arctic–cold Eurasia temperature pattern, Journal of Climate, 33, 5565–5587, 2020.

Yiou, P., Jézéquel, A., Naveau, P., Otto, F. E. L., Vautard, R., and Vrac, M.: A statistical framework for conditional extreme event attribution, Advances in Statistical Climatology, Meteorology and Oceanography, 3, 17–31, https://doi.org/10.5194/ascmo-3-17-2017, 2017.

Yiou, S., Balembois, F., Schaffers, K., and Georges, P.: Efficient laser operation of an Yb : S-FAP crystal at 985 nm, APPLIED OPTICS, 42, 4883–4886, <GotoISI>://000184940000014, 2003.

https://doi.org/10.5194/wcd-2022-9
Preprint. Discussion started: 17 February 2022

Zappa, G., Shaffrey, L. C., Hodges, K. I., Sansom, P. G., , and Stephenson, D. B.: A Multimodel Assessment of Future Projections of North Atlantic and European Extratropical Cyclones in the CMIP5 Climate Models, Journal of Climate, p. 5846–5862, 2013.

Zscheischler, J., Martius, O., Westra, S., Bevacqua, E., Raymond, C., Horton, R. M., van den Hurk, B., AghaKouchak, A., Jézéquel, A., and Mahecha, M. D.: A typology of compound weather and climate events, Nature reviews earth & environment, pp. 1–15, iSBN: 2662-138X Publisher: Nature Publishing Group, 2020.